EXPOSED COLUMN BASE CONNECTIONS SUBJECTED TO AXIAL COMPRESSION AND FLEXURE

by

Ivan Gomez
Amit Kanvinde
University of California, Davis

Gregory Deierlein
Stanford University

Final Report Presented to the

American Institute of Steel Construction

April 2010

Executive Summary

This report presents results of an experimental study investigating the response of exposed column base connections subjected to axial compression and strong-axis bending. This investigation is the second phase of a broader study whose ultimate aim is the development of improved design guidelines for column base connections. A review of existing design procedures and published research reveals that current approaches to characterize the strength of exposed column base connections loaded by axial compression and flexure are not supported by adequate experimental validation. Thus, the main objectives of this study are to evaluate existing strength prediction approaches and propose refinements based on experimental verification.

The main scientific basis of this study consists of a series of seven large scale experiments on exposed column base connections subjected to a combination of axial compressive load and cyclic lateral deformations. The tests investigate the effect of various parameters on the response of the connections, including (1) the base plate thickness (2) anchor rod layout (3) presence and level of axial load (4) anchor rod strength and (5) applied loading history. The column base connection tests are complemented by ancillary tests to characterize material properties of the anchor rods, base plate, grout and concrete.

An evaluation of the experimental data relative to the existing design approaches reveals that existing strength prediction methods (such as those outlined in the *Design Guide 1* published by the AISC) may be highly conservative (i.e. the average test-to-predicted ratio for connection strength is 1.86). The methods outlined in the *Design Guide* assume that failure of the base connection is governed by lowest base moment which activates the limit state of only one component in the connection (e.g. anchor rod capacity or yielding of the base plate in flexure). However, the experimental data suggests that the ultimate strength of the connection is governed by the formation of a plastic mechanism wherein multiple limit states are activated. To overcome this conservatism, a method for characterizing the strength of base connections is proposed. The method incorporates several favorable features from existing approaches such as a method, outlined in the *Design Guide 1,* which assumes a rectangular shaped bearing stress distribution. However, the improved method proposes two key refinements, which include (1) incorporation of a mechanism-based approach for determination of the ultimate connection strength and (2) consideration of alternate yield line patterns and the ultimate strength of the plate material for determination of the bending capacity of the base plate. The resulting approach is shown to characterize the strength of the base connection with significantly improved accuracy, such that on average, the test-to-predicted ratio for connection strength is 0.99, with a coefficient of variation of 6%.

All the experimental specimens show outstanding ductility (deformation capacities in excess of 6% column drift) and hysteretic energy dissipation. Only two of seven specimens show catastrophic failure, due to fracture of one anchor rod. This suggests that under seismic loading conditions, reliable inelastic action is possible in the base connection.

The report concludes by presenting strategies for incorporating the findings of this study into design guidelines and outlining on-going and future work.

Acknowledgments

This project was funded by the American Institute of Steel Construction (AISC) and the National Science Foundation (Grant Number NSF-CMMI 0421492). Trans Bay Steel Corporation of Fairfield, California and PDM Steel Service Centers, Inc. of Stockton, California generously donated steel materials and fabrication for this research and their donations are gratefully acknowledged. The authors also thank Mr. Tom Schlafly and Mr. Kurt Gustafson of AISC and Mr. Rick Drake of Fluor Corporation who provided valuable advice and reviewed the testing plans. In addition, the research team is grateful to the AISC research committee for valuable feedback and comments. The large scale experiments described in this report were conducted at the Network for Earthquake Engineering Simulation (NEES) equipment site at the University of California at Berkeley in Richmond, California. The authors are grateful to the site staff (Don Clyde, Dr. Shakhzod Takhirov, Nathaniel Knight, David MacLam, Donald Patterson and Jose Robles) for assistance during all phases of planning and testing. The authors would like to thank Chris Smith of Stanford University for providing assistance with the test setup.

The findings and opinions developed in this report are those of the authors and do not necessarily represent those of the National Science Foundation (NSF), the American Institute of Steel Construction (AISC) or other sponsors.

Table of Contents

Appendices

List of Tables

List of Figures

List of Symbols

A_b	-	Unthreaded area of anchor bolt
$A_{footing}$	-	Concrete footing area
A_{plate}	-	Area of base plate
A_1	-	Bearing area
A_2	-	Maximum area of the portion of the supporting foundation that is geometrically similar to and concentric with the loaded area
a_1, a_2, a_3, a_4	-	Isotropic hardening parameters
B	-	Base plate width
b	-	Strain-hardening ration
b_e	-	Effective bending width of yield line
b_f	-	Flange width
C	-	Anchor rod compression force
$C.O.V.$	-	Coefficient of variation
d	-	Column depth
d_o, d_f	-	Measured original and necked diameter, respectively
E	-	Young's modulus
E_o	-	Initial elastic tangent
e	-	Load eccentricity (applied base moment over applied axial force)
e_{crit}	-	Critical eccentricity
e_{kern}	-	Kern of the base plate
F_u	-	Ultimate strength
$F_{u,plate}$	-	Measure ultimate strength of base plate material

$F_{u,rod}$	-	Measure ultimate strength of anchor rod
F_y	-	Yield Strength
$F_{y,plate}$	-	Measure yield strength of base plate material
$F_{y,rod}$	-	Measure yield strength of anchor rod
f , f_1 , and f_2	-	Bearing stresses
f_c' , f_g'	-	Compressive strength of concrete and grout, respectively
$f_c^{bearing}$	-	The design bearing strength of concrete
$f_g^{bearing}$	-	Bearing strength of grout
$f_{\max}$	-	Maximum bearing stress under the base plate
g	-	Edge distance of anchor rod
I_x	-	Strong axis second moment of area
k_{column}	-	Elastic stiffness of column
L	-	Distance between anchor rods
L	-	Lever arm distance (centerline of anchor rod to column flange corner) of the base plate in bending
L	-	Column cantilever length (bottom of base plate to location of applied lateral load)
M	-	Base moment
M_{base}	-	Applied base moment
M_{comp}	-	Bending moment (expressed as per-unit-width) across an assumed yield line on the compression side of the connection, produced by the bearing stresses acting upwards on the base plate
M_{tens}	-	Bending moment (expressed as per-unit-width) across an assumed yield line on the tension side of the connection, produced by the tensile forces from the anchor rods acting downwards on the base plate

$M_{pl,comp}$, $M_{pl,ten}$	-	The flexural demand on the compression side and tension side of the base plate, respectively
M_{base}^{comp} , M_{base}^{tens} , $M_{base}^{tens-inclined}$ and M_{base}^{rods}	-	The applied base moment corresponding to each of four failure mechanisms; base plate flexure on the compression side, base plate flexure on the tension side assuming straight yield lines, base plate flexure on the tension side assuming inclined yield lines, and anchor rod tension, respectively
m	-	Plate bending cantilever length
N	-	Base plate length
n	-	Number of anchor rods
P	-	Axial compressive load
P	-	Applied axial load
P_{test}	-	The force in the anchor rod at peak drifts of every loading cycle based on observed strain data (and the calibrated material model)
P_{TSB} , P_{RSB} and P_{LNT}	-	The force in the anchor rod calculated as per the TSB, RSB and LNT method, respectively
R_{plate}	-	Capacity of base plate in flexure
R_{rod}	-	Capacity of anchor rod in tension
T	-	Anchor rod tensile force
T_{rod}	-	Tensile force in both of anchor rods
$T_{u,bolt}$	-	Ultimate capacity of anchor rods
t_f	-	Thickness of the flange
t_p	-	Base plate thickness
Y	-	Bearing length

Z_x	-	Plastic section modulus
β	-	Elastic rotational stiffness the base connection.
ε	-	Average true fracture strain across necked cross section of tension coupon
ϕ	-	Diameter
ϕ	-	Resistance factor

Chapter 1

Introduction

1.1 INTRODUCTION

This report describes the second phase of large scale testing conducted as part of a comprehensive project whose main objective is to characterize the performance and behavior of column base plate connections under various loading conditions. The project was initiated in response to a request for proposal by the American Institute of Steel Construction (AISC RFP 6807, 2006). This report focuses on the behavior of exposed column base connections subjected to combinations of axial and flexural loading. A previously published companion report (Gomez *et al.*, 2009) addresses the response of column base connections subjected to combinations of axial and shear loading.

1.2 GENERAL

Observations of earthquake damage (Tremblay *et al.*, 1995) and previous experimental studies have indicated that exposed column base connections are susceptible to various failure modes, including weld fracture, base plate yielding, anchor rod fracture and concrete/grout crushing (e.g. see DeWolf & Sarisley, 1980; Astaneh-Asl & Bergsma, 1993; Fahmy *et al.*, 1999; Burda & Itani, 1999). Column base connections, used in virtually all types of steel structures, incorporate multiple components interacting under a variety of loading conditions. Despite these complexities, current guidelines for base connections, such as the *Steel Design Guide Series 1* (Fisher & Kloiber, 2006) published by the AISC, are based on assumptions that have not been thoroughly verified by experimental evidence. Moreover, standards for seismic design of base connections, such as recommendations featured in the AISC Seismic Provisions (2005), provide only qualitative guidance regarding the desired modes of the connection response, rather than approaches which quantitatively characterize the connection behavior. Several analytical studies have examined the response of column base connections, but lack sufficient experimental validation. Given this background, the main objective of the current study is

to conduct experiments on exposed column base connections and analyze the data to assess current strength design approaches and, where appropriate, propose revised guidelines.

Seven large scale experiments of exposed column base connections subjected to combined flexural and axial loading form the main scientific basis of this study. These tests are supported by analyses and ancillary material tests. The large scale tests were conducted at the Network for Earthquake Engineering Simulation (NEES) Structures Laboratory at the University of California at Berkeley in Richmond, California.

The large scale tests investigate the effect of various parameters on the base connection response, including the (1) axial load level, (2) base plate thickness, (3) anchor rod strength, (4) anchor rod layout and (5) loading history. All the experiments feature specimens that were fabricated and erected in accordance with standard construction practice and guidelines, including recommendations from the AISC *Steel Design Guide Series 1* (Fisher & Kloiber, 2006).

Chapter 2 presents a detailed review of literature relevant to this study, including a discussion of (1) current design standards (from both American and international codes), (2) previous experimental and analytical studies and (3) the specific objectives of the current study. Chapter 3 presents a detailed description of the large scale base connection tests, including a summary of the ancillary material tests. Included in Chapter 3 are data on load and deformation response and measured strains, as well as visual, photographic and video observations. Chapter 4 presents a detailed analysis of the data in the context of existing design approaches. In addition to detailed analysis of the test data, Chapter 4 proposes an improved design approach for the strength capacity of column base connections. The improved design approach considers observed test specimen response and a favorable combination and modification of features from previous analytical design methods. Chapter 5 summarizes the conclusions of the study and outlines future and ongoing work.

The report is supported by several appendices which document additional data and information in detail. Appendix A presents details of the materials used in the base connection specimen (i.e. anchor rods, base plate, concrete and grout) along with ancillary material tests. Appendix B archives an extended collection of experimental data (i.e. load and displacement histories) recorded from all seven base connection tests. Appendix C reports anchor rod force data determined from a calibrated plastic material model which uses recorded strain data. Appendix D presents the mathematical formulation for the design approaches featured in the report and Appendix E presents a computer program based on this formulation. Appendix F briefly summarizes a list of past experimental programs investigating exposed base connections subjected to flexure.

This research project, being supported by the NEES initiative, requires the dissemination and archival of experimental data through the NEES Central Data Repository. Thus, data from all the experiments, including photographic and video records, may be obtained at http://central.nees.org (Experiment ID: 1195).

Chapter 2

Background and Objectives

2.1 INTRODUCTION

This chapter presents a review of literature relevant to exposed column base connections and provides background for the current investigation. Specifically, the literature review focuses on experimental and analytical investigation of the flexural response of exposed steel column base plate connections. For a similar review of literature on shear transfer mechanisms in column base plate connections, refer to the companion report by Gomez *et al.* (2009). The chapter begins by summarizing current strategies used in the United States and abroad for the design of exposed column base connections subjected to combinations of flexural and axial load. Next, test observations are outlined from past experimental and analytical investigations from around the world. The chapter concludes by describing the objectives of the current study in the context of professional and research needs. To complement the literature review, Appendix F presents a brief summary of experimental programs conducted worldwide featuring exposed base connection prototypes under flexural loading.

For further information, comprehensive literature reviews on the topic of column base connections are included in the first edition of the AISC *Steel Design Guide 1* (DeWolf & Ricker, 1990) as well as a synthesis report sponsored by the AISC (Grauvilardell *et al.*, 2005). The synthesis report summarizes conclusions regarding the behavior of several configurations of column bases from a number of experimental and analytical studies. In addition, the synthesis report presents a comprehensive description of key unresolved academic and practical issues regarding base connection behavior. This study aims to address some of these unresolved issues.

2.2 CURRENT DESIGN PROVISIONS AND DESIGN GUIDES

Column base connections may be broadly categorized as those that are designed for quasi-static gravity and wind loads and those that are designed to withstand seismic loads under which inelastic cyclic deformations are expected. For static loading, the main objective of the design process is to ensure that the critical load combinations can be sustained by the base connection without failure of any of the connection components (i.e. the base plate, the anchor rods, or the concrete/grout footing). In these cases, the design is based on conventional strength checks, wherein the design strength of the various components (e.g. the base plate or anchor rods) are checked against the corresponding required strengths in those components (e.g. bending in the base plate or axial tension in the anchor rods). The majority of research and current design provisions for column base connections address the load capacity and demand of these components.

In the case of seismically designed base connections, inelastic cyclic loading of the column base is expected and should be accounted for in design, especially in steel moment resisting frames. Thus, in addition to strength, the deformation capacity of the various connection components is important. Given the complexity of inelastic cyclic loading and the interaction of multiple mechanisms, the design provisions for seismically designed column base connections are not as developed as those designed for quasi-static loads.

Sections 2.2.1 through 2.2.3 reviews current design approaches for the strength column base connections exposed to axial and flexural quasi-static loading. Design provisions for seismic loading, which rely on these basic strength characterization approaches, are discussed subsequently in Section 2.2.4.

2.2.1 Design Approaches for Column Base Connections under Combined Axial Load and Flexure – United States

Current approaches for the design of column base connections in the United States are typically based on recommendations of the AISC *Steel Design Guide Series 1 – Column Base Plates* (Fisher & Kloiber, 2006), which is referenced by the current (13^{th}) edition of

the Steel Construction Manual (AISC, 2005) for column base design. In addition, the AISC *Steel Design Guide Series 10 – Erection Bracing of Low-Rise Structural Steel Buildings* (Fisher & West, 2003) provides further information relevant to column base design and construction. This section reviews both the *Design Guide 1* and the *Design Guide 10* in the context of the design for flexural loading. Two strength prediction approaches for flexural loading featured in the *Design Guide 1*, the elastic and ultimate method, are first summarized.

2.2.1.1 The Ultimate and Elastic Design Approach

As illustrated in Figure 2.1, the underlying assumption for the design of column bases subjected to flexural loading is that the axial force and moment applied to the base connection are resisted by either bearing stresses in the concrete/grout (for low load eccentricities[1]) or by a combination of bearing in the concrete/grout and tension in one row of anchor rods (for large load eccentricities). A key component of strength prediction for base connections is the accurate characterization of the bearing stresses imposed on the concrete/grout by the base plate, from which the anchor rod forces are derived through static equilibrium. Crushing of the concrete/grout is precluded in current design methods by selecting a large enough base plate area to limit the maximum bearing stress to the crushing strength of the concrete/grout. Once the bearing stress distribution is characterized, the base connection is assumed to fail when one of three failure modes occurs: (1) the base plate reaches its capacity in bending due to bearing stresses from the concrete/grout, (2) the anchor rods reach their axial tensile capacity due to uplift of the base plate, or (3) the base plate reaches its capacity in bending due to tensile forces in the anchor rods. Schematic illustrations of these three failure modes are illustrated in Figure 2.2. The reader is referred to several structural steel textbooks for the theoretical background of these approaches (i.e. Blodgett, 1966; McGuire, 1968; Gaylord & Gaylord, 1972; Salmon & Johnson, 1980; Ballio & Mazzolani, 1983).

The elastic approach, featured in the first edition of the *Design Guide 1* (DeWolf & Ricker, 1990) and listed in the Appendix of the second edition of the *Design Guide 1*

[1]Eccentricity is defined as the ratio of the applied moment to the applied axial force

(Fisher & Kloiber, 2006) assumes a triangular/trapezoidal (i.e. linear) bearing stress distribution at the interface between the steel base plate and the supporting concrete/grout. In contrast, the ultimate approach, featured only in the second edition of the *Design Guide 1*, assumes a rectangular (i.e. constant) bearing stress distribution. The ultimate strength design method was recently proposed by Drake and Elkin (1999) to correspond with Load and Resistance Factor Design (LFRD) methodology. The procedure was later modified by Doyle and Fisher (2005) by redefining the critical eccentricity, of which characterizes "small" and "large" moment conditions. For "small" moment conditions, the applied moment is resisted only by bearing on the concrete/grout base. For "large" moment conditions, the applied moment is resisted by a combination of anchor rod tension and bearing. The methodology and formulation of the design procedures, outlined in Appendix D, provide equations of the critical eccentricity and definitions of "small" and "large" moment conditions.

As noted by Soifer (1966), base connection design is analogous to the design of a reinforced concrete section under combined axial load and bending. The anchor bolts under tension are analogous to reinforcing bars and bearing between the base plate and the supporting concrete/grout is analogous to compression in a concrete beam.

In addition to the elastic and ultimate design approaches, which assume triangular and rectangular bearing stress distributions, respectively, several other studies have developed additional models to characterize the bearing stress distribution within base connections (e.g. Fling, 1970; Stockwell, 1975; Thornton, 1990a & 1990b; Hogan & Thomas, 1994; Ranzi & Kneen, 2002; Cowie *et al.*, 2004).

2.2.1.2 Steel Design Guide Series One, 1st Edition (DeWolf & Ricker, 1990)

In 1990, the American Institute of Steel Construction (AISC) released a report by DeWolf & Ricker (1990) which presented a compilation of existing information on the design of steel column base connections. This report, part of the AISC *Steel Design Guide Series One – Column Base Plate*, outlines methods for base connection design, including bases subjected to axial compression, flexure and shear. The elastic method

(i.e. the triangular stress block approach) is recommended for flexural design. However, the *Design Guide* mentions the lack of experimental data investigating base connections subjected to axial load and moment.

2.2.1.3 Steel Design Guide Series One, 2nd Edition (Fisher & Kloiber, 2006)

The second edition of the AISC base connection design guide (Fisher & Kloiber, 2006) develops the first edition design guide by incorporating new research on column base connections and a new Occupational Safety and Health Administration (OSHA) regulation (under the *Safety Standards for Steel Erection)* requiring a minimum of four anchor rods for most base plate connections (OSHA, 2001). The axial-flexural strength design of base connections is based on the ultimate method proposed by Drake and Elkin (1999), which assumes a rectangular bearing stress distribution. The elastic method (which assumes a triangular stress distribution) is featured in the appendix of the *Design Guide 1*. In addition, the AISC *Steel Design Guide Series Seven – Industrial Buildings – Roofs to Anchor Rods* (Fisher, 2005) features many topics regarding base connection design, many of which are repeated in the second edition of the *Design Guide 1*, including design equations and design examples for column anchorage.

2.2.1.4 Steel Design Guide Series 10 (Fisher & West, 1997)

The AISC *Steel Design Guide Series 10 - Erection Bracing of Low-Rise Structural Steel Buildings* (Fisher & West, 1997) provides information and examples to aid the design of temporary lateral support systems and components for low-rise buildings. A summary of column erection procedures, as well as column base design methods, are presented. The *Design Guide 10* indicates that steel frames are under the highest risk of collapse in their lifetime during construction when the first series of columns are erected. The *Design Guide 10* evaluates an extensive set of failure modes for overturning moments but does not present capacity equations. Instead, the *Design Guide 10* provides a general overview of several possible failure modes, including: (1) fracture of the welds connecting the column to the base plate, (2) bending failure of the base plate, (3) tension fracture of the anchor rods, (4) buckling of the anchor rods, (5) anchor rod nuts pulling or pushing through the base plate hole (6) anchor rod pull out from the concrete footing (7) anchor

rod straightening within the concrete footing (for rods with embedded hook bends), (8) anchor rod push out through the bottom of the footing (for anchor rods with leveling nuts), (9) concrete foundation crushing or spalling damage, (10) pier foundation bending failure and (11) concrete footing overturning within the soil. The *Design Guide 10* also discusses the behavior of base connections with shim stack and leveling nut erection procedure details.

Based on results of finite element analyses, the *Design Guide 10* presents guidelines and design equations for inclined yield lines for base plate bending which are not addressed in other design guides (see Fig. 2.4). A literature review by the authors of the *Design Guide 10* did not reveal any existing published procedures to determine the base plate thickness or weld design strength for base plates subjected to this type of yield line pattern.

2.2.2 Design Approaches for Column Base Connections under Combined Axial Load and Tension – European Union

Column base design provisions adopted by the European Union are published in the EuroCode 3 - *Design of Steel Structures* (CEN, 1992). Similar to the AISC *Steel Design Guide 1*, the EuroCode 3 provisions do not explicitly address seismic loading conditions, but rather focus on strength based design. The standard European design method for predicting base connection behavior, such as strength and rotational stiffness, is based on the component approach, in which the connection is modeled as an assembly of individual components (Wald *et al.*, 2008). Components considered in the base connection include (1) bending in the base plate, (2) compression in the concrete/grout, (3) compression in the column flange and web and (4) shear and tension in the anchor rods. In addition, the concrete bearing stress distribution is assumed constant and is not allowed exceed the design bearing strength.

2.2.3 Other Design Guides

A technical manual, prepared for the structural software company RISA Technologies (Horn, 2004), deals with the design of monopole bases and may be adapted to the general design of any column base connections. Monopoles are used extensively in the

telecommunication and transportation industry and are typically exposed to flexural loads due to wind under low axial loads. The manual addresses topics including: (1) an historical perspective of base connection design, including the AISC approach, (2) classical methods for determining bolt forces and concrete stresses for grouted or ungrouted base plates and (3) an evaluation of various methods currently being used to determine base plate bending stresses for plain and stiffened base plates. The manual states that while some state highway departments (e.g. New York) have developed their own design methods, no national industry standard for the design of monopole base plates is available. The manual points out that experimental evidence on base connections is limited and, based on finite element studies, current design practices used by monopole manufacturers may lead to unconservative design. Nevertheless, the manual provides many design procedures, including methods for determining base plate bending stresses, which may be used for column base design.

A report released by the Australian Steel Institute (Ranzi & Kneen, 2002) addresses the design (i.e. strength characterization) of "pinned" base connections. Axial compression, axial tension and shear force loading conditions are examined. However, no design provisions for flexural loading were presented. Nevertheless, an extensive literature review is outlined which discusses numerous approaches for characterizing the bearing stress distribution between the base plate and the supporting grout/concrete as well as the formation of yield lines in the base plate.

2.2.4 Design of Base Plate Connections under Seismic Loads

Column base connections are critical components in structures designed for seismic loading. For many seismically designed structural systems (such as Special Moment Resisting Frames), significant inelastic action (i.e. plastic hinging) is expected in the column base region, either near bottom of the column or within the base connection. Thus, the design of column bases in earthquake resistant structures presents several issues for which more research is needed, including (1) characterization of force and deformation demands in the base connection, (2) characterization of failure mechanisms and deformation capacities of the various connection components, (3) development of

desirable hierarchies of yielding/failure of the base plate connection and (4) utilization of available strength estimates (i.e. from the various sources outlined in the preceding sections) for a capacity based design.

This section outlines two published documents which address the seismic design of column base connections in the United States. However, as outlined below, these guidelines are predominantly qualitative, and thus provide motivation for experimental study.

2.2.4.1 Seismic Provisions for Structural Steel Buildings (AISC, 2005)

The AISC Seismic Provisions (2005) outline requirements for the flexural strength of column bases subjected to seismic loading. The Provisions require that column bases have adequate strength to permit the desired ductile behavior of the supported structure. Three classifications of exposed base connections are discussed for Special Moment Resisting Frames (SMRFs): (1) a rigid base connection in which yielding occurs in the column, (2) a pinned base connection which does not require moment resistance and (3) a partial fixity connection in which inelastic action is shared by both the column and the base connection, either through bending of base plate or yielding of anchor rods. The Seismic Provisions advises that column base connection design is similar to that of beam-to-column connections but mentions the possibility of foundation rocking and rotation, especially for isolated column footings. However, the Seismic Provisions do not offer any quantitative guidelines or methods by which to achieve the various behavioral modes discussed in the document. Moreover, the Provisions note that seismic design guidelines for base connections have not been well developed mainly due to a limited number of analytical and experimental studies on full-scale specimens. The Provisions emphasize that substantial research work is needed in order to better understand column base behavior under seismic loading and to develop improved design procedures.

2.2.4.2 Recommended Seismic Design Criteria for New Steel Moment-Frame Buildings (FEMA 350, 2000)

The Federal Emergency Management Agency (FEMA) Recommended Seismic Design Criteria for New Steel Moment-Frame Buildings (FEMA 350, 2000) classifies exposed column base connections into three different categories: (1) a pinned base with large columns at the bottom level of a structure to limit interstory drift, (2) a connection which provides partial fixity such that the base itself yields before the column hinges and (3) a heavy base connection assembly strong enough to force yielding in the column. Similar to the AISC Seismic Provisions, the FEMA document recommends that the designer should consider the base connection as analogous to a beam-to-column connection and apply similar principles of design and detailing. Several key distinctions between the design of base connections and beam-to-column connections are outlined. In addition, structural performance levels and acceptance criteria of limiting damage states for base connections are discussed. For example, no observable damage or distortion in the base connection is acceptable for immediate occupancy of the structure.

2.2.5 Initial Stiffness Characterization

Simulation of the initial stiffness, as well as the hysteretic response of the base connection, is important in the context of frame analysis. While a base connection will exhibit partial fixity behavior in general, it is typically modeled as either completely fixed or pinned. Simulating the connection as pinned may result in large drift estimates in the first story of a structure, thereby requiring the use of larger (heavier) structural members. On the other hand, if the connection is modeled as fixed, it should be designed to minimize base rotations through the use of additional/larger anchor rods or a thicker/stiffened base plate. The accurate simulation of the moment-rotation behavior of a base connection is important for the accurate modeling and design of an entire structure.

Picard *et al.* (1987) presents the results of an experimental investigation on the behavior of steel column base connections to determine the initial stiffness of the column base. The flexural stiffness about both principal axes of a base connection was studied. Picard *et al.* argues that while these connections are generally considered “pinned”, modeling

the actual rotational stiffness has a beneficial effect on column stability and frame behavior. Melchers (1992) presents a simple mathematical model, which considers the contributions of anchor rod extension and base plate deformation, for the prediction of the elastic stiffness of base connections. The model is based on experimental evidence and considers both two-bolt and four-bolt base assemblies. Wald and Jaspart (1998) discuss the influence of column base rotational characteristics and derive specific design criteria for the stiffness classification of semi-rigid and rigid joints. Wald *et al.* (1995) proposed an analytical model, based on the component method featured in the EuroCode 3 (CEN, 1992), to determine the moment resistance and the rotational stiffness of column bases under axial and flexural forces. A parametric study of the base plate thickness and the anchor bolt length is also presented.

2.3 PREVIOUS ANALYTICAL STUDIES

Several analytical studies have been conducted on base plate connections, including both conventional mechanical modeling as well as finite element method (FEM) computer simulation. This section briefly describes key analytical investigations on column bases subjected to flexure. The reader is referred to the base plate research synthesis (Grauvilardell *et al.*, 2005) for a detailed assessment of various analytical studies.

DeWolf (1982) published experimental data (refer to Appendix F for details of this experimental study and other) and proposed design methods for column base plates under axial compression as well as flexural moment with or without axial compression. The paper presented two types of design procedures (the ultimate method and the elastic method, see Section 2.2.1.1) adapted from structural engineering textbooks (McGuire, 1968; Gaylord & Gaylord, 1972). DeWolf argued that the procedure assuming ultimate strength considerations (i.e. the ultimate method which assumes a rectangular bearing stress distribution) is the preferred approach since it more closely reflects experimental data. Based on tests data, very thick base plates were shown to reduce the connection capacity due to excessive bearing on the grout/concrete, resulting in crushing damage. Furthermore, it was suggested that designing anchor rods to remain elastic may be unnecessarily costly.

Numerous analytical studies were carried out by researchers in Greece, including the development of a design procedure for the derivation of base connection moment-rotation curves (Ermopoulos & Stamatopoulos, 1996a). Additional studies include (1) a closed-form analytical model for the determination of the response of exposed column bases under cyclic loading (Ermopoulos & Stamatopoulos, 1996b), (2) an analytical model that describes the non-linear bearing stress distribution under the base plate (Ermopoulos & Michaltsos, 1998) and (3) a simulation of the dynamic behavior of column base connections (Michaltsos & Ermopoulos, 2001). Another analytical evaluation of the bearing stress distribution under the base plate, acted upon by axial forces and flexure, is presented by Sophianopoulos *et al.* (2005). In addition, Stamatopoulos & Ermopoulos (1997) developed moment-axial interaction curves for the ultimate behavior of column base connections. The proposed methodology is based on the consideration of three failure modes according the level of applied loading. In addition, the rotational stiffness of the base connection was formulated.

Ohi *et al.* (1982) provided an extensive mathematical treatment for the ultimate strength of steel column bases using upper and lower bound theorems of plasticity and Sato (1987) presented ultimate strength models for rigid column bases. In addition, Sato proposed a model for the rotational stiffness of rigid base connections. The models were compared to experimental data and their application on the response of an entire structure was evaluated. Tamai and Kanazawa (2001) provided a numerical model for the inelastic behavior of exposed column bases under axial force and flexure.

All the analytical studies discussed above assume the formation of straight yield lines in the base plate, which form parallel to the column flange due to tensile forces of the anchor rods (see Figure 2.3). However, as observed in the present study and discussed later in detail in Chapter 3, more complicated yield line patterns may develop. Targowski *et al.* (1993) studied base plate column connections under bending which exhibited complex yield lines, and a special minimization procedure was used to predict the base connection peak strength. In addition, as mentioned before, the AISC *Steel Design Guide*

Series 10 (Fisher & West, 2003) addresses inclined yield lines based on FEM simulations.

Wald *et al.* (1995) developed a method for predicting the stiffness of steel column bases consistent with the component method (explained in Section 2.2.2) for beam-to-column connections in accordance with the EuroCode 3 Annex J (CEN, 1992). In this method, the rotational stiffness is determined by evaluating the stiffness coefficients of the multiple components of the base connection. In addition, a parametric study of the base plate thickness and the anchor bolt length is presented. Jaspart and Vandegans (1998) also presented an application of the component method for column bases to predict the moment-rotation response.

Fahmy (2000) studied the seismic behavior of moment resisting steel column bases. In addition to an extensive literature review, description of experimental results and analytical (FEM) simulations, the report presents a comprehensive formulation for base connection design. Multiple failure modes were explored and categorized into two classifications, non-dissipative and dissipative mechanisms. Non-dissipative mechanisms do not provide stable energy dissipation and are triggered by brittle failure modes (e.g. premature fracture of the welds or anchor rods). Base connections categorized as dissipative mechanisms, suitable for seismic design, are classified into three main groups: (1) a strong-column weak-base connection in which yielding occurs in one or more components of the base connection, (2) a weak-column strong-base connection in which plastic hinging occurs only in the column and (3) a balanced mechanism connection in which yielding of the base connection and column occurs simultaneous. These three behavior classifications are characterized by a plastic moment ratio between the column plastic moment and the sum of the moment capacities of the base connection components. This connection strength parameter, defined from a plastic analysis of the column base connection, is derived to help designers choose a desired failure mode of the base connection. The reader is referred to Fahmy (2000) for a derivation and analysis of this connection strength parameter.

2.4 PREVIOUS EXPERIMENTAL STUDIES

Based on an extensive literature search, 39 past experimental programs on column bases were reviewed and are summarized in Appendix F. The reader is referred to a synthesis report of base connection research (Grauvilardell *et al.*, 2005) for a comprehensive evaluation of several of these test programs. This section outlines previous experimental studies which use test prototypes constructed under current standards or which may be compared with the results of the current study. Many previous test programs were conducted outside of the United States (including Japan, Europe, Australia and Canada) and may not be directly comparable to structural details in the United States since different materials, geometries and construction practices were employed. Thus, only 13 of the 39 test programs were identified as using experimental prototypes similar to current base connection details in the United States; 236 specimens from these 13 test programs were tested under moment (both cyclical and monotonic) with or without axial loads. The main parameters of all published tests include base plate dimensions, column type and anchor rod size and layout.

A significant number of the 236 relevant base connection tests (90 specimens) were conducted as part of an investigation by the Tennessee Valley Authority. The specimens were loaded monotonically under flexural or shear with compression to examine the effects of base plate flexibility and preloading of the anchors on the distribution of anchor loads under varying loading conditions. Cook and Klingner (1992) and Cannon (1992) issued publications based on these 90 tests to investigate ductile, multiple-anchor, steel to concrete connections. Based on the experimental results, behavioral models for anchorage design were formulated and design guidelines were developed. Zhang *et al.* (2001) performed 17 tests investigating the seismic response of multiple-anchor steel base to concrete connections. Observations indicated that anchors in cracked concrete would most likely behave in a ductile manner under seismic loading. These two test programs focused on the behavior of bolts or studs embedded in concrete in the context of concrete anchorage design, rather than column base connection design (e.g. grout between the base plate and concrete was not included, a typically standard detail for column bases).

Test programs in the United States which examined column base connections representative of current details include Burda and Itani (1999), Lee and Goel (2001) and Astaneh *et al.* (1992). Burda and Itani (1999) investigated six specimens under cyclic moment plus axial compression. The report by Burda and Itani presents experimental results and analyzes on the effect of base plate flexibility on the overall seismic response and behavior of steel moment frames. Both experimental and analytical (FEM) investigations were carried out to determine the cyclic behavior of column base plate assemblies under large deformations. In addition, analytical investigations were carried out to study the response of steel frames with several different base connection configurations. The investigations showed that base connections with thinner base plates result in greater ductility than connections with thicker base plates and, from frame analyses, certain structures designed as pinned bases may require as much as 50% more steel than structures designed with fixed bases.

Lee and Goel (2001) tested column base connections subjected to weak-axis bending. Four specimens were tested under cyclic deformations, including two specimens with a four anchor rod configuration and two with a six rod configuration. Lee *et al.* (2002) conducted a numerical (FEM) parametric study based on the experimental data. The parametric study revealed that the use of thick base plates should be avoided to prevent grout crushing. In addition, the study showed that a minimum base plate thickness should be provided to avoid high stresses in the anchor bolts. Furthermore, the study revealed that base plates designed by the Drake and Elkin Method (i.e. the ultimate/rectangular method featured in the AISC *Design Guide 1* (Fisher & Kloiber, 2006) and explained in Section 2.2.1.1) did not behave as intended. Based on analytical results, the effects of a relative strength ratio among the connection elements (e.g. column, base plate and anchor rods) on the seismic connection behavior were investigated. The desired connection behavior at the ultimate state was proposed with intent to maximize the connection ductility under seismic loading conditions. Suggested values for the strength ratio between the anchor rods and column are given as well as a revised value of the resistance factor for the base plate flexural strength.

Astaneh *et al.* (1992) studied six specimens tested under cyclic flexural deformations with constant axial compression. The tests indicate that base connections with greater axial compressive load showed a greater moment capacity. In contrast, the energy dissipation and ductility was greater for base plates with lighter axial loads. All specimens sustained 0.02 radian rotations without excessive yielding or fracture of the base connection components. Beyond the elastic limit of the connection (about 0.01 radian rotation) the hysteretic strength was stable and exhibited little deterioration. In the context of seismic design, it was proposed that the governing failure mode should be plastic hinging at base end of the column or yielding of the base plate in bending. It was recommended that the anchor rod be designed to sustain little or no yielding to prevent rod fracture.

2.5 OBJECTIVES OF CURRENT RESEARCH

As discussed in the preceding sections, several topics regarding flexural behavior of exposed base connections are unresolved and may be addressed through further experimentation and analysis. Thus, the specific objectives of the current study discussed in this report are to –

1. Synthesize experimental data and assess existing design approaches based on their ability to characterize the base connection strength and their ability to accurately reflect the observed failure and deformation modes.
2. Propose refined strength prediction methods which overcome the limitations of the existing models and consider:
   - Interactions of all mechanisms in the base plate assembly, rather than the consideration of failure of only one component.
   - Inclined yield line patterns for base plate bending, which, in certain situations, may be more consistent with actual behavior than the formation yield lines parallel to the column flange assumed in current design.
3. Determine the strength, ductility and hierarchy of failure modes associated with the base connection components. In addition, address failure mechanisms that were not investigated experimentally.
4. Assess the effect of cyclic degradation on available strength.

In addition to the specific objectives discussed in this report, other aspects of the study are ongoing, including (1) the development of finite element models to generalize results of the experimental study, (2) the development of methods to characterize initial stiffness of the connections, (3) the development of suitable cyclic moment-rotation hinge models for computer modeling of base connections and their effect on frame behavior subjected in nonlinear time-histories and (4) the characterization of force and deformation demands in base connections due seismic loading or inelastic behavior.

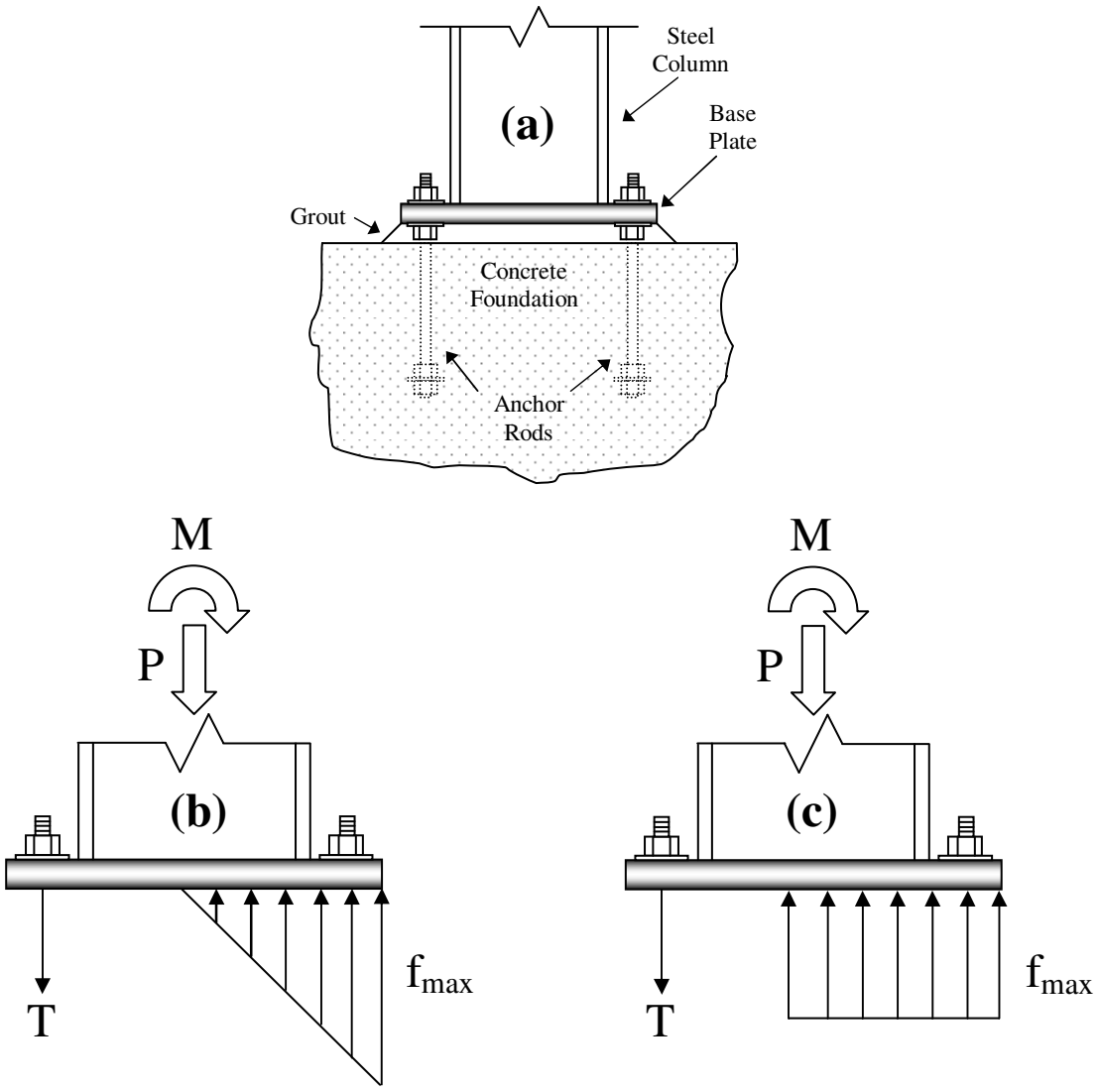

Figure 2.1 – (a) Schematic of a typical exposed column base connection with free body diagrams of (b) the elastic design method and (c) the ultimate design method

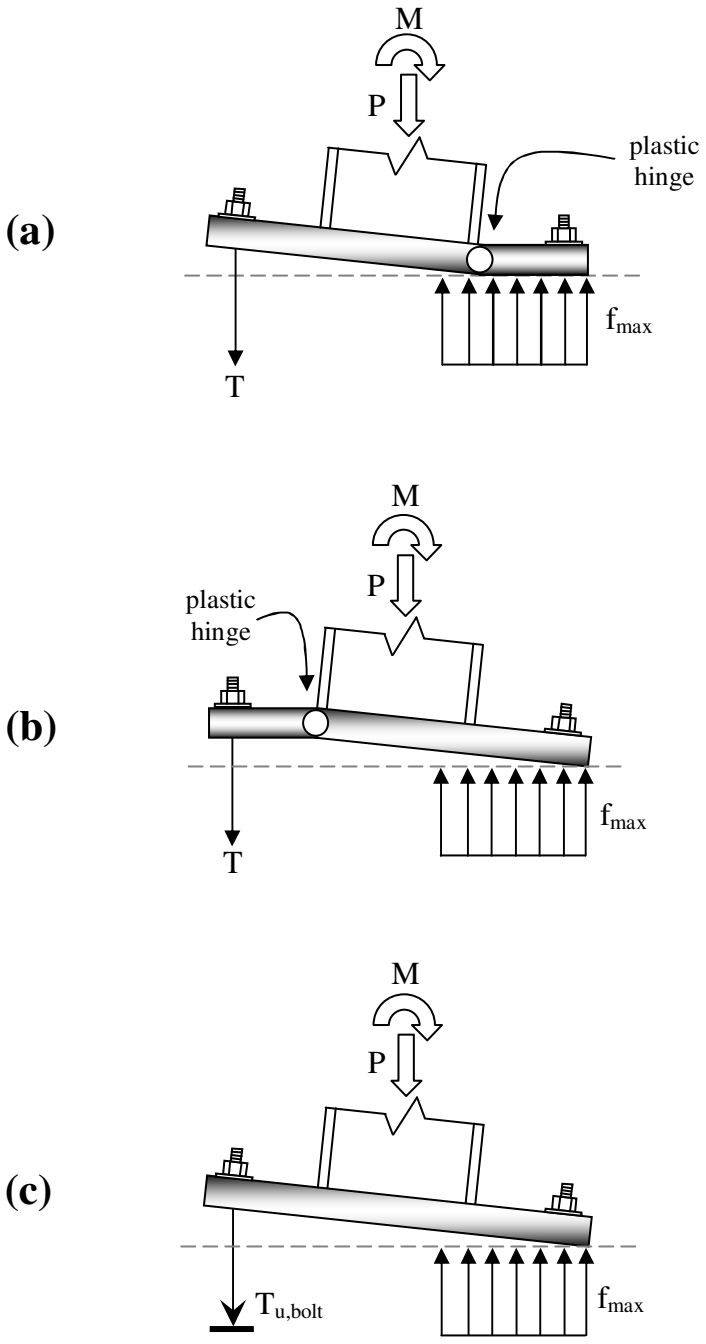

Figure 2.2 – Schematics of the three typical flexural failure modes assumed for base connections – (a) plate bending capacity on the compression side, (b) plate bending capacity on the tension side, and (c) anchor rod tensile capacity

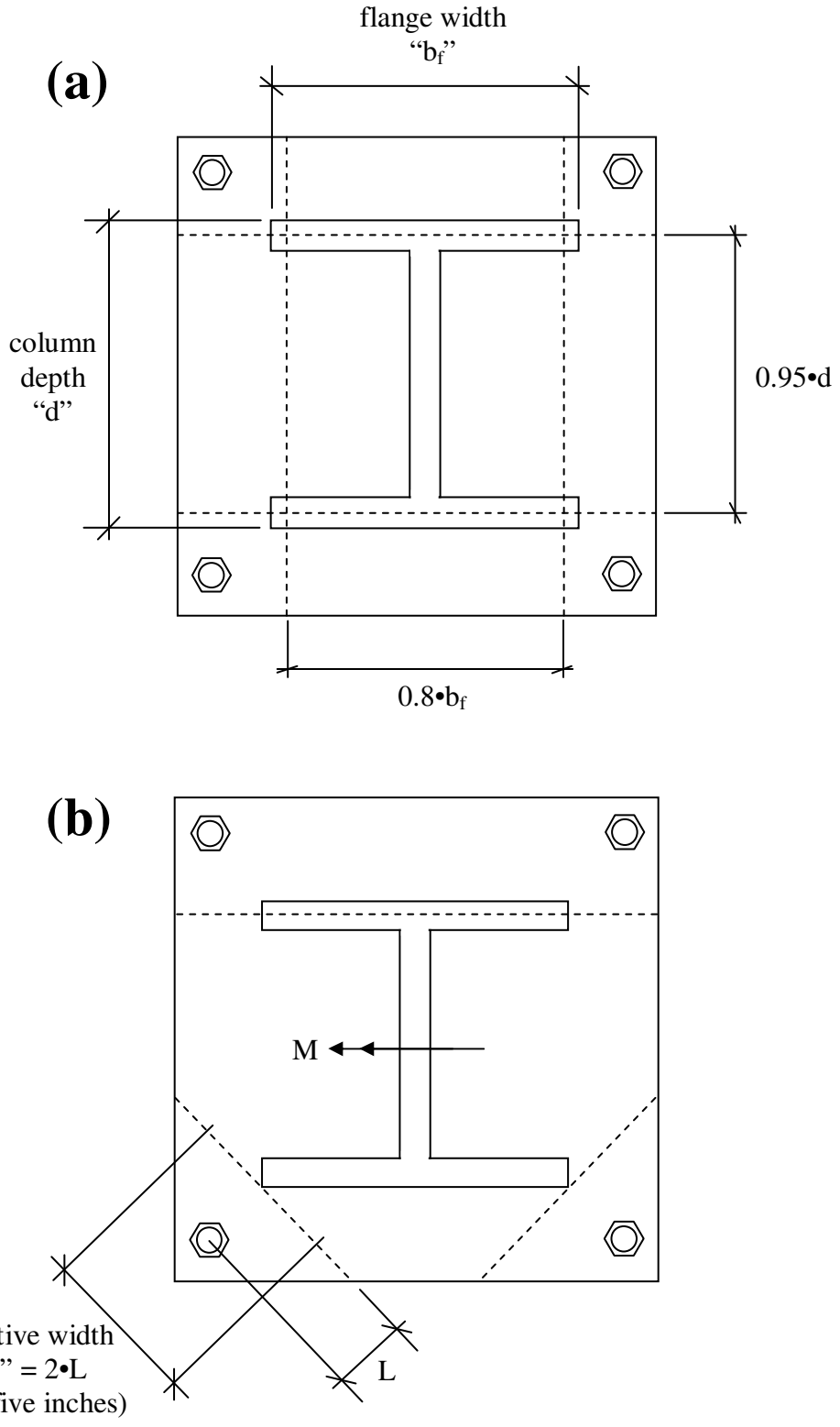

Figure 2.3 – Assumed base plate bending lines (a) from conventional design approaches (e.g. AISC *Design Guide 1*) and (b) for outset anchor rods (e.g. *Design Guide 10*)

Chapter 3

Experimental Program and Test Results

3.1 INTRODUCTION

This chapter presents results and observations from seven large scale experiments of exposed column base connections subjected to flexural and axial compression loading. The main experimental parameters investigated include base plate thickness, level of applied axial load, anchor rod grade, number of anchor rods, and lateral loading protocol (i.e. monotonic or cyclic). The base connection detail investigated for six of the seven tests, shown schematically in Figure 3.1, represents typical construction practice of exposed column base connections in the United States. Data on these experiments, along with ancillary data characterizing the materials used in the test specimens provide the basis to evaluate design guidelines and capacity predictions, such as those presented in the AISC *Steel Design Guide Series 1* (Fisher & Kloiber, 2006). A detailed assessment of current design procedures, along with a critical analysis of the test data, is provided in Chapter 4. This chapter describes the experimental program in detail, including an overview of the large scale test setup, testing procedures, test results and experimental observations. To complement the key data and representative response plots presented in this chapter, detailed test data for all experiments is provided in Appendix B. This chapter also presents a summary of the ancillary tests, including anchor rod tension tests, tension tests on coupons extracted from the base plate material, standard concrete cylinder compression tests and grout cylinder compression tests. Further results of the ancillary tests are provided Appendix A.

3.2 ANCILLARY TESTS

Four types of ancillary tests were conducted to characterize mechanical properties of the materials used in the column base connection specimens. These include (1) anchor rod tension tests, (2) tension tests on coupons extracted from the base plate material, (3) standard concrete cylinder compression tests, and (4) grout cylinder compression tests.

Tables 3.1-3.4 summarize key results obtained from the ancillary tests, further details of which are reported in Appendix A.

3.2.1 Anchor Rod Tension Tests

Tension tests were conducted on samples taken from the same batch of anchor rods used for the base connection tests. All anchor rods were 3/4" in diameter and were either ASTM F1554 Grade 36 ksi or Grade 105 ksi material. Four unthreaded rod specimens (two for each rod grade) were tested quasi-statically under monotonic tension (as per ASTM A370, 2007) to determine the anchor rod stress-strain properties. Two uniaxial strain gages were attached to the rods to identify initial yielding behavior. As summarized in Table 3.1, the mean ultimate strength $F_{u,rod}$ is 71.3 ksi for the Grade 36 rod and 146.5 ksi for the Grade 105 rod. These values are within the ASTM specified ultimate strength range of 58-80 ksi for Grade 36 anchor rod material and 125-150 ksi for Grade 105 anchor rod material (AISC, 2005). The average yield strength $F_{y,rod}$ (as determined by the 0.2% offset method) is 48.6 ksi for the Grade 36 rod and 114.0 ksi for the Grade 105 rod. The yield strength of the Grade 36 rod is approximately 35% greater than the minimum specified strength of 36 ksi, and the yield strength of the Grade 105 rod is approximately 8.6% greater than the minimum specified strength of 105 ksi. Ductility is characterized in terms of the ratio of the pre- to post- fracture cross section diameter. The Grade 36 rod material is approximately 40% more ductile than the Grade 105 rod material.

Note that the material properties of the anchor rods were sampled from the unthreaded region of the rod. As explained in a subsequent section, the anchor rods used in the base plate tests included threads which extended above the surface of the concrete; therefore, most of the plastic deformation (and fracture in some instances) during the large scale tests occurred in the rod threaded region. According to Table 7-18 in the AISC Steel Construction Manual (AISC, 2005), the minimum root diameter for a standard 3/4" anchor rod is 0.642". Thus, the net tensile area is 73.3% of the gross bolt area (often approximated as 75%).

3.2.2 Tension Tests on Coupons Extracted From the Base Plate Material

Tension tests were conducted on steel coupons extracted from the base plates used in the base connection tests. These included plates of 1.0", 1.5", and 2.0" thickness, all of ASTM A36 Grade 36 ksi material. Six reduced scale tension coupons (two for each plate thickness) were tested quasi-statically under monotonic tension (as per ASTM A370, 2007) to determine the base plate material stress-strain properties. An extensometer was attached to the 0.357" diameter tension coupons to measure displacement behavior. As summarized in Table 3.2, the mean ultimate strength $F_{u,plate}$ is 68.7 ksi for the 1.0" thick plate, 67.9 ksi for the 1.5" thick plate, and 72.1 ksi for the 2.0" thick plate. These values are within the ASTM specified ultimate strength range of 58-80 ksi for Grade 36 plate material (AISC, 2005). The average yield strength $F_{y,plate}$ (as determined by the 0.2% offset method) is 40.4 ksi for the 1.0" thick plate, 37.0 ksi for the 1.5" thick plate, and 38.4 ksi for the 2.0" thick plate. On average, the yield strength is approximately 7% greater than the minimum specified strength of 36 ksi for all plate thicknesses.

3.2.3 Standard Concrete Test Cylinders

Seven concrete footings were cast for the large scale tests using commercial ready-mixed concrete specified with a 3,000 psi twenty-eight day compressive strength and 3.0" slump. The concrete was delivered in one truck and the slump was measured on-site as 2.5". At the time of testing, all concrete pedestal specimens were air cured beyond 28 days (i.e. between 1-4 months), since the testing itself extended over a period of 12 weeks. For this reason, a total of 17 concrete compression test cylinder specimens were collected from the concrete truck (as per ASTM C31, 2008) and tested (as per ASTM C39, 2005) at three different curing ages (32, 73, and 131 days). At 32 days, the concrete compressive strength was measured as 3,860 psi (standard deviation = 144 psi). Although the concrete cylinders were not tested after exactly 28 days, this 32-day measured strength is the closest to the 28-day compressive strength of the test cylinders. The 32-day strength is 29% greater than the specified 28-day strength (3,000 psi). The average ultimate compressive strength of test cylinders tested at the conclusion of the test program (tested at 131 days of curing) was 4,440 psi (standard deviation = 233 psi), about 48% greater than specified at 28 days (3,000 psi). The average ultimate

compressive strength of the concrete cylinders is shown in Table 3.3, along with other information such as concrete density. The concrete strength at different curing ages is plotted in Figure 3.2. Also shown in the Figure is the cure age and corresponding strength of the concrete used in the base connection experiments on the day of testing, as well as the standard deviation of the cylinder test strength (shown as error bars on the plot). Detailed information regarding the concrete compression tests, including the concrete mix design, is in Appendix A.

3.2.4 Grout Test Cylinders

General construction, mineral-aggregate, non-shrink grout was installed between the steel base plate and concrete pedestal for all large scale tests. The approximate grout pad thickness was 2" for all base plate tests and the water content (7/8 gallons of water per each 50 pound bag of grout) had a "stiff, damp pack" consistency specified by the manufacturer. Fifteen grout cylinders (five samples each for three different curing ages), measuring 6" tall and 3" in diameter, were tested in compression at a loading rate of approximately 3.5 kips/second. The standard ASTM method for testing grout strength (ASTM C109, 2007), also known as a "grout cube test", was not used since it is applicable for masonry grout applications. In fact, based on an extensive literature search, the design strength of a grout pad has not been thoroughly investigated. Thus, for the purposes of this test program, and explained later, the strength of a grout pad is treated in a similar fashion as concrete, hence the necessity for compression cylinder tests. Other than the smaller cylinder size, the grout was tested and collected using the same methods as for standard concrete cylinders (i.e. ASTM C31 and ASTM C39). The average compressive strength of the grout is presented in Table 3.4, along with other information such as grout density. Between 33 to 120 days of curing, the average compressive strength of the grout ranged from 7,350 to 9,550 psi, approximately twice as large as the compressive strength of the supporting concrete. The grout strength at different curing ages is plotted in Figure 3.3. Also shown in the Figure is the cure age and corresponding strength of the grout used in the large-scale experiments at the time of testing, as well as the standard deviation of the cylinder test strength (shown as error bars on the plot). See

Appendix A for more detailed information regarding the grout, including the test results of each individual compression test and product data from the manufacturer.

3.2.5 Summary of the Ancillary Tests

Table 3.5 summarizes relevant data from the ancillary tests which is subsequently used for evaluating various strength prediction approaches for each individual large scale experiment. Referring to Figures 3.2 and 3.3 introduced earlier, the strength of the concrete and the grout on the date of large scale testing is estimated through linear interpolation of the strengths measured for the ancillary tests with respect to the cure ages.

3.3 LARGE SCALE EXPERIMENTS: TEST SETUP AND PREPARATION

Table 3.6 presents the test matrix for the large scale base connection tests, including the following key information about each experiment: base plate thickness, anchor rod grade and quantity, and applied loading. The dimensions of the two base plate footprints examined in this study are shown schematically in Figure 3.4. Referring to Table 3.6, four of the specimens (i.e. Tests #1, #2, #5 and #7) were identical with respect to specimen construction, i.e. they all featured a 1" thick base plate with four 3/4" diameter anchor rods (all ASTM F1554 Grade 105 ksi). However, different types of loadings (axial as well as flexural) were applied to these nominally identical specimens. Test #1, tested under monotonic lateral loading and zero axial load, provides a "backbone" curve, which can be used for (1) assessing the connection strength under monotonic loading and (2) providing a benchmark case for evaluating cyclic strength and stiffness degradation, as well as visual cyclic damage. Test #2 was identical to Test #1, except that cyclic loading was applied as per the SAC loading protocol (Krawinkler *et al.*, 2000; to be described in a subsequent section). Tests #5 and #7 involved the application of axial compression (i.e. gravity) loads (92.5 kips for Test #5, and 152.5 kips for Test #7), enabling a direct assessment of the effect of axial load on the connection behavior. Test #4 and #6 interrogate alternate base plate thicknesses and their effect on the strength and the modes of failure of the base connection. Tests #4, #5, and #6 are similar except for the base plate thickness, thus providing a direct evaluation of the effect of the plate

thickness (i.e. plate flexibility). Moreover, Test #4 represents a design example presented in the AISC *Steel Design Guide 1* (Fisher & Kloiber, 2006) based on a 720 kip-in moment and a 90 kip axial load designed using the ultimate (i.e. rectangular stress block) approach. This test allows for a direct examination of the level of safety provided by current design procedures. Test #3 examines an alternate bolt pattern, featuring eight, instead of four bolts (see Figure 3.4a for the base plate footprint). This layout is presented as an example of a "rigid base" plate assembly for moment frames in the commentary of the AISC Seismic Provisions (2005). The aim of this eight rod experiment is to investigate whether the failure modes, yield lines, or strength is affected by the additional anchor rods.

3.3.1 Specimen Construction

All large scale specimens were constructed in accordance with the AISC *Design Guide 1* (Fisher & Kloiber, 2006) to reflect current construction practice. A stepped steel reinforced concrete pedestal was used for each base connection test to represent the foundation/footing. Figure 3.5a shows a representative photograph of the concrete pedestal while Figure 3.5b illustrates the pedestal geometry and reinforcement bar layout. The concrete pedestal was stepped to provide a 576 in^2 concrete area situated concentrically under the base plate. Note the area of the base plate (and the approximate area of the grout pad below it) was 196 in^2. The purpose of the stepped geometry was to provide a realistic degree of confinement for the concrete when subjected to bearing pressures by the base plate. Numerous studies (including Fisher & Kloiber, 2006) suggest that the ratio between the area of the base plate and the concrete footing has a significant effect on the bearing strength of the concrete. For the specimens investigated in this study, the ratio of the concrete footing area to the area of the base plate ($A_{footing} / A_{plate}$) equals 2.93. The footing itself was reinforced with #3 (3/8" diameter) steel reinforcing bars to provide confinement to the concrete in the bearing area. Due to the steel reinforcement, the bearing strength of the stepped concrete area is expected to be greater than assumed by current design approaches, which disregard the effect of rebar on the bearing strength. A discussion of the bearing strength of the concrete and grout is presented in Chapter 4. The embedment depth of the anchor rods was 22 inches,

measured from the top surface of the concrete to the anchorage at the bottom of the rods. The bottom (embedded) ends of the anchor rods were attached to 2.75" by 2.75" by 9/32" steel square plate washers sandwiched between two standard nuts. This embedment depth ensured that the rods achieved their full tensile capacity (i.e. failure of the concrete by anchor rod pullout/breakout was prevented). The concrete pedestals were post-tensioned to the laboratory strong floor to provide a fixed boundary condition at the foundation. The post tensioning fixtures were located outside the zone of the column base plate bearing stresses.

3.3.2 Erection Procedure

In current construction practice, various methods are used for the erection and vertical alignment of columns on a concrete foundation. The most popular methods, described in the *Design Guide 1* (Fisher & Kloiber, 2006), include (1) setting (leveling) nuts and washers, (2) setting plates, and (3) steel shim stacks. Setting plates (also known as leveling plates) are an effective method for setting column base elevations but are somewhat more costly than setting nuts and washers (Fisher & Kloiber, 2006). In the setting plate method, a thin steel plate is placed on the foundation (which also doubles as a base plate template) and is set using either jam nuts or shims. Grout is spread under the setting plate and it is then tapped down to elevation. Another popular method involves the use of steel shim stacks under the column. This procedure ensures that all compressive loads are transferred from the base plate to the foundation without stressing the anchor rods (Fisher & Kloiber, 2006). The erection procedure chosen for all large scale specimens in the current test program was the setting nut method. A recent requirement by OSHA, which necessitates the use of four anchor rods, has made the setting nut and washer method of column erection highly popular, since the method offers the convenience of avoiding the need for either a setting plate or shim stacks (Fisher & Kloiber, 2006). In this procedure, four or more anchor rods are utilized, and the column is set by sandwiching the base plate with two nuts and two heavy washers connected to the anchor rods. The elevation and vertical alignment of the column can be adjusted by turning the nuts. It is important to note that the anchor rods are loaded in compression due to temporary construction loads and thus their capacity in compression (i.e. buckling,

etc.) should be checked, as well as the possibility of rod push out through the bottom of the footing. For this reason, it is recommended to use the setting nut and washer method only for columns that are not loaded heavily during erection. A photograph illustrating the leveling nut detail is shown in Figure 3.6. The top plate washers shown in this figure were used only for temporary erection of the column. After consultation with the research group, the top washers were later replaced with smaller plate washers to represent standard geometry (see Figure 3.7). The lower plate washer (adjacent to the leveling nut) measured 2.75" by 2.75" by 9/32" with a hole diameter of 7/8 inches while the upper plate washer measured 2" by 2" by 7/32" with a hole diameter of 7/8 inches. The upper plate washer, made of black steel with a Rockwell hardness value between C40 and C54, was sized according to the *Design Guide 1* (Fisher & Kloiber, 2006) to accommodate the 3/4" diameter rods and 1-5/16 inch anchor rod hole in the base plate. Under typical construction practice, the anchor rod hole in the base plate is generously oversized (hole diameter approximately 1.7 times the anchor rod diameter; see Table 2.3 in the *Design Guide 1*) to accommodate construction tolerances. The bottom washers were made from Grade 2 low carbon steel. ASTM A536 Grade A heavy hex nuts were used for every test to connect the base plate and anchor rods. The top nuts were tightened snug by hand and torqued an additional 1/8 turn using a wrench immediately prior to testing. Other than this, the rods were not pre-stressed to any specified force. This erection procedure was selected based on consultation with an AISC advisory group, since it was considered to be the most representative of standard construction practice.

In this context, it is relevant to discuss recommendations outlined in a report by Astaneh-Asl (2008) which suggests that leveling nuts may provide a stiff load path in the base connection for the compressive forces due to flexure, such that compression may be resisted by the anchor rods, rather than by concrete/grout bearing. Astaneh-Asl's study indicates that a review of engineering literature search did not find any published document on tests or analysis of behavior of base plates with leveling nuts. Because of this, it was recommended by Astaneh-Asl that the nuts below the base plates should be used only for leveling purposes during construction. After the base plate is leveled and is in its correct elevation, it is recommended that the base plate should be supported on

wedges at its edge and the nuts below the base plate should be turned away from the base plate leaving a gap between the base plate and the nut below, preventing compression in the anchor rods. However, consultations with contractors indicate that in typical construction practice, the nuts below the base plate are not, in general, turned away from the plate. Thus, the detail used in the current experimental study (i.e. leaving the leveling nuts in contact with the base plate) is assumed to be most representative of typical construction practice.

3.3.3 Grout Pad

For all base connection tests, a "stiff, damp pack" mix (as defined by the product manufacturer; with 7/8 gallons of water per 50 pounds of grout) of high-strength, non-shrink, general construction grout was installed underneath the base plate, which was elevated two inches due by the leveling nuts (see Figure 3.6). The base plate and concrete pedestal were moistened prior to grout installation to ensure proper application. Grout was spread under the base plate and packed flush with the base plate perimeter using a trowel. A representative picture of the grout pad after testing, shown in Figure 3.8, indicates that the method resulted in a flat and level pad surface with few air voids.

3.3.4 Column

All test specimens had an A992 Grade 50 W8×48 cantilever column welded to the center of the base plate. The column cross-section had a flange width–thickness ratio of $b_f / 2t_f = 5.92$ which is less than the limiting maximum value of $0.3\sqrt{E/F_y} = 7.29$ (for F_y = 50 ksi, E = 29,000 ksi steel) permitted by the AISC Seismic Provisions (2005). The column size, as well as width-thickness ratio, was selected to prevent yielding and local buckling of the column before failure of the base connection. As described later strain gages attached to the base end of the column indicate that the column remained elastic during every test.

3.3.5 Weld Detail between the Base Plate and the Column

The base plate to column weld detail was selected based on a survey of current design practice for SMRF systems. As shown in Figure 3.9, the weld detail consisted of a partial joint penetration (PJP) weld with reinforcing fillet welds. In the PJP detail, a bevel groove weld was installed from the outside flange face through approximately 75% of the flange thickness and a 1/2 inch reinforcing fillet weld was provided on the inside of the flange. The PJP weld and the throat of the reinforcing fillet weld together provide a total throat area about 25% larger than the flange. The web was also welded to the base plate with 1/2 inch fillet welds. All welds were fabricated using E71T-1 filler metal and the flux-cored arc welding (FCAW) process. Previous qualification test data (Fisher, 2005) demonstrates that the E71T-1 weld metal provides high levels of fracture toughness (i.e. the Charpy V-Notch toughness test data at 0°F temperature were in the range of 57 ft-lbs to 91 ft-lbs for the weld metal and the weld yield strength was between 76 ksi and 83 ksi). Recent experimental evidence (Myers *et al.*, 2009), indicates that this type of weld detail in base plates provides excellent performance.

3.3.6 Base Plate

The two base plate footprints used in the large scale tests are shown schematically (with dimensions) in Figure 3.4. Recall that the base plate footprint was identical for six test specimens, except for Test #3, which featured eight anchor rods holes instead of four. Each base plate measured 14” by 14” in area and was fabricated from Grade A36 steel. The base plates were either 1.0, 1.5, or 2.0 inches in thickness. The plates included 1-5/16” diameter anchor rod holes sized according to recommendations in the *Design Guide 1* (Fisher & Kloiber, 2006). allowing construction tolerances for the 3/4” anchor rods.

3.4 TEST SETUP

All base connection tests were conducted at the UC Berkeley Network for Earthquake Engineering Simulation (NEES) Structures Laboratory in Richmond, California. Figure 3.10a schematically illustrates the test setup. A photograph of the setup taken during testing is shown in Figure 3.10b. For all tests, the column was loaded transversely, in the

direction of the column major axis bending, with the load applied 92.5 inches above the top of the base plate to approximately represent the point of inflection in the bottom story of a fixed-base moment frame (roughly 2/3rd of the story height). A restraint bracing system (also shown in Figure 3.10) was provided to prevent lateral (out-of-plane) deformations of the specimen. One MTS Series-244 220-kip actuator provided the lateral loading. The head of the actuator was supported by a pulley arrangement with a counterweight (not indicated in Fig. 3.10a but partially visible in Fig. 3.10b) to ensure that the self-weight of the actuator would not be supported by the specimen itself. For four tests (i.e. Tests #4, #5, #6 and #7), axial loads were applied through a loading beam attached to the top of the column (see Figure 3.10ba). Pre-stress rods, load cells, and hydraulic jacks installed between the loading beam and the strong floor enabled the application and measurement of gravity loads. Swivels were provided at each end of the pre-stress rod assembly (as well as the gravity beam to column connection) to preclude transfer of moment from the gravity loading assembly and the specimen itself. The swivels were located such that the resultant axial load was concentric with the center of the base connection column, minimizing second order (P-Δ) effects. The total self weight of the gravity system was approximately 2,250 pounds. This weight was added to the axial loads recorded from the load cells on the pre-stress rods to determine the net axial load imposed on the base connection.

3.4.1 Loading Protocol

Table 3.7 indicates both the axial and lateral loading applied to the base connections. As indicated in the Table, the lateral loading for Test #1 comprised of a single monotonic push to 10.6% drift (i.e. 9.7" lateral displacement at the load-line of the actuator), which was the stroke limit of the actuator. The lateral loading rate for Test #1 was approximately 0.18% drift per minute. For the other six tests, cyclic lateral displacement-controlled loading was applied. Illustrated in Figure 3.11, cyclic lateral loads were applied according to a displacement history based on the SAC loading protocol (Krawinkler *et al.*, 2000) to represent deformation histories that are consistent with seismic demands in moment frame buildings. The SAC loading protocol is expressed in terms of story drift ratios. For the purposes of test control, these were converted to

actuator displacements by multiplying them with the distance from the top of the base plate to the center of the actuator head (92.5 inches for all tests). The test observations are presented in terms of story drift ratios. The initial loading rate for the cyclic tests was about 2.1% drift per minute. Referring to Table 3.7, constant axial compressive loading was applied to four specimens to represent gravity loading in the column. For Tests #4, #5, and #6, 92.5 kips of axial compressive load was applied (this includes the self-weight of the gravity system test apparatus) while for Test #7, 152.5 kips was applied.

In four of the six cyclic experiments (i.e. Test #3, #4, #5, and #7), sudden failure (i.e. a large drop in resistance) was not obtained during the regime of the SAC loading history. Thus, additional cycles for these tests were appended to the SAC protocol at the maximum available drift level (i.e. at the stroke limit of the actuator). Cyclic loading was applied at the maximum amplitude until minimal response degradation was observed, i.e. an approximately stable hysteretic response was achieved. Details of the entire loading history for each test are listed in Table 3.7 while Appendix B presents the applied load histories for each test.

3.4.2 Instrumentation, Photography, and Video

Figure 3.12 illustrates the typical instrumentation layout for the base connection tests. In addition to the loads and displacements monitored by the actuator, instrumentation was installed on the specimen and loading frame to measure displacements, rotations and strains. These instruments include position transducers attached to the base plate (see Figure 3.12b) and concrete pedestal to measure motion in three dimensions enabling a monitoring of the base plate behavior as well as relative slip between the concrete pedestal and laboratory strong floor. Based on test data, the concrete pedestal did not slip, rotate, nor show uplift relative to the laboratory strong floor. Displacement transducers were installed to monitor incidental out-of-plane motion of the test loading frame (see Figure 3.12c). For all tests, the maximum out-of-plane deformations were minimal (less than 0.5 inches). Strain gages were attached to the column at two locations (three inches and 36 inches from the top of the base plate) to monitor column yielding and deformations (see Figure 3.12c). Several strain gages were also installed on the surface of

the base plate (see Figure 3.12b). In addition, two uniaxial strain gages were attached to every anchor rod (at two inches below the upper threads; about two inches below the surface of the concrete) to measure rod axial strain (see Figure 3.12a). At the location of the strain gages, the anchor rods were unthreaded and rod surface was de-bonded from the concrete (using duct tape and industrial lubricant) over a section of the rod (approximately 1") immediately below the top surface of the concrete to enable the conversion of strain readings to a corresponding force. In addition, six high definition cameras (three still and three video) were employed to document every test. Data recorded from all the instrumentation channels, including the still and video camera recordings, is archived in the NEES Central Data Repository.

3.5 TEST RESULTS OF LARGE SCALE TESTS

This section outlines various aspects of the experimental response of the column base connection large scale tests. Qualitative observations, including a detailed discussion of the observed damage states and failure modes, are first summarized, followed by a brief discussion of quantitative observations. An extensive analysis of test data is presented in Chapter 4.

3.5.1 Qualitative Observations of Specimen Response

In this section, relevant observations for each test are described qualitatively and a summary of the observations is presented in Table 3.8. Figures 3.13-3.19 include annotated plots of the column drift versus the base moment for every test. In addition, Figure 3.20 shows the backbone (or envelope) curves of every test. For a convenient assessment of the effect of different parameters on test response, the backbone curves are grouped into four categories including (1 - see Figure 3.20a) the effect of axial load, (2 - see Figure 3.20b) the effect of plate thickness, (3 - Figure 3.20c) effect of different anchor rod layouts, and (4 - Figure 3.20d) the effect of the loading protocol (i.e. monotonic or cyclic).

3.5.1.1 Test #1

Test #1 was loaded monotonically without any axial (gravity) load, and the resulting plot of the column drift versus the base moment is shown in Figure 3.13. Based on this figure and visual observations during and after testing, the observed experimental response is now summarized –

- Referring to Figure 3.13, elastic response is observed up to a column drift level of approximately 1%, after which yielding and a further increase in connection strength is observed. This increase in strength continues until a drift of approximately 8%, where a slight reduction in strength (approximately 3%) is observed. Based on video evidence, this reduction is accompanied by spalling grout at the extreme compression edge of the base plate. Subsequent to this, a relatively stable response (i.e. no change in moment) was observed until the stroke limit of the actuator (10.6% drift) was reached, at which point the specimen was unloaded and the test was stopped.
- Grout damage (defined as any evidence of grout cracking or spalling) initiated at about 3% drift on the tension side of the base connection. Referring to Figure 3.21, grout crushing was caused by the base plate folding down at its corners, due to the downward clamping force caused by the anchor rods. At 6% drift, grout spalling initiated on the extreme compression edge of the connection.
- Plate yielding (as evidenced by flaking of lime dust painted on the surface of the base plate) initiated at 1.3% drift on the compression side and 2.3% drift on the tension side.
- The strain gage data collected from the anchor rods indicate that yielding of the anchor rods occurred at a column drift of approximately 1%. This is based on the assumption that the rods yielded at a strain of 2,000 microstrain, which is consistent with the rod ancillary tests.
- Fracture initiation of the weld connecting the base plate to the column was observed at 3.7% drift. A crack formed at the corner of the flange to base plate interface (see Figure 3.22). At the end of testing, the crack grew to about a length of 0.3 inches.

- The specimen was gradually unloaded at the end of the experiment. The unloading stiffness was nearly identical to the initial (elastic) loading stiffness, even though the connection sustained significant plate and grout damage.

3.5.1.2 Test #2

The specimen investigated in Test #2 is nominally identical to the one used in Test #1, except that it was loaded cyclically under the SAC loading protocol (recall Section 3.4.1). The column drift versus base moment is plotted in Figure 3.14. For reference, the envelope curve from Test #1 is overlaid on the plot. Based on this figure and visual observations during and after testing, the observed experimental response is now summarized –

- It is striking to note that for the entire experiment (i.e. before anchor rod fracture), the envelope of the moment-drift curve of Test #2 closely follows that of Test #1 (see Figures 3.14 and 3.20d). Although the envelope is similar, slight strength degradation is observed for the cyclic test (approximately 5% drop in base moment between cycles at drifts larger than 4%).
- The cyclic loading produces a pinched hysteretic response with slight strength degradation. This pinching response may be attributed to the interaction of the anchor rods with the base plate. For example, when the base plate is pushed in one direction, the anchor rods on the tension side of the column engage with the base plate (i.e. the anchor rod nut/washer comes into bearing contact with the top of the base plate), and subsequently yields. When the loading is reversed, the base plate loses contact with the nut/washer of the elongated anchor rod, resulting in a change in displacement with an insignificant change in force. The force increases again when the anchor rods on the opposite side of the base plate are engaged.
- One of the anchor rods fractured during the first excursion at the 7% drift level (see Figure 3.23). At this point, the resistance of the connection dropped by nearly half (56% drop in base moment). However, the connection reached its peak strength prior to anchor rod fracture.

- Grout damage initiated during the 2% drift cycles. At the end of the experiment, grout damage included crushing at the bearing sides of the base plate (see Figure 3.24 for a representative post-test grout damage photograph).
- Plate yielding initiated during the 3% drift cycles and rod yielding was recorded at 1% drift.
- Unlike Test #1, no fracture initiation of the column-to-plate weld was observed.

3.5.1.3 Test # 3

The specimen investigated in Test #3 is geometrically similar to that of Test #2 with the exception that it consists of eight anchor rods instead of four. The outer anchor rods of the specimen of Test #3 (see Figure 3.4a for a definition of outer anchor rod) are in the same location as the anchor rods of al the other test specimens. Column drift versus base moment is plotted in Figure 3.15. Based on this figure and visual observations during and after testing, the observed experimental response is now summarized –

- The yield lines in the base plate of Test #3 are distinct from the other tests. Due to the eight-rod pattern, yield lines formed parallel to the web of the column across approximately the whole length of the base plate, rather than the corners of the plate. Consequently, as shown in Figure 3.25, crushing/spalling damage to the grout pad occurred at the sides of the base plate, rather than the bearing regions of the connection. Base plate yielding initiated during 2% drift cycles (sooner than Test #2) and grout damage initiated during 2% drift cycles (similar as Test #2).
- The envelope of the response of Test #3 is similar to the response of Test #2. As shown in Figure 3.20c, Test #3 resisted a 16% larger base moment than Test #2 and was also more ductile.
- Unlike Test #2, no anchor rod fracture was observed in Test #3; up to the maximum applied drift amplitude of 9%.
- In comparison to Test #2, the hysteretic response for Test #3 shows less pinching, presumably due to the anchor rods being engaged with the base plate for a larger portion of the unloading regime (see Figures 3.14 and 3.15).

- Yielding of the outer anchor rods initiated at 1% drift while the inner rods yielded at 2% drift.
- Fracture initiation of the column-to-plate weld was observed during 2% drift cycles and grew to less then one inch in length by the end of testing.

3.5.1.4 Test #4

The column drift versus base moment for Test #4 (1.5" thick base plate, Grade 36 anchor rods, 92.5 kips axial compression load) is plotted in Figure 3.16. Based on this figure and visual observations during and after testing, the observed experimental response is now summarized –

- Qualitatively, the envelope of the moment-drift response of Test #4 is similar to that of Tests #1, #2 and #3 (see Figure 3.20). However, a marked increase in the initial stiffness is observed, probably due to the presence of axial compression load.
- The hysteretic response of Test #4 is distinct from Test #2, wherein the unloading cycles of Test #4 exhibits pinching (see Figure 3.16). Two types of yielding were observed in the base connection; yielding of the anchor rods in axial tension and yielding of the base plate in flexure. Moreover, each of these yielding mechanisms is associated with the opening and closing of a gap, either between the base plate and grout, or the anchor rod nut and base plate. This contact behavior results in a decrease or increase in stiffness, i.e. a pinched hysteretic response, as observed in the moment-drift plots. This behavior is similar to reinforced concrete members where the reinforcing bars yield, the concrete cracks and the cracks close upon load reversal. The presence of axial load delays the opening of these gaps thereby affecting the base moment at which pinching is observed. Thus, for the tests without any axial load, the pinching is observed at zero moment, whereas for tests with axial load, the pinching is observed at higher levels of base moment.
- Four threads on every anchor rod were stripped (sheared off) due to the base plate bearing on the lower (leveling) nuts (i.e. compression in the anchor rod). This damage was observed only after testing and it was not possible to identify at what drift level this damage occurred.

3.5.1.5 Test #5

The specimen of Test #5 is geometrically similar to the specimen of Test #2. The only difference between both tests is the application of a 92.5 kip gravity axial load for Test #5, as compared to zero gravity load for Test #2. The column drift versus base moment is plotted in Figure 3.17. Based on this figure and visual observations during and after testing, the observed experimental response is now summarized –

- The shape of envelope of the moment-drift response of Test #5 is qualitatively similar to that of Test #2 except that a higher initial stiffness is observed (see Figure 3.20a). The hysteretic response is similar to that of Test #4, including the pinching behavior as explained in Section 3.5.1.4. However, this phenomenon is less prevalent as compared to Test #4.
- Grout damage initiated during 4% drift cycles, much later than in Test #2. Grout damage observed at the end of testing included crushing at the corners of the base plate (see Figure 3.8).
- Plate yielding was observed during 1.5% drift cycles (sooner than in Test #2, where it was observed at 3%) and rod yielding was recorded at 1.5% drift (later than in Test #2, where it was observed at 1%).
- Fracture initiation at the column-to-plate weld was observed during 6% drift cycles.

3.5.1.6 Test #6

Referring to Table 3.8, the specimen of Test #6 was similar to Tests #5, except that it featured a thicker (2.0") base plate. Cyclic lateral deformations were applied to the specimen under a constant gravity load of 92.5 kips. The column drift versus base moment is plotted in Figure 3.18. Based on this figure and visual observations during and after testing, the observed experimental response is now summarized –

- The shape of envelope of the moment-drift response of Test #6 is similar to that of Test #4 (see Figure 3.20b). For both of these tests, base plate yielding was not observed.

- The hysteretic response is similar to that of Test #4 and #5, including pinching behavior followed by an increase in resistance at higher drift levels due to the engagement of the anchor rods as explained in Section 3.5.1.4.
- Grout damage initiated at a relatively small drift level (i.e. 1% drift). In addition, three anchor rods exhibited stripping (shearing) of at most two threads below the bottom (leveling) nuts. The onset of early grout damage and thread stripping may be attributed to the rigidity of the plate.
- One of the anchor rods fractured during the 7% drift cycles. Even after rod fracture, the connection maintained substantial resistance (69% of the base moment prior to fracture), probably due to a redistribution of forces through grout bearing in the connection.
- One of the top plate washers fractured during the 7% drift cycles (see Figure 3.26).

3.5.1.7 Test #7

The specimen of Test #7 is geometrically similar to the specimens of Test #2 and #5 with the exception that it was subjected to the highest level of axial compressive load (152.5 kips). The column drift versus base moment is plotted in Figure 3.19. Based on this Figure and visual observations during and after testing, the observed experimental response is now summarized –

- The shape of envelope of the moment-drift response of Test #7 is qualitatively similar to that of Test #2 and #5 except that a higher initial stiffness and peak base moment is observed (see Figure 3.20a). The hysteretic response is similar to that of Test #5, including the pinching behavior explained in Section 3.5.1.4.
- Grout damage initiated during 3% drift cycles, similar to that of Test #5. Grout damage observed at the end of testing was similar to that of Test #5 (i.e. crushing only at the corners of the base plate).
- Plate yielding was identified during 3% drift cycles (later than Test #5) and rod yielding was recorded at 1.5% drift (similar to Test #5).
- Fracture initiation of the column-to-plate weld was observed during the 7% drift cycles; the crack grew less than half an inch during loading.

3.5.1.8 Summary of Observed Damage and Failure

Various behaviors related to the damage and failure of the base connection were noted during the tests, including (1) yielding of the base plate (for all tests except #4 and #6), (2) crushing/spalling of the grout pad (for every test), (3) yielding (for every test) and fracture (for Tests #2 and #6) of the anchor rods, (4) fracture initiation of the weld connecting the base plate to the column (for Tests #1, #3, #5, and #7), (5) dishing (for most tests) and fracture (for Test #6) of the upper plate washers, (6) stripping of the anchor rod threads below the bottom (setting) nut (for Tests #4 and #6), and (7) dishing of the lower plate washers (for most tests). These behavioral observations are summarized in Table 3.8.

3.5.1.9 Deformation of the Base Plate

The test specimens with a 1.0" thick base plate (Tests #1, #2, #3, #5, and #7) exhibited large base plate plastic deformations, whereas the other two specimens (Tests #4 and #6) did not show any evidence of yielding, either from stain gage data or flaking of lime powder applied to the plate. Figure 3.23 shows photographs of the permanently deformed base plate for the monotonic Test #1, clearly indicating the yield line formations on the tension side of the connection. A schematic illustration of this yield line pattern is illustrated in Figure 3.27a. This type of yield pattern was also observed for the cyclic tests with 1.0" thick base plates (Tests #2, #5 and #7). The test with eight anchor rods (Test #3) had a distinct yield pattern and is shown in Figures 3.25 and 3.27b. As evident from these figures, yield lines for Test #3 occurred on the sides of the base plate parallel to the column web. The onset of plate yielding for every test, defined as when the painted-on lime powder flaked off of the base plate, is listed in Table 3.8. Note that for all specimens with 1.0" thick base plates, plate yielding occurred after about 1.5% drift levels. Note that for Tests #1, #2, #5 and #7, plate flexural yielding on the tension side (due to prying forces in the anchor rods) is much more extensive than plate flexural yielding on the compression side (due to bearing on the grout pad or leveling nuts).

3.5.1.10 Grout Damage

All tests sustained some level of crushing or spalling damage to the grout pad under the base plate. For all tests, considerable grout crushing was observed under the lower plate washers, which were subjected to compression forces from the leveling nut detail. Tests #1, #2, #4, and #6 showed grout crushing damage at the extreme bearing interface of the base plate and grout pad. For Tests #5 and #7, most of the grout crushing was in the vicinity of the anchor rod plate washers. Test #3 (the specimen with eight anchor rods) exhibited a distinct pattern of grout damage, where crushing was observed at the sides of the base plate, parallel to the column web. Representative photographs of the grout damage are shown in Figures 3.8, 3.24, 3.25, 3.28. The drift level corresponding to the onset of grout damage, defined as any visually observable cracking or spalling of the grout, is summarized in Table 3.8. For all tests, grout damage initiated at drift levels of 1% or higher and no damage to the concrete pedestal footing (due to crushing or cracking) was observed. A detailed analysis of the bearing behavior of both the grout and concrete will be addressed in Chapter 4.

3.5.1.11 Response of the Anchor Rods

As discussed in the preceding sections, Tests #2 and #6 sustained anchor rod fracture. In each of these tests, one of the anchor rods fractured during the 7% amplitude drift cycle. For Test #2, the anchor rod fractured during the first excursion of the 7% drift cycles (at 6.92% drift) and fracture occurred in the threaded region of the rod within the base plate thickness (i.e. between the two nut and washer assemblies – see Figure 3.23). The anchor rod of Test #6 fractured during first cycle of 7% drift (at negative 7.15% drift) below the leveling nut. The exact instant of anchor rod fracture is indicated in the moment-drift curves in Figure 3.14 and 3.18 for Test #2 and #6, respectively.

Yielding of the Grade 105 anchor rods is assumed to occur at 60 ksi (2,000 microstrain), based on the uniaxial ancillary tension test data (refer Appendix A). Note that yielding in the rods occurred initially in the threaded region. The strain gages attached to the anchor rods indicate that the base plate tests with four Grade 105 rods and axial load (i.e. Tests #5, #6, #7) yielded at 1.5% drift. For the tests with four Grade 105 rods and no axial load

(Tests #1 and #2), rod yielding initiated at about 1% drift. For the test with four Grade 36 rods (Test #4), anchor rod yielding (also based on the uniaxial ancillary tension test data, assumed to occur at 49 ksi – 1,750 microstrain) initiated at 3% drift. For the test with eight anchor rods (Test #3), yielding of the outer rods occurred at 1% drift while yielding of the inner rods occurred at 2% drift. Figure 3.28 illustrates the significant elongation of the anchor rods due to extensive yielding.

Two strain gages were attached to each anchor rod for every test as shown in Figure 3.12a. A representative plot of the anchor rod strain for the cyclic tests is shown in Figure 3.29 (shown here for Test #2). Note the significant compressive strains sustained by the anchor rod as the cyclic loading progressed. As the grout pad deteriorated due to cyclic bearing damage, and as the rods elongated due to tension yielding, compressive forces in the base connection were transferred to the anchor rods through the leveling nuts. Stress-strain data from the ancillary tests, together with cyclic constitutive material models, were used to infer the anchor rod forces based on the measured strains. Analysis of the anchor rod strain data is presented in Chapter 4. Results of the anchor rod response (i.e. the strains) for all the tests are archived in Appendix B.

In addition to data provided by strain gages, the anchor rod elongation can be quantified by monitoring the vertical displacement of the anchor rods at the peak drift of every cyclic drift excursion. A representative plot of the anchor rod elongation is presented in Figure 3.30 (shown here for Test #4; similar plots for all tests shown in Appendix B). Note that elongation, is effected to various mechanisms, including (a) anchor rod yielding in the rod threaded region, (b) yielding in the rod unthreaded region (c) compression in the anchor rod from cyclic drift reversal due to bearing on the leveling nuts, and (d) grout damage.

3.5.2 Quantitative Descriptors of Test Response

Table 3.9 summarizes key quantitative data measured from the base connection tests, including the maximum base moment, the moment at 4% drift level, the moment at assumed connection yield (1% drift), the maximum drift reached in the test, the

maximum rotation, energy dissipation, and elastic stiffness. For reference, Table 3.9 lists the predicted strengths estimated by the general design procedure presented in AISC *Design Guide 1* (Fisher & Kloiber, 2006). Strength predictions are discussed in detail in Chapter 4.

3.5.2.1 Maximum Base Moment

Introduced previously, plots of the column drift ratio versus base moment[1] for all experiments are illustrated in Figures 3.13-3.19 and archived in Appendix B. Chapter 4 shows strength estimates as per current design guidelines (Fisher & Kloiber, 2006) overlaid on the test response plots.

The maximum base moment for every test, averaged from both loading directions, is listed in Table 3.9. For every cyclic test, the difference in peak moment for each loading direction is less than 2%. For Test #1, the maximum moment occurred at the largest applied drift level. Thus, for this test, which was stopped due to the actuator stroke limit, a peak base moment was not obtained. However, based on the shape of the moment-drift curve and the extent of damage observed in the connection, the connection is assumed to have reached a plastic mechanism in the base connection and the peak moment may be approximately estimated as the observed maximum base moment.

Also included in Table 3.9 is the maximum base moment capacity as predicted by the rectangular stress block method presented in AISC *Design Guide 1* (Fisher & Kloiber, 2006). This approach is the most popular method for characterizing the strength of base connections subject to axial load and flexure. These strength estimates are calculated from measured material data (rather than nominal values) in order to eliminate bias due to material variability. In addition, the strength estimate does not include resistance factors (ϕ-factors). As shown in Table 3.9, the rectangular stress block method is rather conservative for all tests except Test #6. In fact, the predicted strengths (except for Test

[1]The column base moment is defined as the lateral resistance recorded by the actuator times the distance between the point of application of the load and the top of the base plate (about 92.5" for all tests). In the tests where it is applied, the axial load is introduced through tension rods whose line of action passes through the center of the base plate. Thus, no additional moment from second order (P-Δ) effects is generated due to the axial load.

#6) are conservative even for the base moment at 4% drift, the ductility required by the AISC Seismic Provisions (2005; Section 9.2a) for connections in special moment frames subjected used for seismic load resisting systems. Chapter 4 presents a more detailed discussion of the connection strength calculated by several strength prediction approaches.

3.5.2.2 Maximum Observed Drift Capacity and Energy Dissipation Capacity

All the base connections showed excellent ductility, measured in terms of drift capacity. Five of the seven large scale tests (i.e. Test #1, #3, #4, #5, and #7) were stopped prior to sudden failure because the stroke limits of the actuator were reached. Table 3.9 lists the maximum drifts applied to all the experiments, including the two tests (Tests #2 and #6) where rod fracture was observed. The monotonic test (Test #1) was deformed up to 10.6% drift, Test #7 deformed up to 8% drift, and Tests #3, #4, and #5 deformed up to 9% drift. The variability in maximum drift between the tests is attributed to slight differences in the location of specimen installation during each test set-up. Thus, all the specimens were not installed in exactly the same location with respect to the mid-stroke of the actuator. Test #2 was stopped at 6.92% drift after a large (56%) drop in base moment due to anchor rod fracture while Test #6 was continued to 8% drift cycles after one rod fractured during the first cycle of the 7% drift amplitudes (at negative 7.15% drift). Except for Test #2 and #6, all tests exhibited substantial resistance and generally maintained at least 80% of the peak base moment up to the end of the loading history. When evaluated in the context of connection ductility guidelines, such recommended by the AISC Seismic Provisions (2005), which requires beam-column connections to exhibit stable hysteretic response until 4% drift, the column base connections tested in this study exhibit excellent performance.

In addition to the moment-drift plots shown in Figures 3.13-3.19, Figure 3.31 shows a representative plot of the base moment plotted against the connection rotation[2].

[2]To eliminate contributions from base slip and column deflection, connection rotation is defined as the difference of the lateral deflection of the column at location of applied lateral load and the average lateral

Connection rotation does not include the deformations of the column itself (which are elastic, since the column is not observed to yield in any of the experiments) and the lateral slip of the base plate. Similar plots for all the tests are presented in Appendix B. Since these plots isolate the connection response, they may be used to inform boundary conditions in analytical models or calibrate hysteretic models for the connections. The maximum rotation of the base connection is listed in Table 3.9 for every experiment.

Hysteretic energy dissipation is often used as an indicator of the cyclic deformation capacity of structural components. Table 3.9 lists a hysteretic energy dissipation measurement for each of the specimens. The energy dissipation was determined by numerically integrating the base moment versus plastic drift plots. The values of energy dissipation summarized in Table 3.9 are normalized by the elastic energy absorption associated with connection yielding (defined at 1% drift for all tests), defined as the product of yield moment and yield rotation. To eliminate the effects of different levels of maximum deformation applied to each experiment, the energy dissipation data is calculated up to the end of the 6% drift cycles. Figure 3.32 plots dissipated energy versus cumulative drift for all cyclic tests up to and including the 6% drift cycles. Referring to this figure, two factors are assumed to effect energy dissipation of the base connection, the relative strength and the influence of the hysteretic pinching behavior. Furthermore, the eight rod specimen dissipates more energy than the four rod specimen.

3.5.3 Contributions to Specimen Deformations

Several mechanisms contribute to the observed deformations including (1) deformations (i.e. bending) of the base plate (2) deformations of the anchor rods (3) deterioration of the grout/concrete footing (4) flexural bending of the column and (5) lateral slip of the base plate relative to the foundation. For flexible columns, the contribution of column bending to the drift deformation is relatively large. The deformation contribution to the column drift corresponding to anchor rod deformations, base plate bending deformations, and concrete/grout deterioration depends on the base connection assembly. For example, for

---

slip of the base plate, divided by the column cantilever length, minus the applied lateral load divided by the elastic rotational stiffness of column

thick (rigid) base plates (i.e. Test #4 and #6), the contribution of deformation corresponding to base plate bending are negligible compared to the drift deformations due to flexure of the column or elongation of the anchor rods.

3.5.4 Connection Stiffness

It is important to quantify the elastic rotational stiffness of the base connection to assess the connection fixity, especially for the accurate modeling of the component for structural frame analysis. The elastic rotational stiffness of each large scale specimen was measured by determining the average slope of the lateral force versus lateral displacement plots at small (i.e. elastic) displacements (specifically ±0.25" lateral displacement). Within this range, the total displacement of the column at the location of the applied load can be expressed as –

$$\Delta = P \cdot \left(\frac{1}{k_{column}} + \frac{L^2}{\beta} \right) \tag{3.1}$$

Where:

L = column cantilever length (bottom of base plate to location of applied lateral load)
= 92.5 inches

P = applied axial load

k_{column} = elastic stiffness of column = $(3EI_x) / L^3$

E = Young's modulus = 29,000 ksi for steel

I_x = Strong axis second moment of area = 184 in^4 for a W8 x 48 beam

Solving for β provides the rotational stiffness constant of the base connection. From the values of β in Table 3.9, it is evident that the rotational stiffness is rather insensitive to all parameters except the level of axial load. In fact, the experiments with axial load show rotational stiffnesses which are approximately five times as large as the rotational stiffnesses for the experiments without axial load. In addition, it is observed that the eight-rod Test #3 is only 11% stiffer than the four-rod Test #2.

3.5.5 Base Plate Lateral Slip Response

Shear forces imposed on the test specimen base were resisted by friction between the steel plate and grout pad. Given the large aspect ratio of the specimens (height of column to base plate width = 6.6), the compressive stress in the bearing region is sufficient to carry the required shear through friction. A calculation, considering the total compressive force under a given moment assuming a lever arm equal to the base plate width, indicates that column base cannot slide unless the friction coefficient is less than approximately 0.2. According to previous experimental results by Gomez *et al.* (2009), the coefficient of friction between steel and grout is 0.45. The maximum slip observed for all tests was only 0.34 inches, where most of the slip occurred after significant damage to the grout. A representative plot of the plate slip versus lateral force is shown in Figure 3.33 (shown here for Test #4). Plate slip versus lateral force plots for all tests are presented in Appendix B.

Table 3.1 – Summary of anchor rod tension tests

Nominal rod grade (ksi)	$F_{y,rod}$[1] (ksi)	$F_{u,rod}$[2] (ksi)	E[3] (ksi)	ε[4]
36	48.6	71.3	29,440	1.13
105	114.0	146.5	29,440	0.81

[1]Measured yield stress, based on 0.2% offset method
[2]Measured ultimate strength
[3]Measured Young's modulus
[4] $\varepsilon = \ln\left(d_0 / d_f\right)^2$ = average true fracture strain across necked cross section of tension coupon

Table 3.2 – Summary of tension tests on coupons extracted from the base plate material

Base plate thickness (inches)	$F_{y,plate}$[1] (ksi)	$F_{u,plate}$[2] (ksi)	E[3] (ksi)
1.0	40.4	68.7	31,400
1.5	37.0	67.9	31,200
2.0	38.4	72.1	33,900

[1]Measured yield stress, based on 0.2% offset method
[2]Measured ultimate strength
[3]Measured Young's modulus

Table 3.3 – Summary of concrete compression tests

Cure time (days)	Samples collected	Average concrete density (lbs/ft^3)	Average compressive strength (psi)	Standard deviation of compressive strength (psi)
32	6	143	3,860	144
73	5	146	4,160	61.0
131	6	146	4,440	233

Table 3.4 – Summary of grout compression tests

Cure time (days)	Samples collected	Average grout density (lbs/ft^3)	Average compressive strength (psi)	Standard deviation of compressive strength (psi)
33	5	127	7,350	957
61	5	127	9,110	691
120	5	131	9,550	2,370

Table 3.5 – Summary of material test data

Large scale test number[1]	Anchor rod yield strength (ksi)	Anchor rod ultimate strength (ksi)	Base plate yield strength (ksi)	Base plate ultimate strength (ksi)	Concrete compressive strength (psi)	Grout compressive strength (psi)
1	114.0	146.5	40.4	68.7	3,965	7,413
2	114.0	146.5	40.4	68.7	4,016	7,854
3	114.0	146.5	40.4	68.7	4,140	8,923
4	48.6	71.3	37.0	67.9	4,247	9,245
5	114.0	146.5	40.4	68.7	4,314	9,349
6	114.0	146.5	38.4	72.1	4,347	9,401
7	114.0	146.5	40.4	68.7	4,394	9,475

[1]From which coupon was extracted

Table 3.6 – Base plate test matrix

Large scale test number	Base plate thickness (inches)	Anchor rod grade (ksi)	Number of anchor rods	Imposed gravity load (kips)	Lateral loading protocol
1	1	105	4	0	Monotonic
2	1	105	4	0	Cyclic
3	1	105	8	0	Cyclic
4	1-1/2	36	4	92.5	Cyclic
5	1	105	4	92.5	Cyclic
6	2	105	4	92.5	Cyclic
7	1	105	4	152.5	Cyclic

Table 3.7 – Base plate test loading details

Test number	Net axial compressive load (kips)	Lateral loading protocol	Peak column drift (%)[1]	Notes
1	0	Monotonic	10.58	Test stopped at peak drift and unloaded to zero load
2	0	Cyclic	6.92	SW rod fractured during first excursion at 7.0% drift (at 6.92% drift) - test was stopped and unloaded to zero load
3	0	Cyclic	9.20	After the general loading protocol, the test was cycled 9.25 times at 9% drift - test was stopped at zero load
4	92.45	Cyclic	9.24	After the general loading protocol, the test was cycled 4 times at 9% drift; test was stopped at zero drift
5	92.35	Cyclic	9.21	After the general loading protocol, the test was cycled 3 times at 9% drift; test was stopped at zero load
6	92.55	Cyclic	7.15	SE rod fractured during first excursion at 7% drift (at negative 7.15% drift); test continued through both 8% cycles
7	152.55	Cyclic	8.21	After the general loading protocol, the test continued with two slow cycles followed by three fast cycles at 8% drift - test was stopped at zero drift

[1]Either peak imposed drift or max drift due to anchor rod fracture

Table 3.8 – Base plate test qualitative observations

Test number	Drift level at initial grout damage	Observed post-test grout crushing damage	Drift level at initial plate yielding	Drift level at initial anchor rod yielding	Drift level at anchor rod fracture	Drift level at weld fracture initiation	Evidence of anchor rod thread stripping	Drift level at upper plate washer fracture
1	3.12% (tension side) 5.71% (compression side)	Compression side at the edge of the grout pad; tension side at the corners of the grout pad	1.30% (compression side) 2.34% (tension side)	0.94%	No fracture	3.66%	Unable to determine	No fracture
2	2nd excursion at 2%	Tension/compression sides of the grout pad	1st excursion at 3%	1%	1st excursion of 7%	No fracture initiation	No	No fracture
3	1st excursion at 2%	Sides where the anchor rods were located (i.e. weak axis sides)	1st excursion at 2%	1% (outer rods) 2% (inner rods)	No fracture	4th excursion at 2%	Unable to determine	No fracture
4	4th excursion at 2%	Tension/compression sides of the grout pad	No significant yielding	3%	No fracture	No fracture initiation	All rods are stripped about four threads	No fracture
5	1st excursion at 4%	Only at the corners of the grout pad	1st excursion at 1.5%	1.5%	No fracture	2nd excursion at 6%	Unable to determine	No fracture
6	4th excursion at 1%	Tension/compression sides of the grout pad	No significant yielding	1.5%	2nd excursion of 7%	No fracture initiation	Three rods are stripped a couple of threads	1st excursion at 7%
7	4th excursion at 3%	Only on one side, at the corners, of the grout pad	1st excursion at 3%	1.5%	No fracture	2nd excursion at 7%	Unable to determine	No fracture

Table 3.9 – Base plate test results

Test number	Average peak base moment (kip-in)	Predicted base moment[1] (kip-in)	Test-to-predicted base moment	Average column drift at peak moment (%)	Average base moment at 4% drift (kip-in)	Average base moment at yield – i.e. 1% drift (kip-in)	Peak column drift (%)	Max base rotation (radians)	Energy dissipated after 6% drift (kip-in)	Energy norm after 6% drift	Base plate connection rotational stiffness (kip-in/ rad)
1	1,110	648	1.71	10.58	970	490	10.58	0.0984	19,700	40.3	86,100
2	1,080	644	1.68	5.60	1,050	540	6.92[3]	0.0631[3]	73,900	137.0	85,500
3	1,250	n/a[2]	n/a	4.42	1,240	600	9.20	0.0860	89,700	149.5	94,800
4	1,130	934	1.21	4.08	1,120	880	9.24	0.0856	98,900	113.0	501,900
5	1,570	514	3.05	6.35	1,470	780	9.21	0.0829	115,000	148.1	310,700
6	1,645	1,700	0.97	4.58	1,640	890	7.15[3]	0.0611[3]	113,000	127.5	456,900
7	1,785	706	2.53	6.49	1,690	990	8.21	0.0721	136,000	137.2	475,600

[1]Based on the rectangular stress block method featured in the AISC *Design Guide 1* (Fisher & Kloiber, 2006)
[2]The rectangular stress block method is not applicable for the eight-rod Test #3
[3]At rod fracture

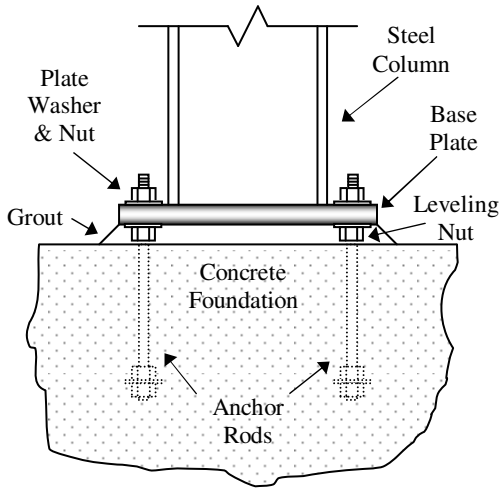

Figure 3.1 – Schematic of a typical exposed column base connection

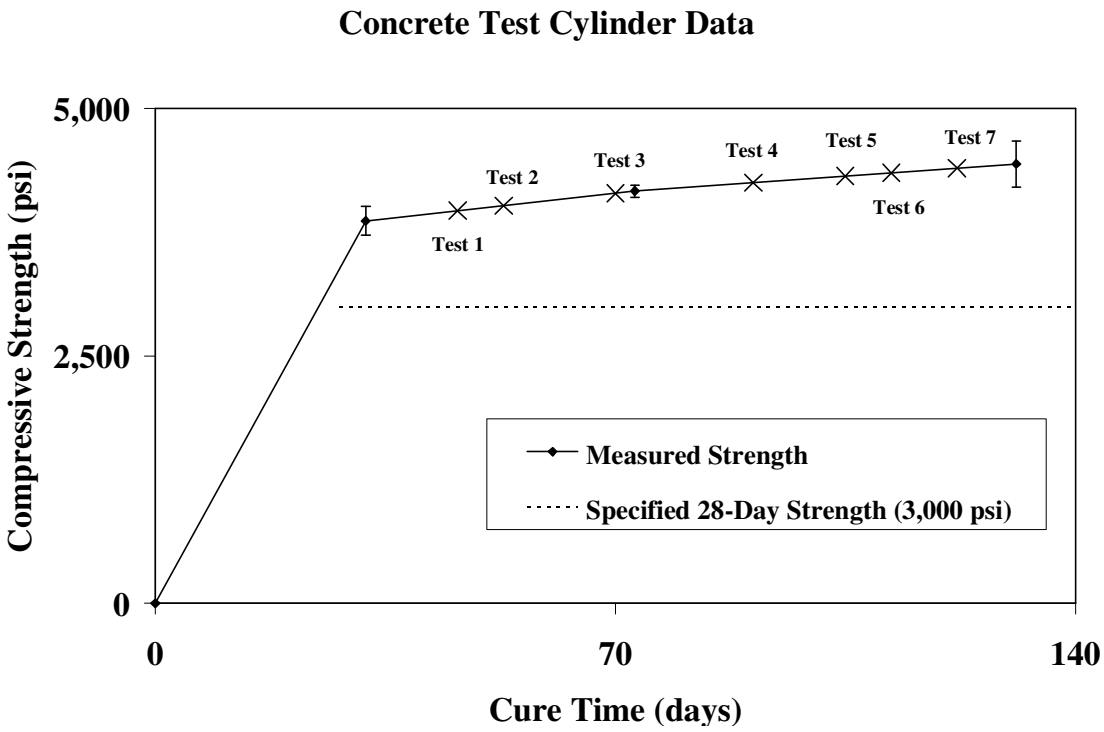

Figure 3.2 – Results of the concrete test cylinders

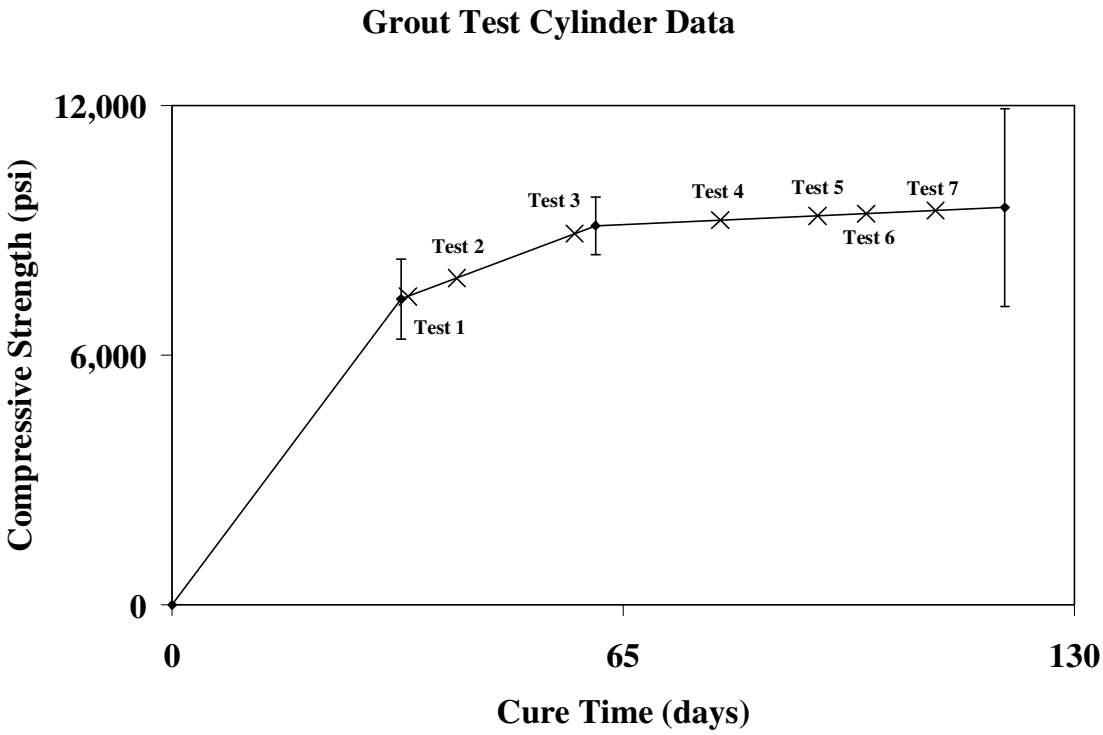

Figure 3.3 – Results of the grout test cylinders

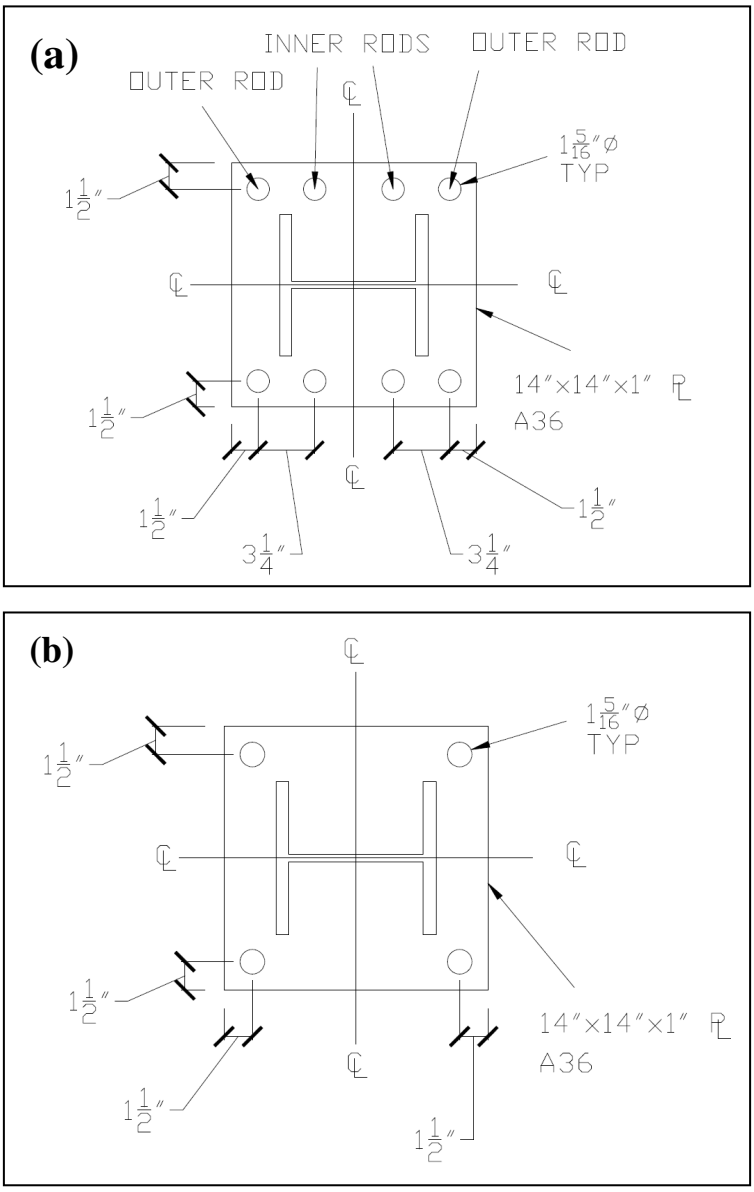

Figure 3.4 – Base plate footprints for (a) Test # 3 and (b) all other tests

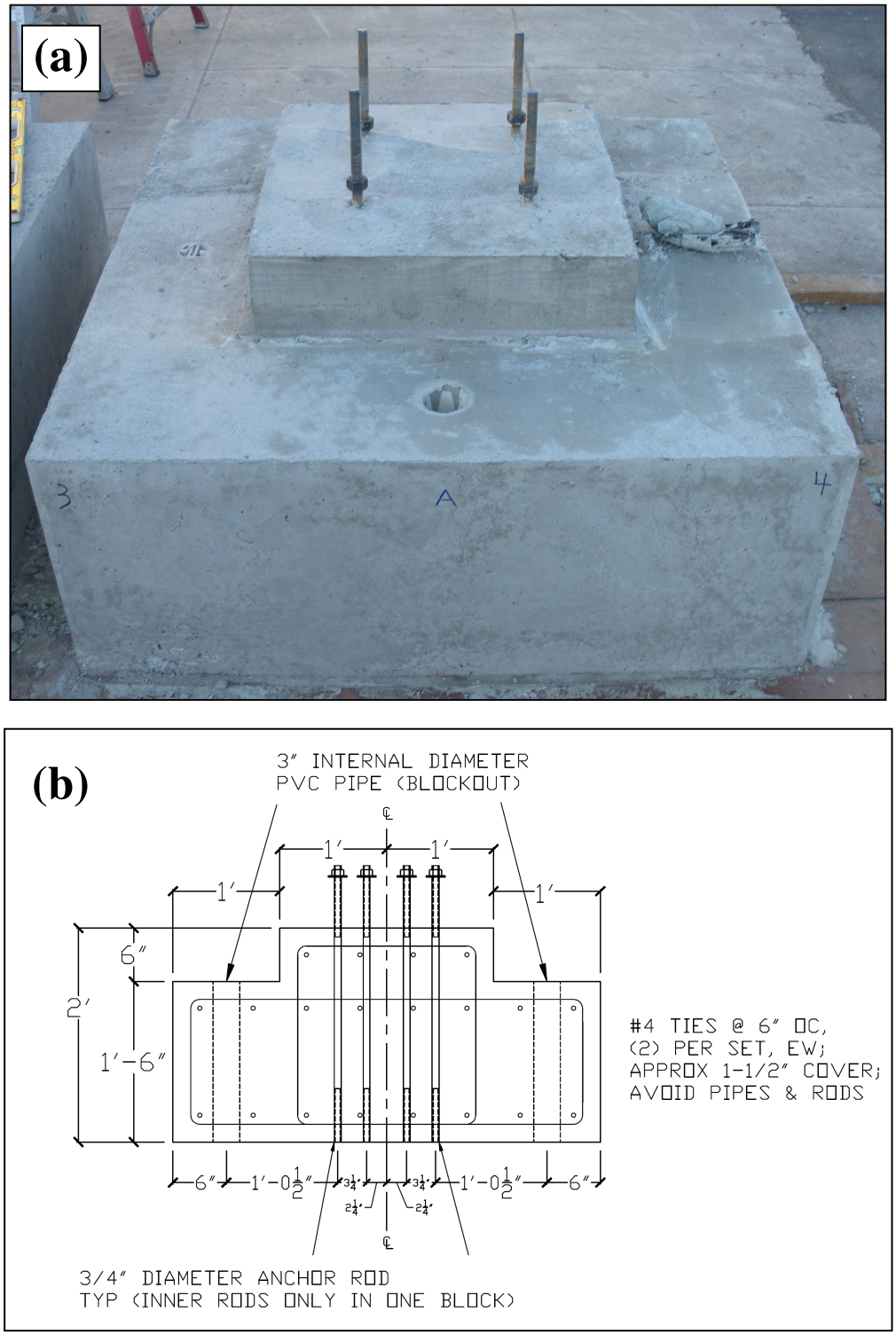

Figure 3.5 – (a) Photograph and (b) schematic illustration of the concrete footing pedestal

Figure 3.6 – Leveling (setting) nut detail

Figure 3.7 – Detail of anchor rod nut and washer assembly

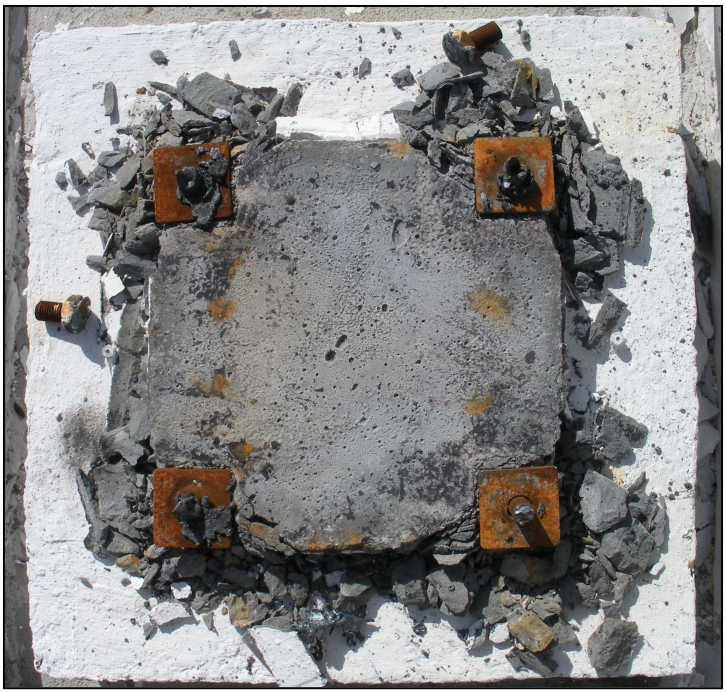

Figure 3.8 – Representative photograph of the grout pad after testing (shown here for Test #5)

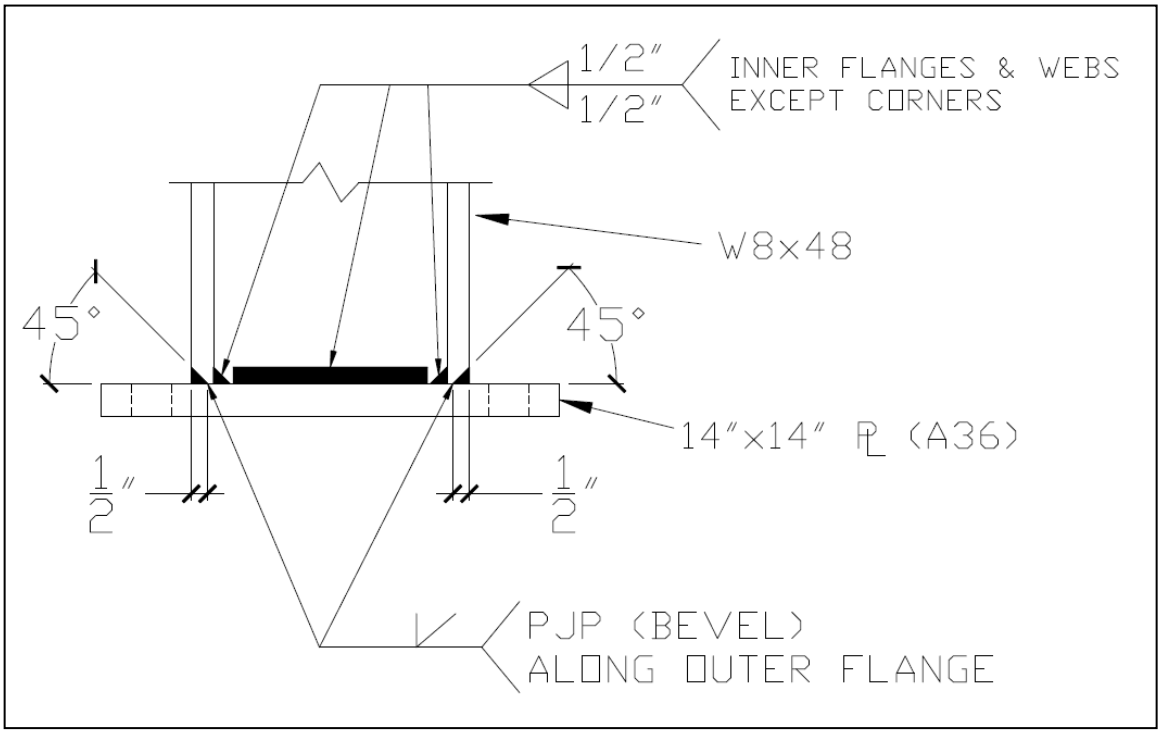

Figure 3.9 – Column to base plate weld detail

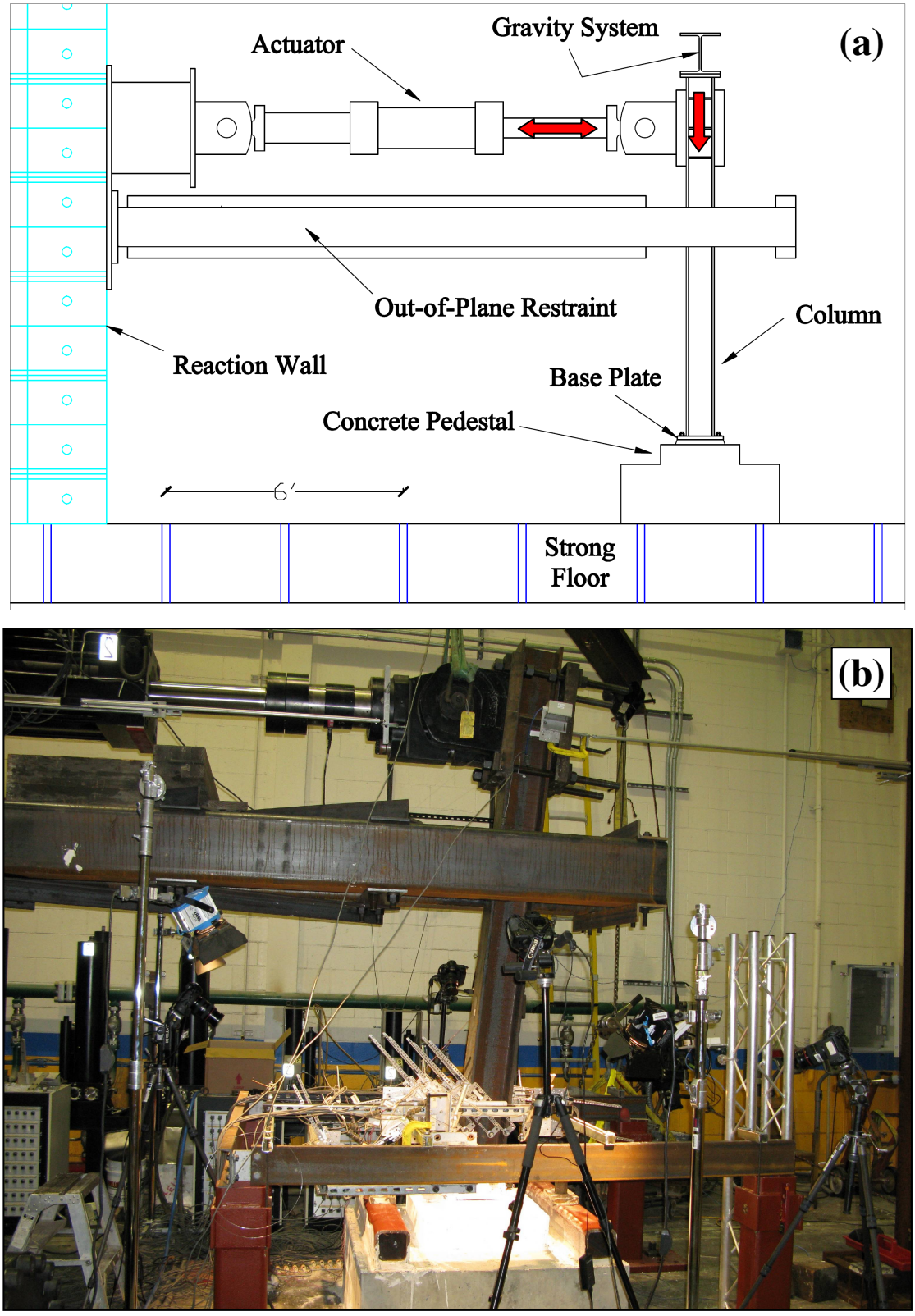

Figure 3.10 – Typical test setup (a) schematic and (b) photograph

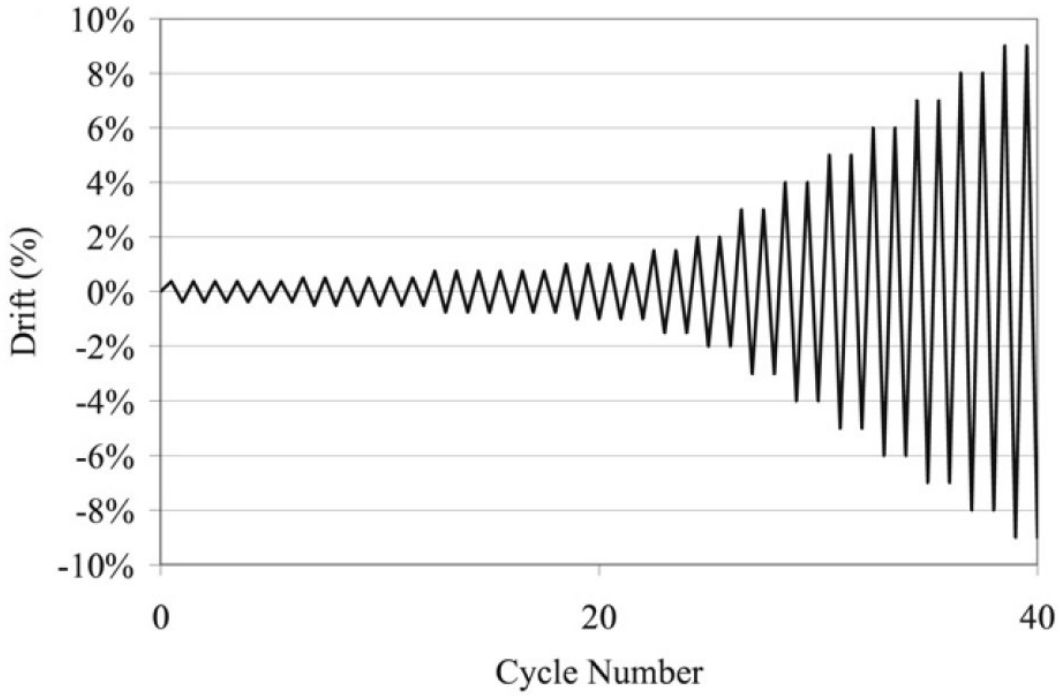

Figure 3.11 – Typical cyclic loading protocol

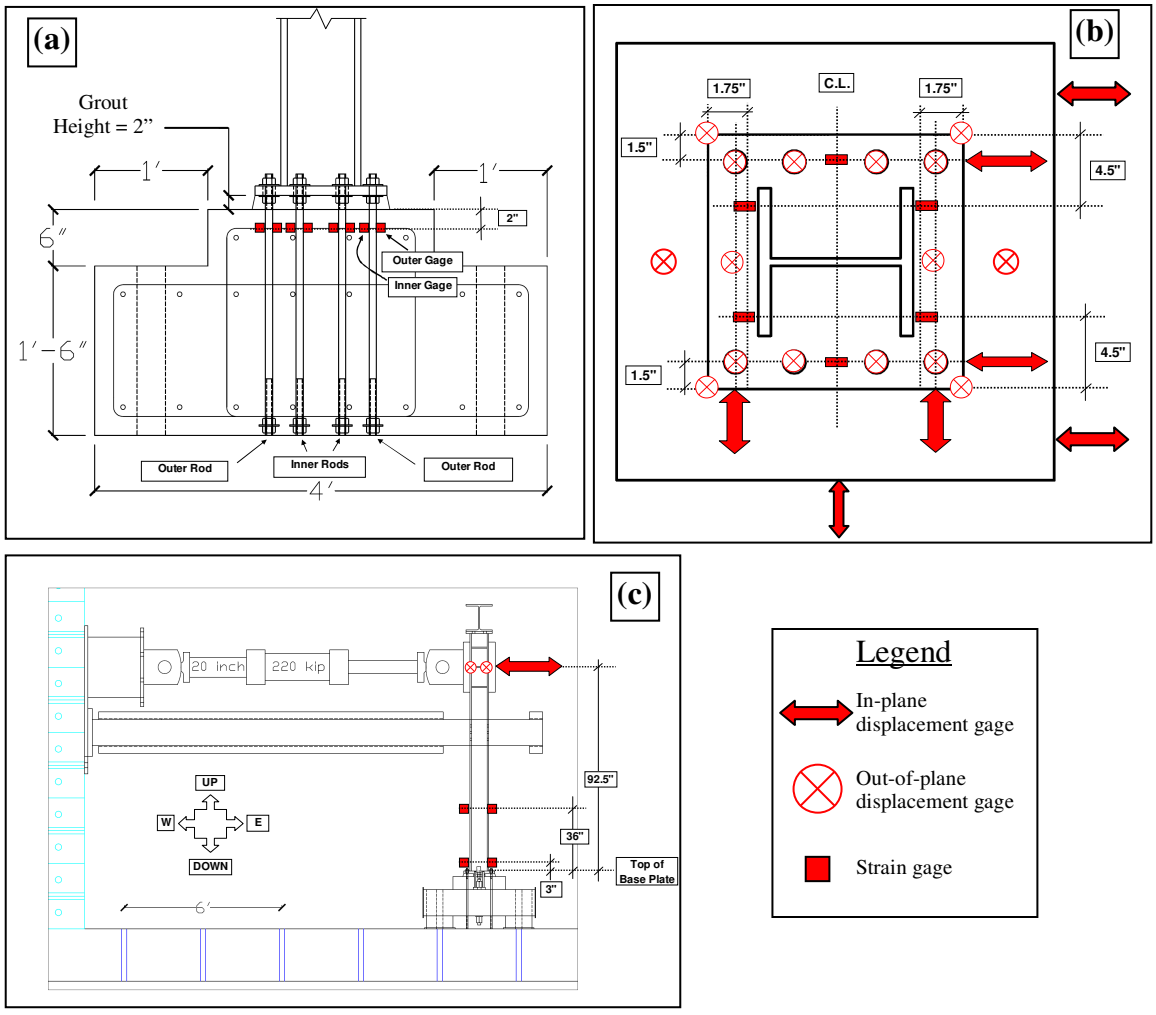

Figure 3.12 – Typical instrumentation layout

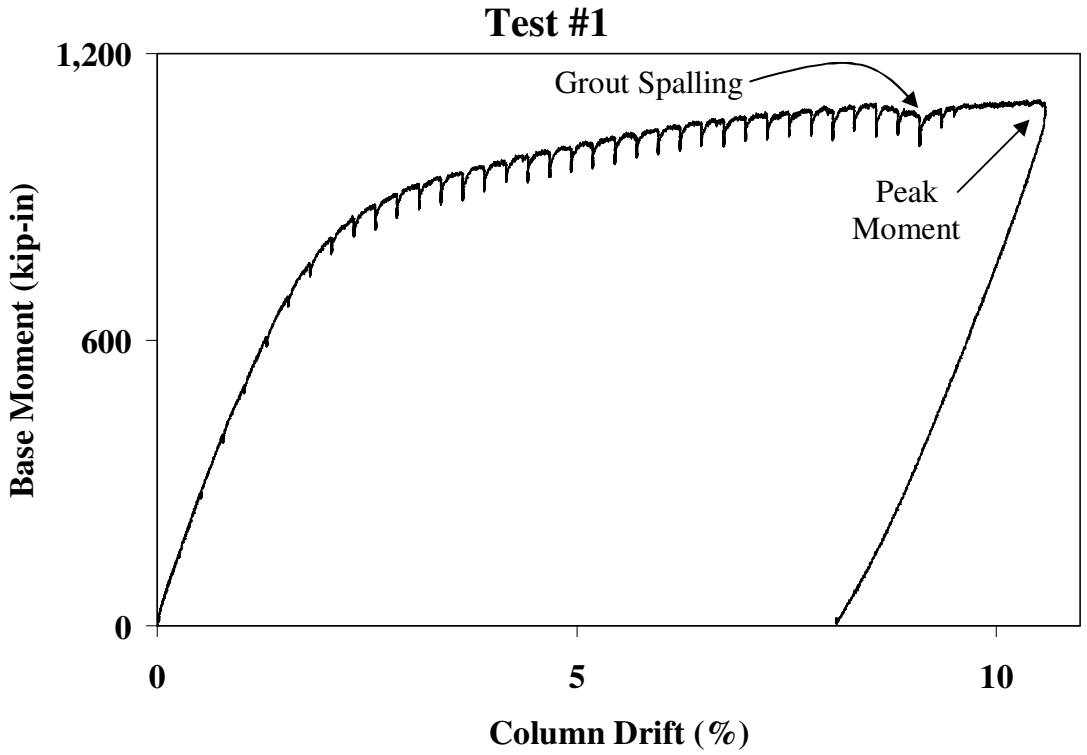

Figure 3.13 – Test #1 response – 1.0" thick base plate, four Grade 105 rods, zero axial load

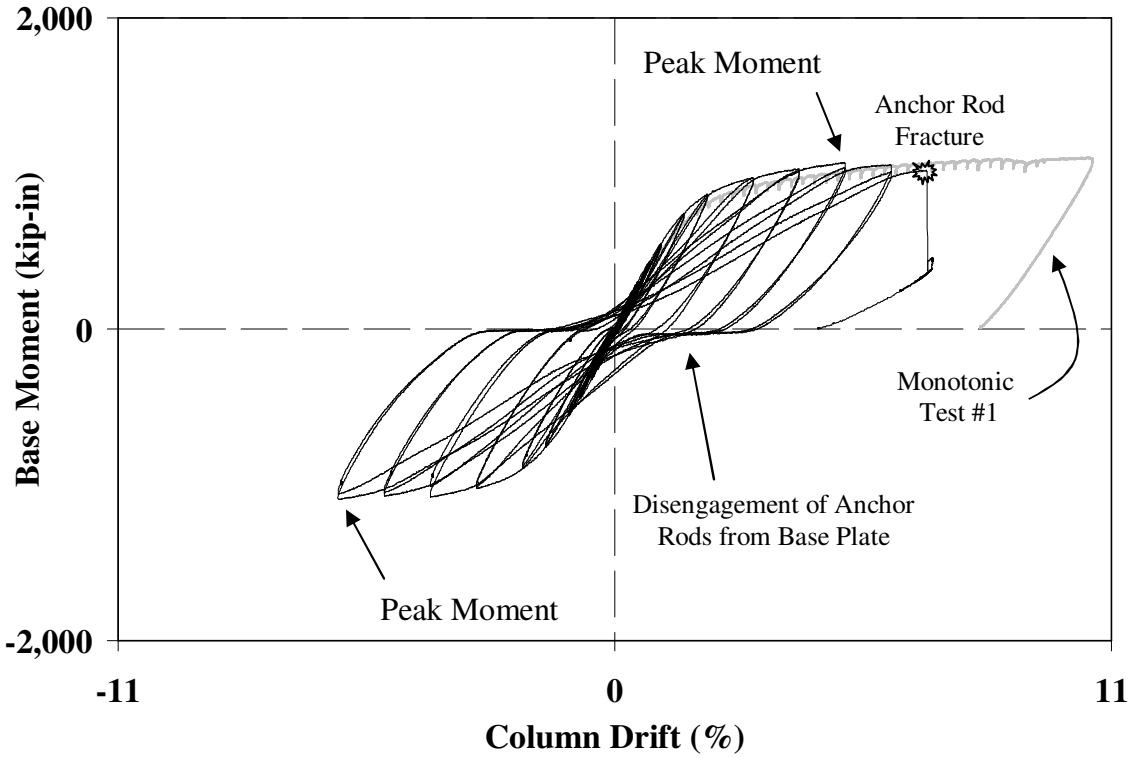

Figure 3.14 – Test #2 response – 1.0" thick base plate, four Grade 105 rods, zero axial load

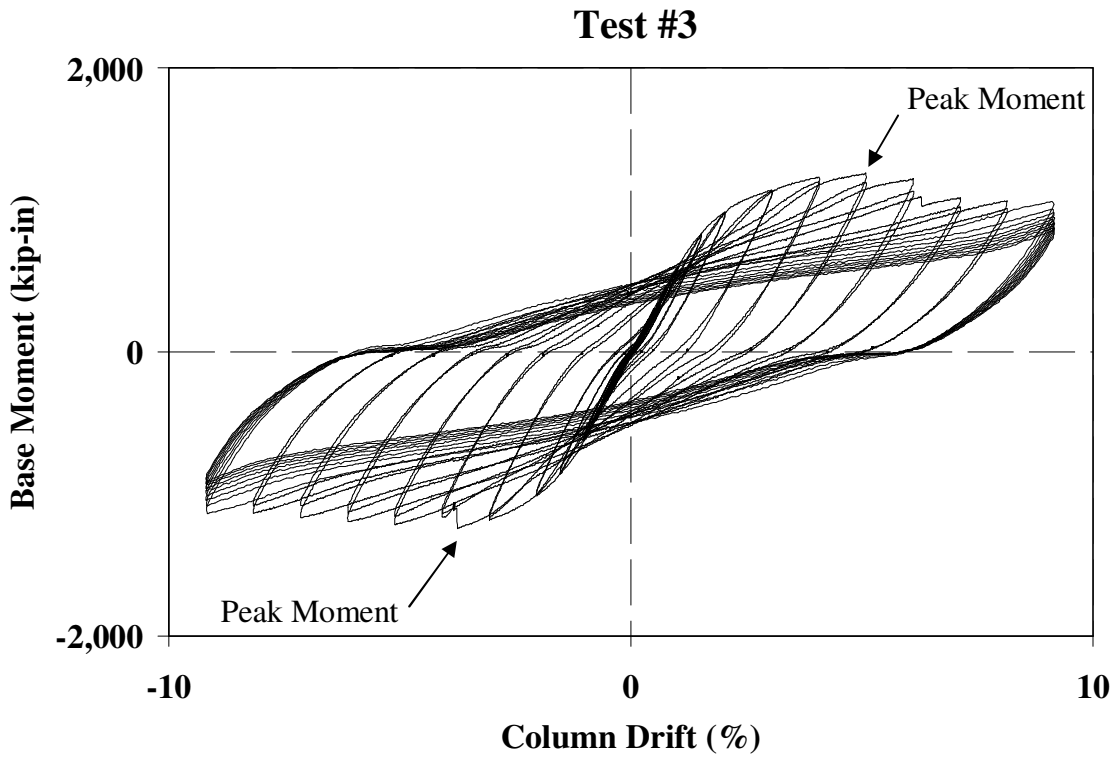

Figure 3.15 – Test #3 response – 1.0" thick base plate, eight Grade 105 rods, zero axial load

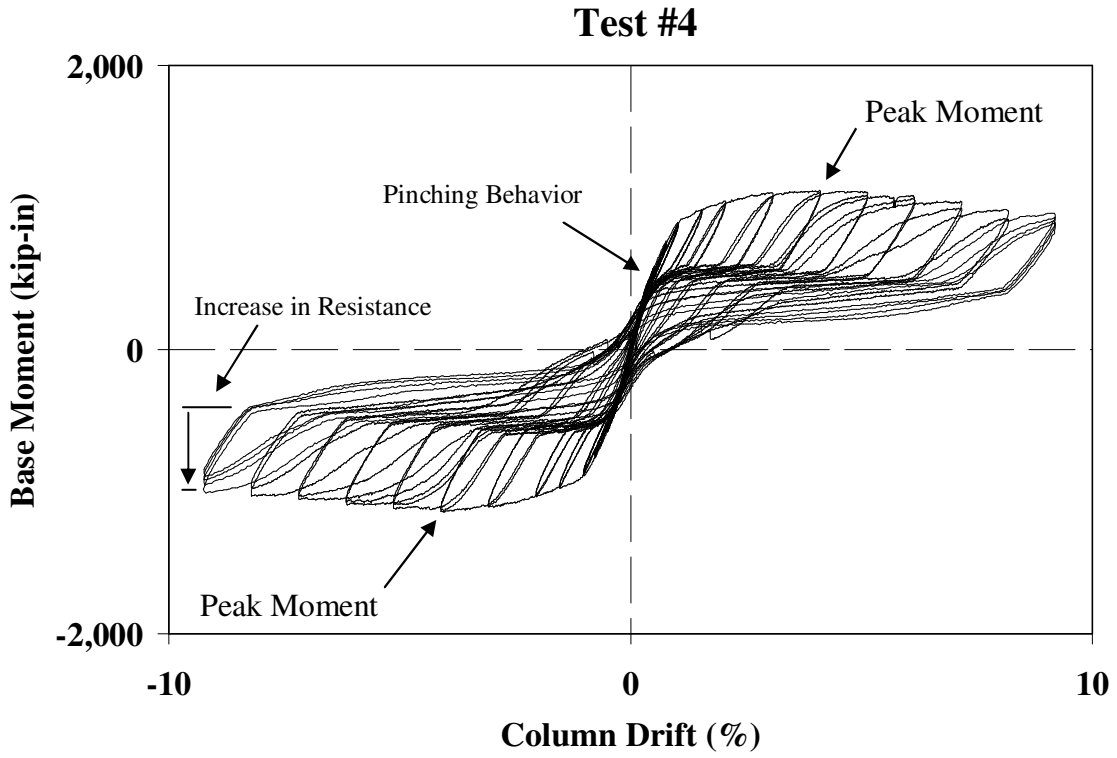

Figure 3.16 – Test #4 response – 1.5" thick base plate, four Grade 36 rods, 92.5 kips axial load

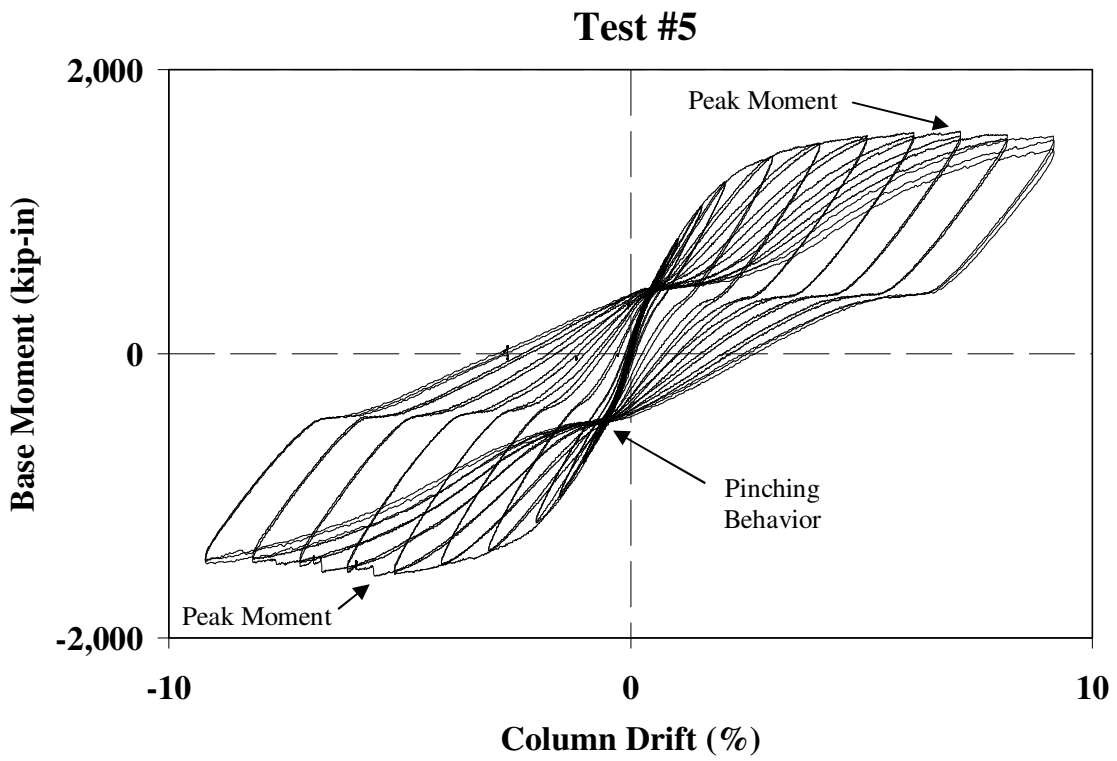

Figure 3.17 – Test #5 response – 1.0" thick base plate, four Grade 105 rods, 92.5 kips axial load

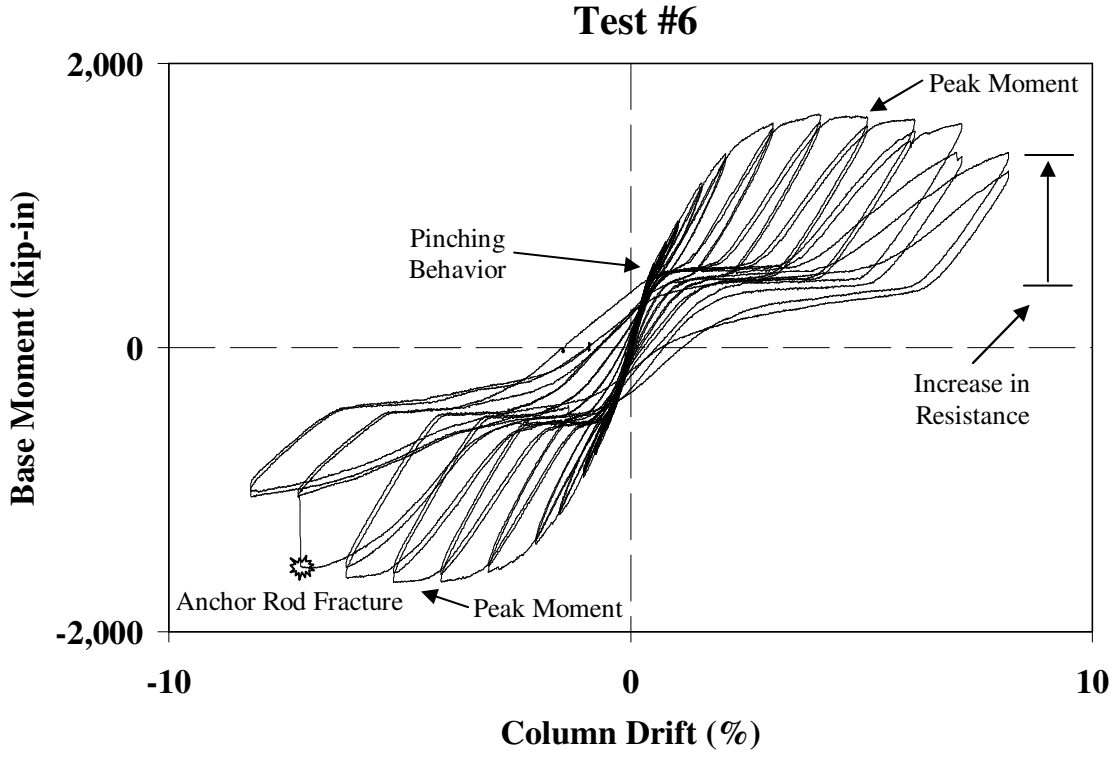

Figure 3.18 – Test #6 response – 2.0" thick base plate, four Grade 105 rods, 92.5 kips axial load

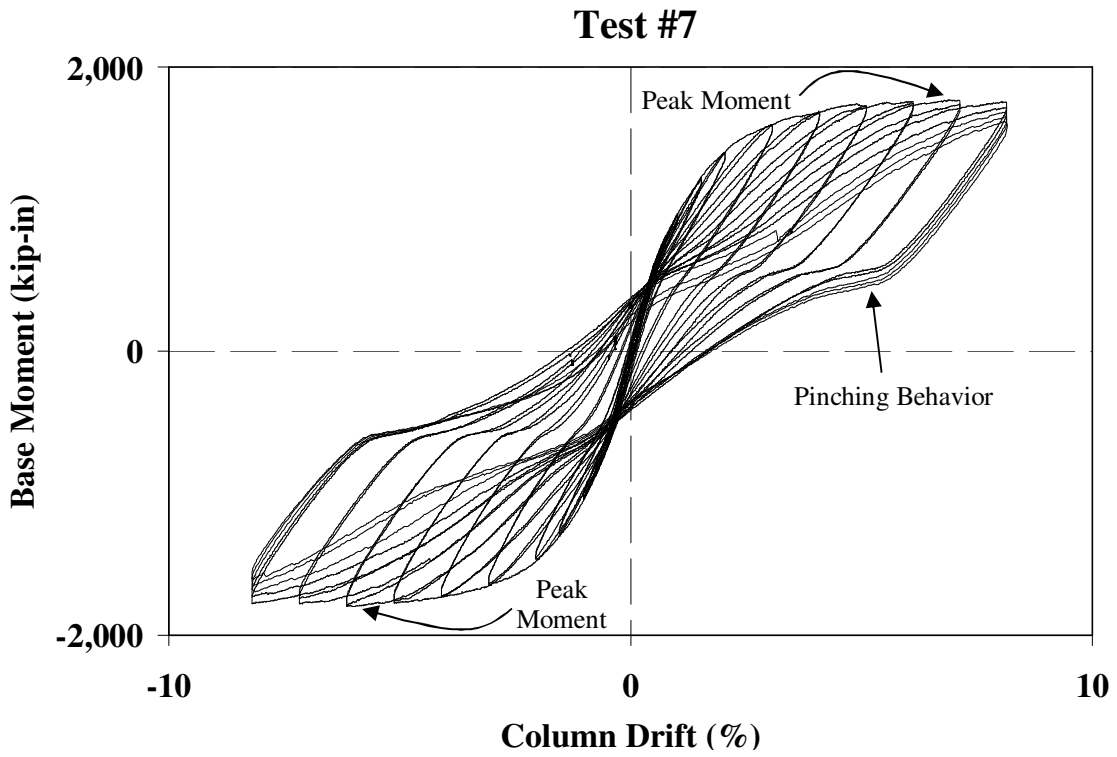

Figure 3.19 – Test #7 response – 1.0" thick base plate, four Grade 105 rods, 152.5 kips axial load

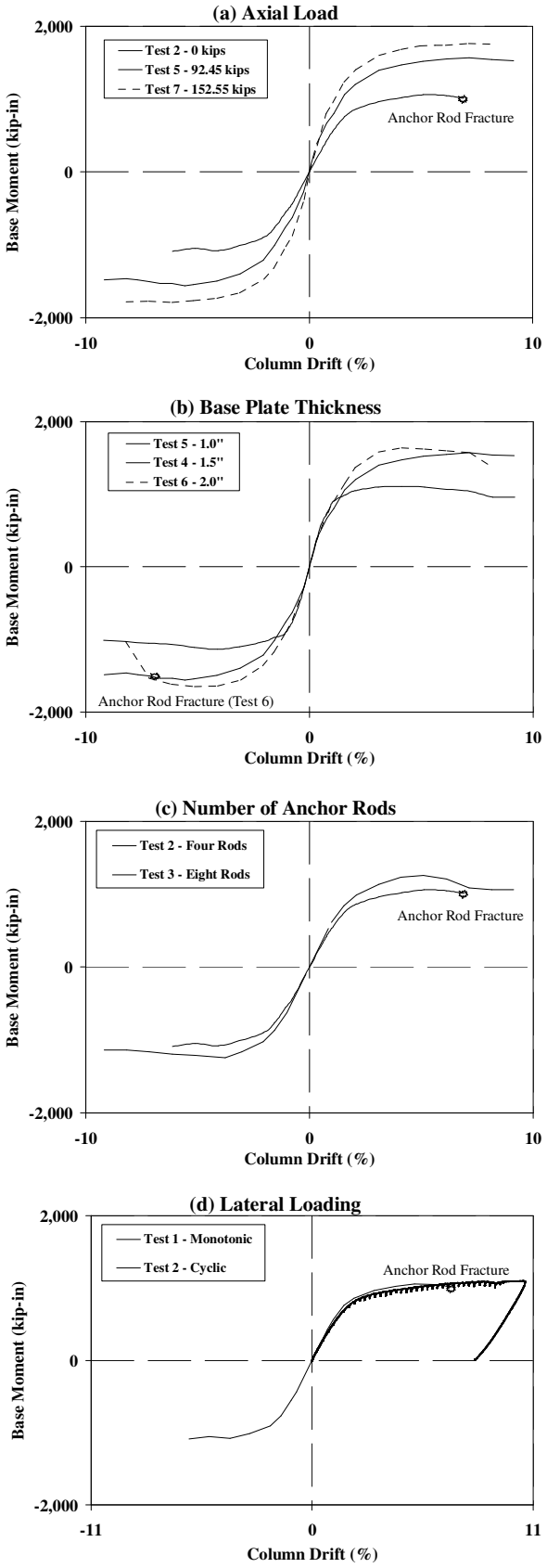

Figure 3.20 – Envelope (backbone) curves of the experimental response

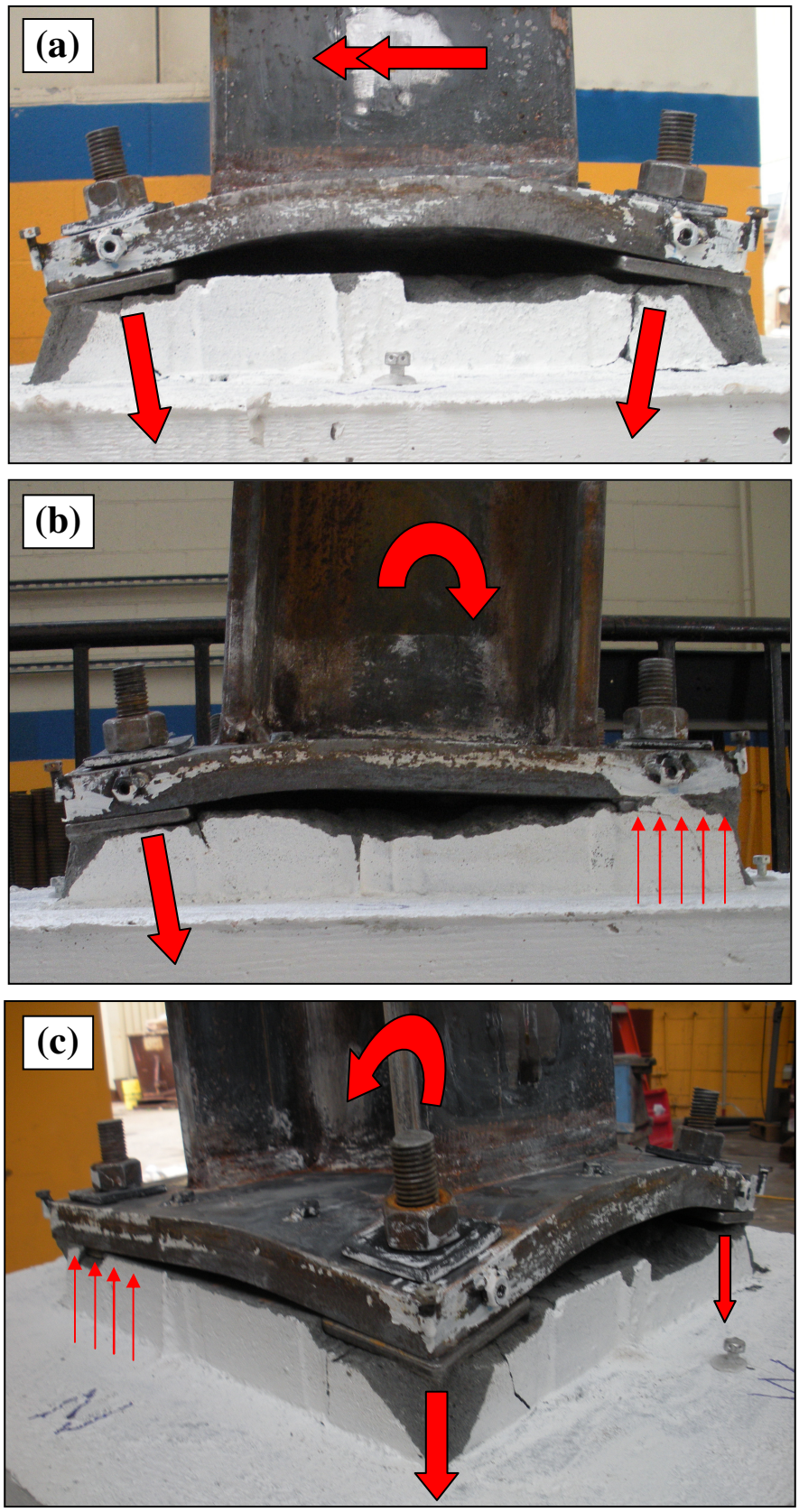

Figure 3.21 – Post-test (a) tension side view (b) side view and (c) isometric view of the plastic deformation of Test #1 with schematics of ideal imposed and resisting forces

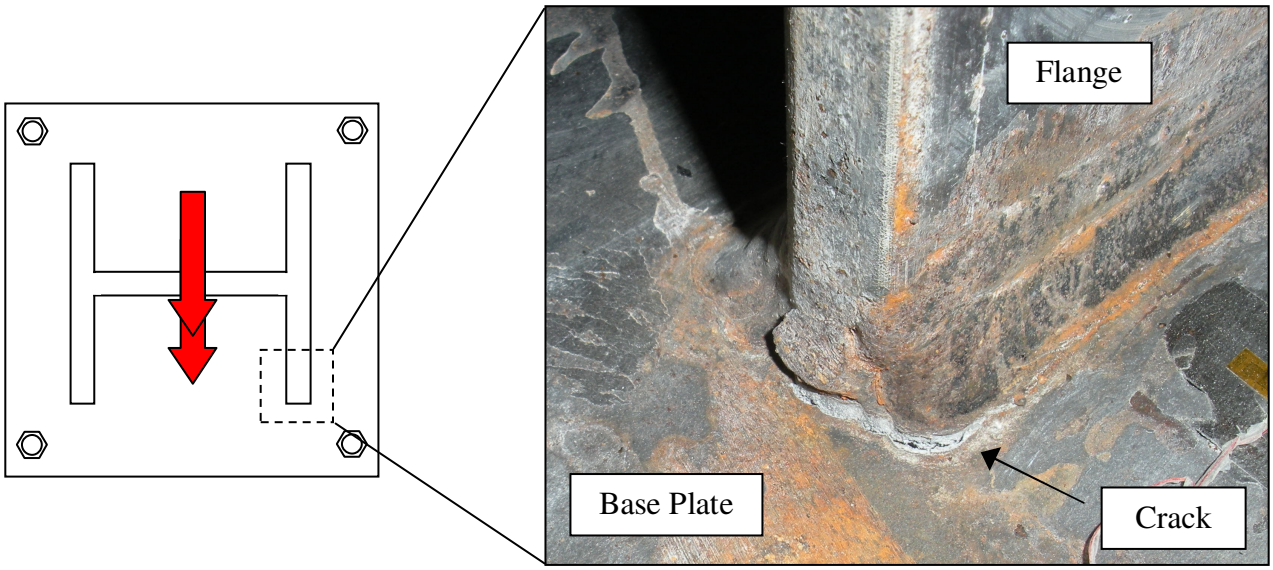

Figure 3.22 – Fracture initiation of the column to base plate weld (shown here for Test #1)

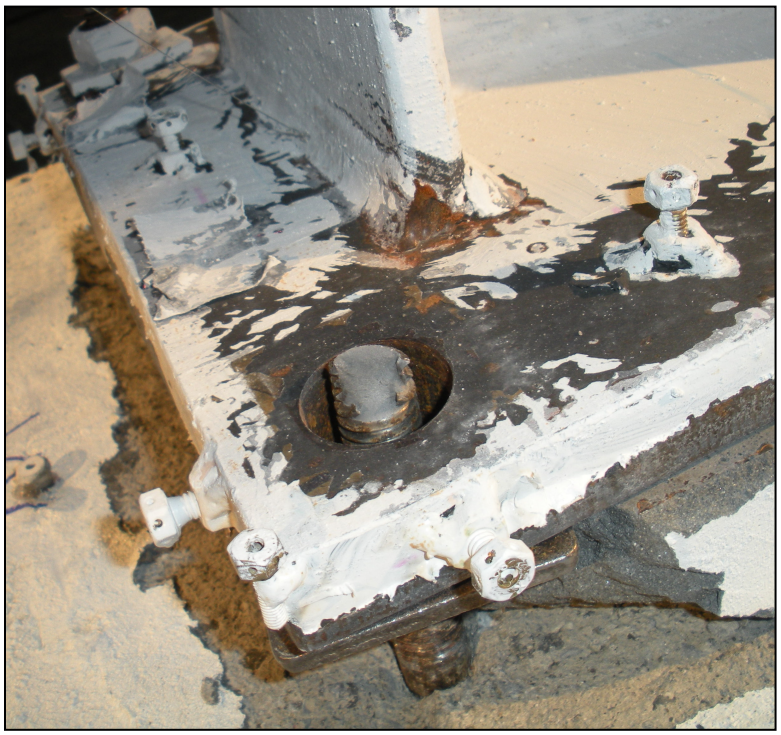

Figure 3.23 – Fracture of anchor rod from Test #2

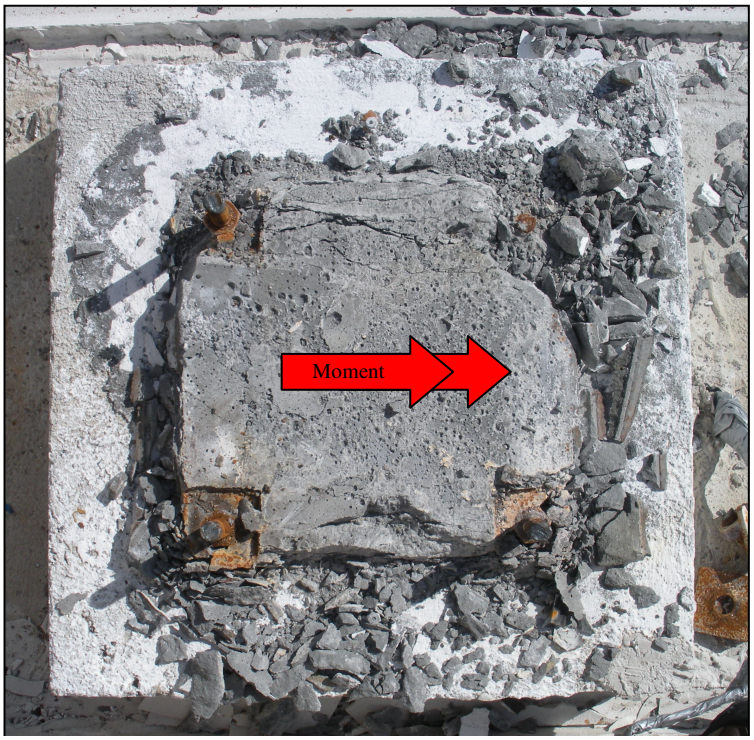

Figure 3.24 – Post-test photograph of typical grout damage (shown here for Test #6)

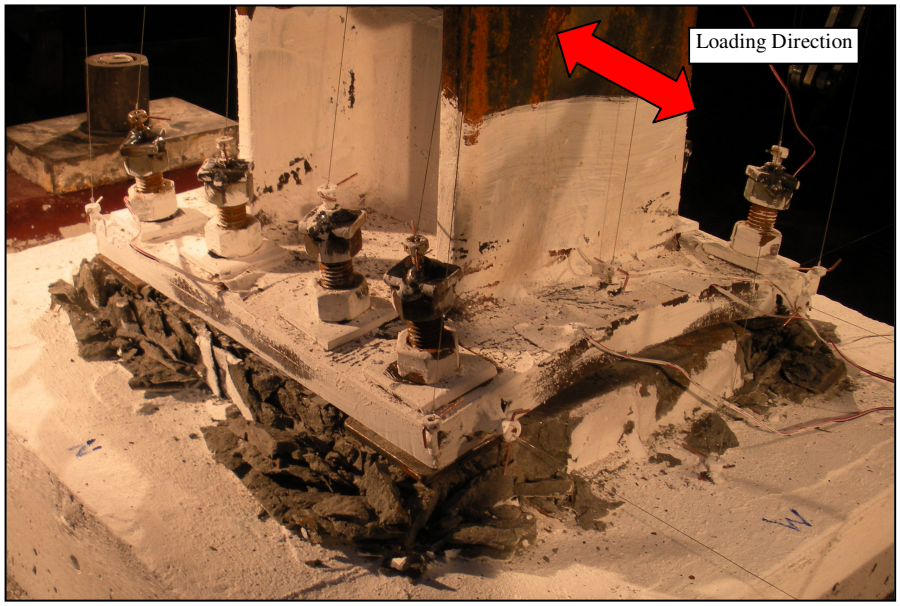

Figure 3.25 – Post-experiment photograph of Test #3

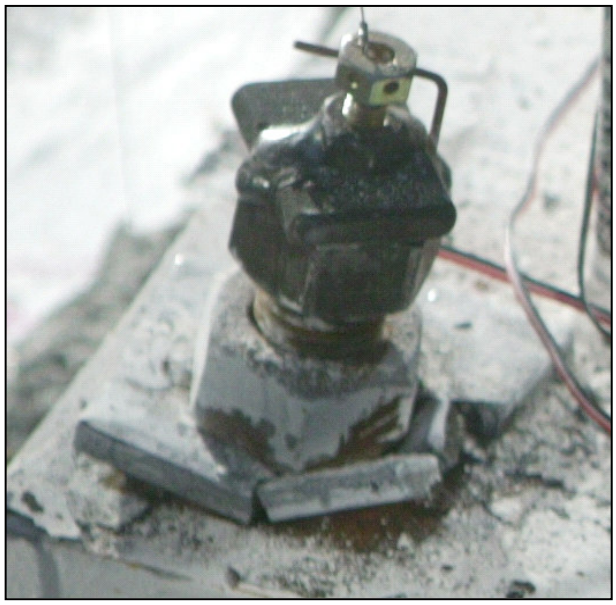

Figure 3.26 – Fracture of top plate washer of Test #6

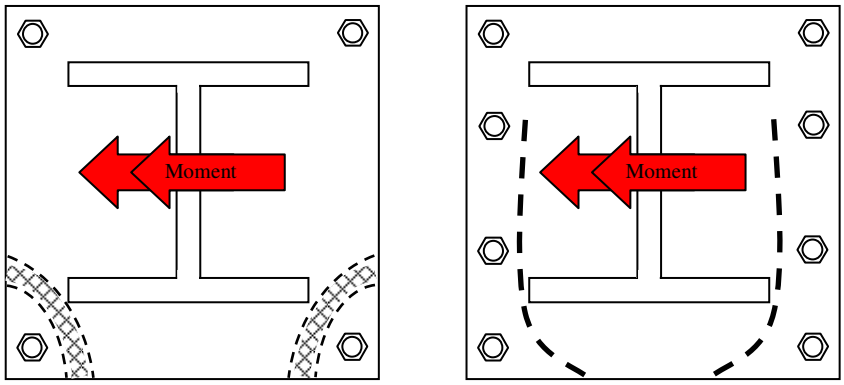

(a) Four Rod Detail **(b) Eight Rod Detail**

Figure 3.27 – Schematic of tension side base plate yield lines

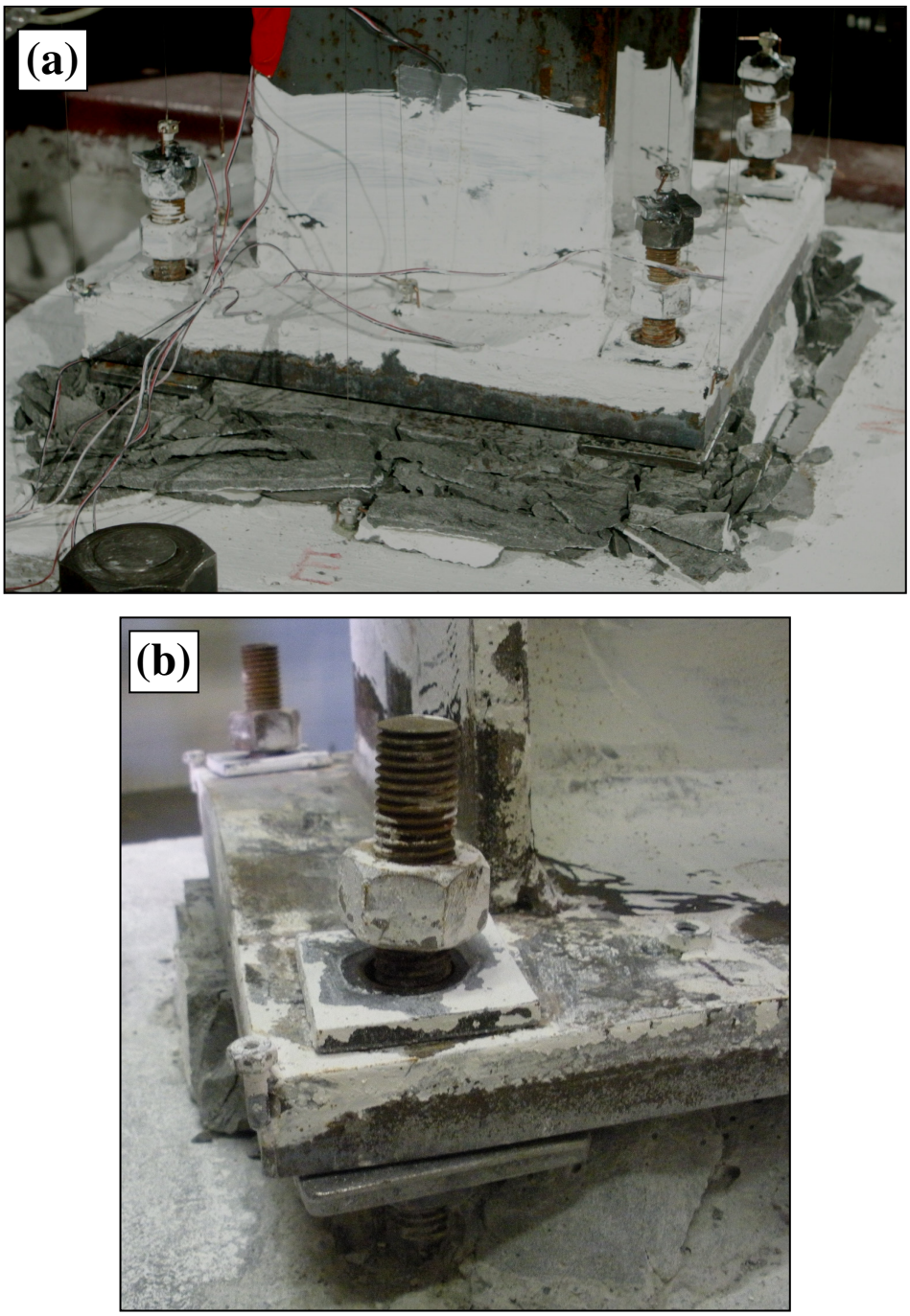

Figure 3.28 – (a) Photograph illustrating anchor rod yielding (shown here for Test #4) and (b) representative close-up of anchor rod yielding

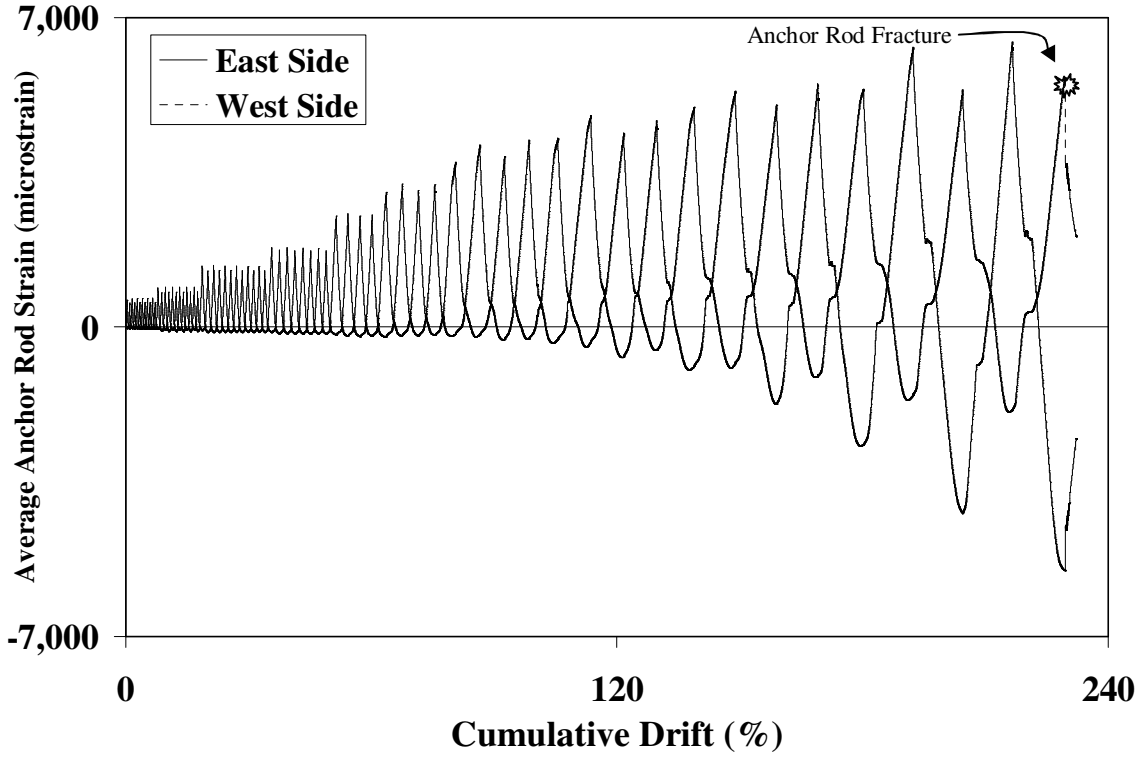

Figure 3.29 – Typical anchor rod response (shown here for Test #2)

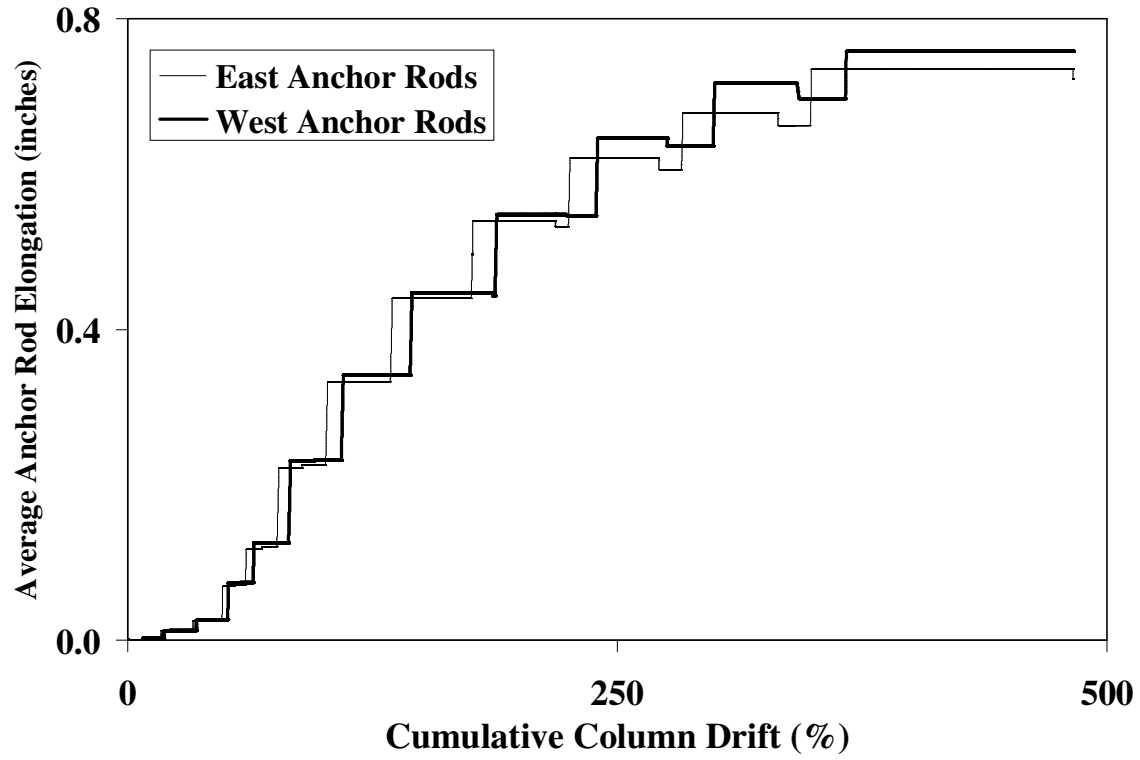

Figure 3.30 – Plot representing anchor rod elongation (shown here for Test #4)

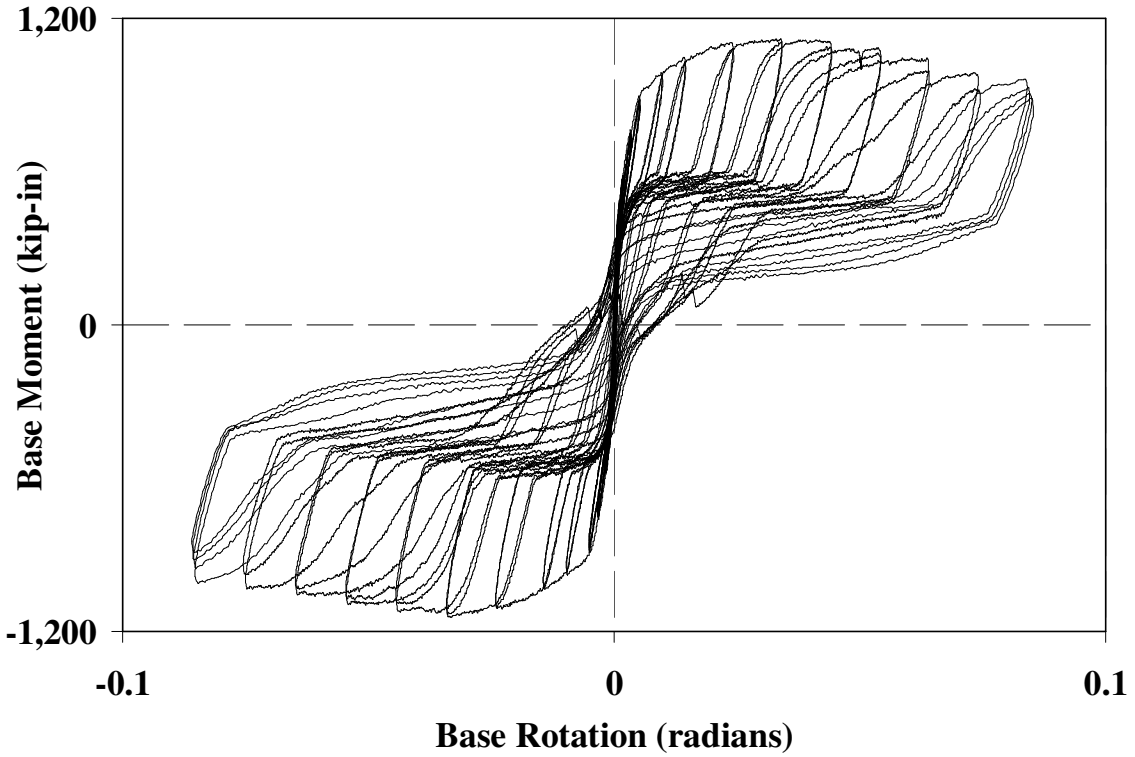

Figure 3.31 – Typical rotation-moment response (shown here for Test #4)

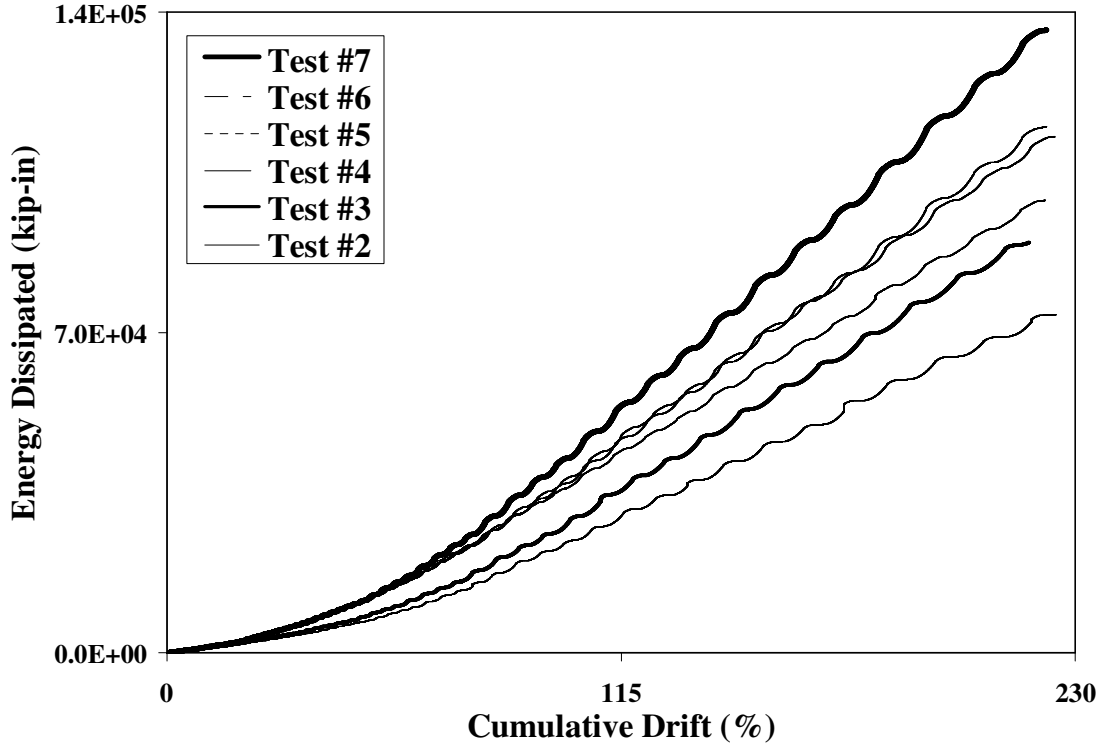

Figure 3.32 – Energy dissipation versus cumulative drift plot for every test

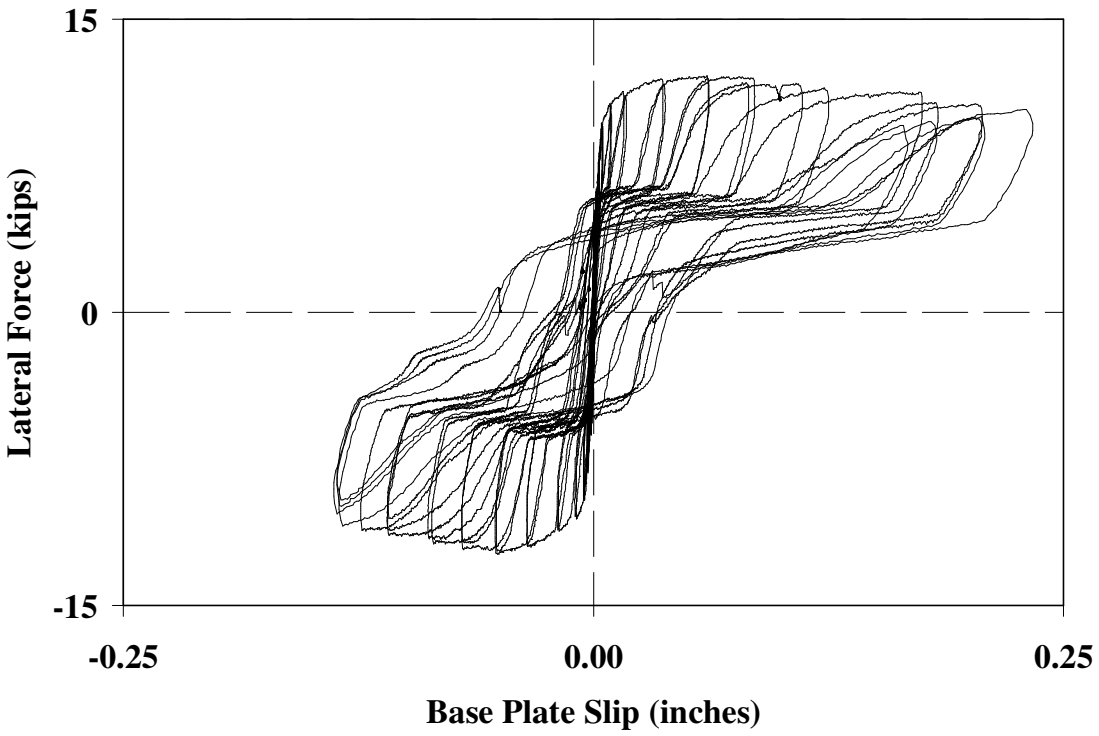

Figure 3.33 – Typical base plate slip response (shown here for Test #4)

Chapter 4

Analysis of Test Data and Strength Prediction Methods

4.1 INTRODUCTION

This chapter presents a detailed analysis of the experimental data described in Chapter 3, with the main objective of evaluating various strength prediction approaches for exposed column base connections subjected to a combination of flexural and axial loading. As discussed previously, several types of data were recovered from the column base connection tests, including hysteretic force-deformation data, as well as material strength data, both of which provide the main basis for evaluating various strength prediction methods. The force-deformation data is complemented by strain data from the anchor rods, which can be related to anchor rod forces to examine the stress distributions within the connection. In addition to the experimental strength and deformation measurements, other information, such as visual, photographic and video observations provide qualitative insights into base connection behavior.

This chapter begins by evaluating strength prediction methods for exposed column base connections, including two methods (the triangular and rectangular stress block methods) featured in the AISC *Steel Design Guide 1* (Fisher & Kloiber, 2006). Both of these methods are evaluated based on their ability to characterize the peak moment of the base connection, forces in the anchor rods and deformation (yield line) patterns in the base plate. Measured (rather than specified/nominal) material properties (for the anchor rods, base plate steel, grout, and concrete) obtained from the ancillary tests are used in the analysis of all approaches in order to accurately characterize each material. Based on the experimental data, test observations and corresponding analysis, a new method, combining favorable features from existing approaches, is presented and discussed. The chapter concludes by discussing both the implications of the proposed strength prediction method and the results of the experiments in the context of structural design.

4.2 EVALUATION OF CURRENTLY USED STRENGTH PREDICTION METHODS

Outlined previously in Section 2.2.1.1, two design methods, the elastic and the ultimate methods, featured in the AISC *Steel Design Guide 1* (Fisher & Kloiber, 2006), are the most common methods used in the United States for characterizing the strength of exposed column base connections subjected to flexure and axial loading. The elastic method, referred to as the Triangular Stress Block (TSB) method, assumes that the combination of applied axial force and moment is resisted through the development of a triangular/trapezoidal compressive stress distribution in the concrete/grout foundation below the base plate and, as the base plate uplifts, the development of tensile forces in the anchor rods. The ultimate strength method, referred to hereafter as the Rectangular Stress Block (RSB) method, is similar to the TSB method, except that it assumes the development of a rectangular bearing stress distribution that approximates the ultimate compression/tension force in the concrete/grout. Figure 2.1, introduced previously, illustrates the assumed stress distributions for both methods and Appendix D presents the theory of these methods in detail. The following sections discuss both of these methods and evaluate their efficacy based on two criteria (1) their ability to characterize the maximum moment capacity of the connection under a constant axial load, and (2) their ability to characterize the anchor rod forces in the base connection. In addition, agreement of the experimentally observed plastic deformation patterns with assumed yield line patterns is discussed and analyzed. The sections conclude by summarizing the advantages and disadvantages of both design approaches.

4.2.1 The Triangular Stress Block (TSB) Method

The TSB approach considers two flexural loading conditions, characterized by either a low or high load eccentricity[1]. Under low eccentricity, the applied axial force and moment combination is assumed to be resisted exclusively through the development of a linear (i.e. triangular or trapezoidal shaped) bearing stress distribution beneath the base plate. The separation between the low and high eccentricity case is defined by a critical eccentricity as calculated per Equation (D.1) in Appendix D. This definition of the critical eccentricity is different than the critical eccentricity presented in the *Design*

[1]Load eccentricity is defined as the applied base moment divided by the applied axial load.

Guide 1 (Fisher & Kloiber, 2006). The critical eccentricity presented in the *Design Guide 1* (defined as one-sixth the base plate length; often called the kern of the base plate) does not consider the effect of the applied axial load[2]. As discussed previously by Drake and Elkin (1999) and verified during this study, defining the critical eccentricity as the kern of the base plate may result in unphysical, but otherwise mathematically acceptable, solutions which require compression in the anchor rods during high eccentricity (i.e. uplift) conditions in order to satisfy equilibrium. When the load eccentricity exceeds the critical eccentricity, the applied axial force and moment combination can no longer be resisted by bearing stresses alone and equilibrium requires the development of tensile forces in the anchor rods.

For low load eccentricities, failure of the connection is a result of flexural yielding of the plate from bearing stresses acting beneath the base plate[3]. For high load eccentricities, the base plate is assumed to lift off from the concrete/grout foundation. Consequently, it is somewhat challenging to generate a bearing stress distribution which explicitly satisfies both equilibrium and compatibility. Therefore, the high eccentricity condition is analyzed through the simplifying assumption that the maximum bearing stress is equal to the limit of the bearing strength of the concrete.[4] From this assumption, the principles of statics may be applied to determine both the forces in the anchor rods as well as the area over which bearing is active. Accordingly, under high eccentricity, concrete crushing is not considered explicitly as a failure mode, since the formulation cannot characterize the strain in the concrete/grout at the extremity of the base plate. In reality, concrete/grout crushing is a possible mode of failure (as observed during testing) although it is not

[2]As a clarification, in the *Design Guide 1*, the kern of the base plate is assumed invariant with respect to the level of axial load present in the base connection, i.e. it is always assumed as one-sixth of the base plate width. While this is based on a conventional strength of materials approach, it does not yield physically acceptable solutions when a large axial load is present. For example, if an axial load close to the bearing strength of the foundation is present, then obviously even a slightly eccentric load cannot be resisted by the bearing distribution alone. The modified definition of the kern outlined in Appendix D adjusts for this effect.

[3]Concrete/grout crushing/bearing failure is precluded as per the guidelines described in the AISC *Design Guide 1*, which requires base plate dimensions large enough to limit bearing stresses to the concrete ultimate bearing strength.

[4]Other bearing stress distributions may satisfy equilibrium, but none can be shown to explicitly satisfy compatibility and thus are all arbitrary. Consequently, a stress distribution which prescribes that the maximum bearing stress equals the limit strength of concrete is conservative for connection strength prediction, since it provides the most severe condition for flexural yielding of the base plate.

specifically addressed in the *Design Guide 1*. Thus, the only failure modes possible under high load eccentricities are (1) flexural yielding of the base plate due to bearing stresses (2) flexural yielding of the base plate due to forces imposed by the anchor rods on the tension side of the connection and (3) tensile failure of the anchor rods themselves. Consequently, the design of base connections involves determining a combination of anchor rod size/strength and layout, as well as base plate size and thickness/strength, such that each of these failure modes is precluded. The AISC *Design Guide 1* (Fisher & Kloiber, 2006) presents several design examples based on both the TSB and RSB methods.

4.2.1.1 Predictions of Maximum Moment Capacity

Evaluating the predicted ultimate strength with respect to the observed peak strength during testing provides the best assessment of TSB and RSB methods. However, it is interesting to note that both methods outlined in the *Design Guide 1* (Fisher & Kloiber, 2006) do not explicitly outline a procedure to characterize the strength capacity of the base connection, but rather require that all components in the connection (i.e. anchor rods and base plate) be designed to withstand force demands corresponding to an applied base moment and axial force combination. Thus, TSB method, as outlined in the *Design Guide 1* implicitly assumes that the connection will reach a limit state and fail when any one of the components reaches its individual limit state. Consequently, this type of "first-yield" estimate of the base connection is the only strength estimate available for comparison with the experimental data. Thus, this “first-yield” capacity is evaluated in this section for the TSB method, as well as in Section 4.2.2.1 for the RSB method.

Low and high eccentricity loading situations, as modeled by the TSB and RSB methods, are common for statically loaded column base connections. However, under seismic conditions (e.g. as simulated in the current experiment study), a base connection may be loaded in a non-proportional manner, such that the axial load is held constant[5] while flexural deformations are varied and reversed. Thus, for purposes of evaluating the

[5]Certain situations of seismic loading may induce overturning moments in the structure such that the axial load would not remain constant.

experimental results from this study, the maximum moment capacity of the base connection under a given axial load is calculated and compared to test data.

The analytical procedure of the TSB and RSB method, based on equations derived in Appendix D, is implemented through a computer program presented in Appendix E. The axial load, base plate geometry and concrete/grout strength are input parameters while the applied moment is increased in a stepwise fashion. For each value of applied moment M_{base}, the load eccentricity is determined as being either low or high as per Equation (D.1) in Appendix D. Correspondingly, the bearing stress distribution under the base plate is determined, and three key output quantities are calculated for each value of applied moment including (1) the tensile force T_{rod} in both of the anchor rods, (2) the bending moment[6] M_{comp} (expressed as per-unit-width) across an assumed yield line on the compression side of the connection, produced by the bearing stresses acting upwards on the base plate (see Figure 2.3a and D.1 for an illustration of the assumed yield line, which is oriented parallel to the column flange and located near the edge of the column flange) and (3) the bending moment M_{tens} (expressed as per-unit-width) across the same assumed yield line on the tension side of the connection, produced by the tensile forces from the anchor rods acting downwards on the base plate.

Figure 4.1 shows the evolution of each of these three quantities (M_{comp}, T_{rod} and M_{tens}) with respect to the applied base moment M_{base} for Test #4. The plot includes two vertical axes; the left vertical axis corresponds to the tensile force demand on both anchor rods while the right vertical axis corresponds to the flexural demand on a per-unit-width of the base plate. Also shown in Figure 4.1 are the capacities of the base plate in bending and the anchor rods in tension. The bending capacity of the base plate R_{plate} is determined based on the plastic section modulus and yield strength of the base plate, while the tensile capacity of the anchor rod R_{rod} is calculated based on the measured ultimate tensile

[6] Note that M_{comp} and M_{tens} represent internal bending moments of the base plate, in contrast to the value of M_{base} which reflects the moment applied to the column base connection.

strength of the anchor rods. From Figure 4.1, the value of the base moment M_{base} corresponding to each of the three failure mechanisms (i.e. M_{base}^{comp}, M_{base}^{tens} and M_{base}^{rods}) may be calculated. Similar capacity/demand plots are generated for each test specimen and are presented in Appendix E.

Referring to the plot in Figure 4.1, several observations regarding the TSB prediction method may be made –

- Both the force in the anchor rod T_{rod} and bending moment on the tension side of the base plate M_{base}^{tens} are zero for low moments (less than 595 kip-in for Test #4) due to the low eccentricity condition discussed above.
- At zero applied base moment, a bending moment demand is imposed on the compression side of the base plate due to the imposed axial compressive load. This is due to the upward bearing pressure on the base plate.
- For lower base moments, (less than 3,324 kip-in for Test #4), the flexural demand on the compression side of the base plate M_{comp} is greater than the flexural demand on the tension side (M_{tens}).
- At higher base moments (greater than 5,937 kip-in for Test #4), the TSB is unable to provide a solution. At this base moment value, the extent of the bearing length approaches the location of the anchor rods and tension forces in the rods asymptotically approach infinity. Due to this situation, the TSB method is invalid for base plate geometries under certain load combinations. In practice, this represents situations where the size of the base plate and/or the location of the anchor rods must be modified to produce acceptable solutions.[7]

[7] Recall that grout failure is not considered a limit state, since it is assumed that the base plate size is selected to limit the stresses in the grout. However, the method cannot directly account for grout spalling/failure due to large strains, since the strains cannot be estimated within the framework of the method. In reality, it is expected that the grout will fail/spall before the large moments shown in Figure 4.1 are reached.

Figures 4.2-4.8 plot the column drift versus base moment curves for the seven experiments. For each plot, the three values of M_{base}, corresponding to the three failure modes (i.e. M_{base}^{comp}, M_{base}^{tens} and M_{base}^{rods}) described in the preceding discussion, are overlaid on the test response. As per current design procedures, featured in the *Design Guide 1* (Fisher & Kloiber, 2006), the *minimum* of these values reflects the design strength of the column base connection. Table 4.1 compares the predicted base moment, corresponding to each failure mode, with the peak base moment (averaged from both loading directions) and the base moment at 4% drift (also averaged from both loading directions) observed in the experiments. A 4% drift level is approximately representative of peak drift demands in moment frames based under rare earthquakes (Gupta and Krawinkler, 1999). In addition to plate bending capacity based on the plastic section modulus and yield strength of the plate material (i.e. $R_{plate} = Z_x \cdot F_y$) as assumed by the *Design Guide 1* procedure (Fisher & Kloiber, 2006), Table 4.1 lists the predicted base moment considering the ultimate strength of the plate material (i.e. assuming full strain hardening; $R_{plate} = Z_x \cdot F_u$). Also included in the Table are predicted base moments considering alternate bending yield line patterns on the tension side of the base plate not addressed in the *Design Guide 1*. A description and analysis of alternate yield lines is presented in Section 4.2.1.3.

A closer examination of Figures 4.2-4.8 and Table 4.1 reveals several key points which provide insight into the efficacy of the TSB method as applied by the *Design Guide 1* (Fisher & Kloiber, 2006). In summary, these are –

- For five tests (i.e. Tests #1, #2, #4, #5 and #7), the lowest predicted M_{base} corresponds to flexural yielding of the base plate on the compression side, i.e. M_{base}^{comp} governs the capacity of these test specimens under the applied axial load. In these cases, it is observed that this value of M_{base}^{comp} is significantly lower (i.e. the predictions are very conservative) as compared to the maximum moment measured experimentally (i.e. the average test-to-predicted ratio is 2.04). For one test (i.e. Test #6), the lowest M_{base} corresponds to the tensile capacity of the anchor rods, i.e. M_{base}^{rods}

governs the capacity of this test specimen under the applied axial load. In this case, it is observed that the value of M_{base}^{rods} is close to the maximum base moment measured experimentally (i.e. test-to-predicted ratio for this test is 0.97). Recall that Test #6 contained a base plate which remained elastic during testing resulting in failure of the anchor rods (rather than failure of the plate). No specimens were controlled by flexural yielding of the plate on the compression side (M_{base}^{tens}).

- Considering the design procedure outlined by the AISC *Design Guide 1* (Fisher & Kloiber, 2006), i.e. choosing the *minimum* of the three failure modes as the design strength of the connection ($M_{base} = \min\{ M_{base}^{comp}, M_{base}^{tens}, M_{base}^{rods} \}$), the TSB method is significantly conservative in it predictions of ultimate connection strength (average test-to-predicted ratio = 1.86 for all tests except Test #3). As discussed in the preceding bullet point, this may be attributed to the fact that the TSB model erroneously predicts base plate yielding on the compression side as being the governing condition in a majority of the experiments.
- Considering the ultimate strength (rather than yield strength) of the base plate material for flexural failure provides better agreement with test data (average test-to-predicted ratio = 1.37 for all tests except Test #3). However, this does not fundamentally correct the incorrect identification of base plate yielding as the governing failure mode.
- Disregarding yielding of the base plate on the compression side, the TSB predictions are accurate (average test-to-predicted ratio = 0.97 for all tests except Test #3).
- The conservatism of the TSB method increases as the level of axial load increases. Larger axial loads increase the flexural demand on the compression side of the connection, which is the controlling failure mode for most of the configurations.

Results from Test #3 are not included in the above discussion since they cannot be directly interpreted relative to the TSB method due to the indeterminate nature of the anchor rod layout. These are discussed separately in Section 4.5.

4.2.1.2 Characterization of the Anchor Rod Forces

While the previous section addresses the efficacy of the TSB method with respect to characterizing the connection strength, an examination of strain data recorded from the large-scale specimen anchor rods provides valuable insight into the ability of the method to characterize the stress distributions within the base connection. In the absence of direct measurements of bearing stresses under the base plate, this type of information is valuable as it may provide a better assessment of the TSB method, while helping to explain the trends in strength prediction.

As discussed in Chapter 3, two strain gages were attached to each anchor rod in every large-scale specimen. As shown in Figure 3.12a, two uniaxial strain gages were attached to the unthreaded circumference of the anchor rods approximately two inches below the surface of the concrete (as well as two inches below the rod threaded circumference). The anchor rods themselves were de-bonded from the surrounding concrete in the immediate vicinity of the strain gages through the use of duct tape and industrial lubricant, such that strain in the anchor rods was not affected through bonding with the concrete. Two strain gages were attached to each anchor rod (on opposite sides, in the direction of loading), to differentiate between axial loading as well as bending in the anchor rods. The average of the two strains, which approximately equals the axial strain, is considered for analysis in this section. Figure 4.9 plots the evolution of strain recorded from each anchor rod of Test #4; similar plots for all tests are archived in Appendix B. As indicated by the strain data, for all cyclic tests, the anchor rods were subjected to reversed cyclic axial loading with both tensile and compressive cycles well in excess of the anchor rod material yield strain (e.g. peak strains as large as ±6,000 microstrain were recorded for some tests). As explained in the previous chapter, the large compressive strains observed from the anchor rod strain data (e.g. see Figure 4.9) are a result of the leveling nut detail. As expected, during the initial stages of loading, the strain history for the rods is biased in the tensile direction due to the undamaged grout pad preventing bearing on the leveling nuts which would result in compression of the anchor rods. During larger drift cycles, the magnitude of compressive strain excursions increases due to crushing and deterioration of the grout pad, as well as stretching of the anchor rods such that the plate washer lifts up and goes

into bearing sooner. Typically, compressive strains are considerable during 5% drift for Test #2 and #3, 2% drift for Test #4, and 6% drift for Test #5, #6, and #7.

Since the rods undergo yielding under reversed cyclic loading, it is not possible to convert the strain data to force by means of an elastic analysis. For this purpose, a cyclic plasticity model, with bi-linear stress-strain response and kinematic hardening assumptions (i.e. the Steel01 material model from OpenSees, 2006) is calibrated to the anchor rod tensile material properties observed in the ancillary tests (presented previously in Chapter 3). Recall that the anchor rod ancillary tests are monotonic tension tests and do not provide information about cyclic hardening. For the purposes of this discussion, where the main objective is a qualitative evaluation of the TSB method, it is assumed that the cyclic hardening is purely kinematic and isotropic hardening is negligible. This assumption, while not ideal, reflects material response with reasonable accuracy for several structural steels (Kanvinde & Deierlein, 2004). Appendix C presents details of the calibrated stress-strain model. Forces estimated by the material model are henceforth referred to as "measured" anchor rod forces, to distinguish them from predictions of anchor rod force from the base connection design methods.

Based on the calibrated material model, the strain history for each anchor rod is converted into a corresponding force history and is compared to the anchor rod forces predicted by the TSB method at the same instant of loading (i.e. under the same load-moment combination). Figure 4.10 plots anchor rod force histories of both the observed data and predicted values for Test #4[8]. Using results from this type of plot, Figures 4.11-4.17 plot the ratio P_{TSB} / P_{test}, where P_{test} is the force in the anchor rod at peak drifts of every loading cycle based on observed strain data and P_{TSB} is the force in the anchor rod during an identical loading combination (i.e. the same applied base moment and axial load) calculated as per the TSB method. Also shown in the Figures are curves representing similar estimates of anchor rod force from two other methods which will be discussed later. Due to damage (i.e. de-bonding) of some strain gages during testing,

[8] Since the TSB method involves calculation of only the tensile forces in the anchor rods, Figure 4.10 shows only the tensile forces, and data when the rod was in compression is omitted for clarity.

strains were not recorded for the entire loading history for some tests. For the monotonic test (Test #1), similar data is shown in Figure 4.11. However, since monotonic stress-strain data for the rod material is available directly from ancillary tests, the plots are generated based on a polynomial curve fit to this data.

Referring to Figures 4.11-4.17, several observations may be made regarding the efficacy of the TSB method in predicting anchor forces in the base connection –

- Referring to the monotonic Test #1 (see Figure 4.11), the TSB method accurately predicts forces in the anchor rods for drift levels higher than 0.5% (P_{TSB} / P_{test} is between 0.96-1.00). The accuracy tends to decrease at very high drift levels (greater than 9%), while for very low drifts (less than 0.5%) the estimates deviate significantly from the measured forces.
- For Test #2, the TSB method results in predictions of anchor rod forces that are larger (by up to 35%) than the "measured" rod forces for drift levels less than 1%. At higher drift levels, the TSB predictions are lower than measured, but within 15% of the measured values.
- For Tests #4 and #5, the TSB predictions are significantly lower than the measured anchor rod forces at drift levels less than 1.5%. At higher drift levels, the predictions are within 15% of the measured values.
- For Test #6, the anchor force predictions are accurate (i.e. within 10%) after 1% drift cycles.
- For Test #7, the anchor force predictions are not accurate. After 1.5% drift cycles, the method over- and under- predicts the anchor rod forces by up to 30%.

In summary, based on the specimens examined, the TSB method accurately predicts anchor rod forces (within 15%) for base connections with lower axial forces (i.e. zero to 90 kips axial compression) at drift levels greater than 1.5%. Recall that the TSB method is based on the assumption of a triangular bearing stress block with the concrete/grout crushing strength at the base plate extremity and lower elsewhere. This assumption is not, in general, consistent with the stresses developed during low drifts (i.e. moments) as well

as during high axial forces where large regions of the grout or concrete may experience a uniform stress equal to the crushing strength. Although speculative, this provides a possible explanation for the observed trends. Other factors may contribute to the differences between estimated and calculated anchor rod forces. These include (1) errors in the estimated forces, especially since they are estimated through a simplified constitutive model and (2) effects not considered in the analysis, e.g. prying forces in the rods, which may be generated due to the corners of the base plate bearing on the grout, as can be seen in Figure 3.21a.

4.2.1.3 Application of the TSB Method Considering Inclined Yield Lines

As discussed in the previous subsection, the TSB method accurately predicts anchor rod forces under certain situations. However, characterization of these forces is only one component of the strength prediction methodology. The anchor rod forces are subsequently used to determine the base moment M_{base} at which the base plate will yield under flexure on the tension side due to the tensile forces developed in the rods. For this purpose, the *Steel Design Guide 1* (Fisher & Kloiber, 2006), based on assumptions by Blodgett (1966), considers yield lines parallel and close to the edge of the column flange for both compression and tension side flexure (see Figure 2.3a and D.1). Once the anchor rod force is calculated, the lever arm corresponding to this force is determined as the distance between the center of the anchor rods and the assumed yield line, measured perpendicular from the yield line. However, an examination of damage patterns during the experiments (refer Figure 3.21 and 3.27 introduced previously) suggests that yield lines may form at an angle to the column flange when the anchor rods are close to the corner of the base plate and outset from the column footprint. In fact, the AISC *Steel Design Guide 10* (Fisher & West, 2003) considers inclined yield lines due to outset anchor rods and presents design recommendations based on analytical models. Figure 2.3b, introduced earlier, illustrates the location and orientation of the assumed inclined yield line prescribed by the *Design Guide 10*. Referring to the Figure, the yield line is constructed perpendicular to the lever arm (defined as the line from the center of the anchor rod to the corner of the flange) and the effective bending width is calculated as twice the length of this lever arm. Based on test observations (recall Figure 3.12), another

assumed yield line formation due to outset anchor rods disregards an effective bending width and assumes that the bending width extends to the perimeter edges of the base plate. Due to observed specimen behavior, only the latter inclined yield line assumption is considered. The maximum strength of the base connection calculated as per the outset yield line approach, denoted as $M_{base}^{tens-inclined}$, is listed in Table 4.1.

Referring to Table 4.1, several observations may be made regarding the efficacy of the TSB method to predict the base connection strength considering inclined yield lines –

- Due to the location of the anchor rods, the calculated strength of the base plate is lower for included yield lines as compared to the straight yielding line for all test specimens.
- Since the assumption of inclined yield lines results in a lower flexural capacity of base plate yielding on the tension side, $M_{base}^{tens-inclined}$ both governs for the tests without axial load (instead of M_{base}^{comp}). This provides an even more conservative estimate of the connection strength as compared to the perpendicular yield line assumption.
- Considering the ultimate strength of the plate material (rather than the yield strength), the inclined yield line approach does not give better agreement with test data when compared with the approach that uses perpendicular yield lines and either the ultimate or the yield strength. However, it is important to note that this apparent lack of accuracy is not a deficiency of using the inclined yield lines, but rather a deficiency of the overall method itself, which considers the first yield of the connection, rather than the development of the mechanism. In fact, the inclined yield lines are consistent with experimental observations, and provide better agreement with test data (as compared to straight yield lines) when used within an approach which considers the development of a mechanism in the base connection.

4.2.1.4 Summary of the TSB Method

Based on experimental results and the discussions presented above, the efficacy of the TSB method in predicting the base connection behavior, as outlined in the *Design Guide 1*[9], is now summarized –

- For the test specimens examined, the TSB method, is significantly conservative in its ability to characterize the strength capacity of a base connection (average test-to-predicted base moment ratio = 1.86 for all tests except Test #3).
- If failure due to base plate bending on the compression side is neglected, the TSB method provides accurate predictions of strength (average test-to-predicted ratio = 0.97 for all tests except Test #3).
- Considering the base plate ultimate strength for flexural failure (rather than the yield strength) provides better agreement with test data (average test-to-predicted ratio = 1.37 for all tests except Test #3).
- For all test specimens examined, the TSB method accurately predicts anchor rod forces (within 15%) for base connections with lower axial forces (i.e. zero to 90 kips axial compression) at drift levels greater than 1.5%. For the monotonic Test #1, the TSB method predicts anchor rod forces within 4% for drift levels higher than 0.5%
- Considering inclined yield lines does not increase the accuracy of the TSB method and results in predictions which are more conservative than assuming conventional yield lines. However, this is an artifact of the overall method which considers only first yield of the connection. In fact, inclined yield lines are observed in the experiments.
- For certain combinations of axial force and moment, the TSB method cannot provide valid solutions (i.e. anchor rod forces), given a base plate size and anchor rod layout. In these cases, the base plate geometry must be modified.

4.2.2 The Rectangular Stress Block (RSB) Method

The AISC *Steel Design Guide 1* (Fisher & Kloiber, 2006) suggests that for determining the base connection strength capacity associated with ultimate limit states, a rectangular

[9] Note that the method is refined by changing the definition of the critical eccentricity – refer Appendix D.

stress block may be more appropriate over a triangular stress distribution as used by the TSB method. In fact, previous test results (i.e. DeWolf, 1982) show that the RSB method is the preferred approach since it more closely reflects actual behavior.

Similar to the TSB approach described in the previous section, the RSB approach categorizes loading conditions as those with either a low or high load eccentricity. Under low eccentricity, the applied axial force and moment combination is assumed to be resisted exclusively through the development of a constant (i.e. rectangular shaped) stress distribution under the base plate, centered under the resultant eccentric load (recall Figure 2.1). The separation between the low and high eccentricity case is defined by a critical eccentricity as calculated per Equation (D.14) in Appendix D. For the high eccentricity condition, the plate is assumed to lift off from the concrete/grout foundation and the concrete on the compression side is on the verge of crushing due to bearing stresses. Similar to the TSB method, this simplifying assumption is conservative in its predictions of the connection capacity. The theoretical assumptions underlying this method are presented in Appendix D of this report, as well as in Chapter 3.3 and 3.4 of the AISC *Steel Design Guide 1* (Fisher & Kloiber, 2006). The discussions of the RSB methods in the subsequent subsections follow a similar format as the discussion section for the TSB method. Thus, some procedural details regarding computation of the various quantities are omitted and the reader is referred to Section 4.2.1 for details regarding procedures of the analysis.

4.2.2.1 Predictions of Maximum Moment Capacity

Figure 4.18 shows the evolution of each of the three quantities representing the base component demands defined earlier (M_{comp}, T_{rod} and M_{tens}) with respect to the applied base moment (M_{base}) for Test #4, as well as the capacity of each component. Similar plots for each test specimen are included in Appendix E. Referring to this plot, several observations regarding the RSB prediction method are now made –

- Both the force in the anchor rod T_{rod} and bending moment on the tension side of the base plate M_{base}^{tens} are zero for low moments (less than 609 kip-in for Test #4) due to the low eccentricity condition discussed above.
- At zero applied base moment, a bending moment demand is imposed on the compression side of the base plate due to the imposed axial compressive load. This is due to the upward bearing pressure on the base plate.
- For lower base moments, (less than 3,961 kip-in for Test #4), the flexural demand on the compression side of the base plate M_{comp} is greater than the flexural demand on the tension side (M_{tens}).
- After a certain value of applied base moment (3,082 kip-in for Test #4), the flexural demand on the compression side of the base plate reaches a maximum value. This is a result of the rectangular stress block becoming active over the entire lever arm length of the compression side of the base plate.
- At higher base moments (greater than 8,086 kip-in for Test #4), the RSB is unable to provide a solution. At this base moment value, the extent of the bearing length approaches the location of the anchor rods and tension forces in the rods asymptotically approach infinity. Due to this situation, the RSB method is invalid for base plate geometries under certain load combinations. In practice, this represents situations where the size of the base plate and/or the location of the anchor rods must be modified to produce acceptable solutions.

Figures 4.19-4.25 plot the column drift versus base moment curves for all experiments discussed in Chapter 3. The three values of M_{base}, corresponding to the three failure modes (i.e. M_{base}^{comp}, M_{base}^{tens} and M_{base}^{rods}) described in the preceding discussion, are overlaid on each of the plots. As per current design procedures, featured in the *Design Guide 1* (Fisher & Kloiber, 2006), the *minimum* of these values reflects the design strength of the column base connection. Table 4.2 compares the predicted base moment, corresponding to each failure mode, with the peak base moment (averaged from both loading directions) and the base moment at 4% drift (also averaged from both loading directions) observed in the experiments. In addition to plate bending capacity based on the plastic section

modulus and yield strength of the plate material (i.e. $R_{plate} = Z_x \cdot F_y$) as assumed by the *Design Guide 1* procedure (Fisher & Kloiber, 2006), Table 4.2 lists the predicted base moment considering the ultimate strength of the plate material (i.e. assuming full strain hardening; $R_{plate} = Z_x \cdot F_u$). Also included in the Table are predicted base moments considering alternate bending yield line patterns on the tension side of the base plate not addressed in the *Design Guide 1*. A description and analysis of alternate yield lines is presented in Section 4.2.2.3.

A close examination of Figures 4.19-4.25 and Table 4.2 reveals several key points which provide insight into the efficacy of the RSB prediction method –

- For five tests (i.e. Tests #1, #2, #4, #5 and #7), the lowest M_{base} corresponds to flexural yielding of the plate on the compression side, i.e. M_{base}^{comp} governs the capacity of these specimens under the applied axial load. In these cases, it is observed that this value of M_{base}^{comp} is significantly lower (i.e. the predictions are significantly conservative) as compared to the maximum moment measured experimentally (i.e. the average test-to-predicted ratio is 2.04 for every tests except #3 and #6). In one test (i.e. Test #6, the test with the thickest (1.5") base plate), the lowest M_{base} corresponds to anchor rod capacity, i.e. M_{base}^{rods} governs the capacity of this test. For this case, it is observed that the value of M_{base}^{rods} is close to the maximum moment measured experimentally (i.e. the test-to-predicted ratio is 0.97 for Test #6). No specimens were controlled by flexural yielding of the plate on the compression side (M_{base}^{tens}).
- Considering the design procedure outlined in the AISC *Design Guide 1* (Fisher & Kloiber, 2006), i.e. by choosing the *minimum* of the three failure modes as the design strength of the connection ($M_{base} = \min\{M_{base}^{comp}, M_{base}^{tens}, M_{base}^{rods}\}$), the RSB method is significantly conservative in its predictions of ultimate connection strength (average test-to-predicted ratio = 1.86 for all tests except Test #3). Thus, the conservatism of the RSB method is similar to that of the TSB method.

- Considering the ultimate strength (rather than yield strength) of the base plate material for flexural failure provides better agreement with test data (average test-to-predicted ratio = 1.40 for all tests except Test #3).
- Disregarding yielding of the base plate on the compression side, the RSB predictions are more accurate (average test-to-predicted ratio = 0.94 for all tests except Test #3).
- The conservatism of the RSB method increases as the level of axial load increases. Larger axial loads increase the flexural demand on the compression side of the connection, which is the controlling failure mode for most tests.

4.2.2.2 Characterization of the Anchor Rod Forces

As discussed in the Section 4.2.1.2, an examination of strain data recorded in the anchor rods during the large scale tests provides valuable insight into the ability of the method to characterize the stress distributions within the base connection.

Figures 4.11-4.17 plot the ratio P_{RSB}/P_{test}, where P_{test} is the force in the anchor rod at peak drifts of every loading cycle based on observed strain data (and the calibrated material model) while P_{RSB} is the force in the anchor rod during an identical loading combination (i.e. the same applied base moment and axial load) calculated as per the RSB method. For the monotonic test (Test #1), similar data is shown in Figure 4.11. However, since monotonic stress-strain data for the rod material is available directly from ancillary tests, the plots are generated based on a polynomial curve fit to this data.

Referring to Figures 4.11-4.17, several observations may be made regarding the efficacy of the RSB method in predicting anchor rod forces in the base connection –

- Referring to the monotonic Test #1 (see Figure 4.11), the RSB method accurately predicts forces in the anchor rods for drift levels higher than 0.5% (P_{RSB}/P_{test} between 0.95-1.00). The accuracy tends to decrease at very high drift levels (greater than 9%), while for very low drifts (less than 0.5%) the estimates deviate significantly from the measured forces.

- The anchor rod forces predicted by the RSB are similar to the predictions of the TSB method (i.e. predicted anchor rod forces for both the TSB and RSB methods are generally within 10% for tests with axial load and within 3% for tests without axial load). Thus, the reader referred to the bullet line summary in Section 4.2.1.3 for a discussion of the efficacy of the TSB method in predicting anchor rod forces.

In summary, based on the specimens examined, the RSB method is similar to the TSB method in its ability to predict anchor rod forces anchor rod forces (within 20%) for base connections with lower axial forces (i.e. zero to 90 kips axial compression) at drift levels greater than 1.5%. This observation is not entirely unexpected. Recall that both the TSB and RSB methods assume that the limit strength of concrete is reached for all high-eccentricity conditions. While this is a conservative assumption, it may not be true, since it cannot satisfy compatibility, especially for low applied moments. Thus, for these cases, the anchor rod force estimates deviate significantly from the measured values.

4.2.2.3 Application of the RSB Method Considering Inclined Yield Lines

This section examines the effect of considering inclined yield lines in conjunction with the RSB method. The base connection capacity calculated as per the outset yield line approach, under the assumption that the inclined yield line width is perpendicular to a lever arm which runs from the center of the anchor rod to the column flange corner, and extends to the perimeter edges of the base plate, is denoted as $M_{base}^{tens-inclined}$ and listed in Table 4.2. Referring to this Table, several observations may be made regarding the efficacy of the RSB method for predicting the base connection strength considering inclined yield lines –

- Due to the location of the anchor rods, the moment demand on the base plate is larger considering inclined yield lines rather than the straight yield line for all test specimens.
- Since the assumption of inclined yield lines results in a lower flexural capacity of base plate yielding on the tension side, $M_{base}^{tens-inclined}$ governs for the tests without axial

load (instead of M_{base}^{comp}). This provides an even more conservative estimate of the connection strength as compared to the perpendicular yield line assumption.

- Considering the ultimate strength of the plate material (rather than the yield strength), the inclined yield line approach does not give better agreement with test data when compared with the approach that uses perpendicular yield lines and either the ultimate or the yield strength.

4.2.2.4 Summary of the RSB Method

Based on experimental results and the discussions presented above, the efficacy of the RSB method in predicting the base connection behavior, as outlined in the *Design Guide 1*, is now summarized –

- For the test specimens examined, the RSB method is significantly conservative in its ability to characterize the strength capacity of a base connection (average test-to-predicted base moment ratio = 1.86 for all tests except Test #3). The accuracy of the RSB method is similar to that of the TSB method.
- If failure due to base plate bending on the compression side is neglected, the RSB method provides accurate predictions of strength (average test-to-predicted ratio = 0.94 for all tests except Test #3).
- Considering the base plate ultimate strength for flexural failure (rather than the yield strength) provides better agreement with test data (average test-to-predicted ratio = 1.40 for all tests except Test #3). This effect is observed for both straight and inclined yield lines.
- For all test specimens examined, the RSB method accurately predicts anchor rod forces (within 25%) for base connections with lower axial forces (i.e. zero to 90 kips axial compression) at drift levels greater than 1.5%. For the monotonic Test #1, the RSB method predicts anchor rod forces within 5% for drift levels higher than 0.5%
- Considering inclined yield lines does not increase the accuracy of the RSB method for predicting strength; in fact this makes the predictions even more conservative.

- For certain combinations of axial force and moment, the RSB method cannot provide valid solutions (i.e. anchor rod forces), given a base plate size and anchor rod layout. In these cases, the base plate geometry must be modified

Based on the experimental results, it is observed that the RSB method, by means of the design procedures outlined in the AISC *Steel Design Guide 1* (Fisher & Kloiber, 2006), is significantly conservative in its predictions of base connection strength capacity. Furthermore, both the TSB and RSB methods give similar predictions of anchor rod forces and the strength capacity of the base connection.

4.2.3 The Leveling Nut (LNT) Method

Recall that a leveling nut detail was used in the test specimens for column erection. This detail consists of a nut and washer assembly bolted on the anchor rods such that the underside of the base plate is in direct contact with the leveling nut detail. This assembly provides a potential load path for compressive (i.e. bearing) forces from the base plate to the connection footing. In fact, during seismic type loading, the grout pad may deteriorate due to cyclic compression damage such that bearing on the compression side may be resisted by the anchor rods through the leveling nut detail (i.e. as observed in the tests). In this case, the base connection may be modeled as a simply supported beam and, given a moment, axial force and distance between the anchor rods, the forces in the anchor rods may be determined conveniently through static equilibrium[10]. This section considers such an approach with the main purpose of examining if this mechanism becomes active at any point in the loading history. Refer to Appendix D for the mathematical formulation of this method. Although a literature search revealed that leveling nut details have not been investigated experimentally in the past, the AISC *Steel Design Guide 10* provides recommendations for leveling nuts in the context of base connection strength design.

Figures 4.11-4.17 plot the ratio P_{LNT}/P_{test}, where P_{test} is the force in the anchor rod at peak drifts of every loading cycle calculated based on observed anchor rod strains and

[10] For a base plate with two bolt lines.

P_{LNT} is the force in the anchor rod during an identical loading combination (i.e. the same applied base moment and axial load) calculated as per the LNT method. Referring to Figures 4.11-4.17, several observations may be made –

- Referring to the monotonic Test #1, the LNT method accurately predicts forces in the anchor rods for drift levels higher than 1.0% (P_{LNT}/P_{test} between 1.04.-1.10). The accuracy tends to increase for higher drift levels, while for very low drifts (less than 1.0%) the estimates deviate significantly from the measured forces.
- In general, the LNT method is not accurate in predicting anchor rod forces at low drift levels (approximately less than 1.5%). This is expected, since the grout in the compression region is relatively intact and providing a load path through grout bearing, rather than compression in the anchor rods.
- For Tests #2, #5, and #6, the LNT method provides extremely accurate anchor rod force predictions (on average within 3% of observed values) at drift levels greater than 2%. This observation is promising since it may support the validity of the procedures used in analyzing the anchor rod forces.
- The LNT method is not accurate in predicting anchor rod forces for Test #4 (over predicts up to 35%) and Test #7 (over predicts up to 50% and under predicts up to 20%).

In summary, based on the specimens examined, the LNT method is very accurate in predicting anchor rod forces for some tests (i.e. Tests #2, #5, and #6) at drift levels greater than 2%. This is consistent with the expectation that as the grout becomes progressively damaged, the leveling nut detail provides a load path for the compressive forces due to the applied base moment. However, it is somewhat challenging to develop a design approach based on the LNT method, since in general (1) the grout may not deteriorate unless large cyclic deformations are applied (2) given that the leveling nut detail is one of many options used for column erection, and is usually decided upon during construction, it is difficult and unreliable to prescribe (3) the anchor rods may not be able to sustain the compressive forces due to mechanisms such as buckling of the rods and stripping of the rod threads.

4.3 CONSIDERATION OF THE FORMATION OF PLASTIC MECHANISM IN THE BASE CONNECTION

The most important observation from the previous sections is that the current approaches for strength prediction (such as those featured in the AISC *Steel Design Guide 1* [Fisher & Kloiber, 2006]) are highly conservative, especially when the strength is controlled by flexural yielding of the base plate on the compressive side. When the strength is controlled by the anchor rod capacity, the TSB and RSB methods are very accurate. In fact, a closer inspection of Tables 4.1 and 4.2 reveals that if only the values of M_{base}^{tens} and M_{base}^{rods} are considered, i.e. the failure on the compression side of the base plate is disregarded, the average test-predicted ratio is 0.98 for both methods, which is more accurate as compared to the test-predicted ratio of 1.86 (for both methods) that was obtained by selecting the minimum of all the three values of M_{base}^{tens}, M_{base}^{comp} and M_{base}^{rods}. This suggests that while yielding on the compression side of the base plate may represent the onset of inelastic behavior of the base connection for some of the experiments, it does not govern the ultimate strength of the connection. In fact, referring to Chapter 3, compression side yielding of the base plate (evidenced by flaking of whitewash applied to the plate) was observed before the peak strength was reached. This suggests that the peak strength of the base connection may be governed by a combination of multiple yielding states (in the base plate or anchor rods), resulting in the formation of a plastic mechanism. This type of mechanism-based analysis for base plates has been investigated in the past (e.g. Ohi *et al.*, 1982). Based on the experimental data and a review of previous mechanism-based approaches (such as Ohi *et al.*, 1982), it is proposed that the ultimate strength of the base connection will be reached when any one of the following yielding scenarios is activated (see Figure 4.26 for a schematic representation of these scenarios) –

A. Flexural yielding of both the tension side *and* compression side of the base plate (see Figure 4.26a).
B. Flexural yielding of the tension side of the base plate *and* axial yielding of the anchor rods on the tension side (see Figure 4.26b).
C. Axial yielding of the anchor rods on the tension side (see Figure 4.26c).

D. Flexural yielding of the compression side of the base plate *and* axial yielding of the anchor rods on the tension side (see Figure 4.26d).
E. Axial yielding of the anchor rods on both sides of the connection (see Figure 4.26e).
F. Crushing of the concrete or grout (see Figure 4.26f)

For example, Scenario A implies that only the flexural yielding on the compression side of the base plate is not sufficient to result in a mechanism; yielding on tension side is required as well. Similarly, all the other scenarios require yielding in one or two components to obtain a mechanism. It is important to note that most of the scenarios discussed above do not form an exhaustive set of possible mechanisms but rather represent actual conditions observed during testing. Based on visual observations of the experiments, Scenarios (A, B and D) were observed for the "thin" base plate specimens (i.e. Test #1, #2, #5, and #7) while Scenario (C) occurred for the "thick" base plate specimens (i.e. Test #4 and #6). Other scenarios may be also possible; for example, yielding of all anchor rods on both sides of the connection (see Figure 4.26e). However, this condition would only occur if a highly rigid base plate was connected to a very rigid/strong foundation. Similarly, it may be possible to consider a situation with a stiff/strong base plate as well as strong anchor rods, where the strength may be reached only through the crushing of the concrete/grout (Scenario F – see Figure 4.26f). In the case of Scenario F, the strength may be estimated by one of two approaches including (1) methods similar to that of flexural design of a reinforced concrete beam, by assuming that the rigid plate enforces a deformation pattern consistent with plane sections and the anchor rods are analogous to reinforcement bars, or (2) by considering the maximum base moment that may be applied to the base plate of a given size (i.e. the maximum valid base moment as per the TSB or RSB methods – refer Appendix D), since this represents the base moment corresponding to the development of the maximum bearing stress condition in the grout/concrete. However, in the absence of experimental data for this type of behavior, Scenario E and F are discussed only for completeness and without theoretical treatment. In all the other mechanisms (A-D), the crushing of the concrete is implicitly assumed, but is not explicitly considered a "yielding" state, since the bearing

stresses predicted by the TSB and RSB methods limited to the concrete/grout bearing strength (at high eccentricities).

The base moment for each mechanism scenario is calculated as the maximum base moment associated with any of the respective yielding states within each scenario. This is consistent with the assumption that a given mechanism scenario will be activated only when all the yielding states within it have been activated. Once the ultimate strength is determined from each scenario, the minimum from all scenarios is selected as the governing scenario.

Within the overall framework of the plastic mechanism based approach, several variants may be adopted to characterize the connection strength. These include the use of the TSB or the RSB method for characterizing bearing stresses, the use of straight or inclined yield lines to characterize yielding of the base plate on the tension side, and the use of the yield or ultimate material strength for the flexural capacity of the base plate. Section 4.6 presents recommendations on the combination of these various options that provides the best overall predictions of experimental response.

4.4 GROUT AND CONCRETE BEARING STRENGTH

As discussed previously, both the TSB and RSB methods utilize a maximum bearing stress value corresponding to the bearing strength of the concrete foundation. The strength of concrete under steel plate bearing has been tested extensively in the past (i.e. Hawkins, 1968a & 1968b; DeWolf, 1978 & 1982). From these investigations, the design bearing strength of concrete is defined in ACI 318-02, Section 10.17, as –

$$f_c^{bearing} = 0.85 \cdot f_c' \cdot \left(\sqrt{\frac{A_2}{A_1}} \right) \leq 1.7 \cdot f_c' \qquad (4.1)$$

Where:

A_1 = bearing area

A_2 = maximum area of the portion of the supporting foundation that is geometrically similar to and concentric with the loaded area

f_c' = compressive strength of the concrete

For the purpose of establishing the concrete bearing strength, the bearing area A_1 is assumed to be equal to the base plate area, even though under flexural loading, the actual bearing area on the concrete may be smaller than the entire base plate (e.g. see DeWolf & Sarisley, 1980). Furthermore, Equation (4.1) assumes concentric axial loading through a rigid plate, rather than eccentric loading or loading through flexible plates. Thus, the design bearing stress from Equation (4.1) may not accurately predict the actual concrete bearing strength in the context of base connections under flexural loading.

In addition, Equation (4.1), as well as current base connection design provisions, do not consider the beneficial effect of reinforcing bar confinement on the concrete bearing strength. The reader is referred to Ahmed *et al.* (1998) regarding the bearing capacity of plain and reinforced concrete loaded over a limited area. The publication includes mathematical equations to characterize the effect of steel reinforcement on the ultimate bearing capacity.

Based on an extensive literature search, no research publications have experimentally investigated the bearing strength of a grout pad, which is characterized by compression loading of a very thin slab of grout over a large bearing area (with respect to the grout height dimension). Consequently, the failure mechanisms of a grout pad may be different than concrete bearing failure, where the height to bearing diameter ratio can be dramatically different. In the absence of experimental or analytical studies in this area, and for the purpose of this report, the bearing strength of grout is calculated in a similar manner to the bearing strength of concrete as per Equation (4.1), with $A_1 = A_2$ –

$$f_g^{bearing} = 0.85 \cdot f_g' \tag{4.2}$$

Where:

f_g' = compressive strength of the grout

Due the difficulty of finishing the concrete foundation to a precise level and elevation, especially in the presence of embedded anchor rods, base plates are rarely set directly on the concrete for building construction (Ricker, 1989). Nevertheless, current design provisions do not explicitly address the grout pad beneath the base plate for strength capacity predictions. For example, the *Design Guide 1* (Fisher & Kloiber, 2006) only recommends that the grout strength be specified as two times the concrete strength. Thus, for the study, the maximum bearing stress under the base plate was determined as the minimum of the strengths of the grout and concrete –

$$f_{\max} = \min\left\{0.85 \cdot f_c' \cdot \left(\sqrt{\frac{A_2}{A_1}}\right) \leq 1.7 \cdot f_c', f_g'\right\} \tag{4.3}$$

Based on ancillary test data and Equations (4.1) and (4.2), the predicted maximum bearing strength for every large-scale test is governed by crushing of the concrete. However, based on test observations, the grout pad crushed while the concrete remained undamaged. This may be attributed to the presence of reinforcement in the concrete footing, which resulted in the increase of the concrete strength above that predicted by Equation 4.3, which disregards the grout.

The *Design Guide 1* (Fisher & Kloiber, 2006) uses a resistance factor (ϕ-factor) when calculating the maximum concrete bearing pressure for base connections under flexural/axial loading. The use of a resistance factor for the concrete bearing pressure is appropriate when concrete crushing controls the design (e.g. in failure Scenario E outlined in the previous Section), however, when the concrete capacity is used to characterize an imposed resisting load (such as a bearing pressure acting on the underside of a base plate), it is more appropriate (and conservative) to omit the resistance factor.

4.5 DISCUSSION OF TEST #3 WITH ALTERNATE ROD PATTERN

Recall that Test #3 examines an alternate bolt pattern, featuring eight, rather than four bolts (see Figure 3.4a). A schematic illustration of this layout is presented as an example of a "rigid base" plate assembly for moment frames in the commentary of the AISC Seismic Provisions (2005). The main objective of this test was to compare the effect of the additional anchor rods on the performance of the base connection. Due to the additional anchor rods, it is not possible to calculate the bearing stress distribution or the anchor rod forces for Test #3 within the framework of the TSB or RSB methods due to the static indeterminacy. The specimens used in Test #3 and Test #2 are identical, with the exception of the number of anchor rods (i.e. Test #2 contained four anchor rods while Test #3 contained eight). Thus, the effect of additional rods may be directly evaluated by comparing test data from these tests. Some of the observations based on such a comparison include –

- Test #3 demonstrates only a moderate increase strength compared to Test #2 (i.e. 16% increase in observed peak base moment).
- Test #2 exhibited anchor rod fracture at approximately 7% drift cycles while Test #3 was able to sustain cyclic deformations up to at least 9% drift.
- It is observed that the initial stiffness of the specimen investigated in Test #3 is 11% higher than that of the specimen investigated in Test #2, indicating that the additional anchor rods may not substantially increase the connection stiffness.

In summary, the presence of the additional anchor rods has only a modest effect on the strength, stiffness and ductility of the base connection. Development and validation of strength prediction models for such anchor rod layouts faces several challenges due to (1) the lack of experimental data for these details, (2) the indeterminate nature of the connection which requires compatibility assumptions and (3) complex yield line patterns which develop in the base plate due to plate bending. However, a general observation is that the eight-rod specimen shows higher strength, stiffness and ductility compared to an identical four-rod connection. Thus, if necessary, the eight-rod detail may be

conservatively designed by ignoring the contributions from the four additional rods. Ongoing finite element simulation studies will be used to develop design guidelines for more unconventional base connection layouts, including those involving indeterminate anchor rod layouts.

4.6 PROPOSED APPROACH FOR STRENGTH PREDICTION

Based on the preceding sections, it is evident that any strength prediction approach for column base connections must incorporate various components including –

1. The selection of an appropriate bearing stress distribution under the base plate (i.e. the TSB method versus the RSB method)
2. The selection of an appropriate yield line pattern in the base plate (i.e. straight yield lines versus inclined yield lines)
3. The development of an appropriate approach which utilizes the overstrength of the connection due to yielding of various components to characterize connection strength (i.e. a single-limit approach versus a mechanism-based approach).
4. The appropriate choice of material properties (i.e. yield versus ultimate strength) for characterizing the flexural capacity of the base plate.
5. The appropriate prediction of the maximum bearing strength (i.e. confined concrete, with or without steel reinforcement, versus unconfined grout)

Various modeling alternatives are available for each of the issues described above. In this study, all the possible combinations of these alternatives were investigated. Based on this investigation, this section proposes the combination of modeling alternatives that result in the best agreement with experimental data not only in terms of the overall test-to-predicted ratios, but also in terms of the test observations of damage and deformation, as well as correlation with the measured anchor rod forces. The key features of the proposed approach are –

1. The compressive bearing stresses are characterized by the rectangular stress block (RSB) method.

2. For the RSB method, the maximum bearing stress is determined as the minimum of the bearing strength of the concrete foundation, and the strength of the unconfined grout pad, as per Equation 4.3.
3. No resistance factors (ϕ-factors) are applied to the maximum bearing stress when calculating the bearing stresses and anchor rod forces as per the RSB method. However, resistance factors should be applied to the maximum bearing stress if concrete/grout bearing failure governs (e.g. the mechanism described in Scenario F).
4. The anchor rod tensile capacity, as well as the base plate flexural capacity, is determined using the *ultimate* material strength.
5. For flexural yielding of the base plate on the tension side, the yield line pattern that gives the lower strength estimate is considered. The two patterns considered include yield lines parallel to the column flange and at an angle to the flange as illustrated in Figure 2.3. In addition, it is assumed that the width of the yield line extends to the perimeter edges of the base plate. For the experiments in this study, the inclined yield lines govern in all cases.
6. A mechanism-based approach is adopted such that the base connection strength capacity is controlled by the formation of a plastic mechanism. Such mechanisms include those illustrated in Figure 4.26 and outlined in Section 4.3. This requires the activation of yielding in various components of the base connection as described in Section 4.3. A mechanism-based approach is distinct from the current approach, which assumes the strength of the connection is based on the base moment required to induce yielding in any one component.

Based on this proposed approach, predictions of the connection strength as well as the associated failure mechanism, are presented in Table 4.3 for all experiments other than Test #3. Referring to this Table, the proposed design method is highly accurate for predicting the peak connection strength (the average test-to-predicted base moment = 0.99, C.O.V. = 0.057). Thus, the proposed method provides significantly more accurate estimates of the base connection strength as compared to existing approaches. Moreover, the predicted failure modes and assumed yield line patterns are consistent with the response observed during testing. Similarly, the consideration of the ultimate material

strength for the anchor rods and base plate is consistent with the large plastic deformations observed during the experiments. Moreover, the test-to-predicted ratios do not show a systematic bias towards any of the test parameters.

Figure 4.27 outlines a brief flowchart for the design of base connections based on this approach given an axial/flexural load case, concrete/grout strength and column dimension. In essence, the design procedure involves iteratively applying the strength prediction approach until a satisfactory solution is determined. However, the flowchart described above does not include the use of resistance factors (ϕ-factors) for the concrete/grout bearing strength and is based only on the expected material strengths, and is presented only to demonstrate the potential incorporation of the proposed strength prediction method into a design methodology.

It is not appropriate to recommend resistance factors for the proposed design approach without a detailed reliability analysis. Moreover, in some situations, the use of the resistance factors may produce unconservative results. For example, the bearing pressure acting upwards on the compression side of the base plate produces a moment in the base plate which must be designed for. If a resistance factor is included in the estimate of the bearing pressure, the moment is reduced, leading to an unconservative assumption. Similarly, the estimates of the anchor rod forces, and consequently the flexural demand on the tension side of the base plate, are impacted by the use of the resistance factor on the bearing pressure. Thus, a detailed reliability analysis (and possibly a sensitivity analysis) should be conducted to determine the appropriate use of resistance factors. However, without the benefit of such a reliability analysis (which may be conducted in the future), some preliminary (and conservative) guidelines for the use of ϕ-factors may be summarized as follows –

- In all mechanisms that involve base plate bending, a resistance factor of 0.9 ($\phi = 0.9$, as per AISC, 2005) is used for the strength of the base plate.
- In all mechanisms that involve anchor rod axial capacity, a resistance factor of 0.75 ($\phi = 0.75$, as per AISC, 2005) is used for the strength of the anchor rod.

- For the mechanisms that involve base plate or anchor rod yielding (i.e. Scenarios A-D in Section 4.3), no resistance factor ($\phi = 1.0$) is used for the maximum bearing strength of the concrete/grout when calculating the bearing stress distribution and anchor rod forces as per the RSB and TSB methods, since it will provide the most conservative results. However, when initially sizing the base plate for axial loads, a resistance factor of 0.65 ($\phi = 0.65$, as per ACI-318, 2002) is used for the bearing strength of the concrete.
- For the mechanism that involves crushing of the concrete/grout (see Scenario E in Section 4.3), $\phi = 0.65$ should be applied to the concrete/grout bearing strength, since it will provide the most conservative design strength.
- Other possibilities might include the application of a ϕ-factor to the strength of the entire connection to limit deformations, and acknowledging that inelastic action will be present if the mechanism-based method is used for design.

While the proposed method is an improvement over the previous approaches, some of the key limitations of the approach are now outlined –

- The proposed method characterizes the strength of the base connection based on the development of a plastic mechanism. Thus, designed as per this method, the base connection will exhibit some degree of inelastic action under extreme loads. It is important to recall that even the RSB method outlined in *Design Guide 1* is intended to reflect the ultimate response of the connection, leading to the use of the rectangular bearing stress block as well as the plastic section modulus of the base plate in flexure. Thus, some level of inelastic action is anticipated and implicit even in the current approach. Consequently, the proposed method is consistent with the intent of current design approach, except that it leverages beneficial effects of inelastic action in various components of the connection. While this may be the desired approach under extreme or seismic loads, under certain situations (i.e. service loads) elastic response may be desired. For these situations, the existing methods (TSB/RSB) may be used without the consideration of a mechanism approach. However, even in these cases, a limited degree of inelastic action may occur (e.g. concrete/grout crushing).

- The method is applicable to exposed rectangular/square shaped base plates connected to H, rectangular, and square shaped columns set on concrete or grout. However, the method is developed for a maximum of two anchor rod bolt lines, set parallel to the base plate edge and situated in the region beyond a line projected by the column flange. Anchor rods positioned at the sides of the base plate or within the flanges of an H-section require additional yield line analysis for base plate bending and is outside the scope of this report. Refer to Murray (1983) for such conditions. Furthermore, specific details such as stiffeners and haunches are not addressed. However, ongoing finite element simulations specifically examine these issues, and future reports will provide more detailed guidelines for strength prediction as well as design of such configurations.
- The formulation of the RSB method may result in invalid or unreasonable solutions based on certain base plate geometry, base moment, and axial load combinations. The mathematical limit of the RSB method is discussed in Appendix D. In practice, this represents situations where the size of the base plate and/or the location of the anchor rods must be modified to produce acceptable solutions. This occurs when a large axial force-moment combination is applied to a small base plate, such that even the development of concrete strength over a large/entire portion of the base plate is not sufficient to resist the applied load-moment combination.
- The method is valid for strong axis bending of the column and may be applicable for weak axis bending as well as loading situations of flexure with axial tension. However, the method cannot be directly applied to situations of biaxial bending.
- The method does not explicitly address failure of the concrete foundation or grout pad as a limit state. While not an issue in the current study, it may be important in situations of a rigid base plate connected to a relatively weak footing.
- The rectangular bearing stress distribution (as well as the triangular distribution) are not based on compatibility criteria, and thus cannot incorporate the effect of base plate flexibility on the bearing stress distributions. While this was not a factor in the current study, it may be an important issue when highly flexible base plates are used.
- The method may produce erroneous (although conservative) results for situations of large eccentricities with low moment (e.g. no axial force and small moment). In these

cases, the maximum bearing stress is set to the crushing strength of the concrete/grout, which may not be physically accurate.

In summary, the proposed strength prediction approach provides a framework for the design of column base connections given axial load and moment combination. However, the seismic design of these connections must be addressed in broader context with a discussion of various issues including (1) the forces and moments which may be used for the design of these connections considering the interaction of building response with the response of the connection (2) the degree to which inelastic action (i.e. ductility) may be allowed in the components of these connections, as well as the connection itself and (3) the failure or yielding modes that are desirable if inelastic action is permitted in these connections. The next chapter provides a discussion of these design issues along with a summary of the entire study.

Table 4.1 – Base connection strength - test results and estimates based on the Triangular Stress Block (TSB) method

Test number	Test-to-predicted ratio[1]	Observed base moment (kip-in)		Predicted base moment M_{base} corresponding to each component capacity (kip-in)						
					Plate flexure considering plate yield strength			Plate flexure considering plate ultimate strength		
						Plate tension side			Plate tension side	
		Average peak base moment	Average base moment at 4% drift	Anchor rod M_{base}^{rods}	Plate compression side M_{base}^{comp}	Straight yield line M_{base}^{tens}	Inclined yield line $M_{base}^{tens-inclined}$	Plate compression side M_{base}^{comp}	Straight yield line M_{base}^{tens}	Inclined yield line $M_{base}^{tens-inclined}$
1	1.65[2]	1,110	970	1,142	671	1,137	524	1,334	1,850	874
2	1.62[2]	1,080	1,050	1,146	666	1,141	524	1,295	1,862	876
3	-	1,250	1,240	1,154	655	1,149	526	1,233	1,885	881
4	1.04[2]	1,130	1,120	1,119	1,084	2,621	1,557	invalid[4]	3,945	2,287
5	3.08[2]	1,570	1,470	1,644	509	1,640	1,074	708	2,306	1,397
6	1.00[3]	1,645	1,640	1,647	invalid[4]	3,980	2,302	invalid[4]	5,624	3,536
7	2.78[2]	1,785	1,690	1,912	643	1,909	1,379	849	2,528	1,681

[1]Based on the *Design Guide 1* approach which assumes that the design strength is a minimum of M_{base}^{rods}, M_{base}^{comp}, and M_{base}^{tens} and considering the yield strength of the base plate material; Test #3 is not applicable

[2]Governed by M_{base}^{comp}

[3]Governed by M_{base}^{rods}

[4]The TSB method can not provide a solution for this case

Table 4.2 – Base connection strength - test results and estimates based on the Rectangular Stress Block (RSB) method

Test number	Test-to-predicted ratio[1]	Observed base moment (kip-in)		Predicted base moment M_{base} corresponding to each component capacity (kip-in)						
					Plate flexure considering plate yield strength			Plate flexure considering plate ultimate strength		
						Plate tension side			Plate tension side	
		Average peak base moment	Average base moment at 4% drift	Anchor rod M_{base}^{rods}	Plate compression side M_{base}^{comp}	Straight yield line M_{base}^{tens}	Inclined yield line $M_{base}^{tens-inclined}$	Plate compression side M_{base}^{comp}	Straight yield line M_{base}^{tens}	Inclined yield line $M_{base}^{tens-inclined}$
1	1.71[2]	1,110	970	1,160	648	1,155	527	1,198	1,901	884
2	1.68[2]	1,080	1,050	1,163	644	1,158	528	1,182	1,910	886
3	-	1,250	1,240	1,169	637	1,164	529	1,153	1,927	889
4	1.21[2]	1,130	1,120	1,149	934	2,750	1,606	n/a[3]	4,263	2,385
5	3.05[2]	1,570	1,470	1,698	514	1,694	1,102	636	2,405	1,438
6	0.97[3]	1,645	1,640	1,700	n/a[3]	4,296	2,400	n/a[3]	6,536	3,774
7	2.53[2]	1,785	1,690	2,005	706	2,000	1,436	856	2,677	1,756

[1]Based on the *Design Guide 1* approach which assumes that the design strength is a minimum of M_{base}^{rods}, M_{base}^{comp}, and M_{base}^{tens} and considering the yield strength of the base plate material; Test #3 is not applicable

[2]Governed by M_{base}^{comp}

[3]Governed by M_{base}^{rods}

[2]Flexural yielding on the compression side is not a possible mode of failure

Table 4.3 – Base connection capacity and prediction results based on the proposed method

Test number	Average observed peak base moment (kip-in)	Predicted peak base moment (kip-in)	Predicted failure mechanism[1]	Test-to-predicted ratio
1	1,110	1,160	D	0.96
2	1,080	1,163	D	0.93
4	1,130	1,149	C	0.98
5	1,570	1,438	A	1.09
6	1,645	1,700	C	0.97
7	1,785	1,756	A	1.02
			Mean =	**0.99**
			COV =	**0.057**

[1]Refer Section 4.3 and Figure 4.26

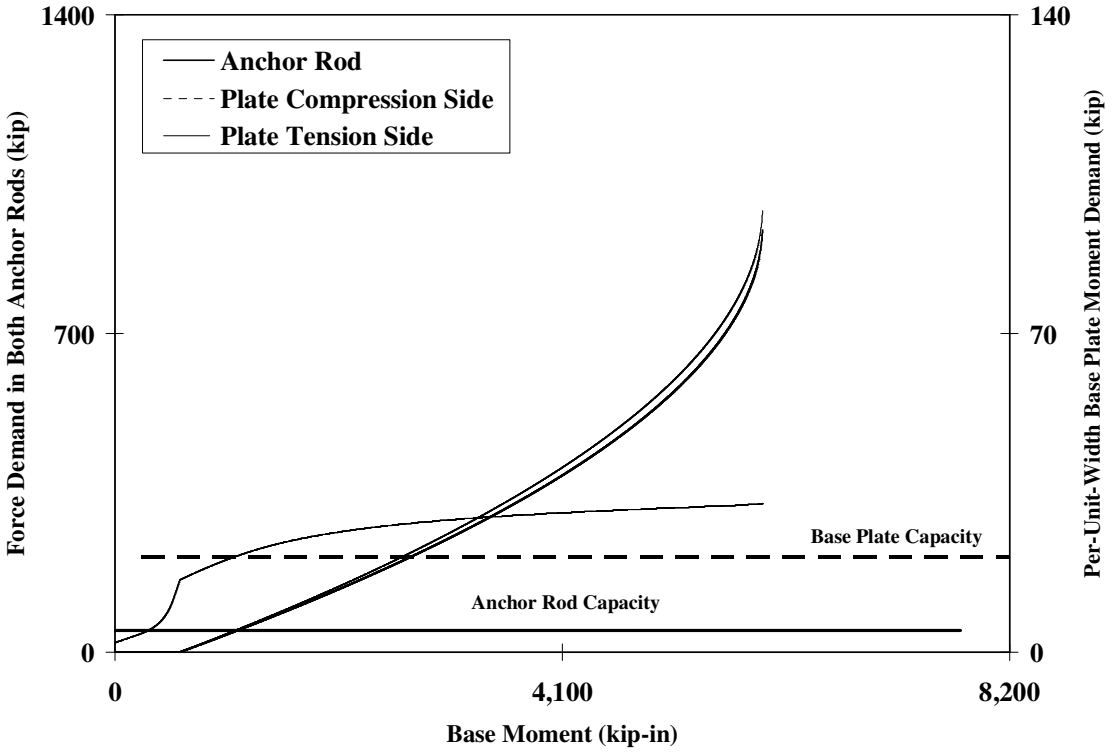

Figure 4.1 – Predicted capacity/demand plot for Test #4 using the TSB method

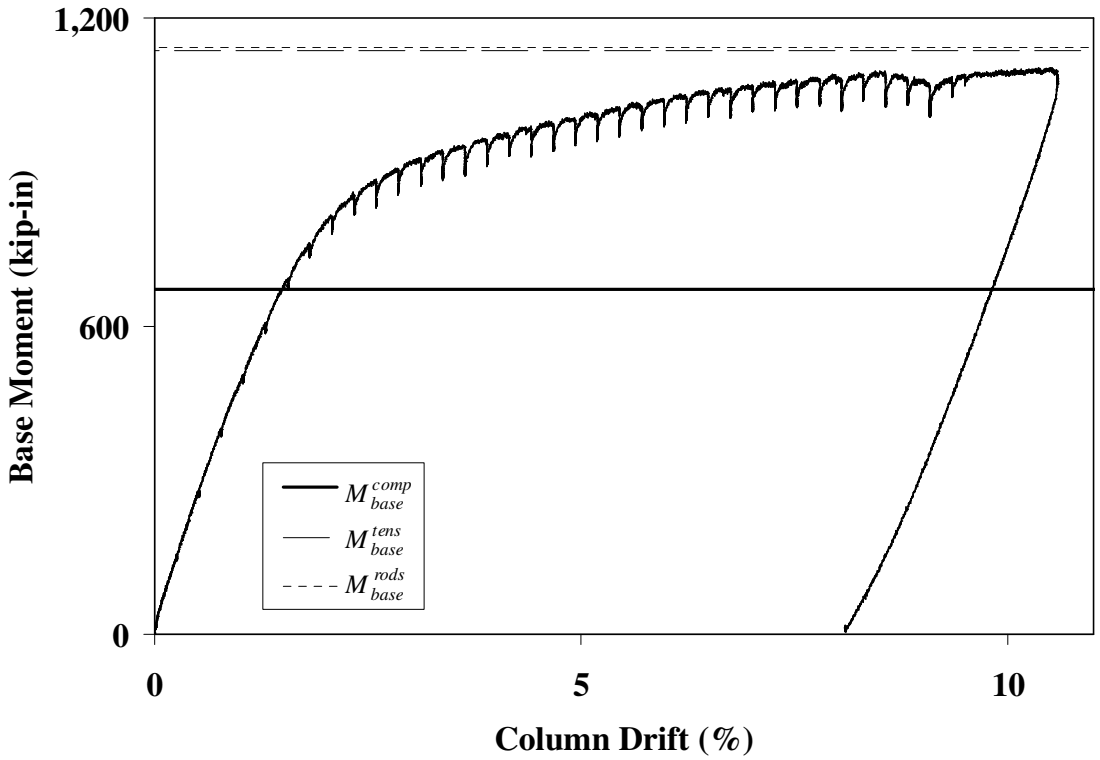

Figure 4.2 – Base moment predictions for Test #1 using the TSB method

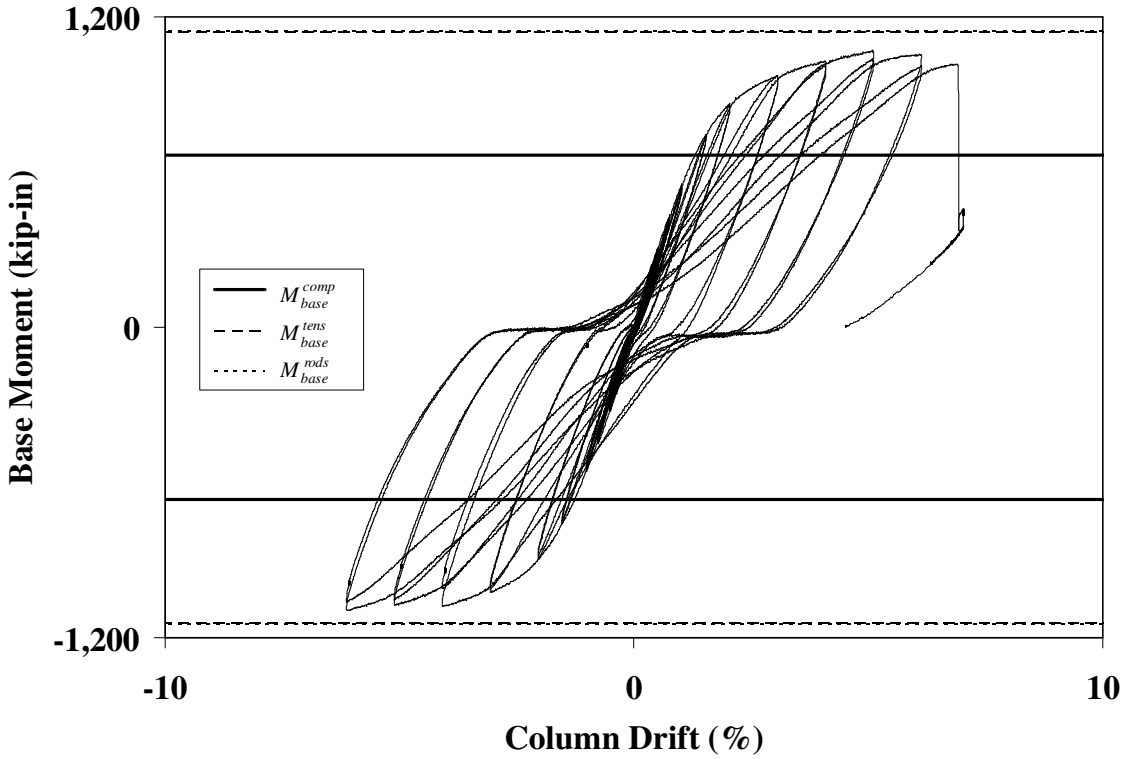

Figure 4.3 – Base moment predictions for Test #2 using the TSB method

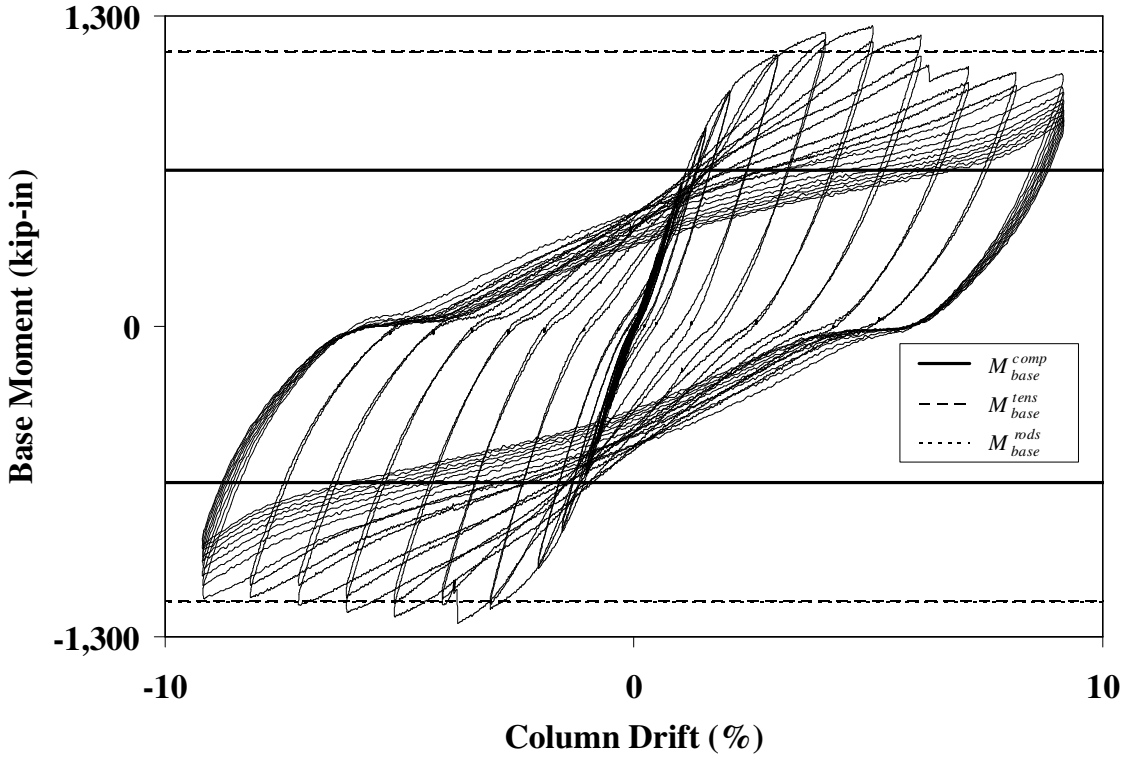

Figure 4.4 – Base moment predictions for Test #3 using the TSB method

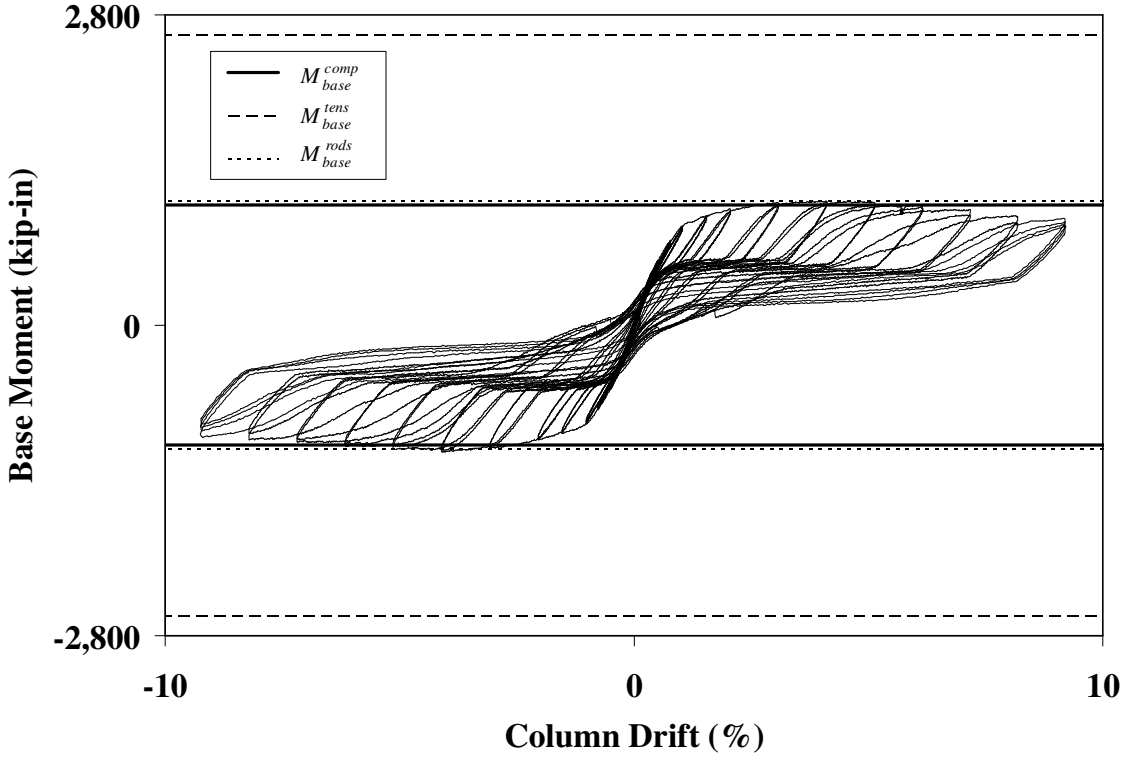

Figure 4.5 – Base moment predictions for Test #4 using the TSB method

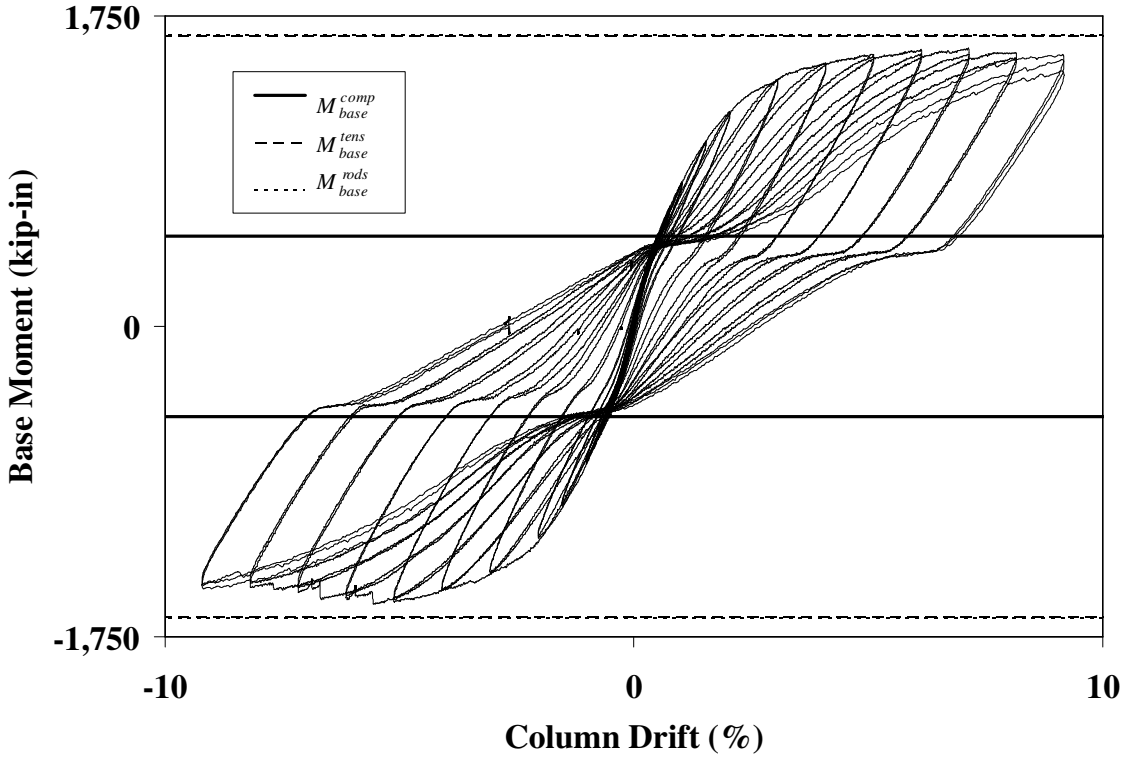

Figure 4.6 – Base moment predictions for Test #5 using the TSB method

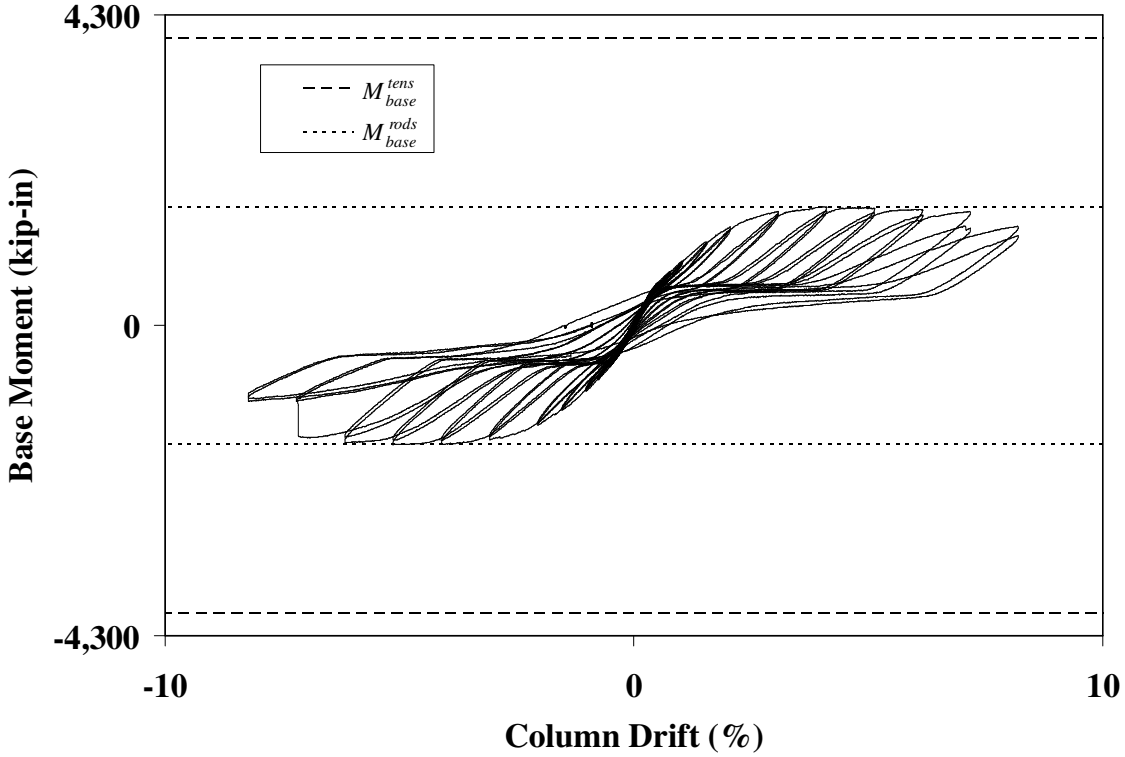

Figure 4.7 – Base moment predictions for Test #6 using the TSB method

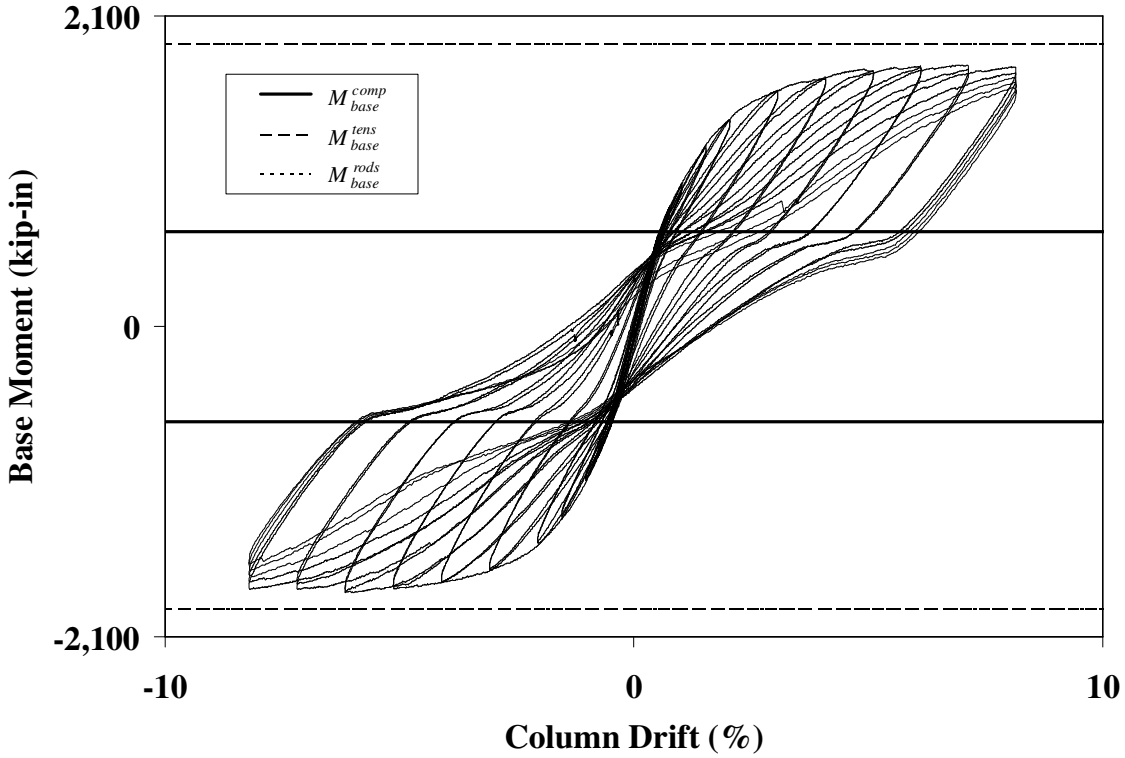

Figure 4.8 – Base moment predictions for Test #7 using the TSB method

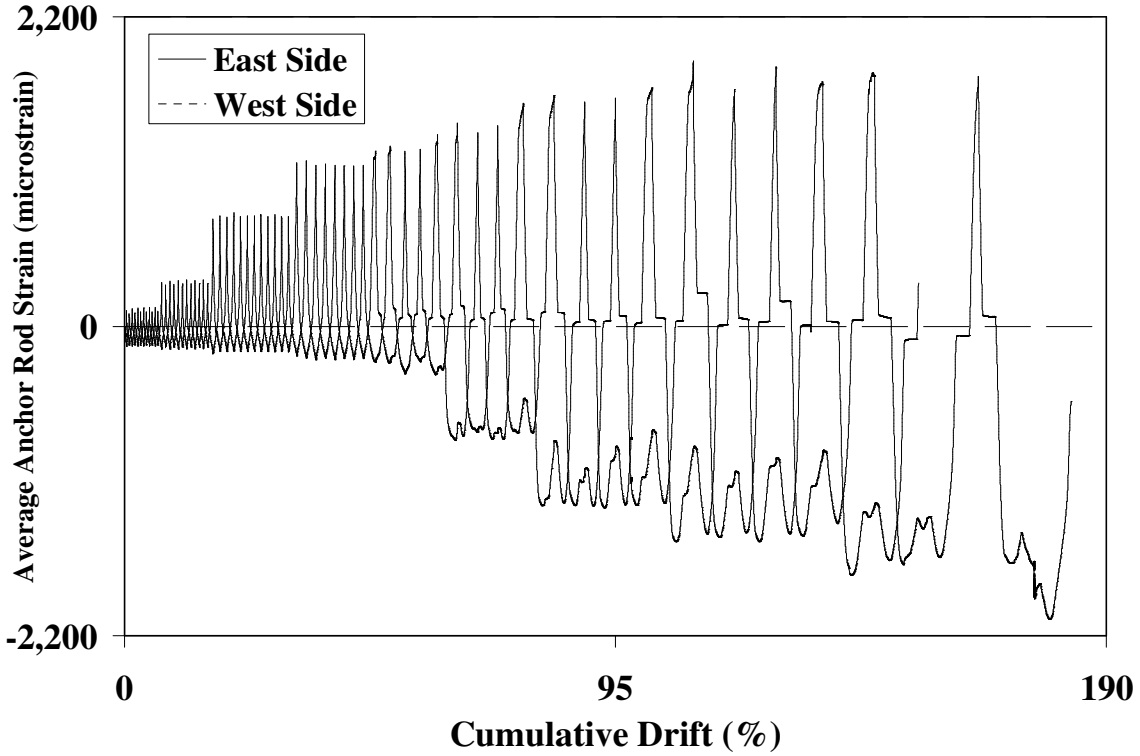

Figure 4.9 – Observed strain history for the anchor rods in Test #4

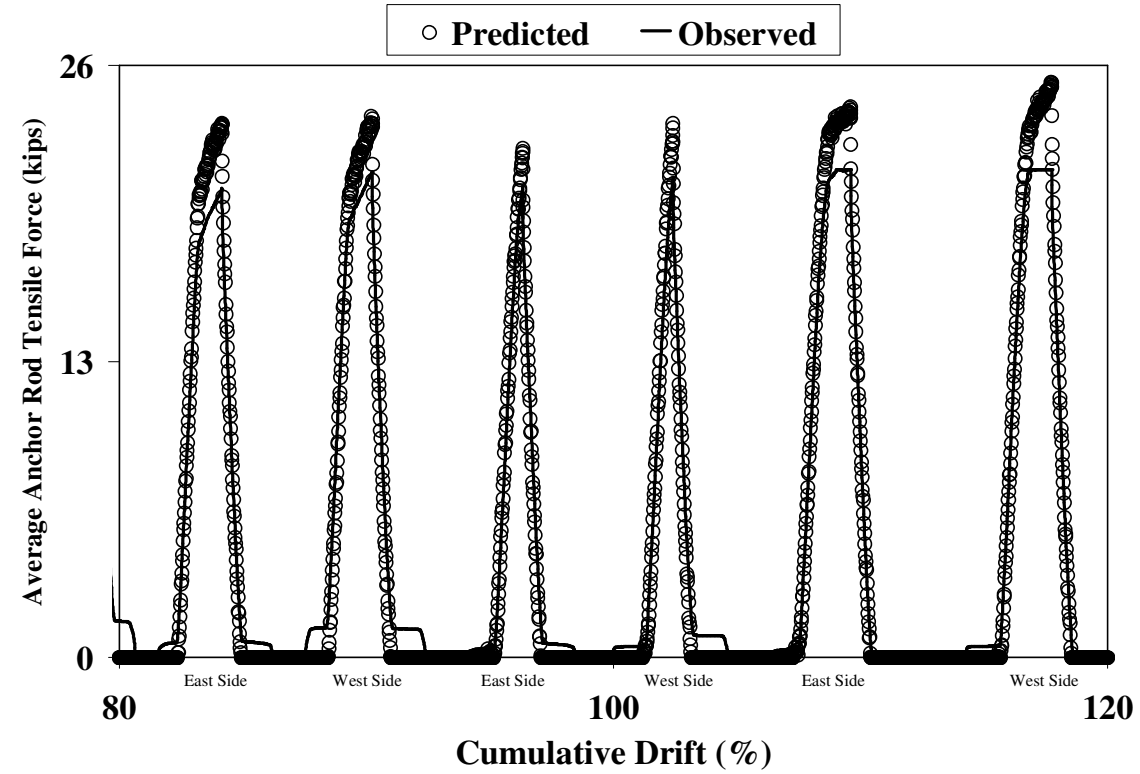

Figure 4.10 – Observed and predicted anchor rod forces, as per the TSB method, for Test #4

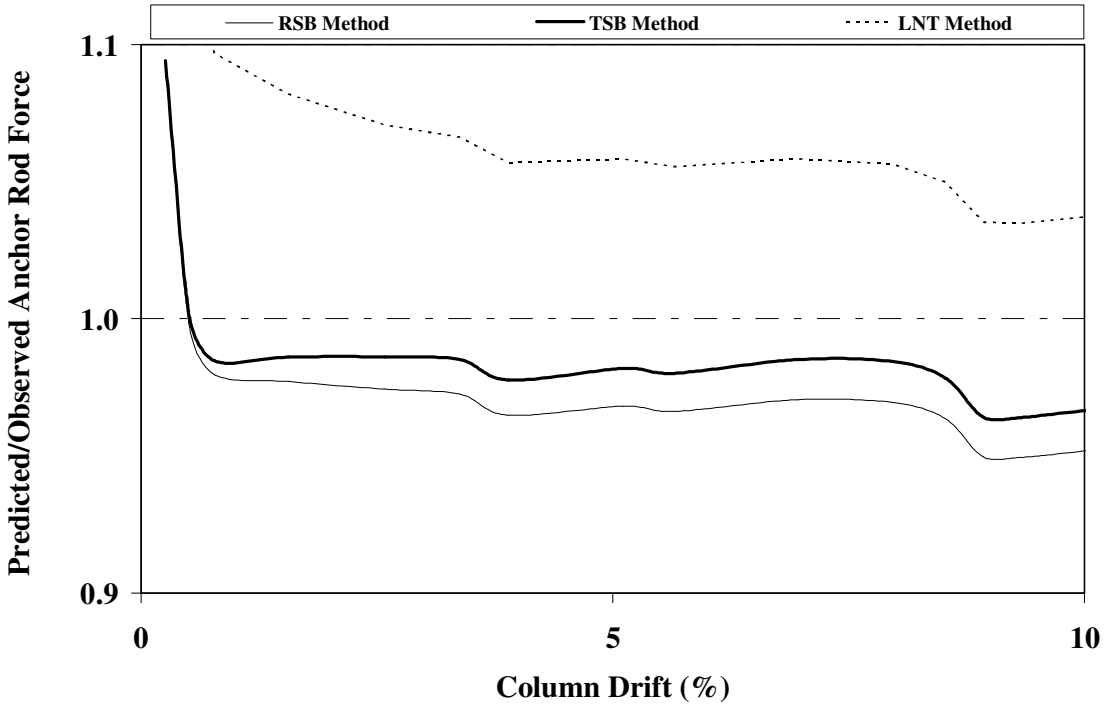

Figure 4.11 – Anchor rod force predictions for Test #1

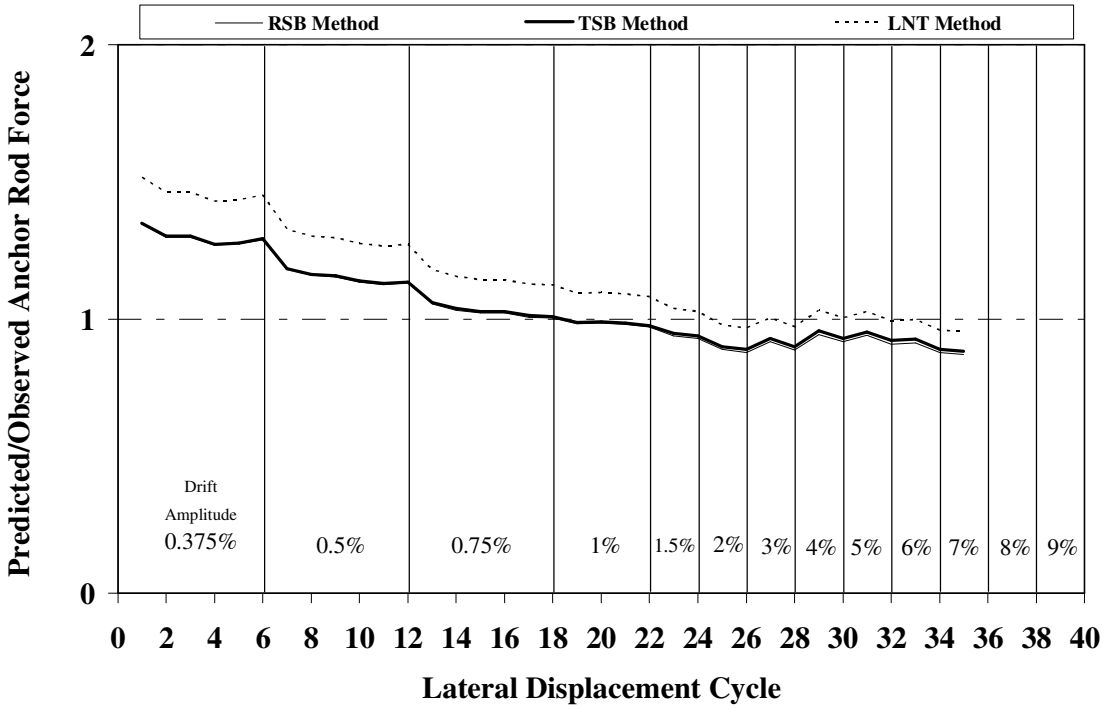

Figure 4.12 – Anchor rod force predictions for Test #2

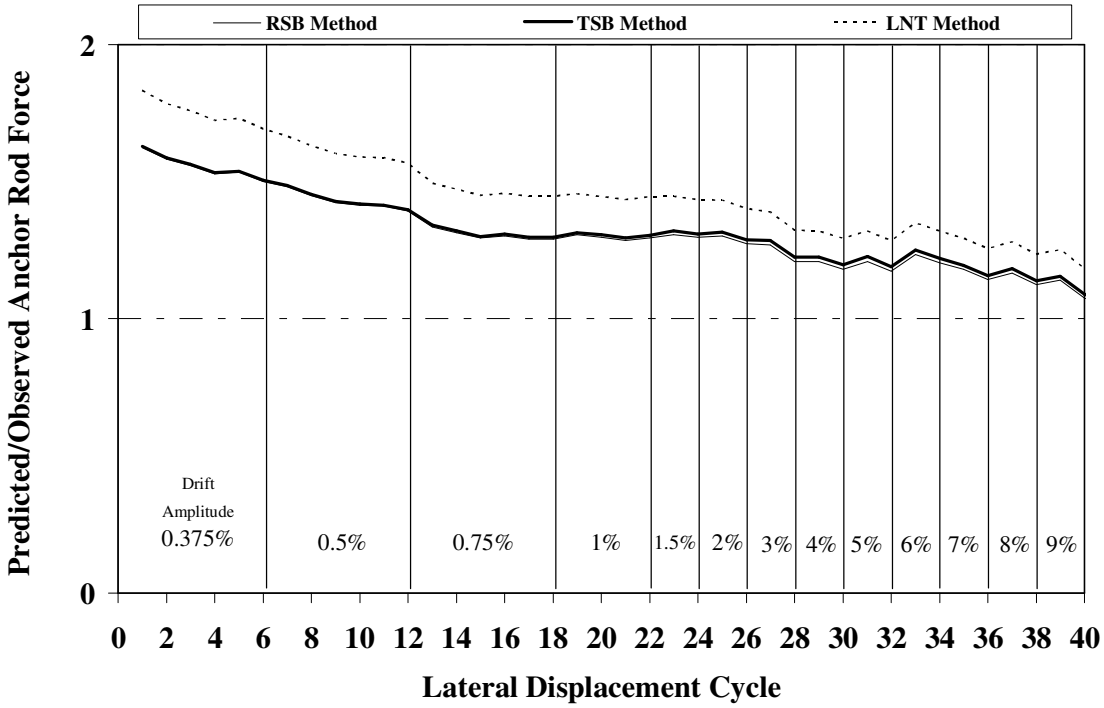

Figure 4.13 – Anchor rod force predictions for Test #3

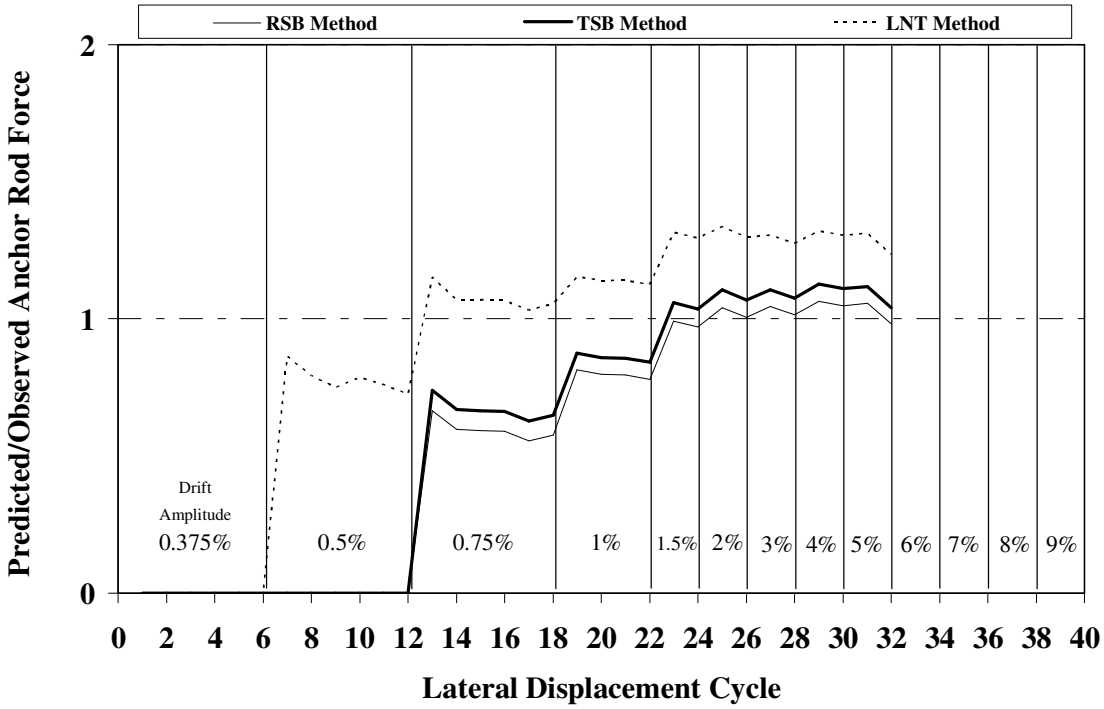

Figure 4.14 – Anchor rod force predictions for Test #4

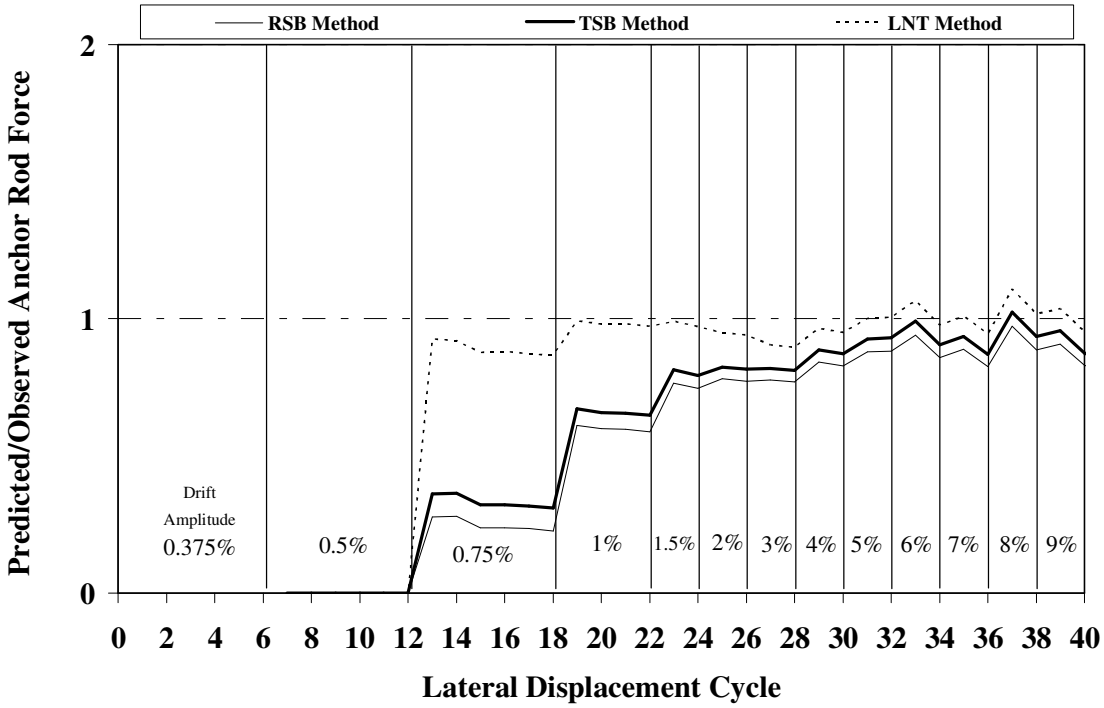

Figure 4.15 – Anchor rod force predictions for Test #5

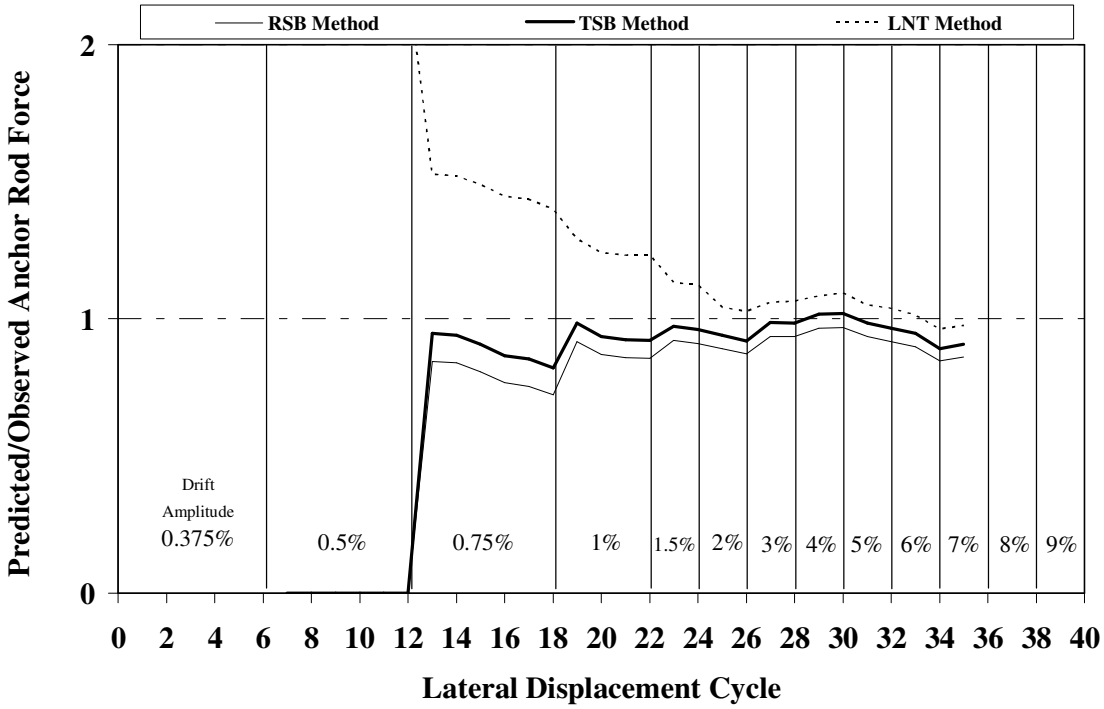

Figure 4.16 – Anchor rod force predictions for Test #6

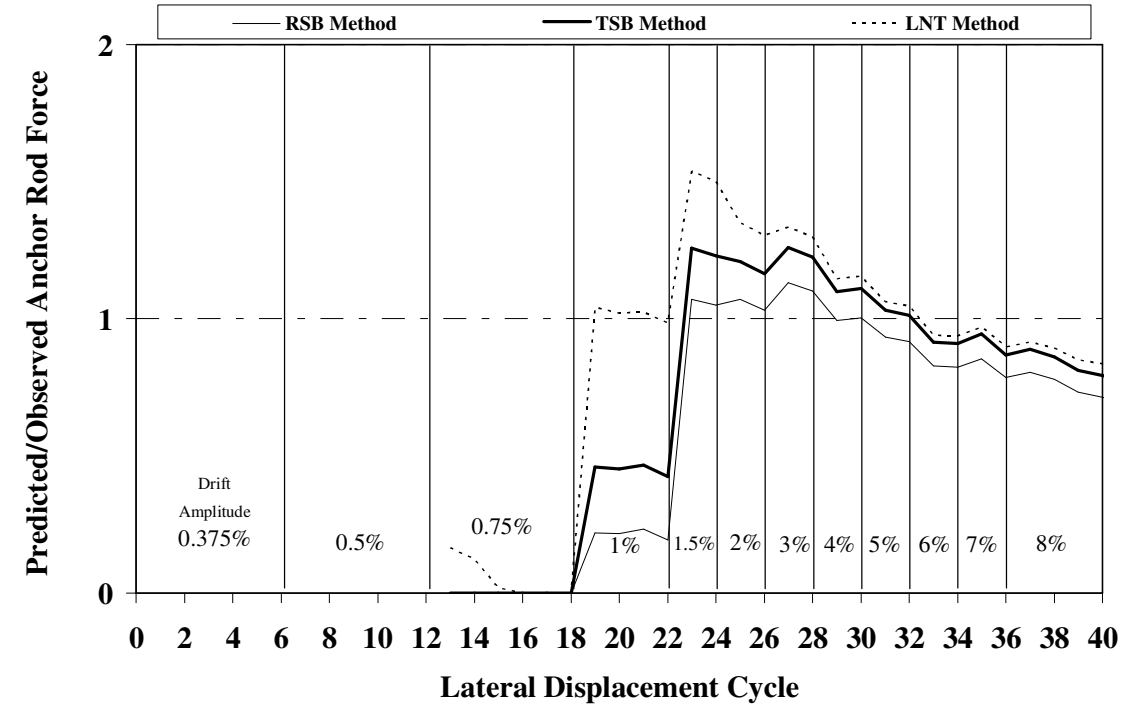

Figure 4.17 – Anchor rod force predictions for Test #7

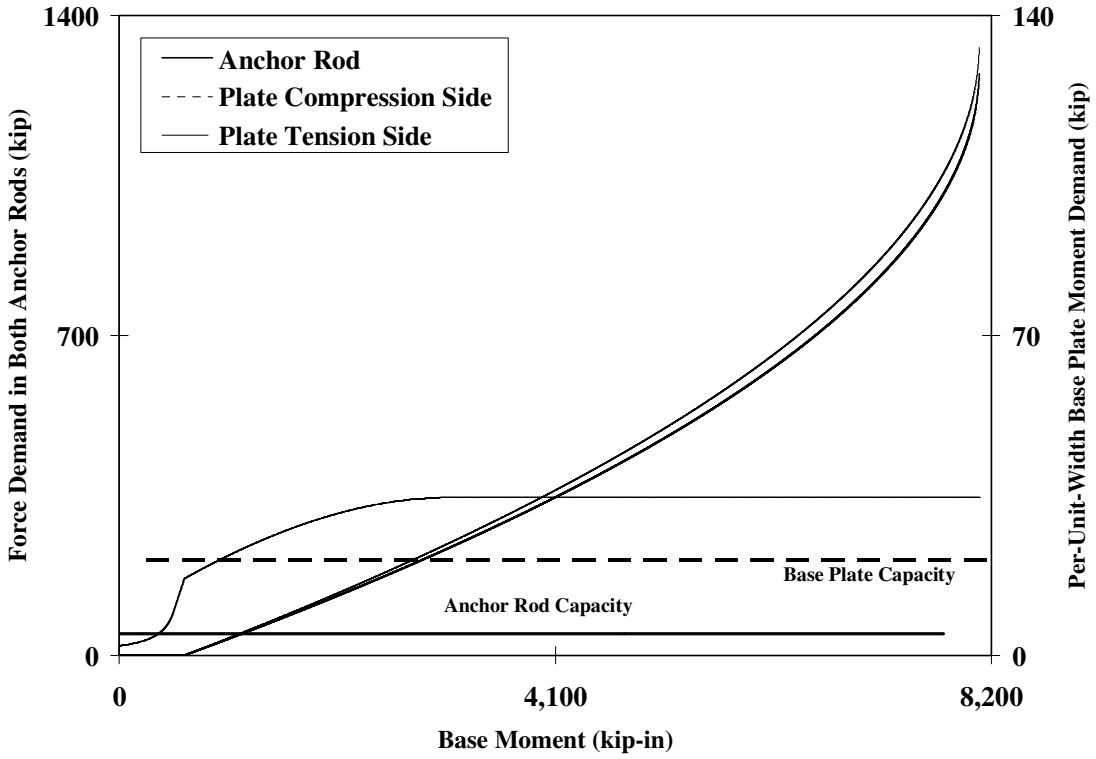

Figure 4.18 – Predicted capacity/demand plot for Test #4 using the RSB method

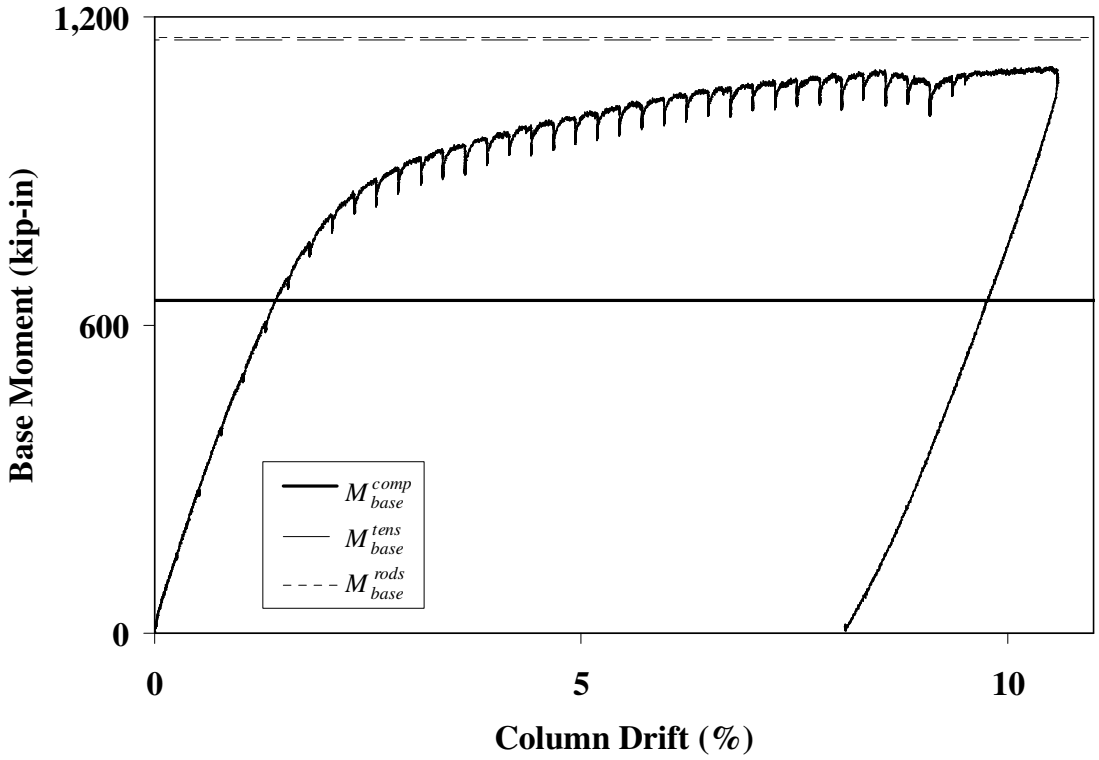

Figure 4.19 – Base moment predictions for Test #1 using the RSB method

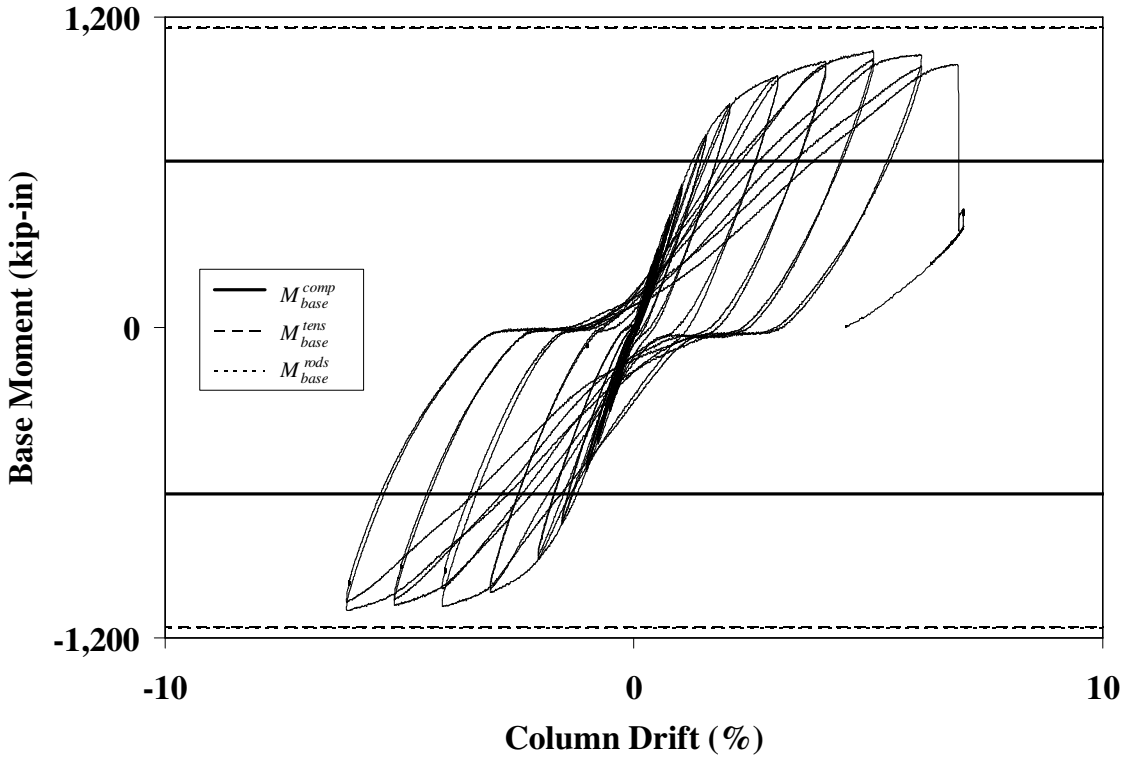

Figure 4.20 – Base moment predictions for Test #2 using the RSB method

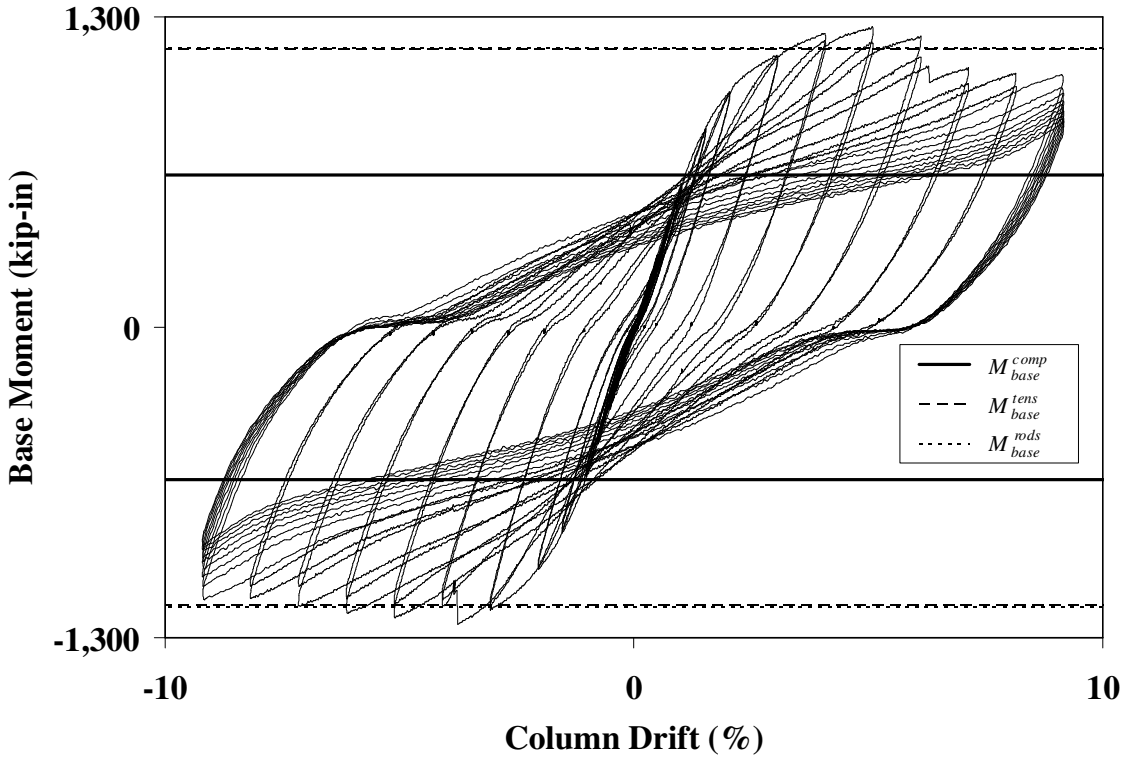

Figure 4.21 – Base moment predictions for Test #3 using the RSB method

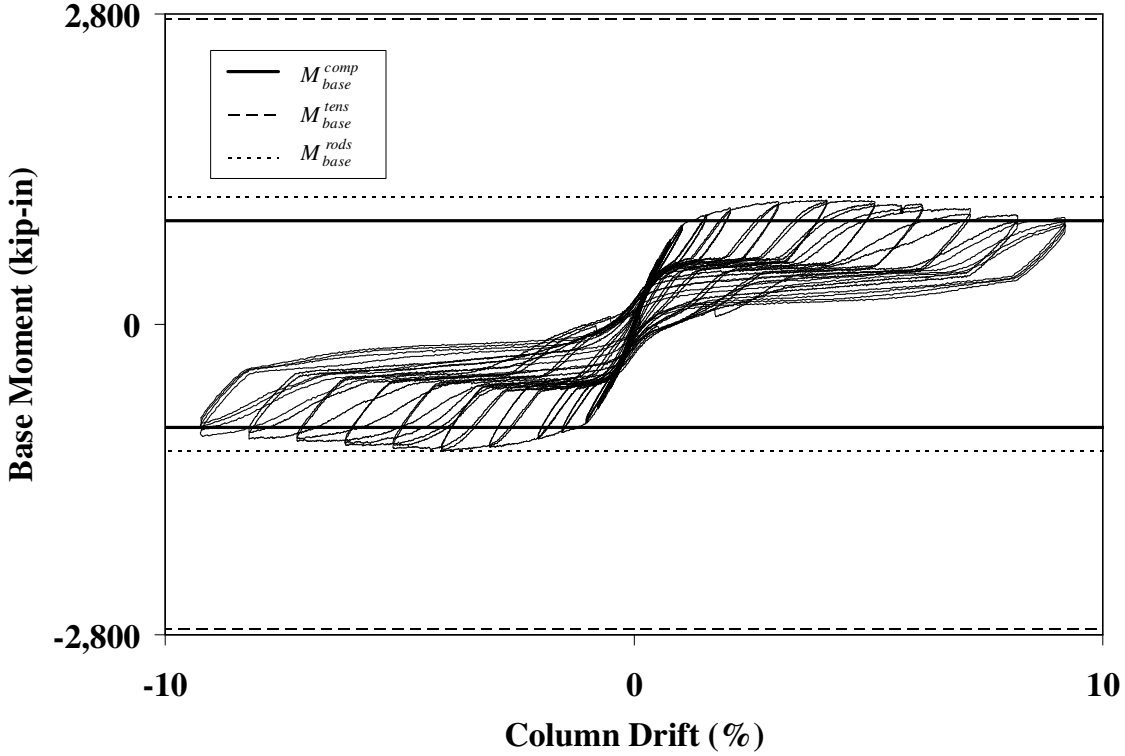

Figure 4.22 – Base moment predictions for Test #4 using the RSB method

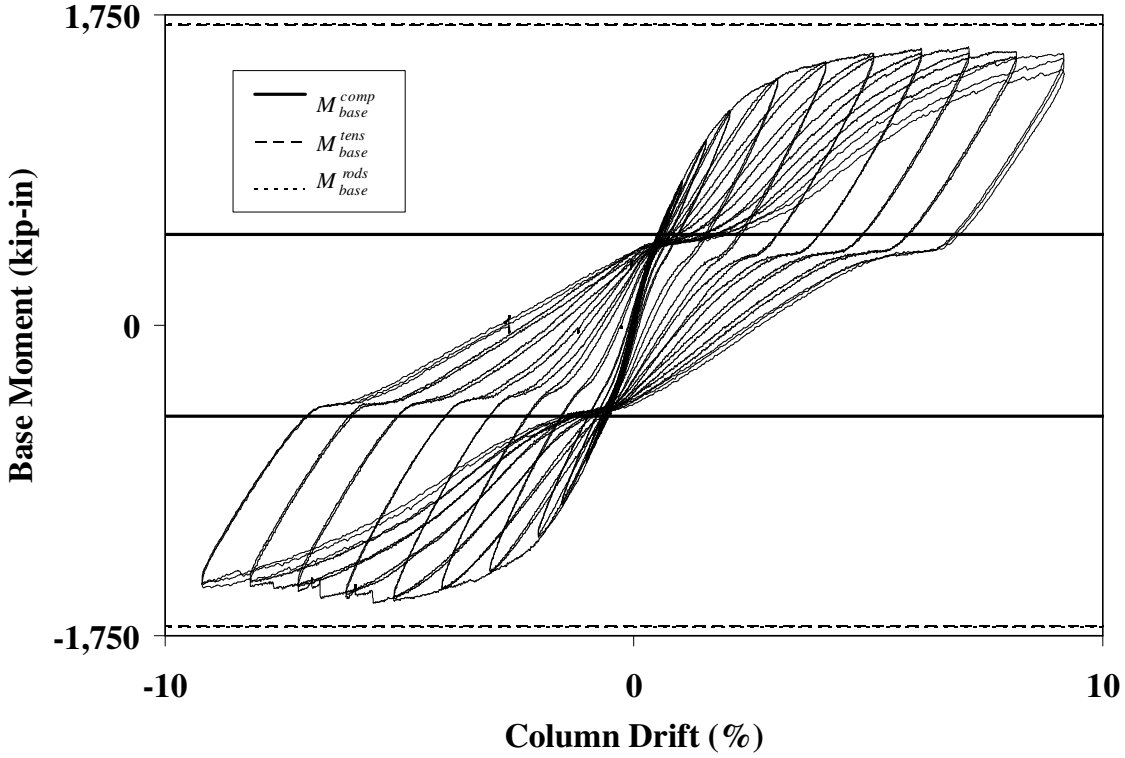

Figure 4.23 – Base moment predictions for Test #5 using the RSB method

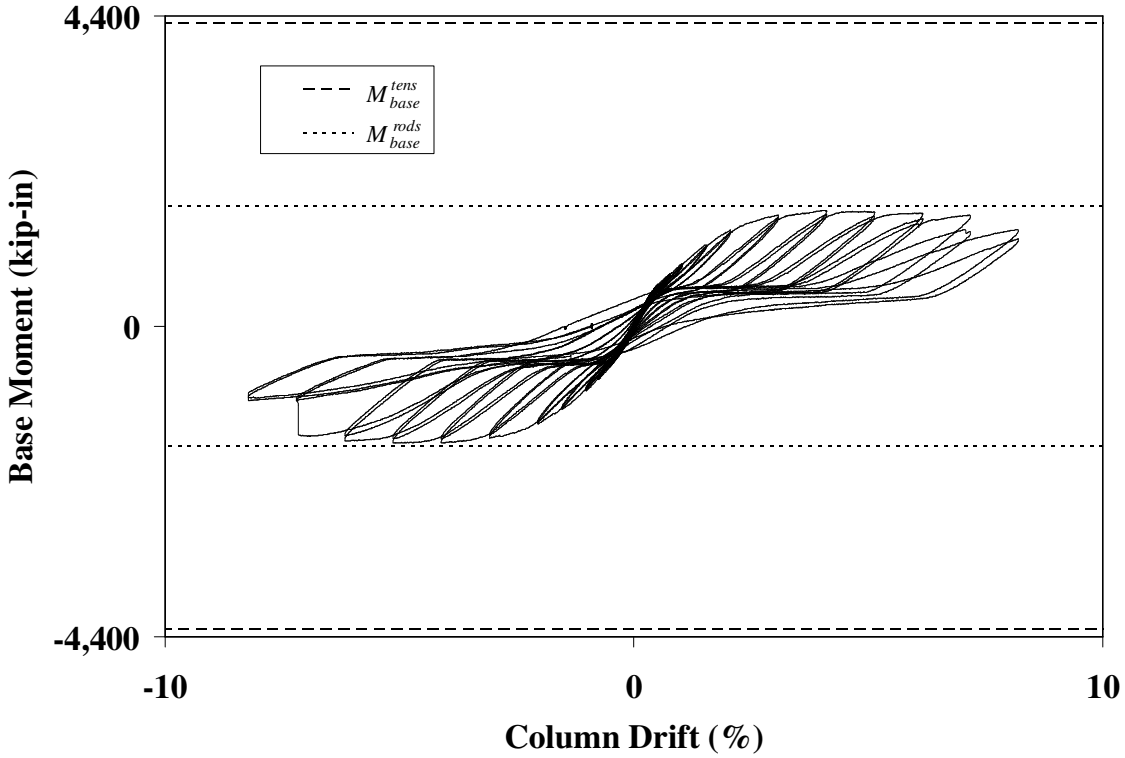

Figure 4.24 – Base moment predictions for Test #5 using the RSB method

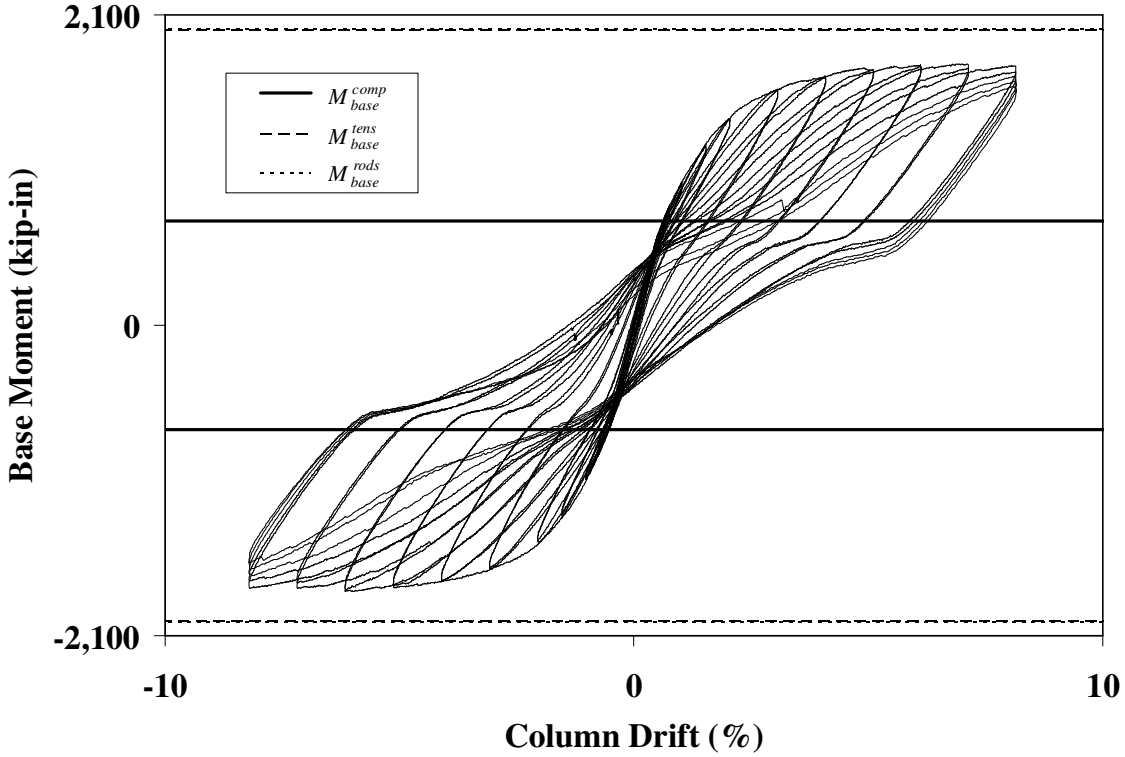

Figure 4.25 – Base moment predictions for Test #7 using the RSB method

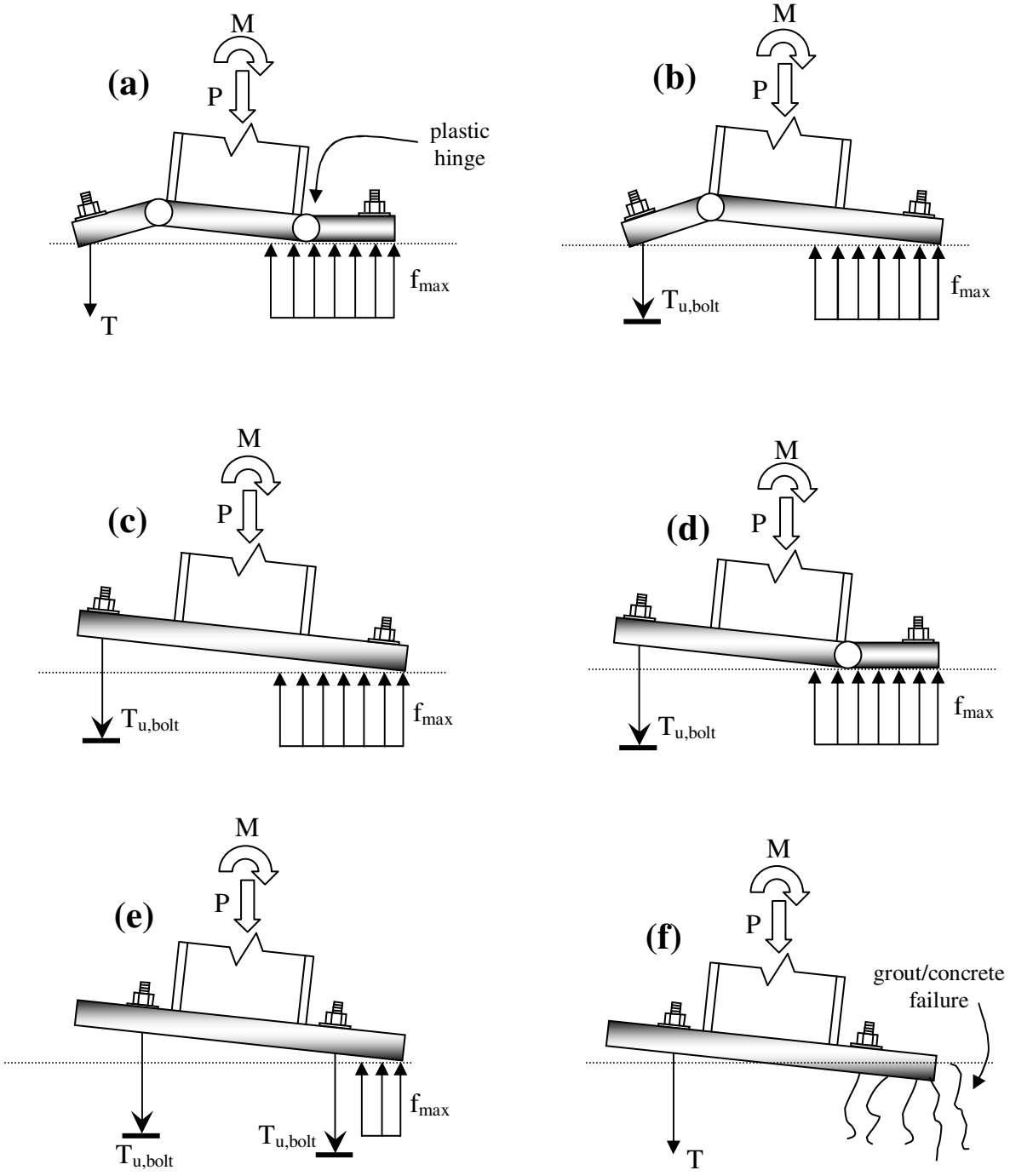

Figure 4.26 – Various plastic mechanism scenarios (a) Mechanism A (b) Mechanism B (c) Mechanism C (d) Mechanism D (e) Mechanism E (f) Mechanism F

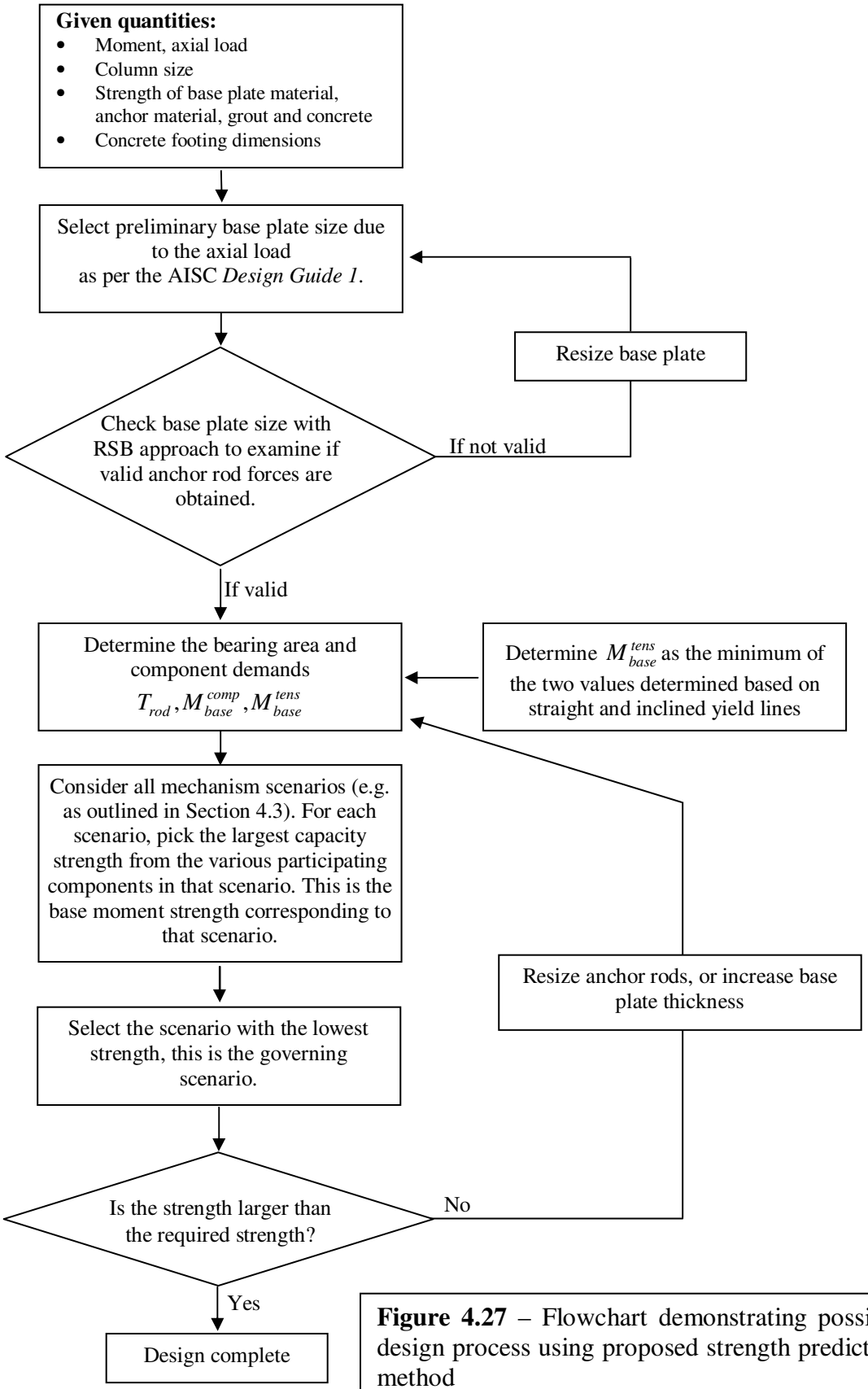

Figure 4.27 – Flowchart demonstrating possible design process using proposed strength prediction method

Chapter 5
Summary and Conclusions

5.1 SUMMARY

Current guidelines for the design of column base connections subjected to combinations of axial force and flexure, such as those featured in the AISC *Steel Design Guide Series 1* (Fisher & Kloiber, 2006), have not been adequately verified through experimental testing. As a result, current design guidelines are based on a combination of analytical methods, engineering intuition and generalization of limited test data. To address these issues, this report presents observations of seven large scale tests on exposed column base connections subjected to flexure and axial loading and addresses several topics regarding the flexural behavior of exposed base connections through a detailed analysis of these experiments.

The experiments examine the effect of several parameters on the response of base connections including (1) the base plate thickness, (2) the level of axial load, (3) the layout and strength of the anchor rods and (4) the loading history. The experimental specimens were fabricated and erected based on typical construction practice, and were subjected to cyclic and monotonic lateral deformations with or without constant axial compressive loads. Data collected from the experiments includes load-deformation response, anchor rod strains, photographic images and video recordings. All data is achieved and available for public download at the NEES Central Data Repository at http://central.nees.org (Experiment ID: 1195).

The main contribution of this study is the examination and assessment of current strength prediction methods for column base connections, as well as several proposed modifications to improve the accuracy of these methods. The proposed design method of the base plate connection is based on a plastic mechanism approach to evaluate the strength. This is in contrast to current methods which assume that the connection strength is governed by the “first yield” failure of only one component. In addition, the proposed

method considers the development of alternate yield lines patterns which are more realistic than the yield lines typically assumed by current design methods. Incorporating and modifying favorable aspects from various existing approaches, the proposed method results in accurate estimates of base connection strength and reduces the conservatism that is observed for all the existing design approaches.

In addition to providing test data which may be used to validate analytical models, the experiments provide valuable insights into the failure modes, deformation patterns and component capacities for base connections. The following sections provide a brief summary of the current study, including results of the experimental observations and the evaluation, development and applicability of strength prediction methods. The chapter concludes with a description of ongoing and future work.

5.2 EXPERIMENTAL STUDY

Seven tests were conducted on large-scale prototypes of exposed column base connections subjected to flexural and axial compression loading. The main experimental parameters investigated include base plate thickness (1", 1.5" and 2.0"), level of applied axial load (zero, 92.5 and 152.5 kips), anchor rod strength (Grade 36 and 105), number of anchor rods (four and eight rod footprint) and lateral loading type (monotonic and cyclic flexure). In all cases, the column was designed to remain elastic during loading. In addition, ancillary tests were conducted to characterize the materials used, including (1) anchor rod tension tests, (2) tension tests on coupons extracted from the base plate material, (3) standard concrete cylinder compression tests and (4) grout cylinder compression tests.

The column base connection specimens were constructed in accordance with the AISC *Design Guide 1* (Fisher & Kloiber, 2006) to reflect typical construction practice. Each test specimen consisted of an A992 Grade 50 W8×48 cantilever column welded to the center of a 14"-by-14" base plate using a partial joint penetration (PJP) weld detail. The specimens were erected atop a concrete footing through the use of setting (leveling) nuts.

High-strength, non-shrink, general construction grout was packed underneath the base plate.

For all tests, the column was loaded transversely, in the direction of the column major axis bending, with the load applied 92.5 inches above the top of the base plate to approximately represent the point of inflection in the bottom story of a fixed-base moment frame (roughly 2/3rd of the story height). Cyclic lateral loads were applied according to a displacement history based on the SAC loading protocol (Krawinkler *et al.*, 2000) to represent deformation histories that are consistent with seismic demands in moment frame buildings. In addition, for most tests, constant axial compressive loading was applied to represent gravity loading in the column.

Various qualitative observations regarding the damage and failure of the base connection include (1) yielding of the base plate, (2) crushing/spalling of the grout pad and (3) yielding and fracture of the anchor rods. A majority of the tests exhibited a combination of these mechanisms prior before reaching their ultimate strength. No damage to the concrete foundation was observed. All the base connections showed excellent ductility and endured 6% or greater drift amplitudes. Only two tests exhibited sudden failure (due to anchor rod fracture) while all other tests were stopped (typically at 9% drift cycles) due to the stroke limit of the actuator.

In addition to moment-drift hysteretic response plots, various experimental measurements were recovered, including the maximum base moment, maximum column drift, column drift at first yield (approximately 1% for every test), maximum base rotation, connection energy dissipation, initial elastic stiffness and lateral slip of the base plate relative to the foundation. In addition, anchor rod strain data was collected and subsequently converted to anchor rod forces in order to evaluate the assumed bearing stress distributions within the connection.

5.3 EVALUATION OF EXISTING STRENGTH PREDICTION METHODS

Experimental data is used to evaluate two strength prediction methods of exposed column bases under flexure featured in the AISC *Steel Design Guide 1* (Fisher & Kloiber, 2006). The methods are evaluated based on their ability to characterize the peak moment of the base connection, forces in the anchor rods and deformation (yield line) patterns in the base plate. Measured (rather than specified/nominal) material properties (for the anchor rods, base plate steel, grout and concrete) are used in the analysis of all approaches to accurately characterize each material. One strength prediction method, the Triangular Stress Block (TSB) method assumes that the combination of applied axial force and moment is resisted through the development of a triangular/trapezoidal compressive stress distribution in the concrete/grout foundation under the base plate and, as the base plate uplifts, the development of tensile forces in the anchor rods. The Rectangular Stress Block (RSB) method is similar to the TSB method, except that it assumes the development of a rectangular (rather than a triangular) bearing stress distribution.

The TSB and RSB approaches each consider two flexural loading conditions, characterized by either a low or high load eccentricity. Under low eccentricity, the applied axial force and moment combination is assumed to be resisted exclusively through the development of a bearing stress distribution beneath the base plate. The distinction between the low and high eccentricity case is defined by a critical eccentricity based on the base plate dimensions, the maximum bearing pressure and the level of applied axial load. When the load eccentricity exceeds the critical eccentricity, the applied axial force and moment combination can no longer be resisted by bearing stresses alone and equilibrium requires the development of tensile forces in the anchor rods.

For low load eccentricities, failure of the connection is a result of flexural yielding of the plate from bearing stresses acting beneath the base plate. For high load eccentricities, the base plate is assumed to lift off from the concrete/grout foundation and is analyzed through the simplifying assumption that the maximum bearing stress is equal to the limit of the bearing strength of the concrete. From this assumption, the principles of statics may be applied to determine both the forces in the anchor rods as well as the area over

which bearing is active. The only failure modes possible under high load eccentricities are (1) flexural yielding of the base plate due to bearing stresses, (2) tensile failure of the anchor rods as the base plate uplifts and (3) flexural yielding of the base plate due to tensile forces imposed by the anchor rods. Consequently, the design of base connections involves determining a combination of anchor rod size/strength and layout, as well as base plate size and thickness/strength, such that each of these three failure modes is prevented. For the test specimens examined and based on procedures outlined in the *Design Guide 1*, both the TSB and RSB methods are conservative in their ability to characterize the strength capacity of the base connection. The average test-to-predicted base moment ratio equals 1.86 for both methods and all tests, excluding the eight anchor rod Test #3. If failure due to base plate bending on the compression side is neglected, the TSB and RSB methods provide accurate predictions of strength (average test-to-predicted ratio = 0.96 for both methods and all tests other than Test #3). For all tests, both the TSB and RSB methods accurately predict anchor rod forces (within 20%) for base connections with low axial forces (i.e. zero to 90 kips axial compression) and for drift levels greater than 1.5%. Considering inclined yield lines for base plate bending does not increase the accuracy of the TSB and RSB method and results in predictions which are more conservative than assuming conventional yield lines prescribed by the *Design Guide*. For certain combinations of axial force and moment, the TSB and RSB method cannot provide a valid solution for the anchor rod forces. In these cases, the base plate area and/or anchor rod location must be modified.

Overall, the TSB and RSB methods give similar predictions of anchor rod forces and the strength capacity of the base connection. Thus, based on the current investigation, it is difficult to judge whether the TSB or RSB method is more accurate in characterizing the bearing stress distribution. However, based on previous experimental studies (e.g. DeWolf, 1982) and considerations of ultimate limit state design, the RSB method may be more appropriate.

It is important to note that application of the TSB and RSB methods are just one part of the strength prediction process. Several other issues should be considered for predicting

the base connection capacity, including (1) quantifying the maximum bearing strength, (2) characterization of complex yield lines, (3) the choice of the appropriate material strength (i.e. yield or ultimate strength) of the various connection components and (4) the consideration of a mechanism-based approach which accounts for inelastic overstrength in the connection after the weakest component has yielded.

5.3 PROPOSED METHOD FOR STRENGTH PREDICTION OF COLUMN BASE CONNECTIONS

To overcome the limitations of the current design approach, a new method incorporating favorable features from existing approaches was presented. The key features of the proposed approach are –

1. The compressive bearing stresses are characterized by the rectangular stress block (RSB) method.
2. The maximum bearing stress is determined as the minimum of the bearing strength of the concrete foundation and the bearing strength of the grout pad.
3. The anchor rod tensile capacity, as well as the base plate flexural capacity, is determined using the *ultimate* material strength.
4. For flexural yielding of the base plate on the tension side, inclined yield lines are considered.
5. A mechanism-based approach is adopted such that the base connection strength capacity is controlled by the formation of a plastic mechanism. Thus, the strength is determined based on a combination of individual component failures.

The proposed design method is highly accurate for predicting the peak connection strength (e.g. the average test-to-predicted base moment = 0.99, C.O.V. = 0.057). Thus, the proposed method provides a more accurate estimate of the base connection strength as compared to existing approaches. Moreover, the predicted failure modes and assumed yield line patterns are consistent with the response observed during testing. In addition, the test-to-predicted ratios do not show a systematic bias towards any of the test parameters.

While the proposed method is an improvement of the previous approaches, a summary of the key limitations and observations of the new approach is now outlined –

- The proposed method characterizes the strength of the base connection based on the development of a plastic mechanism. Thus, designed as per this method, the base connection will exhibit inelastic action under extreme loads.
- The method is applicable to typical base connections set on concrete or grout subjected to strong axis bending of the column and may be applicable for weak axis bending as well as loading situations of flexure with axial tension. However, the method does not consider strain compatibility and thus is applicable for connections with tension in only one anchor rod bolt line. Furthermore, specific details such as stiffeners and haunches are not addressed.
- Due to mathematical limitations, the formulation of the RSB method may result in invalid or unreasonable solutions for certain base plate geometry, base moment and axial load combinations.
- The rectangular bearing stress distribution (as well as the triangular distribution) are not based on compatibility criteria, and thus cannot incorporate the effect of base plate flexibility on the bearing stress distributions. As such, the method may produce erroneous (although conservative) results for situations of (1) large eccentricities with low moment, (2) very thin base plates or (3) very strong foundations.
- The seismic design of these connections must be addressed in broader context with a discussion of various issues including the degree to which inelastic action (i.e. ductility) may be allowed in the components of these connections, as well as the connection itself.

5.5 CONCLUSIONS, DESIGN IMPLICATIONS AND FUTURE WORK

Based on the reported test data and consideration of previously published literature, this study has resulted in improved methods to characterize the strength of column base connections subjected to combinations of axial compression and flexure. These improved methods, as well as general experimental findings, may be suitably incorporated into current design guidelines for the flexural design of column base connections. As the

scope of this report is to present and analyze the experimental data, evaluate existing methods and present improved methods for strength prediction of base connections, complete design guidelines are not presented herein. Future efforts, including collaboration with the AISC oversight committee, may result in specific design guidelines (in the form of reports or papers) or modifications to the AISC *Steel Design Guide 1*. The integration of these findings into design guidelines may involve a consideration of several issues, some of which are outlined below –

1. Owing to the expense associated with large-scale testing, the experiments presented in this report do not include replicate data sets for statistical analysis. Thus, before applying the proposed methods for design, appropriate resistance factors (ϕ-factors) should be developed through examination of previous standards, specifications and similar test data. Moreover, in some situations, the use of the resistance factors may, in some situations, produce unconservative results. For example, the bearing pressure acting upwards on the compression side of the base plate produces a moment in the base plate which must be designed for. If a resistance factor is included in the estimate of the bearing pressure, the predicted base moment may be reduced, leading to an unconservative assumption. Similarly, the estimates of the anchor rod forces, and consequently the flexural demand on the tension side of the base plate, are impacted by the use of the resistance factor on the bearing pressure. Thus, a detailed reliability analysis (and possibly a sensitivity analysis) should be conducted to determine the appropriate use of resistance factors. However, in the absence of such an analysis, this report presents a preliminary proposal for the use of ϕ-factors for various situations.
2. The strength prediction method proposed in this study relies on the assumption of plastic mechanisms or scenarios involving the yielding of several components. These mechanisms are based on failure and deformation modes observed during testing. For incorporation into design guidelines, the proposed strength prediction method may be complemented by additional mechanisms which involve situations that were not explicitly tested in this study, such as a highly flexible base plate attached to a

relatively strong footing or a highly rigid base plate attached to a relatively weak footing.

3. As discussed previously, the proposed strength prediction method assumes the development of a plastic mechanism to characterize the strength of the base connection. Thus, if designed considering this overstrength, the base connection will exhibit some degree of inelastic action under extreme loads. While this may be the desired approach under extreme situations such as seismic conditions, the current method (not considering a mechanism approach) might be more appropriate when elastic response is desired under service loads.
4. One of the tests in this program featured an eight anchor rod layout which is statically indeterminate and, as a result, the prediction of its strength is outside the framework the RSB and TSB methods. However, the response of this specimen was not significantly different from other similar specimens. Thus, this study did not result in the development of design approaches for these situations. Ongoing finite element simulations address these and other non-standard designs and loading conditions, such as bi-axial bending.
5. This study did not feature experiments or analysis involving the combined application of a tensile axial force and flexure. However, based on the results of this study, refined approaches for these types of situations may be developed.
6. While this study focuses on the maximum strength of a base connection, it does not address the axial force and moment demands in the connection; i.e. these are assumed to be "given" quantities. In seismic design, where inelastic action may be anticipated in the base connection, the moment and axial load demands may be a result of the interaction of the base connection hysteretic response with the building response. A detailed analysis of structural response subjected to nonlinear time histories, in conjunctions with nonlinear cyclic moment-rotation hinge models of the base connection, is required to appropriately characterize these moment and axial force demands.
7. All the specimens examined in this study showed a great capacity for inelastic deformation as well as large hysteretic energy dissipation. Moreover, all the components of the connection (i.e. the base plate as well as the anchor rods) were

shown to contribute to this inelastic response. This data may be used to determine the degree of inelastic deformation permissible in the base connection during seismic loading, as well as desirable hierarchies of failure for capacity-based seismic design of the connection.

In summary, several issues remain to be addressed before the results of this study may be incorporated into design recommendations. Owing to these unresolved issues, some of the ongoing and future work includes development of finite element simulations for alternate details, as well as nonlinear time history analysis of structures to characterize demands in base connections. Finally, as discussed in the introduction, the experimental results presented in this report are one part of a comprehensive study on column base connections. While this phase of testing focused on loading combinations dominated by flexural and axial loading, other situations may be dominated by interactions of flexural, shear and axial loading. Axial and shear loading conditions are investigated by a companion report (Gomez *et al.*, 2009).

References

ACI Committee 318. (2002), "Building Code Requirements for Structural Concrete (ACI 318-02) and Commentary (ACI 318R-02)," Farmington Hills, MI.

Adany, S., Calado, L., and Dunai, L. (2000), "Experimental Studies on Cyclic Behavior Modes of Base Plate Connections," *Proceedings of the Third International Conference STESSA 2000* Montreal, Canada.

Ahmed, T., Burley, E., and Rigden, S. (1998), "Bearing Capacity of Plain and Reinforced Concrete Loaded over a Limited Area," *ACI Structural Journal*, May-June 1998, pp. 330- 342.

American Institute of Steel Construction (AISC). (2006), "Fundamentals of Column Bases and Exposed Seismic Base Design," *Request for Proposal (RFP) 6807*, August 11, 2006.

American Institute of Steel Construction (AISC). (2005), "Seismic Design Manual," American Institute of Steel Construction, Chicago, IL.

American Institute of Steel Construction (AISC). (2005), "Steel Construction Manual," 13th Edition, American Institute of Steel Construction, Chicago, IL.

Akiyama, H., Kurosawa, M., Wakuni, N., and Nishinura, I. (1984), "Strength and Deformation of Exposed Type of Steel Column Bases," *Journal of Structural and Construction Engineering*, Transactions of AIJ, No. 342, pp. 46-54. [In Japanese]

Akiyama, H., Yamada, S., Takahashi, M., Katsura, D., Kumura, K., and Yahata, S. (1998), "Full Scale Shaking Test of the Exposed-Type Column Bases," *Journal of Structural and Construction Engineering*, Transactions of AIJ, No. 514, pp. 185-192. [In Japanese]

Astaneh, A., Bergsma, G., and Shen J.H. (1992), "Behavior and Design of Base Plates for Gravity, Wind and Seismic Loads," *Proceedings of the National Steel Construction Conference*, Las Vegas, Nevada, AISC, Chicago, Illinois.

Astaneh-Asl, A. (2008), "Seismic Behavior and Design of Base Plates in Braced Frames," *SteelTIPS*, Technical Information and Product Service, Structural Steel Educational Council.

Astaneh-Asl, A., Bergsma, G. (1993), "Cyclic Behavior and Seismic Design of Steel Base Plates," *Proceedings, Structures Congress*, ASCE 1993; 409–14.

ASTM Standard C31. (2008), "Standard Practice for Making and Curing Concrete Test Specimens in the Field," *ASTM International*, West Conshohocken, PA.

ASTM Standard C39. (2005), "Standard Test Method for Compressive Strength of Cylindrical Concrete Specimens," *ASTM International*, West Conshohocken, PA.

ASTM Standard C109. (2007), "Standard Test Method for Compressive Strength of Hydraulic Cement Mortars (Using 2-in. or [50-mm] Cube Specimens)," *ASTM International*, West Conshohocken, PA.

ASTM Standard A307. (2007), "Standard Test Methods and Definitions for Mechanical Testing of Steel Products," *ASTM International*, West Conshohocken, PA.

Ballio, G., and Mazzolani, F.M. (1983), "Theory and Design of Steel Structures," Chapman and Hall, London and New York, pp. 257-264.

Blodgett, O.W. (1966), "Design of Welded Structures," The James F. Lincoln Arc Welding Foundation, Cleveland, Ohio, pp. 3.3-1 – 3.3-32.

Burda, J.J., and Itani, A.M. (1999), "Studies of Seismic Behavior of Steel Base Plates," Report No. CCEER 99-7, Reno (NV): Center of Civil Engineering Earthquake Research, Department of Civil and Environmental Engineering, University of Nevada, NV.

Cannon, R.W. (1992), "Flexible Base Plates: Effects of Plate Flexibility and Preload on Anchor Loading and Capacity," *ACI Structural Journal*, Volume 89, Issue 3, pp. 315–324.

Carrato. P. (1991), "Testing and Analysis of Base Plate Connections," Anchors in Concrete - Design and Behavior, G.A. Senkiw and H.B. Lacelot III, Editors, ACI Special Publication 130.

Comité Européen de Normalisation (CEN) (1992). "ENV1993 Eurocode 3; Design of Steel Structures," Brussels, Belgium.

Cook, R.A., and Klingner, R.E. (1992), "Behavior of Multiple-Anchor Steel-to-Concrete Connections with Surface Mounted Baseplates," Anchors in Concrete Design and Behavior, G.A. Senkiw and H.B. Lacelot III, Editors, ACI Special Publication 130, pp. 61-122.

Cowie, K., Hyland, C., and Mago, N. (2004), "Column Base Plate Design - Lapping Strip Method," *Proceedings of the 2004 Pacific Structural Steel Conference*, Long Beach, California.

Cui, Y., Nagae, T., and Nakashima, M. (2009), "Hysteretic Behavior and Strength Capacity of Shallowly Embedded Steel Column Bases" *ASCE Journal of Structural Engineering*, [In Print].

DeWolf, J.T. (1978), "Axially Loaded Column Base Plates," *Journal of the Structural Division*, ASCE, Vol. 104, No. ST5, May, pp. 781-794.

DeWolf, J.T. (1982), "Column Base Plates," Structural Engineering Practice, Vol. 1, No.1, pp. 39-51.

DeWolf, J.T., and Ricker, D. (1990), "Design of Column Base Plates," American Institute of Steel Construction (AISC), *Steel Design Guide Series 1*, Chicago, IL.

DeWolf J.T., and Sarisley, E.F. (1980), "Column Base Plates with Axial Loads and Moments," *Journal of the Structural Division*, ASCE, Vol. 106, No. 11, November 1980, pp. 2167-2184

Di Sarno, L., Pecce, M.R., and Fabbrocino, G. (2006), "Inelastic Response of Composite Steel and Concrete Base Column Connections," Tokyo, STESSA 2006. Behavior of Steel Structures in Seismic Areas 2006. Mazzolani, F.M., editor. Published by A.A. Balkema, a member of Sweets & Zeitlinger Publishers, August 2006.

Doyle, J.M. and Fisher, J.M. (2005), "Discussion: Beam-Column Base Plate Design - LRFD Method," *Engineering Journal*, AISC, Fourth Quarter, Chicago, IL.

Drake, R.M. and Elkin, S.J. (1999), "Beam-Column Base Plate Design - LRFD Method," *Engineering Journal*, AISC, Vol. 36, No. 1, First Quarter, pp. 29-38, Chicago, IL.

Eberbach, D.E., (1959), "An Investigation of Base Restraints of Precast Reinforced Concrete Columns," Unpublished Thesis, University of Toronto.

Ermopoulos, J., and Stamatopoulos, G. (1996a), "Mathematical Modeling of Column Base Plate Connections," *Journal of Constructional Steel Research*, Vol. 36, No. 2, pp. 79-100.

Ermopoulos, J., and Stamatopoulos, G. (1996b), "Analytical Modeling of Column Base Plates under Cyclic Loading," *Journal of Constructional Steel Research*, Vol. 40, No. 3, pp. 225- 238.

Ermopoulos, J., and Michaltsos, G.T. (1998), "Analytical Modeling of Stress Distribution under Column Base Plates," *Journal of Constructional Steel Research*, Vol. 46, No. 1-3, Paper No. 136.

Fahmy, M. (2000), "Seismic Behavior of Moment-resisting Steel Column Bases," Ph.D. Dissertation, Department of Civil and Environmental Engineering, University of Michigan, Ann Arbor, Michigan.

Fahmy, M., Stojadinovic, B., and Goel, S.C. (1999), "Analytical and Experimental Studies on the Seismic Response of Steel Column Bases," *Proceedings of the 8th Canadian Conference on Earthquake Engineering*.

Federal Emergency Management Agency (FEMA) (2000), "NEHRP Recommended Provisions for seismic Regulations for New Buildings and Other Structures," Building Seismic Safety Council, Washington, D.C.

Fisher, J.M. (2005), "Design Guide No. 7, Industrial Buildings - Roofs to Anchor Rods," 2nd Ed., *Steel Design Guide Series*, AISC, Chicago, IL.

Fisher, J.W., (2003), "FHWA Bay Bridge Pile Connection Plate Welding Investigation," John W. Fisher And Associates, Inc.

Fisher, J.M., and Kloiber, L.A. (2006), "Steel Design Guide 1 - Base Plate and Anchor Rod Design," 2nd Ed., AISC 801-06, American Institute of Steel Construction, Inc., Chicago, IL.

Fisher, J.M. and West, M.A. (2003), "Design Guide No. 10, Erection Bracing of Low-Rise Structured Steel Buildings," 2nd Printing, *Steel Design Guide Series*, AISC, Chicago, IL.

Fling R.S. (1970), "Design of Steel Bearing Plates," *Engineering Journal*, AISC, Vol. 7, April, pp. 37-40.

Gaylord, E.H., and Gaylord, C.N. (1972), "Design of Steel Structures," 2nd Ed. McGraw-Hill, New York, New York, pp. 479-485.

Gomez, I.R., Kanvinde, A.M., Smith, C., and Deierlein, G.G. (2009), "Shear Transfer in Exposed Column Base Plates," Technical Report submitted to the American Institute of Steel Construction, AISC, Chicago, IL.

Grauvilardell, J.E., Lee, D., Ajar, J.F., and Dexter R.J. (2005), "Synthesis of Design, Testing and Analysis Research on Steel Column Base Plate Connections in High Seismic Zones," Structural Engineering Report No. ST-04-02. Minneapolis (MN): Department of Civil Engineering, University of Minnesota.

Hawkins, N.M. (1968a), "The Bearing Strength of Concrete Loaded Through Rigid Plates," *Magazine of Concrete Research*, Vol. 20, No. 62 (March 1968), pp. 31-40.

Hawkins, N.M. (1968b), "The Bearing Strength of Concrete Loaded Through Flexible Plates," *Magazine of Concrete Research*, Vol. 20, No. 63 (June 1968), pp. 95-102.

Hogan, T., and Thomas, I. (1994) "Design of Structural Connections," (4th Ed.), Australian Institute of Steel Construction, Sydney.

Hon, K.K., and Melchers, R.E. (1988). "Experimental Behavior of Steel Column Bases," *Journal of Constructional Steel Research*, Vol. 9, Paper No. 143, pp. 35-50.

Horn, D., (2004), "Technical Manual 1 - Design of Monopole Bases," RISATech.

Igarashi, S., Kadoya, H., Nakashima, S., and Suzuki, M. (1992), "Behavior of Exposed-Type Fixed Column Base Connected to Riser Foundation," *Proceedings of the Tenth World Conference on Earthquake Engineering*, Madrid, Spain.

Jaspart, J.P., and Vandegans, D. (1998), "Application of Component Method to Column Bases," *Journal of Constructional Steel Research*, Vol. 48, pp. 89-106.

Kallolil, J.J., Chakrabarti, S.K., and Mishra, R.C. (1998), "Experimental Investigation of Embedded Steel Plates in Reinforced Concrete Structures," *Engineering Structures*, Vol. 20, No. 1-2, pp. 105-112.

Kanvinde, A.M., and Deierlein, G.G. (2004), "Micromechanical Simulation of Earthquake Induced Fractures in Steel Structures," TR-145, John A. Blume Earthquake Engineering Center, Stanford University, CA.

Kim, S.E., Lee, D.H., and Cuong, N.H. (2007), "Shaking Table Tests of a Two-Story Unbraced Steel Frame," *Journal of Constructional Steel Research*, Volume 63, Issue 3, March 2007, Pages 412-421.

Korekoda, W., *et al.* (2001), "Elasto-Plastic Behavior of Exposed-Type Steel Column Base with Base Plate Yielding (Part 1 - Experimental Program and Results)," Summaries of Technical Papers of Annual Meeting, Architectural Institute of Japan C-1, pp. 967–970 [In Japanese].

Krawinkler, H., Gupta, A., Medina, R., and Luco, N. (2000), "Loading Histories for Seismic Performance Testing of SMRF Components and Assemblies," SAC Joint Venture, Report no. SAC/BD-00/10. Richmond, CA.

LaFraugh, R.W., and Magura, D.D. (1966), "Connections in Precast Concrete Structures - Column Base Plates," *Journal of the Prestressed Concrete Institute*, Vol. 11, No. 6 (December 1966), pp. 18-39.

Lee, D., and Goel, S.C. (2001). "Seismic Behavior of Column-Base Plate Connections Bending about Weak Axis," Report No. UMCEE 01-09, Department of Civil and Environmental Engineering, University of Michigan, Ann Arbor, Michigan.

Lee, D., Goel, S.C., and Stojadinovic, B. (2002), "Relative Strength Effects on Seismic Behavior of Column-Base Plate Connections under Weak Axis Bending," *Proceedings of the Seventh U.S. National Conference on Earthquake Engineering*, EERI, Boston, Massachusetts.

Li, T., Sakai, J., and Matsui, C. (2000), "Seismic Behavior of Steel-Concrete Composite Column Bases," *Proceedings of the 12th World Conference on Earthquake Engineering*, Paper 1072.

Liu T.C. (2001), "Investigation of Rotational Characteristics of Column 'Pinned' Bases of Steel Portal Frames," *Steel and Composite Structures*, Vol. 1, No. 2, 187-200.

McGuire, W. (1968), "Steel Structures," 1st Ed. Prentice-Hall, Inc., Englewood Cliffs, New Jersey, pp. 987-1004.

Melchers, R.E. (1992), "Column-Base Response under Applied Moment," *Journal of Constructional Steel Research*, Vol. 23, pp. 127-143.

Michaltsos, G.T., and Ermopoulos, J.C. (2001), "Dynamic Response of Column Bases," *Engineering Structures*, Vol. 23, pp. 58-71.

Miyasaka, H., Arai, S., Uchiyama, M., Yamada, T., and Hashimoto, A. (2001), "Elasto-Plastic Behavior of Structural Elements Consist in Exposure Fixed-Type Steel Column Base. Part I – Behavior to Bending Moment," *Journal of Structural and Construction Engineering*, Transactions of AIJ, No 550, December 2001, pp.167-174.

Murray, T.M. (1983), "Design of Lightly Loaded Column Base Plates," *Engineering Journal*, AISC, Vol. 20, No. 4 (Fourth Quarter), 1983, pp. 143-152.

Myers, A.T., Kanvinde, A.M., Deierlein, G.G., and Fell B.V. (2009), "Effect of Weld Details on the Ductility of Steel Column Baseplate Connections," *Journal of Constructional Steel Research*, Volume 65, Issue 6, June 2009, Pages 1366-1373.

Ohi, K., Tanaka, H., and Takanashi, K. (1981), "Ultimate Strength of Steel Column Bases," Bulletin No. 14, Earthquake Resistant Structure Research Center, Tokyo, Japan.

OpenSees, Mazzoni, S., McKenna, F., Scott, M.H., and Fenves, G.L. (2006) "Open System for Earthquake Engineering Simulation, User Command-Language Manual," Pacific Earthquake Engineering Research Center, Berkeley, CA.

Occupational Safety and Health Administration (OSHA). (2001), "Safety Standards for Steel Erection," (Subpart R of 29 CFR Part 1926), Washington, D.C.

Park, Y.M., Hwang, W.S., Yoon, T.Y., and Hwang, M.O. (2005), "A New Base Plate System using Deformed Reinforcing Bars for Concrete Filled Tubular Column," *Steel and Composite Structures*, Vol. 5, No. 5 pp. 375-394.

Penserini, P., and Colson, A. (1989), "Ultimate Limit Strength of Column-Base Connections," *Journal of Constructional Steel Research*, Vol. 14, pp. 301-320.

Picard, A., and Beaulieu, D. (1985), "Behavior of a Simple Column Base Connection," *Canadian Journal of Civil Engineering*, Vol. 12, pp. 126-136.

Picard, A., Beaulieu, D., and Perusse, B. (1987), "Rotational Restraint of a Simple Column Base Connection," *Canadian Journal of Civil Engineering*, Vol. 14, pp. 49-57.

Ranzi, G., and Kneen, P. (2002), "Design of Pinned Column Base Plates," *Steel Construction*, Vol. 36, No. 2 September 2002, Australian Steel Institute, Australia.

Salmon, C.G. and Johnson, J.E. (1980), "Steel Structures," 2nd Ed., Harper and Row, New York, N.Y., 1980, pp. 806-815.

Sato, K. (1987), "A Research on the Aseismic Behavior of Steel Column Base for Evaluating Its Strength Capacity and Fixity," Report No. 69, Kajima Institute of Construction Technology, Tokyo, Japan.

Soifer, H. (1966), "Design of Base Plates and Anchor Bolts with Simple Assumptions," *Civil Engineering*, ASCE, Vol. 36, No. 4, pp. 63.

Somiya, Y., Fukuchi, Y., and Chin, B. (2002), "Experimental Study on Elasto-Plastic Behavior and Strength Estimation of Exposed-Type Column Base with Variable Axial Force," *Journal of Structural and Construction Engineering*, Transactions of AIJ, No. 562, pp. 137-143. [In Japanese].

Sophianopoulos, D.S, Asteris, P.G., and Michaltsos, G.T. (2005), "Equilibrium Based Evaluation of Stress Distribution under Steel Column Base Plates - I: Governing Equations," *Electronic Journal of Structural Engineering*, Vol. 5.

Stamatopoulos, G., and Ermopoulos, J. (1997), "Interaction Curves for Column Base-Plate Connections," *Journal of Constructional Steel Research*, Vol. 44, No. 1-2, pp. 69-89.

Stephenson, J.M. and Tarpy, T.S. (1981), "Moment-Rotation Characteristics of Column Base Plate to Foundation Connections," NTIS Report USGDE81027685, January 1981.

Stockwell, F.W. (1975), "Preliminary Base Plate Selection," *Engineering Journal*, AISC, Vol. 12, No. 3, Third Quarter, pp. 92-99.

Takamatsu, T., and Tamai, H. (2005), "Non-Slip-Type Restoring Force Characteristics of an Exposed-Type Column Base" *Journal of Constructional Steel Research*, Volume 61, Issue 7, July 2005, Pages 942-961.

Tamai. H., and Kanazawa, Y. (2001), "Elasto-plastic Behavior of Exposed-Type Column Base Under Variable Axial Force," *Proceedings of the Sixth Pacific Structural Steel Conference*, Beijing, China Vol.1, pp.260-265.

Targowski, R., Lamblin, D., and Guerlement, G. (1993), "Base Plate Column Connection under Bending: Experimental and Numerical Study," *Journal of Constructional Steel Research*, Vol. 27, pp. 37-54.

Thambiratnam, D.P., and Paramasivam, P. (1986), "Base Plates Under Axial Loads and Moments," *Journal of Structural Engineering*, ASCE, Vol. 112, No. 5, pp. 1166-1181.

Thornton, W.A. (1990a), "Design of Small Base Plates for Wide Flange Columns," *Engineering Journal*, AISC, Vol. 27, No. 3, Third Quarter, pp. 108-110.

Thornton, W.A. (1990b), "Design of Base Plates for Wide Flange Columns - A Concatenation of Methods," *Engineering Journal*, AISC, Vol. 27, No. 4, Fourth Quarter, pp. 173-174.

Tremblay, R., Timler, P., Bruneau, M., and Filiatrault, A., (1995), "Performance of Steel Structures During the 1994 Northridge Earthquake," *Canadian Journal of Civil Engineering*, Vol. 22, pp. 338–360.

Wald, F., Simek, I., and Seifert, J. (1994), "The Tests of the Column-Base Components," *Proceedings of the First International Conference STESSA*, Timisoara, Romania.

Wald, F., Sokol, Z., and Steenhuis, M. (1995), "Proposal of the Stiffness Design Model of the Column Bases," *Proceedings of the Third International Workshop on Connections in Steel Structures*, Trento, Italy.

Wald, F., and Jaspart, J. (1998), "Stiffness Design of Column Bases," *Journal of Constructional Steel Research*, Vol. 46, Nos. 1-3, Paper No. 135.

Wald, F., Sokol, Z., Steenhuis, M., and Jaspart, J. (2008), "Component Method for Steel Column Bases," HERON Vol. 53 No. 1/2.

Yoshimori, K., and Nakashima, S. (2001), "Experimental Behavior of Steel Column Bases Embedded Shallowly into Reinforced Concrete Floor" *Architectural Institute of Japan*, pp.655-656. [In Japanese].

Yoshimori, K., Nakashima, S., and Makimoto, H. (1997), "Influence of Pinned Column Bases on Mechanical Characteristics of Steel Portal Frames," *Architectural Institute of Japan*, pp.475-476. [In Japanese].

Zhang, Y.G., Klingner, R.E., and Graves, H.L. (2001), "Seismic Response of Multiple-Anchor Connections to Concrete," *ACI Structural Journal*, Volume 98, Issue 6, pp. 811-822.

Appendix A

Ancillary Test Data

Table A.1 - Anchor rod tension test results

Test	Rod grade (ksi)	Nominal diameter (inches)	Measured original diameter "d_o" (inches)	Measured necked diameter "d_f" (inches)	Ductility[1] "ε"	Young's modulus "E" (ksi)	Yield strength[2] "$F_{y,rod}$" (ksi)	Ultimate strength "$F_{u,rod}$" (ksi)
1a	36	3/4	0.756	0.430	1.13	29,400	49.0	70.6
1b			0.746	0.422	1.14		48.1	72.1
Mean			**0.751**	**0.426**	**1.13**		**48.6**	**71.3**
2a	105		0.748	0.495	0.83		114.0	146.4
2b			0.747	0.502	0.79		114.0	146.5
Mean			**0.747**	**0.499**	**0.81**		**114.0**	**146.5**

[1]Average true fracture strain across necked cross section of anchor rod coupon = $\ln(d_o / d_f)^2$

[2]Measured yield stress, based on 0.2% offset method

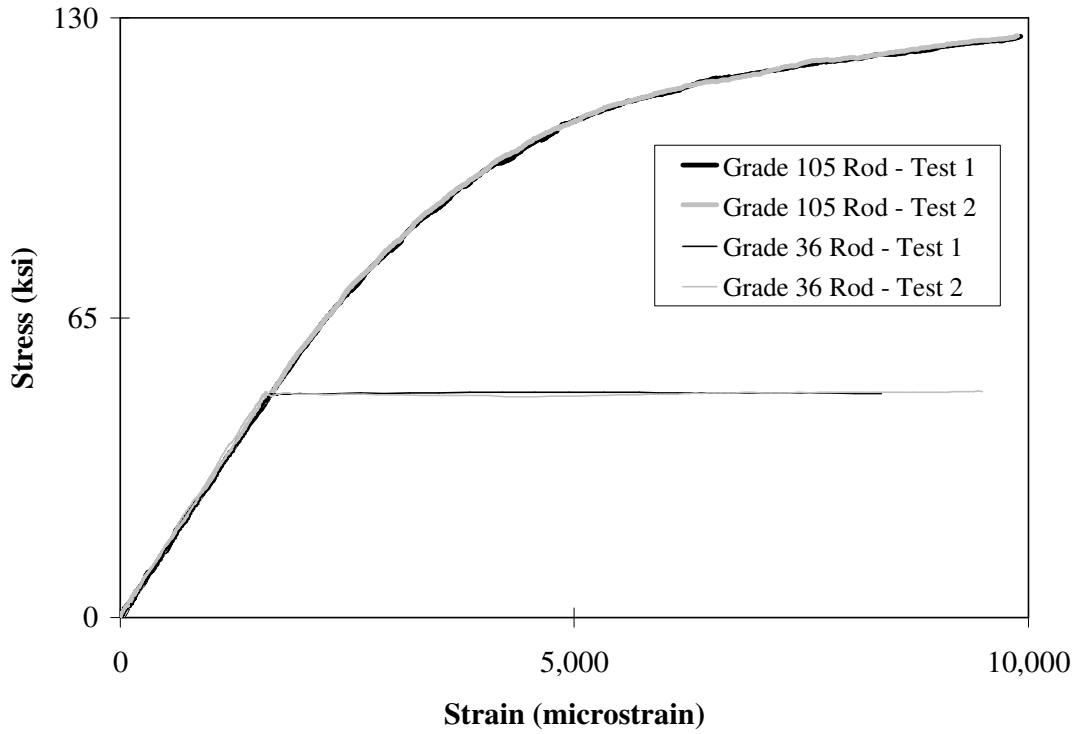

Figure A.1 – Stress-strain response of all anchor rod tension tests

Table A.2 - Tension test results of coupons extracted from the base plate material

Test	Base plate thickness (inches)	Young's modulus "E" (ksi)	Yield strength[1] "$F_{y,plate}$" (ksi)	Ultimate strength "$F_{u,plate}$" (ksi)
1a	1.0	30,900	40.47	69.08
1b		31,800	40.36	68.34
Mean		**31,400**	**40.42**	**68.71**
2a	1.5	31,900	37.01	67.14
2b		30,500	36.92	68.60
Mean		**31,200**	**36.97**	**67.87**
3a	2.0	33,700	40.17	72.65
3b		34,000	36.57	71.50
Mean		**33,900**	**38.37**	**72.08**
Global Average	**-**	**32,100**	**38.58**	**69.55**

[1]Measured yield stress, based on 0.2% offset method

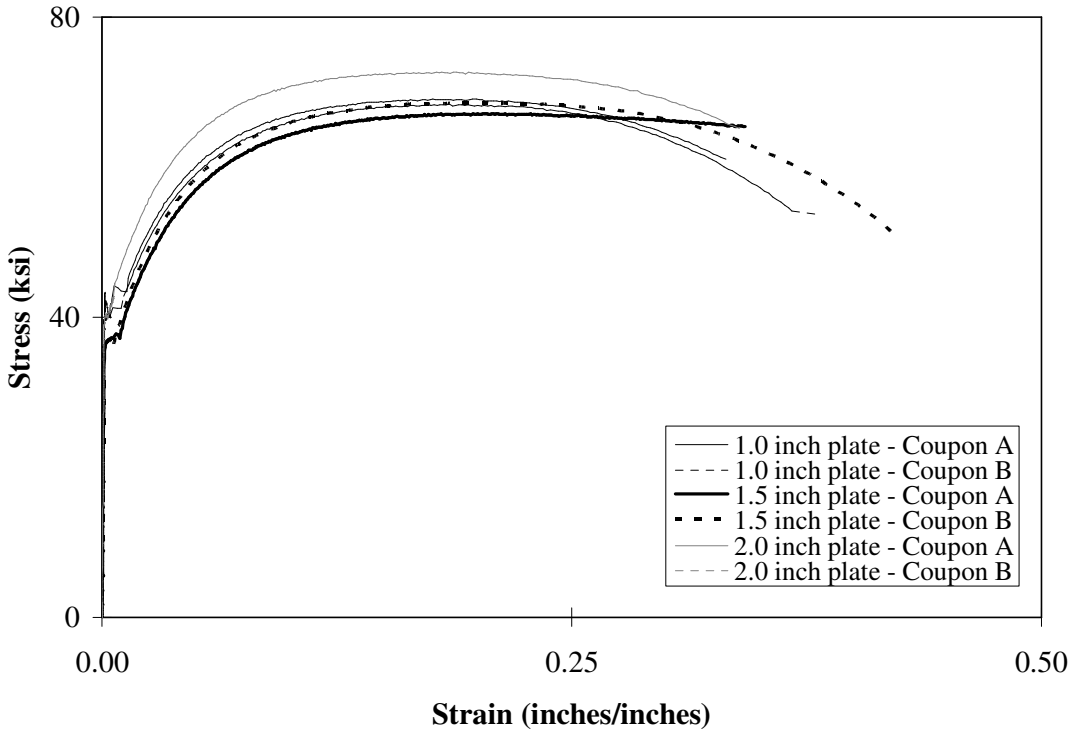

Figure A.2 – Stress-strain response of all base plate material tension tests

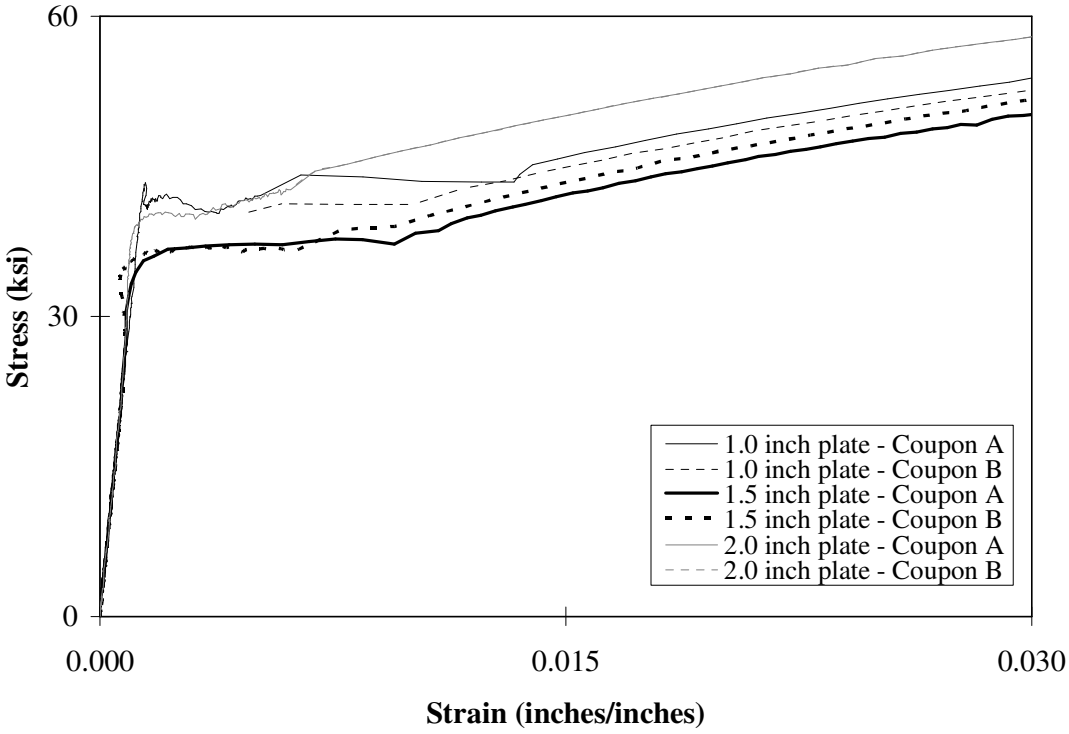

Figure A.3 – Stress-strain response of all base plate material tension tests for strains less than 0.03

Table A.3 – Concrete cylinder compressive strength test results

Specimen	Corresponding large scale test number	Cure age (days)	Cylinder area (in^2)	Density ($pounds/feet^3$)	Compressive strength (psi)
1a1	1,3	32	28.55	143	3,888
1a2	1,3		28.56	143	4,044
1a3	1,3		28.50	144	3,737
1b1	2,4,5,6,7		28.72	142	3,743
1b2	2,4,5,6,7		28.58	145	4,024
1b3	2,4,5,6,7		28.47	142	3,740
Mean	**-**		**28.56**	**143**	**3,860**
COV	**-**		**0.3%**	**0.8%**	**3.75%**
2a1	1,3	73	28.65	146	4,154
2a2	1,3		28.64	146	4,138
2b1	2,4,5,6,7		28.64	146	4,137
2b2	2,4,5,6,7		28.68	147	4,114
2b3	2,4,5,6,7		28.59	145	4,268
Mean	**-**		**28.64**	**146**	**4,160**
COV	**-**		**0.1%**	**0.5%**	**1.46%**
3a1	1,3	131	28.70	144	4,180
3a2	1,3		28.58	146	4,724
3a3	1,3		28.65	146	4,206
3b1	2,4,5,6,7		28.54	145	4,695
3b2	2,4,5,6,7		28.57	146	4,427
3b3	2,4,5,6,7		28.61	146	4,387
Mean	**-**		**28.61**	**146**	**4,440**
COV	**-**		**0.2%**	**0.6%**	**5.25%**

Note: Nominal cylinder size = 6" diameter, 12" height
Measured slump of concrete = 2.5"

Figure A.4 – Photographs showing representative concrete cylinder test (a) before and (b) after failure

SUGAR CITY BUILDING MATERIALS CO.

CONCRETE MIX CODE : SC532213P
DESCRIPTION : 5.25 SACK 1" FA WR AE
DATE : August 7, 2006
PROJECT : UC DAVIS CONCRETE BLOCK/1301 S, 46th ST., RICHMOND
CONTRACTOR : BERKELEY CEMENT
SUB-CONTRACTOR :
CONCRETE USE :
STRENGTH - PSI : 3000 PSI

MIX PROPORTIONS

	SP.GR.	WEIGHT	VOLUME		
CEMENT:CEMEX Type II	3.15	420	2.137		
FLYASH - CLASS F :	2.6	74	0.456	0.15	Flyash % By Weight
1" X #4 Vulcan Pleasanton Pit	2.69	1775	10.57	55.56	Coarse %
3/8" GRAVEL	2.68	0	0.00	44.44	Fine %
TOP SAND: Vulcan Pleasanton	2.64	1420	8.62		
WATER	1	275.00	4.41	33.0 GAL.	
AIR ENTRAPPED	3.0	%	0.81		
TOTAL		3964	27.00	CUBIC FEET	

ADMIXTURES

WATER REDUCER :	WRDA64	20.0	OZS/YD
AIR ENTRAINMENT:	Daravair	1.5	OZS/YD
SET ACCELERATOR:			OZS/YD
MID RANGE WRA :			OZS/YD

PLASTIC PROPERTIES

UNIT WEIGHT :	146.8	PCF
SLUMP RANGE :	3±1	INCHES
AIR CONTENT RANGE :	3-5	PERCENT
W/C - LBS/LBS :	0.56	
W/C - GAL/SACK :	6.28	

REGISTERED PROFESSIONAL ENGINEER ROBERT KUHN No. C39678 Exp. 12-31-07 CIVIL STATE OF CALIFORNIA

Figure A.5 – Concrete mix design from fabricator

Table A.4 – Grout cylinder compressive strength test results

Specimen	Corresponding large scale test number	Cure age (days)	Cylinder area (in^2)	Density ($pounds/feet^3$)	Compressive strength (psi)
1a	1,2,6	33	7.21	131	8,363
1b	1,2,6		7.22	123	7,424
1c	1,2,6		7.22	127	7,202
1d	1,2,6		7.19	128	7,923
1e	1,2,6		7.19	125	5,840
Mean	-		**7.21**	**127**	**7,350**
COV	-		**0.2%**	**2.4%**	**13.0%**
2a	3	61	7.07	132	9,974
2b	3		7.30	123	8,081
2c	3		7.10	126	9,297
2d	3		7.10	130	9,291
2e	3		7.12	126	8,918
Mean	-		**7.14**	**127**	**9,110**
COV	-		**1.3%**	**2.8%**	**7.58%**
3a	4,5,7	120	7.09	131	12,902
3b	4,5,7		7.07	131	8,836
3c	4,5,7		7.09	131	8,468
3d	4,5,7		7.03	132	10,809
3e	4,5,7		7.06	132	6,731
Mean	-		**7.07**	**131**	**9,550**
COV	-		**0.4%**	**0.4%**	**24.8%**

Note: Nominal cylinder size = 3" diameter, 6" height
Water content of grout mix = 7/8 gallons water per 50 pound bag of grout

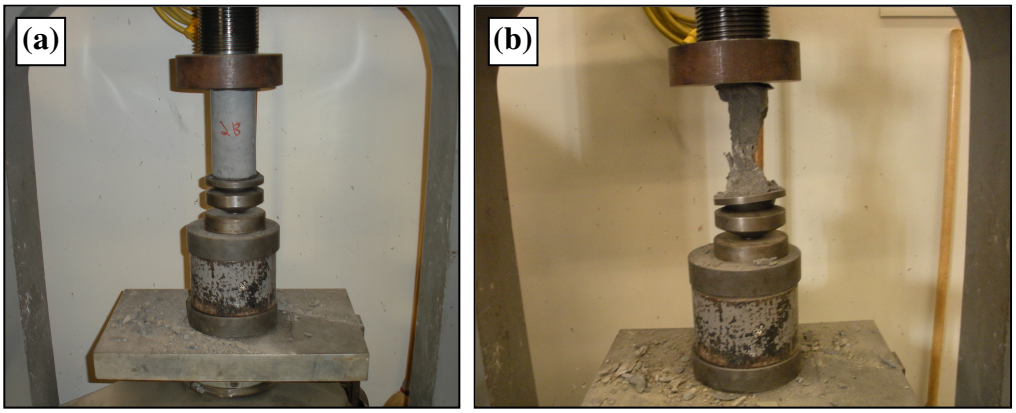

Figure A.6 – Photographs showing representative grout cylinder test (a) before and (b) after failure

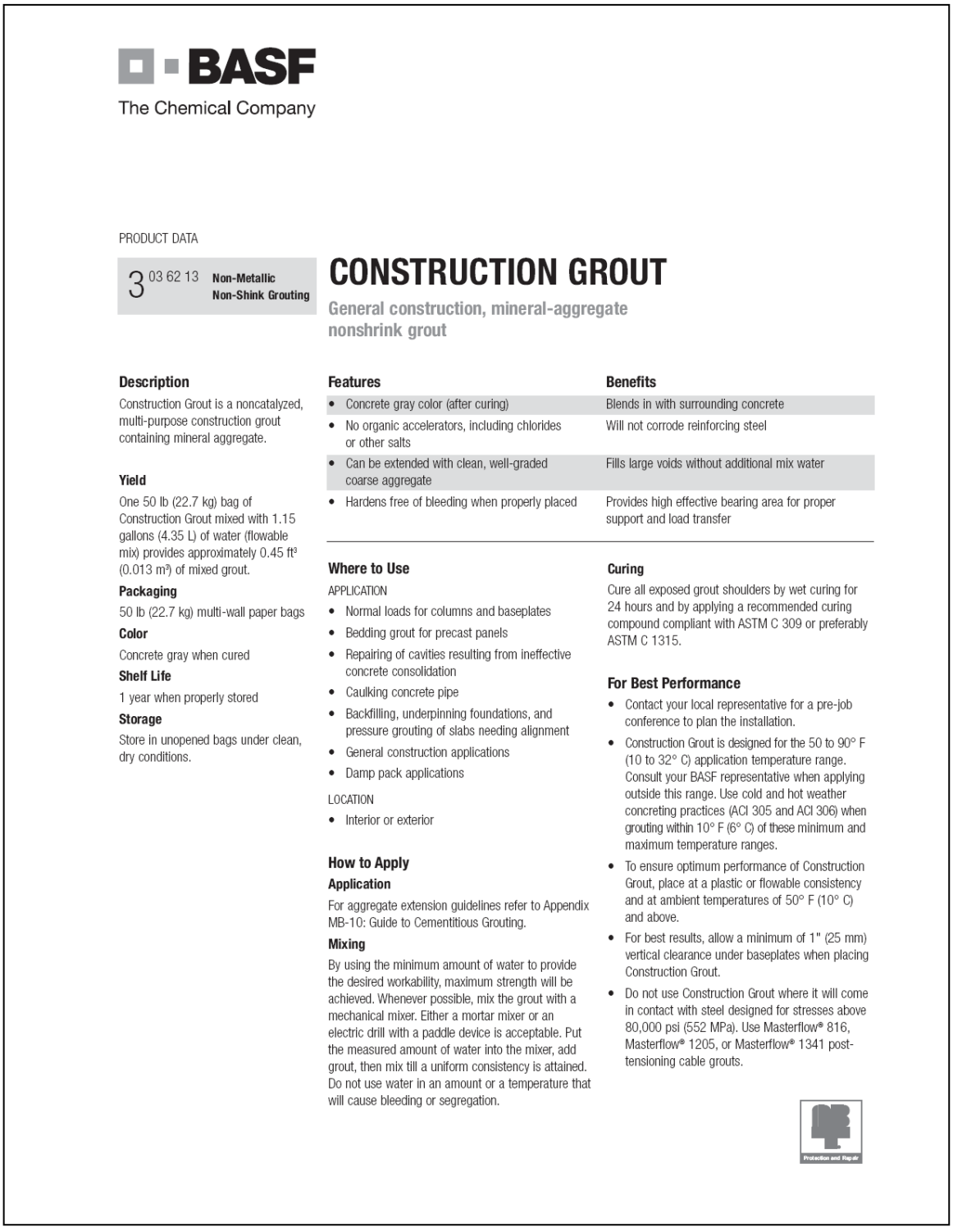

BASF
The Chemical Company

PRODUCT DATA

3 03 62 13 **Non-Metallic Non-Shink Grouting**

CONSTRUCTION GROUT

General construction, mineral-aggregate nonshrink grout

Description

Construction Grout is a noncatalyzed, multi-purpose construction grout containing mineral aggregate.

Yield

One 50 lb (22.7 kg) bag of Construction Grout mixed with 1.15 gallons (4.35 L) of water (flowable mix) provides approximately 0.45 ft³ (0.013 m³) of mixed grout.

Packaging

50 lb (22.7 kg) multi-wall paper bags

Color

Concrete gray when cured

Shelf Life

1 year when properly stored

Storage

Store in unopened bags under clean, dry conditions.

Features	Benefits
• Concrete gray color (after curing)	Blends in with surrounding concrete
• No organic accelerators, including chlorides or other salts	Will not corrode reinforcing steel
• Can be extended with clean, well-graded coarse aggregate	Fills large voids without additional mix water
• Hardens free of bleeding when properly placed	Provides high effective bearing area for proper support and load transfer

Where to Use

APPLICATION

- Normal loads for columns and baseplates
- Bedding grout for precast panels
- Repairing of cavities resulting from ineffective concrete consolidation
- Caulking concrete pipe
- Backfilling, underpinning foundations, and pressure grouting of slabs needing alignment
- General construction applications
- Damp pack applications

LOCATION

- Interior or exterior

How to Apply

Application

For aggregate extension guidelines refer to Appendix MB-10: Guide to Cementitious Grouting.

Mixing

By using the minimum amount of water to provide the desired workability, maximum strength will be achieved. Whenever possible, mix the grout with a mechanical mixer. Either a mortar mixer or an electric drill with a paddle device is acceptable. Put the measured amount of water into the mixer, add grout, then mix till a uniform consistency is attained. Do not use water in an amount or a temperature that will cause bleeding or segregation.

Curing

Cure all exposed grout shoulders by wet curing for 24 hours and by applying a recommended curing compound compliant with ASTM C 309 or preferably ASTM C 1315.

For Best Performance

- Contact your local representative for a pre-job conference to plan the installation.
- Construction Grout is designed for the 50 to 90° F (10 to 32° C) application temperature range. Consult your BASF representative when applying outside this range. Use cold and hot weather concreting practices (ACI 305 and ACI 306) when grouting within 10° F (6° C) of these minimum and maximum temperature ranges.
- To ensure optimum performance of Construction Grout, place at a plastic or flowable consistency and at ambient temperatures of 50° F (10° C) and above.
- For best results, allow a minimum of 1" (25 mm) vertical clearance under baseplates when placing Construction Grout.
- Do not use Construction Grout where it will come in contact with steel designed for stresses above 80,000 psi (552 MPa). Use Masterflow® 816, Masterflow® 1205, or Masterflow® 1341 post-tensioning cable grouts.

Protection and Repair

Figure A.7 – Grout product data from manufacturer (first page)

MBT PROTECTION & REPAIR PRODUCT DATA
CONSTRUCTION GROUT

Technical Data

Composition

Construction Grout is a noncatalyzed hydraulic cement-based grout containing mineral aggregate.

Compliances

- CRD C 621 and ASTM C 1107, Grade C, at flowable or plastic consistency
- City of Los Angeles Research Report Number RR 23137

Typical Properties

Mixed Grout Data* (Flowable Mix)

PROPERTY	VALUE
Approximate Water, gal (L)	1.15 (4.35)
Initial set, hrs, at 70° F (21° C)	6
Final set, hrs, at 70° F (21° C)	8

*At a constant percent of water, consistency will vary with temperature. Final set takes place in approximately 8 hours at a flowable consistency and 70° F (21° C).

Test Data

PROPERTY	RESULTS	TEST METHODS
Flow, %, 5 drops	126 – 145	ASTM C230
Volume change, %, flowable consistency, after 28 days	0.08	ASTM C 1090
Compressive strength, psi (MPa)		ASTM C 942, according to ASTM C 1107

	Consistency		
	Flowable[1]	**Plastic**[2]	**Stiff**[3] (damp pack)
1 day	1,500 (10)	—	—
3 days	5,000 (34.5)	6,000 (41.4)	8,000 (55.2)
7 days	6,000 (41.3)	7,000 (48.3)	9,500 (65.5)
28 days	7,000 (48.0)	8,500 (58.6)	10,000 (69.0)

[1] 140% flow on flow table, ASTM C 230, 5 drops in 3 seconds
[2] 100% flow on flow table, ASTM C 230, 5 drops in 3 seconds
[3] 40% flow on flow table, ASTM C 230, 5 drops in 3 seconds
Test results are averages obtained under laboratory conditions. Reasonable variations can be expected.

- Do not add plasticizers, accelerators, retarders, or other additives unless advised in writing by BASF Technical Services.
- The surface to be grouted should be clean, strong, and roughened to CSP 5 – 9 according to ICRI Guideline 03732 to permit proper bond. For freshly placed concrete, consider using Liquid Surface Etchant (see Form No. 1020198).
- Do not place Construction Grout in lifts greater than 6" (152 mm) unless the product is extended with aggregate to dissipate hydration heat.
- Where precision alignment and severe service, such as heavy loading, rolling, or impact resistance are required, use metallic-reinforced, noncatalyzed Embeco® 885 grout. If the amount of impact resistance needed is not great enough to require metallic reinforcement, use natural-aggregate, Masterflow® 928.
- The water requirement may vary with mixing efficiency, temperature, and other variables.
- The concrete surfaces should be saturated (ponded) with clean water for 24 hours before grouting. Remove water immediately before application.
- Make certain the most current versions of product data sheet and MSDS are being used; call Customer Service (1-800-433-9517) to verify the most current versions.
- Proper application is the responsibility of the user. Field visits by BASF personnel are for the purpose of making technical recommendations only and not for supervising or providing quality control on the jobsite.

Health and Safety

CONSTRUCTION GROUT

WARNING!

Construction Grout contains silica, crystalline quartz; portland cement; limestone; calcium oxide; gypsum; silica, amorphous.

Risks

Product is alkaline on contact with water and may cause injury to skin or eyes. Ingestion or inhalation of dust may cause irritation. Contains small amount of free respirable quartz which has been listed as a suspected human carcinogen by NTP and IARC. Repeated or prolonged overexposure to free respirable quartz may cause silicosis or other serious and delayed lung injury.

Precautions

Avoid contact with skin, eyes and clothing. Prevent inhalation of dust. Wash thoroughly after handling. Keep container closed when not in use. DO NOT take internally. Use only with adequate ventilation. Use impervious gloves, eye protection and if the TLV is exceeded or used in a poorly ventilated area, use NIOSH/MSHA approved respiratory protection in accordance with applicable Federal, state and local regulations.

First Aid

In case of eye contact, flush thoroughly with water for at least 15 minutes. In case of skin contact, wash affected areas with soap and water. If irritation persists, SEEK MEDICAL ATTENTION. Remove and wash contaminated clothing. If inhalation causes physical discomfort, remove to fresh air. If discomfort persists or any breathing difficulty occurs or if swallowed, SEEK IMMEDIATE MEDICAL ATTENTION.

Waste Disposal Method

This product when discarded or disposed of is not listed as a hazardous waste in federal regulations. Dispose of in a landfill in accordance with local regulations. For additional information on personal protective equipment, first aid, and emergency procedures, refer to the product Material Safety Data Sheet (MSDS) on the job site or contact the company at the address or phone numbers given below.

Proposition 65

This product contains material listed by the State of California as known to cause cancer, birth defects or other reproductive harm.

VOC Content

0 g/L or 0 lbs/gal less water and exempt solvents.

For medical emergencies only, call ChemTrec (1-800-424-9300).

BASF Construction Chemicals, LLC – Building Systems
889 Valley Park Drive
Shakopee, MN, 55379
www.BuildingSystems.BASF.com
Customer Service 800-433-9517
Technical Service 800-243-6739

Form No. 1019295 7/07
Printed on recycled paper including 10% post-consumer fiber.

Figure A.8 – Grout product data from manufacturer (second page)

Appendix B

Base Connection Test Data

GUIDE TO BASE CONNECTION TEST DATA

Average Anchor Rod Elongation – average vertical displacement of the anchor rods at the peak drift of every cyclic drift excursion

Average Anchor Rod Strain – axial anchor rod strains, collected from the unthreaded diameter of the rods about one inch below the surface of the concrete foundations, averaged from two rods and two strain gages per rod

Axial Load – average load recorded by the two gravity system load cells plus the self weight of the gravity system

Base Moment – lateral force multiplied by the distance of the point of load application to the top of the base plate (92.5 inches)

Base Plate Slip – lateral displacement of the base plate, averaged at two locations

Base Rotation - the difference of the lateral displacement and the base plate slip, divided by the column cantilever length (92.5 inches), minus the lateral force divided by the elastic rotational stiffness of column

Column Drift (Drift) – lateral displacement divided by the distance of the point of load application to the top of the base plate (92.5 inches)

Lateral Displacement – lateral displacement of the horizontal actuator; equal to the lateral displacement of the column 92.5 inches from the top of the base plate

Lateral Force – load recorded by lateral actuator

Table B.1 – Summary of experimental observations

Test #	Base plate thickness (inches)	Anchor rod grade (ksi)	Number of rods	Axial load (kips)	Lateral loading	Failure mode
1	1.0	105	4	None	Monotonic	• Grout crushing • Base plate tension side flexural yielding
2	1.0	105	4	None	Cyclic	• Grout crushing • Base Plate tension side flexural yielding • Anchor rod fracture
3	1.0	105	8	None	Cyclic	• Grout crushing • Base plate tension side flexural yielding
4	1.5	36	4	92.25	Cyclic	• Grout crushing • Anchor rod yielding
5	1.0	105	4	92.25	Cyclic	• Grout crushing • Base plate tension side flexural yielding
6	2.0	105	4	92.25	Cyclic	• Grout crushing • Anchor rod yielding • Anchor rod fracture
7	1.0	105	4	152.25	Cyclic	• Grout crushing • Base plate tension side flexural yielding

Note: Anchor rod diameter = 3/4”
Base plate width = 14”
Base pate length = 14”
Outer anchor rod edge distance = 1.5”
Column type = W8x48
Average concrete compressive strength = 4,200 psi
Average grout compressive strength = 8,800 psi

Table B.2 – Drift cycle amplitude corresponding to cumulative drift value

Drift cycle amplitude (%)	**Number of cycles**	**Cumulative drift (%)**
0.375	6	9
0.5	6	21
0.75	6	39
1	4	55
1.5	2	67
2	2	83
3	2	107
4	2	139
5	2	179
6	2	227
7	2	283
8	2	347
9+	2+	419+

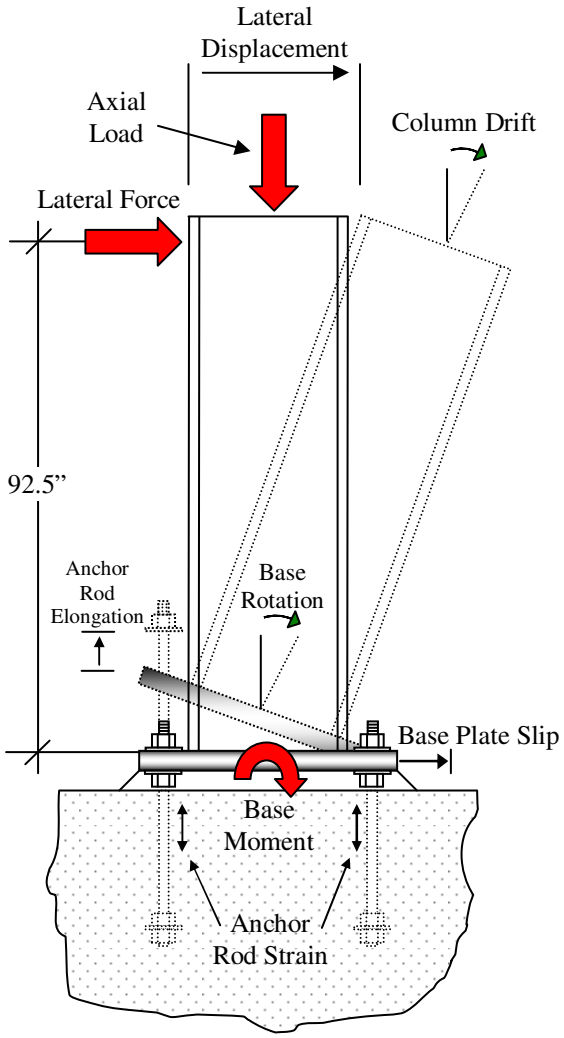

Figure B.1 – Schematic illustration of base connection and measured quantities

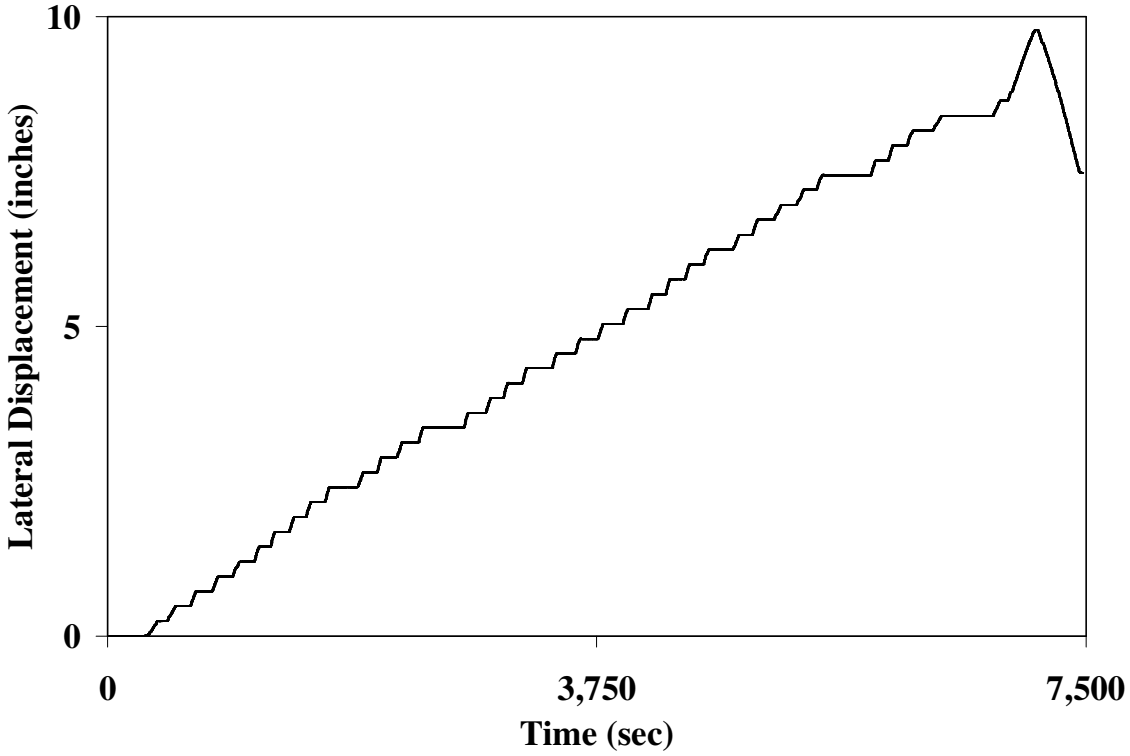

Figure B.2 – Time versus lateral displacement data for Test #1

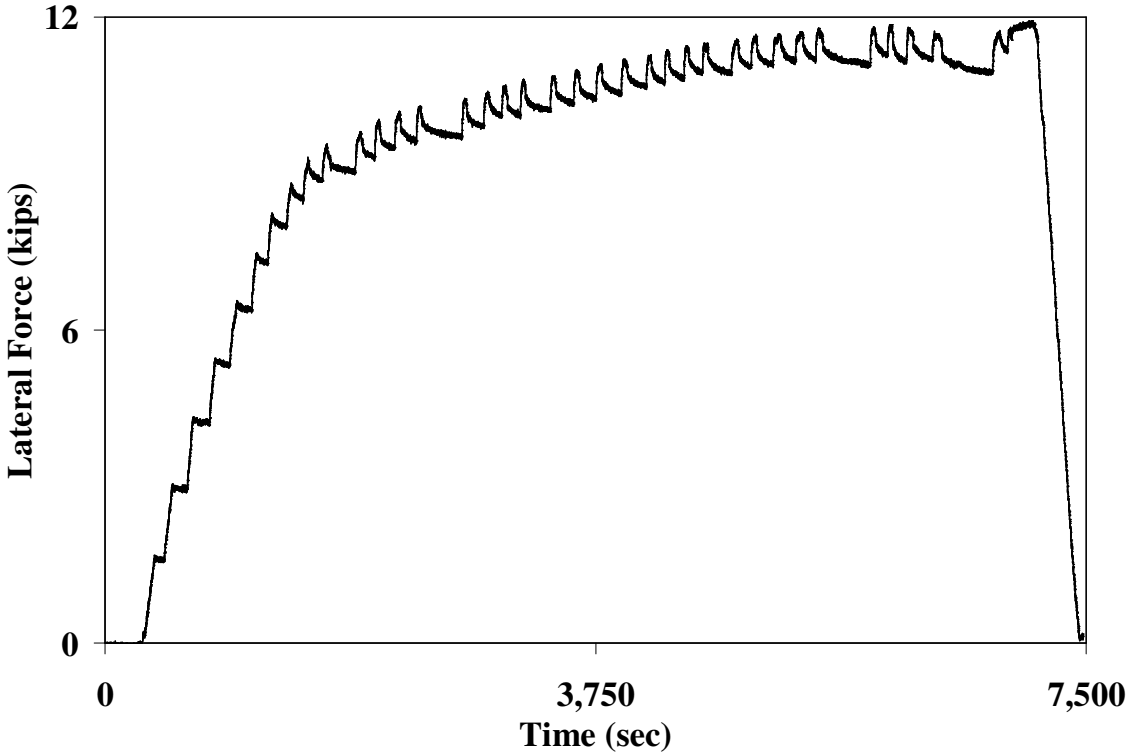

Figure B.3 – Time versus lateral force data for Test #1

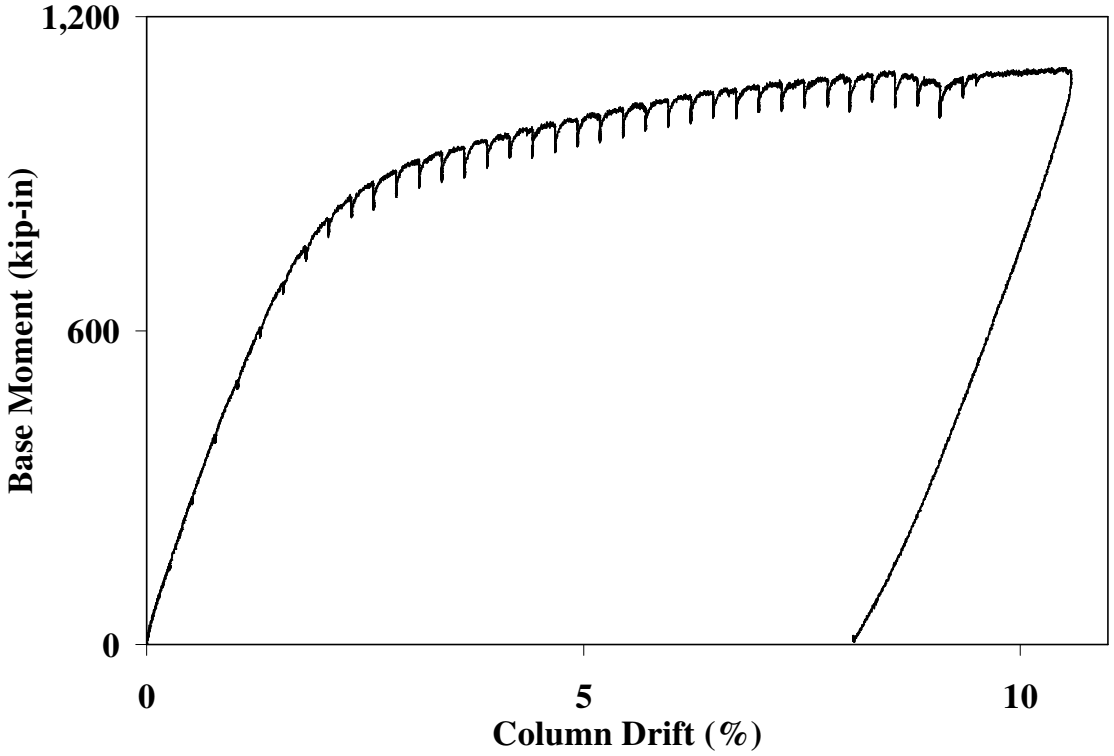

Figure B.4 – Column drift versus base moment data for Test #1

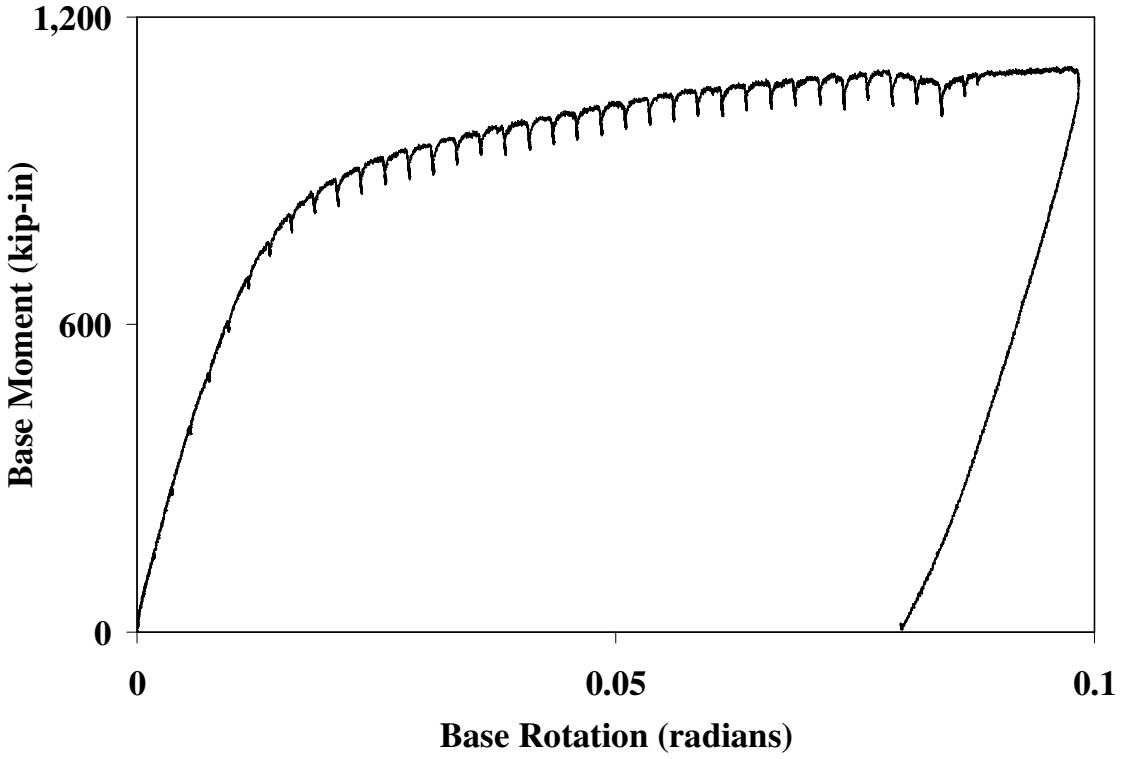

Figure B.5 – Base rotation versus base moment data for Test #1

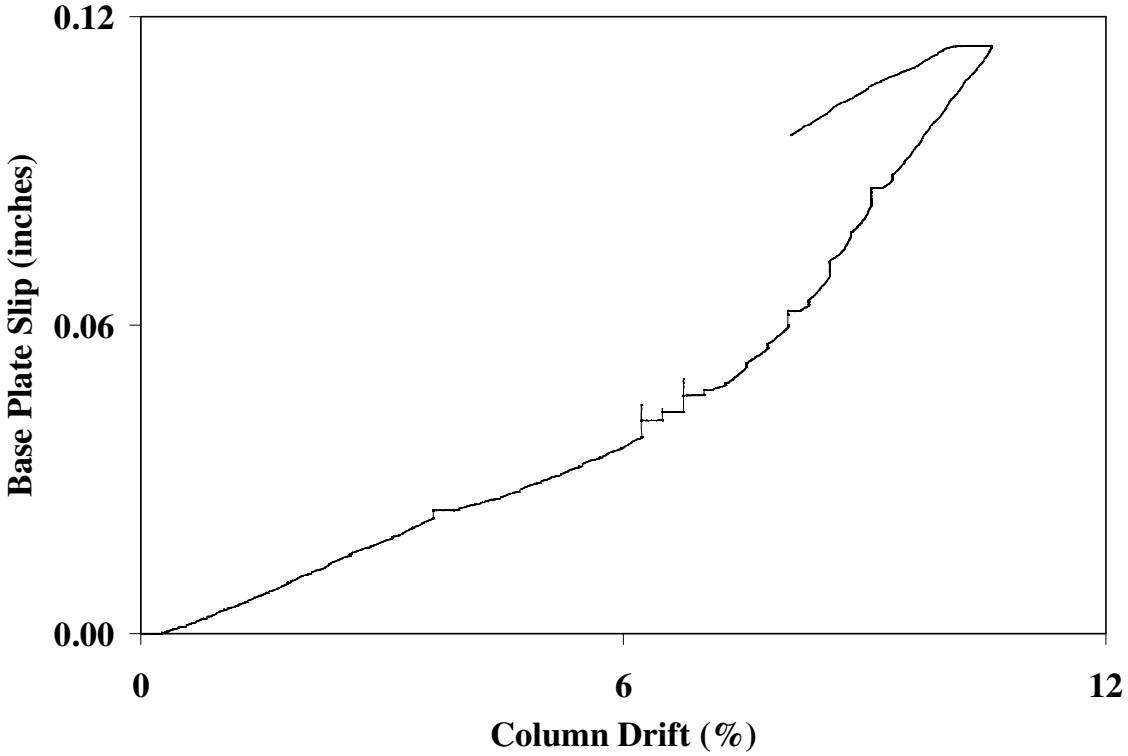

Figure B.6 – Column drift versus base plate slip data for Test #1

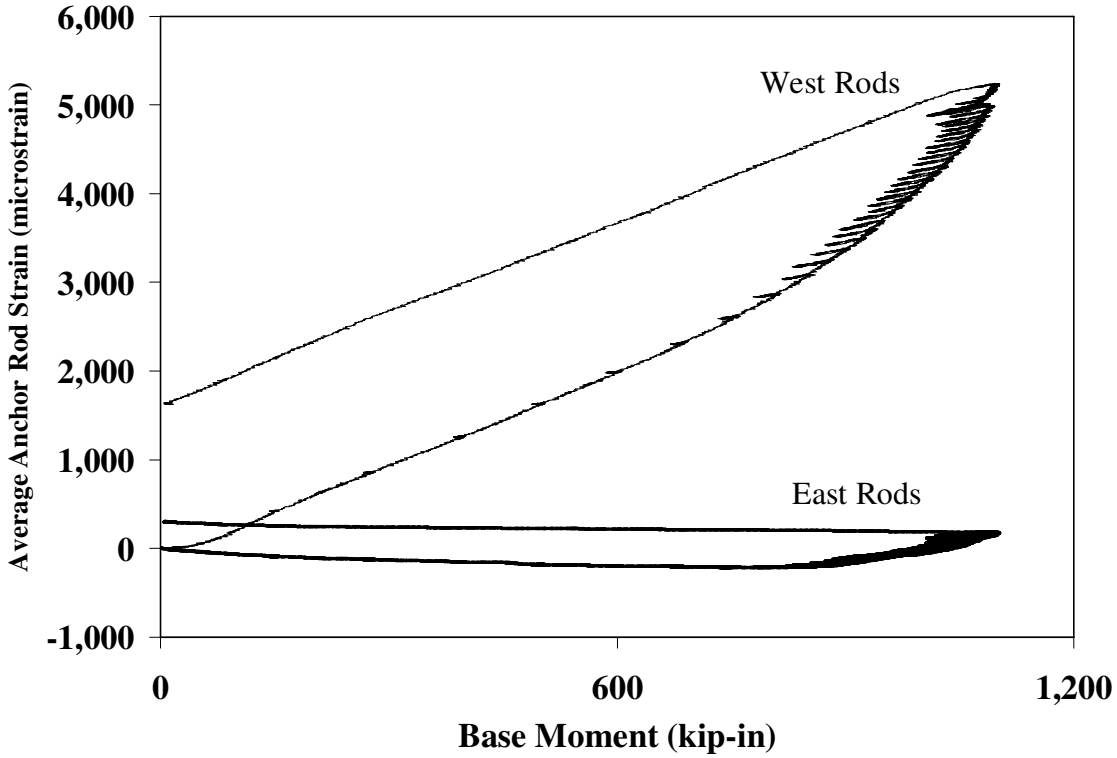

Figure B.7 – Base moment versus anchor rod strain data for Test #1

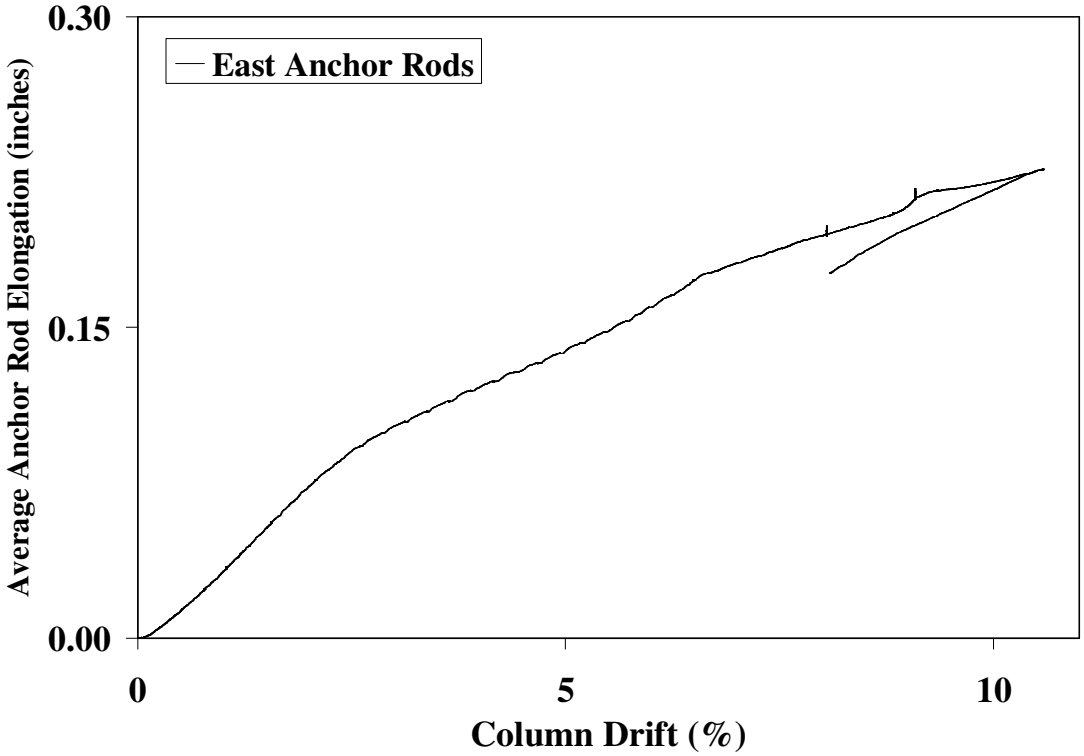

Figure B.8 – Cumulative column drift versus anchor rod elongation data for Test #1

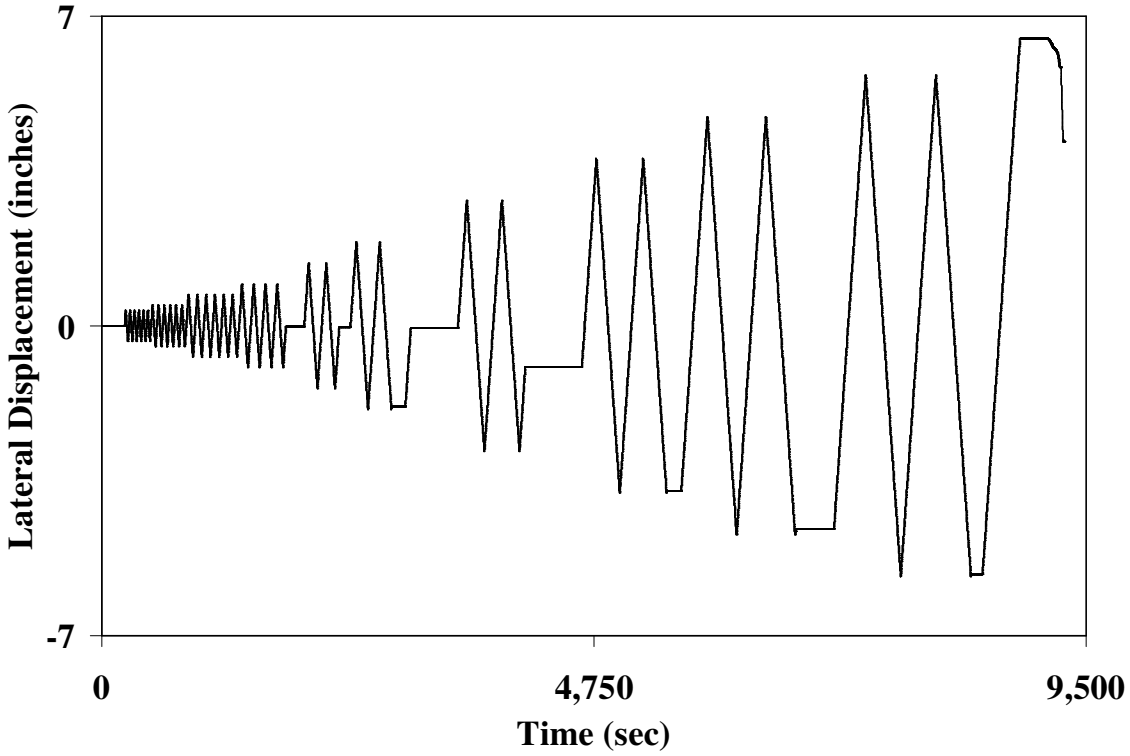

Figure B.9 – Time versus lateral displacement data for Test #2

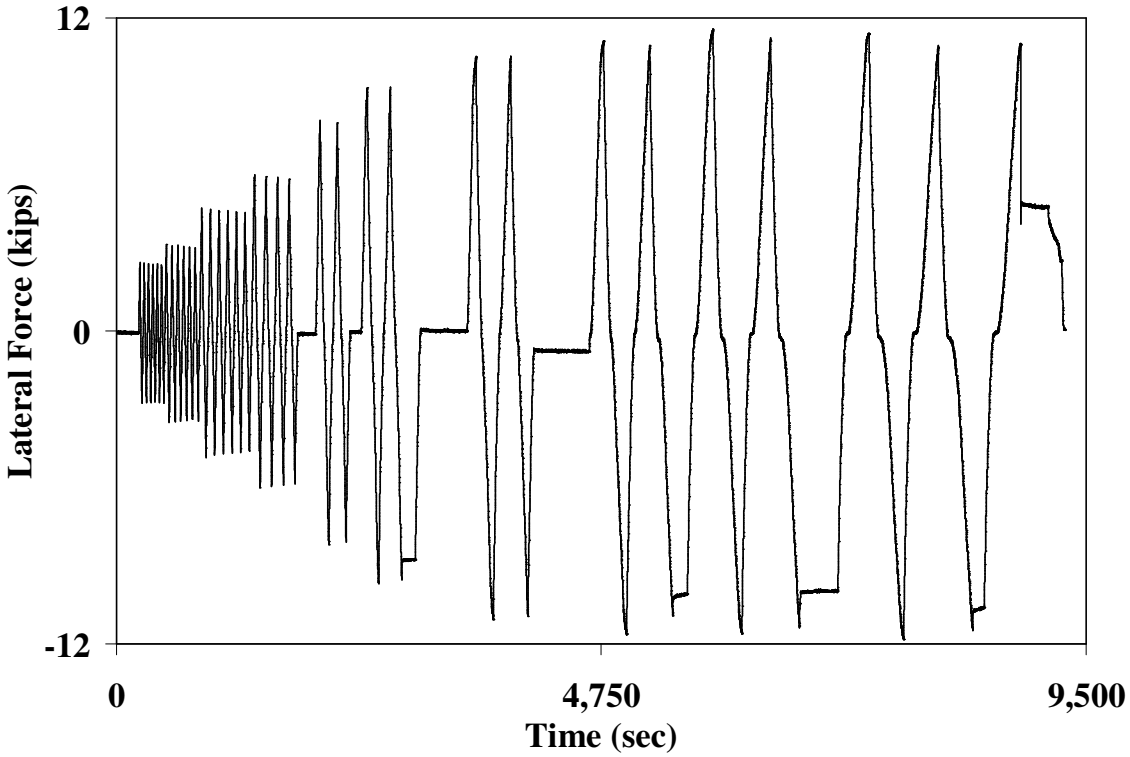

Figure B.10 – Time versus lateral force data for Test #2

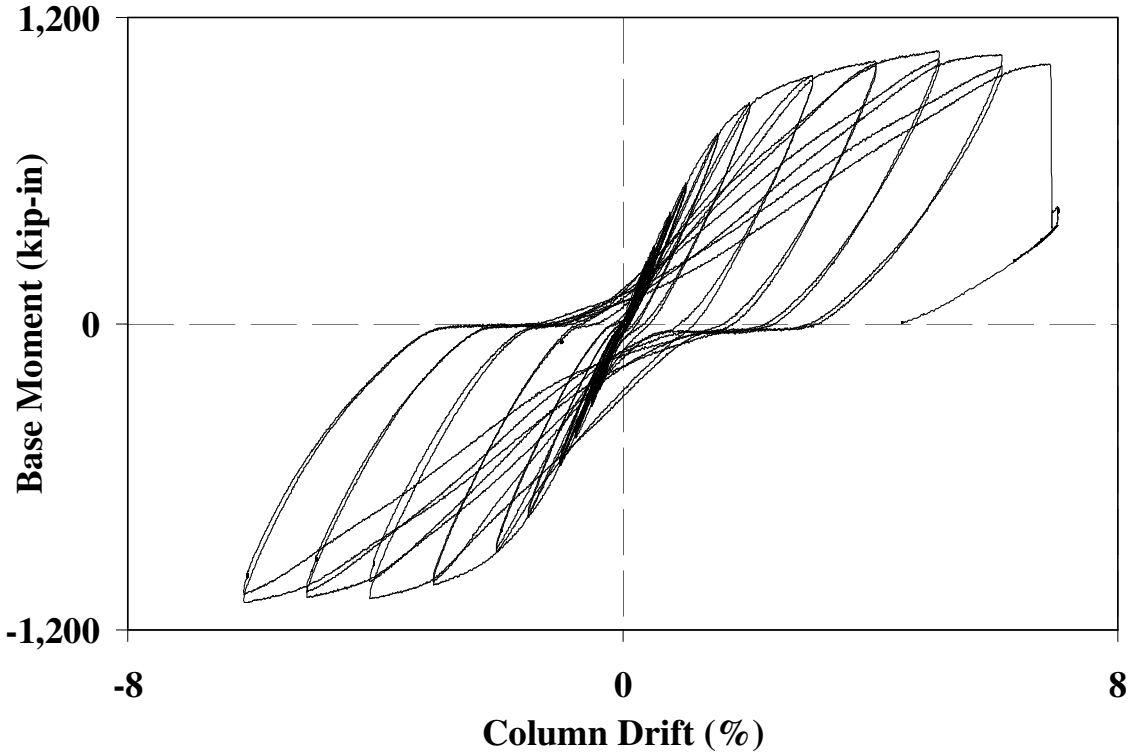

Figure B.11 – Column drift versus base moment data for Test #2

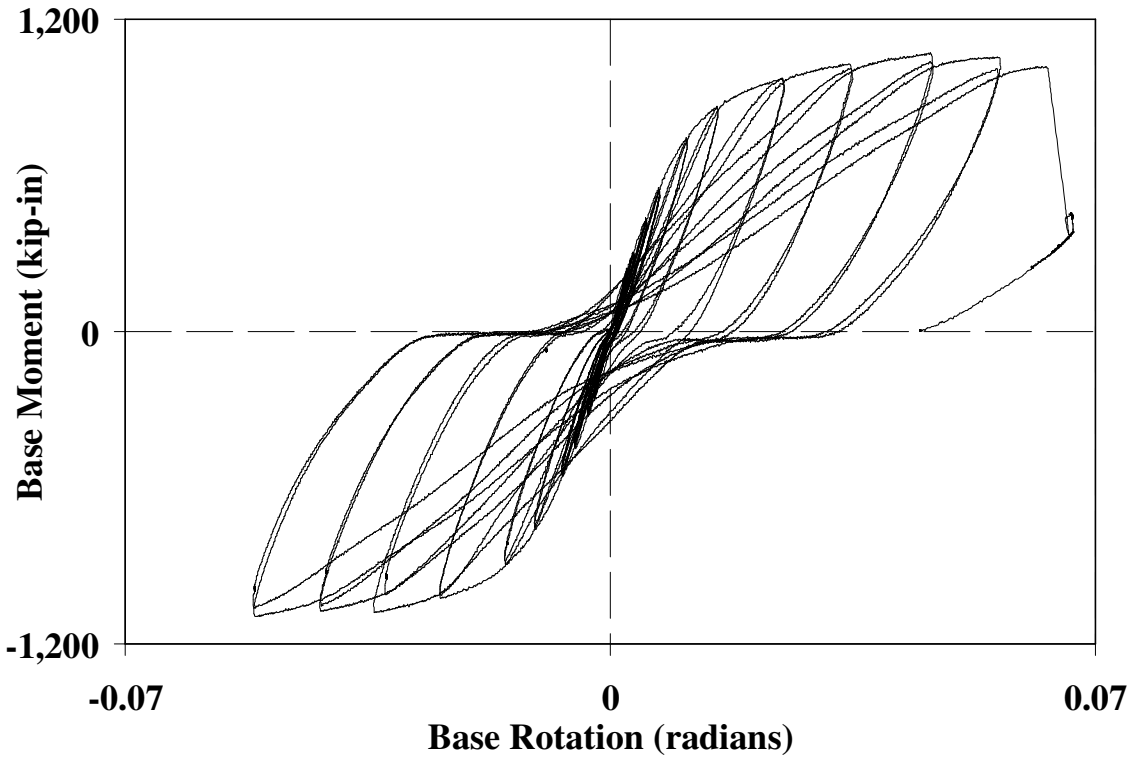

Figure B.12 – Base rotation versus base moment data for Test #2

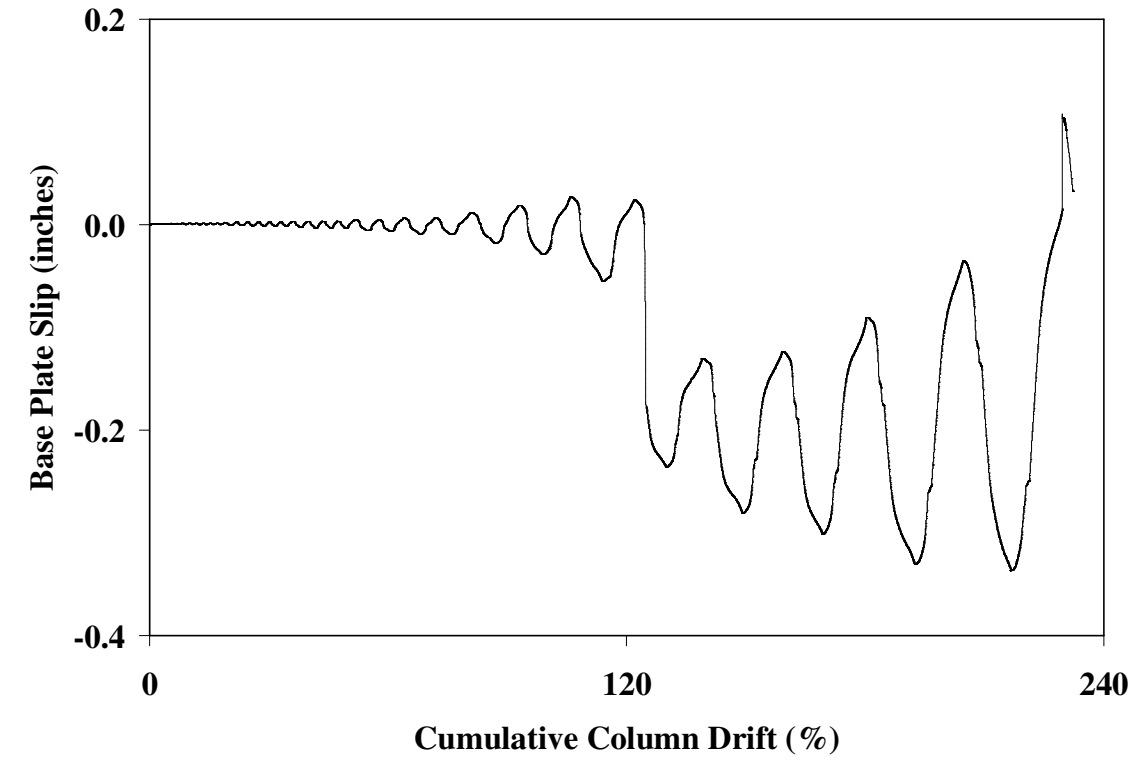

Figure B.13 – Cumulative column drift versus base plate slip data for Test #2

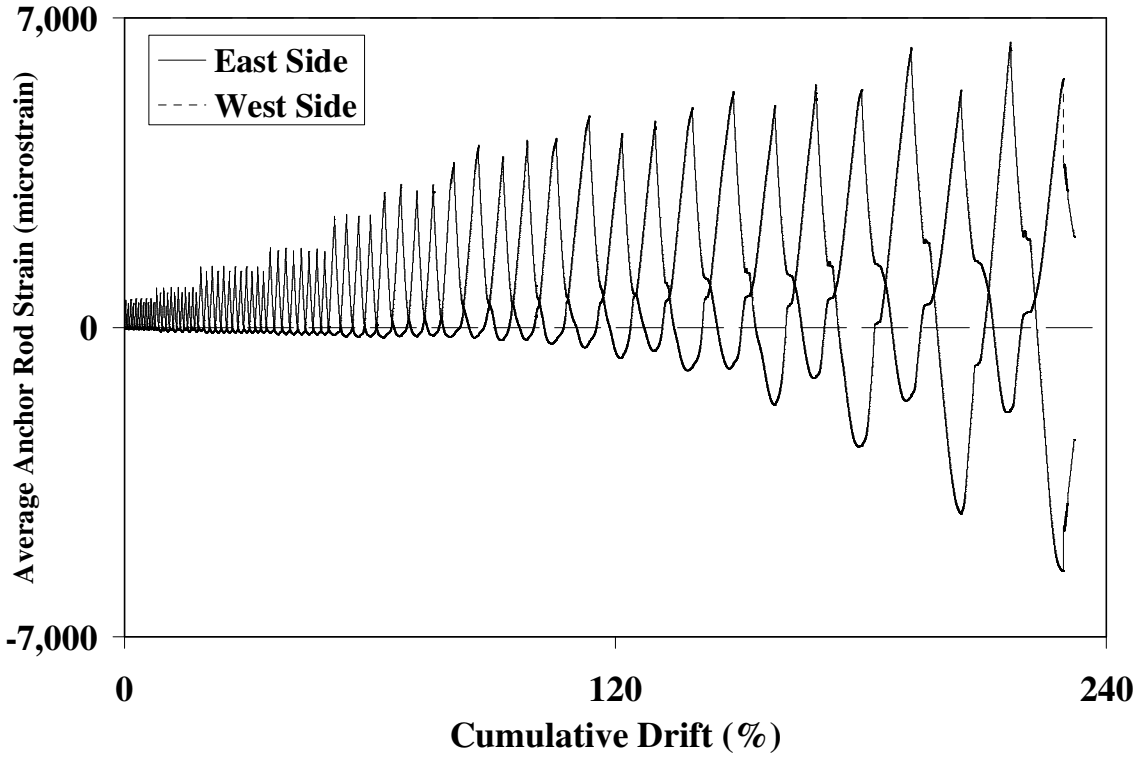

Figure B.14 – Cumulative drift versus anchor rod strain data for Test #2

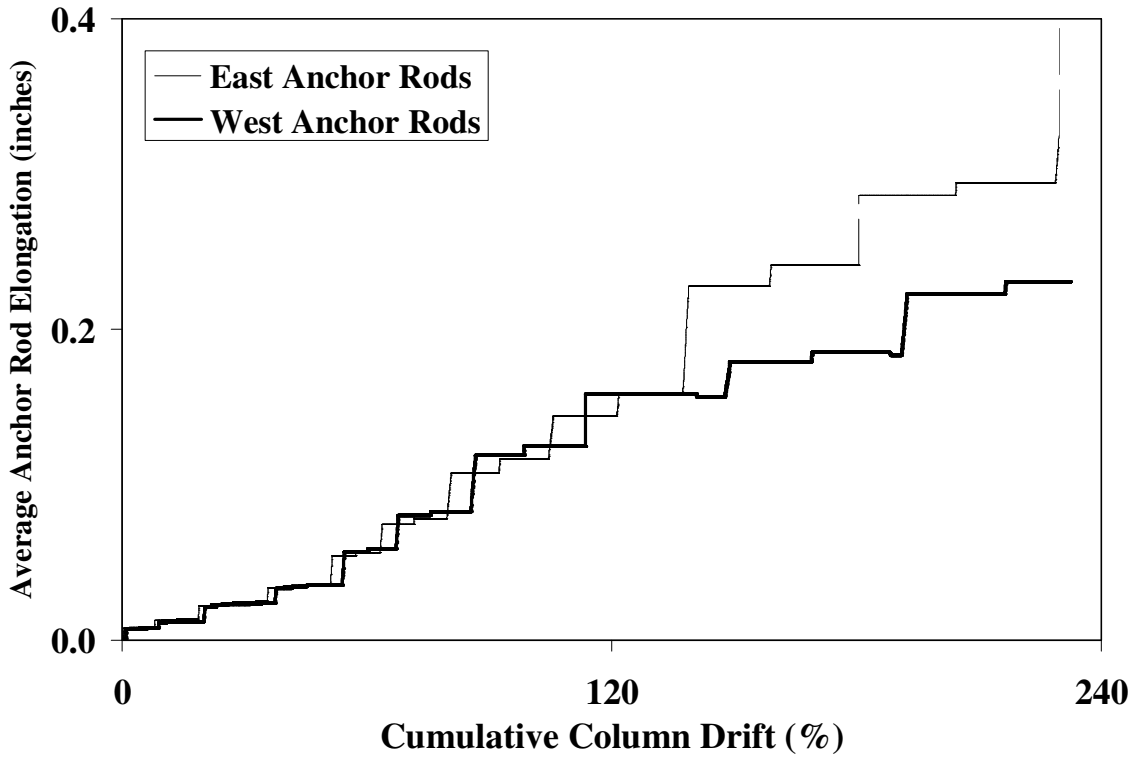

Figure B.15 – Cumulative column drift versus anchor rod elongation data for Test #2

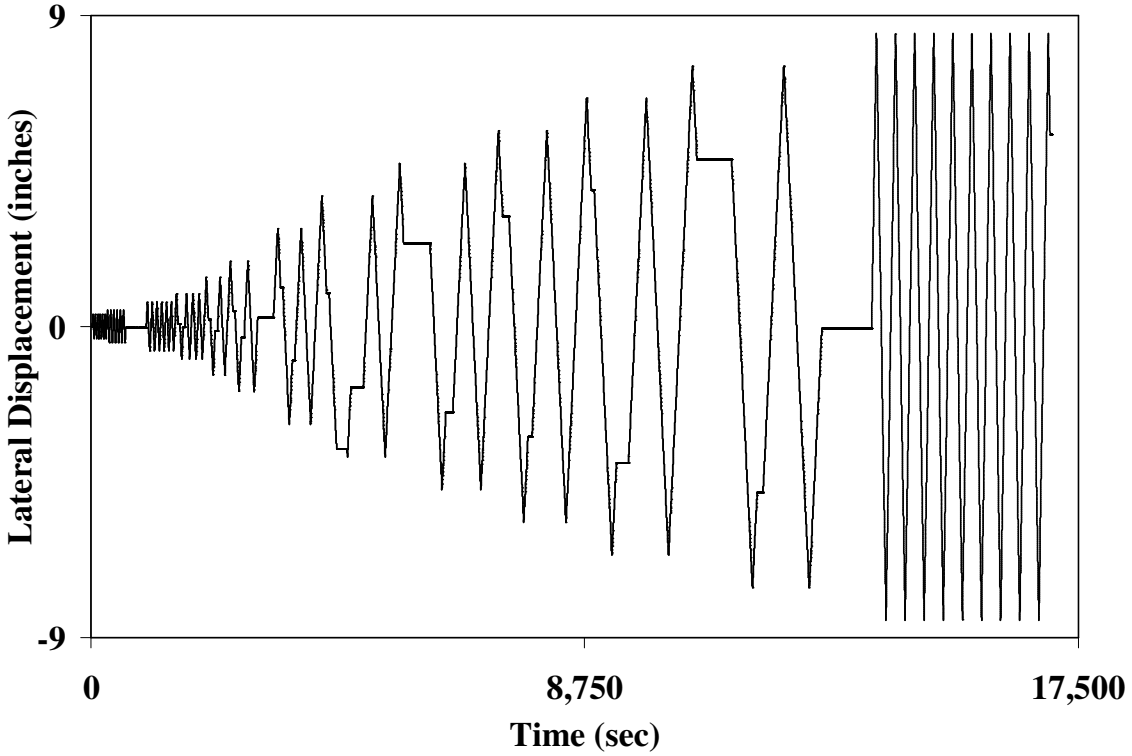

Figure B.16 – Time versus lateral displacement data for Test #3

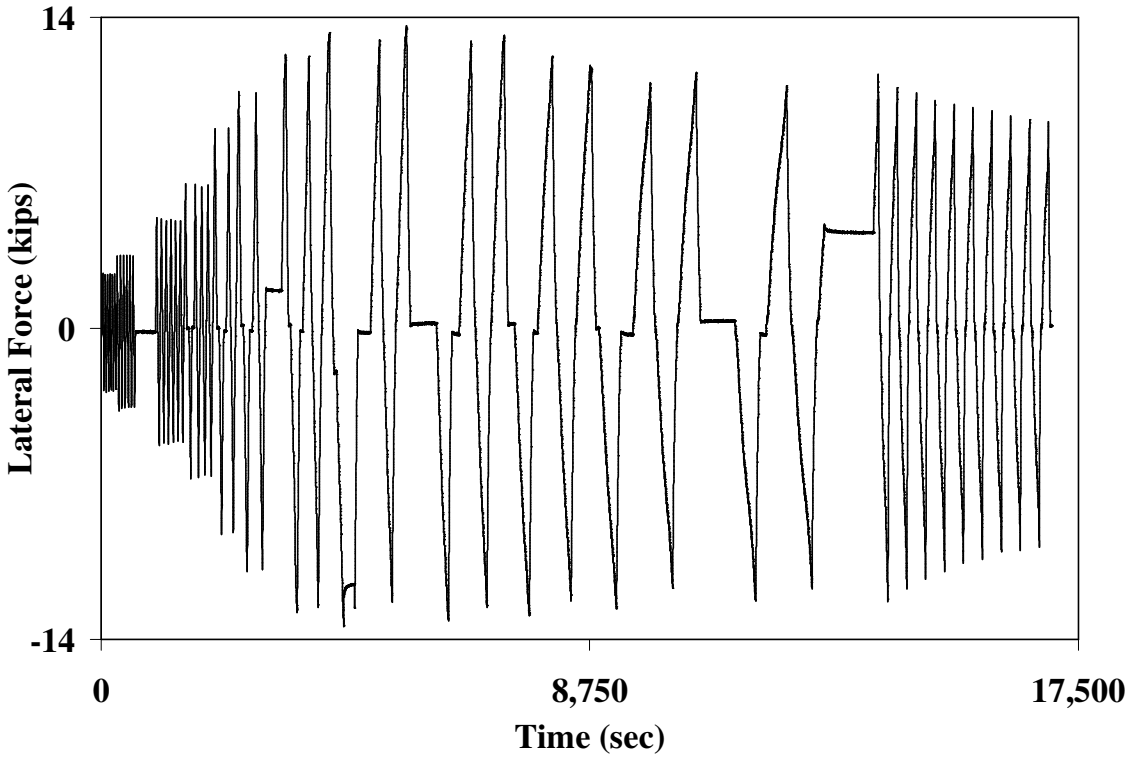

Figure B.17 – Time versus lateral force data for Test #3

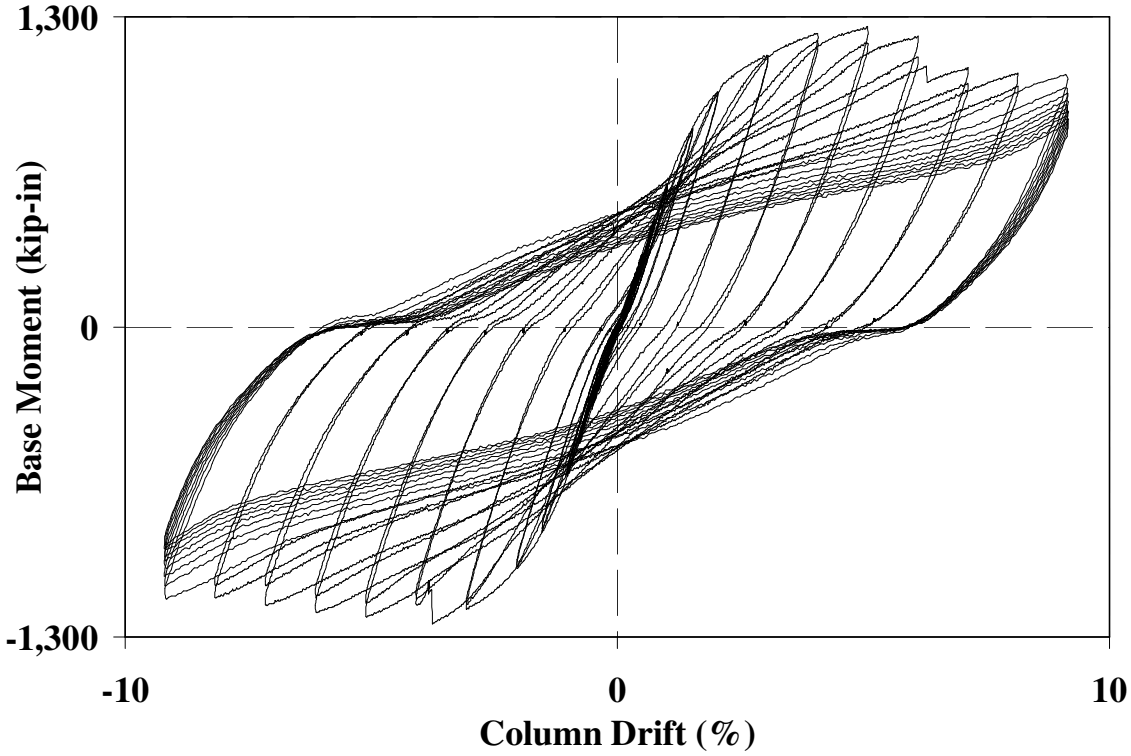

Figure B.18 – Column drift versus base moment data for Test #3

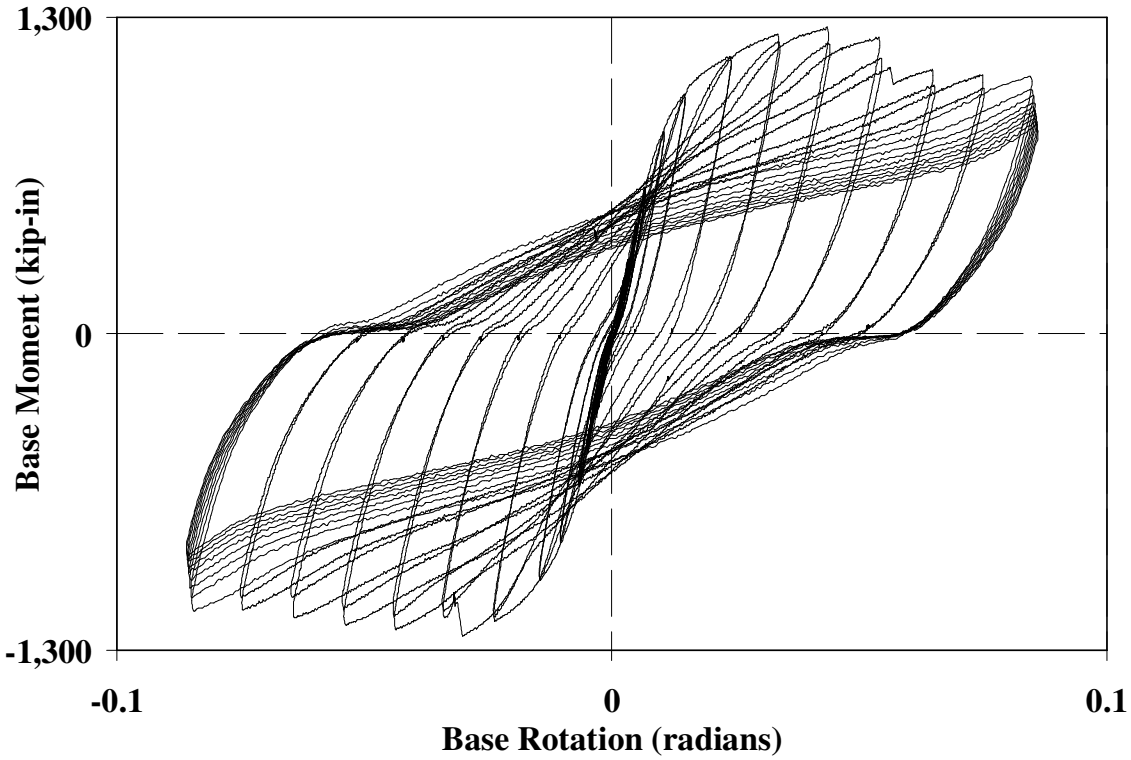

Figure B.19 – Base rotation versus base moment data for Test #3

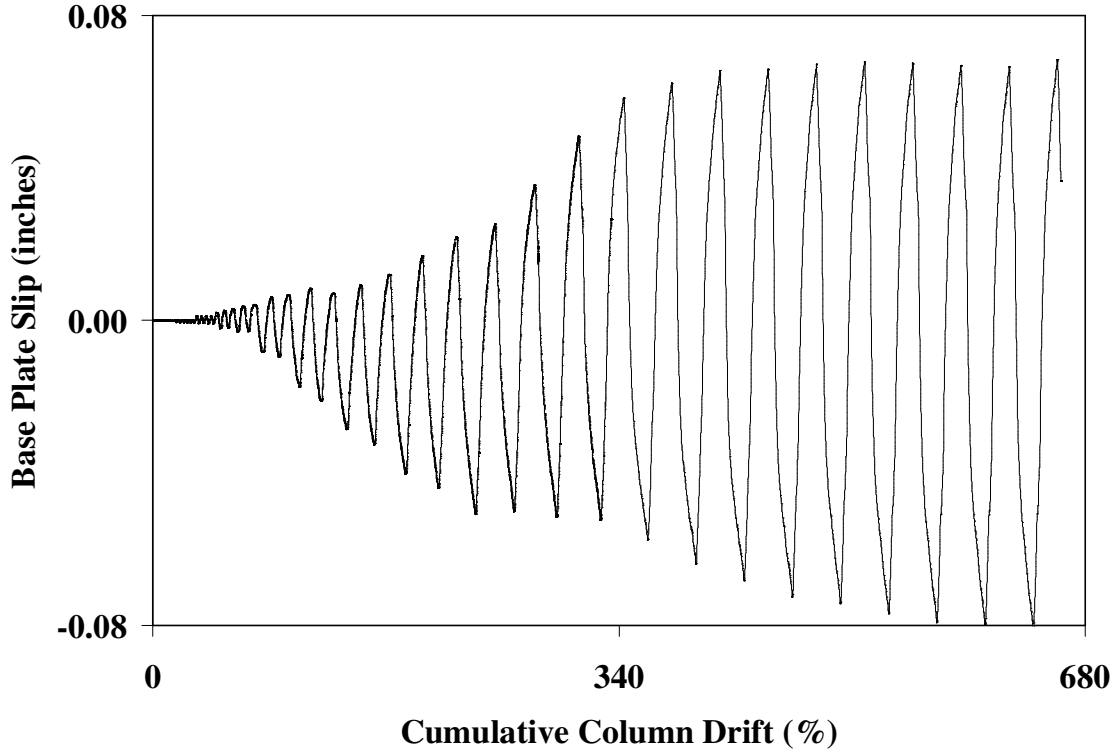

Figure B.20 – Cumulative column drift versus base plate slip data for Test #3

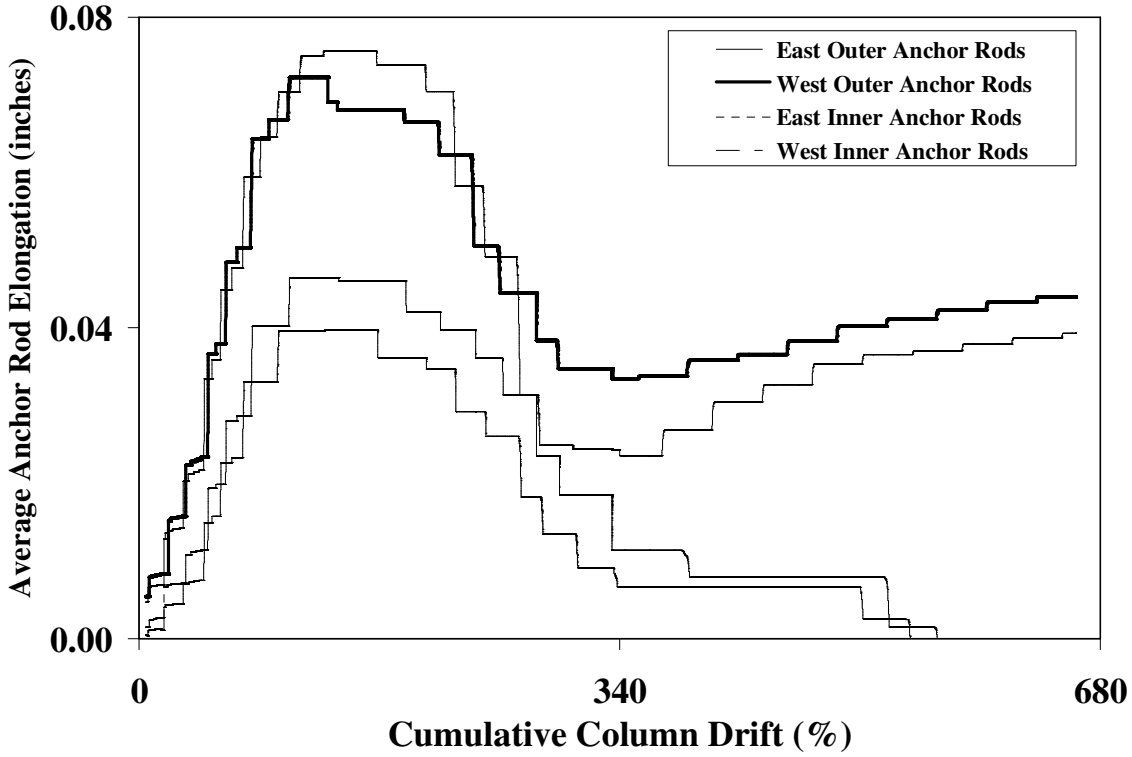

Figure B.21 – Cumulative column drift versus anchor rod elongation data for Test #3

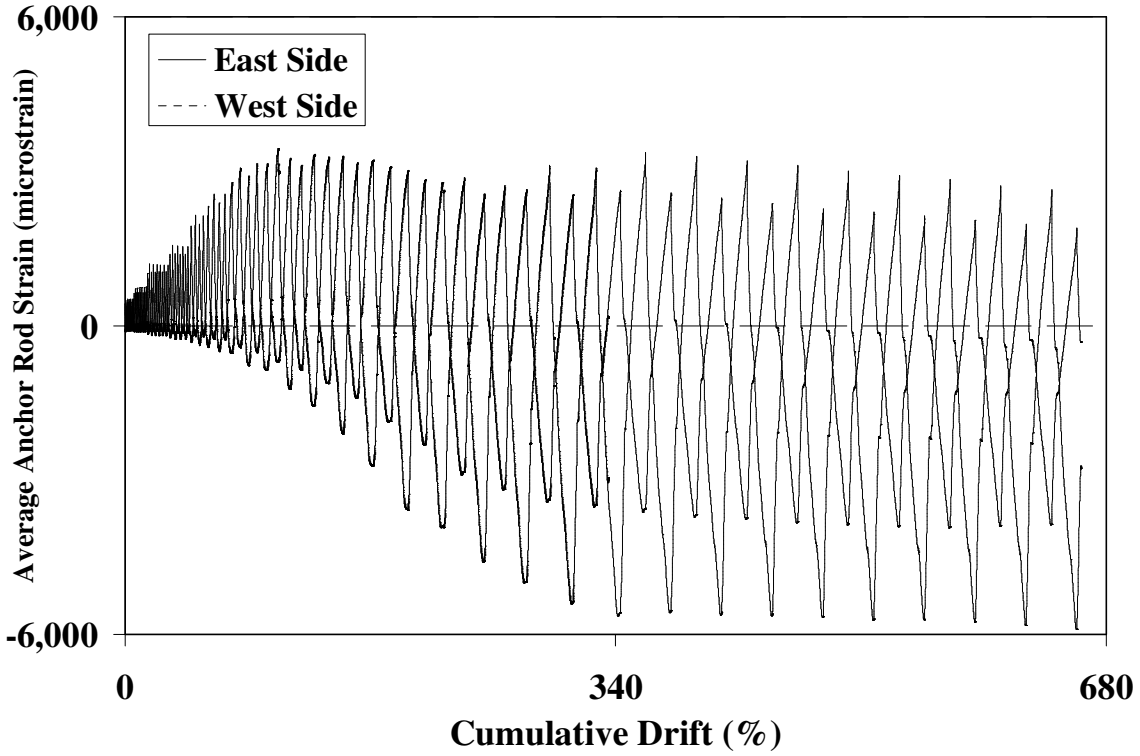

Figure B.22 – Cumulative drift versus outer anchor rod strain data for Test #3

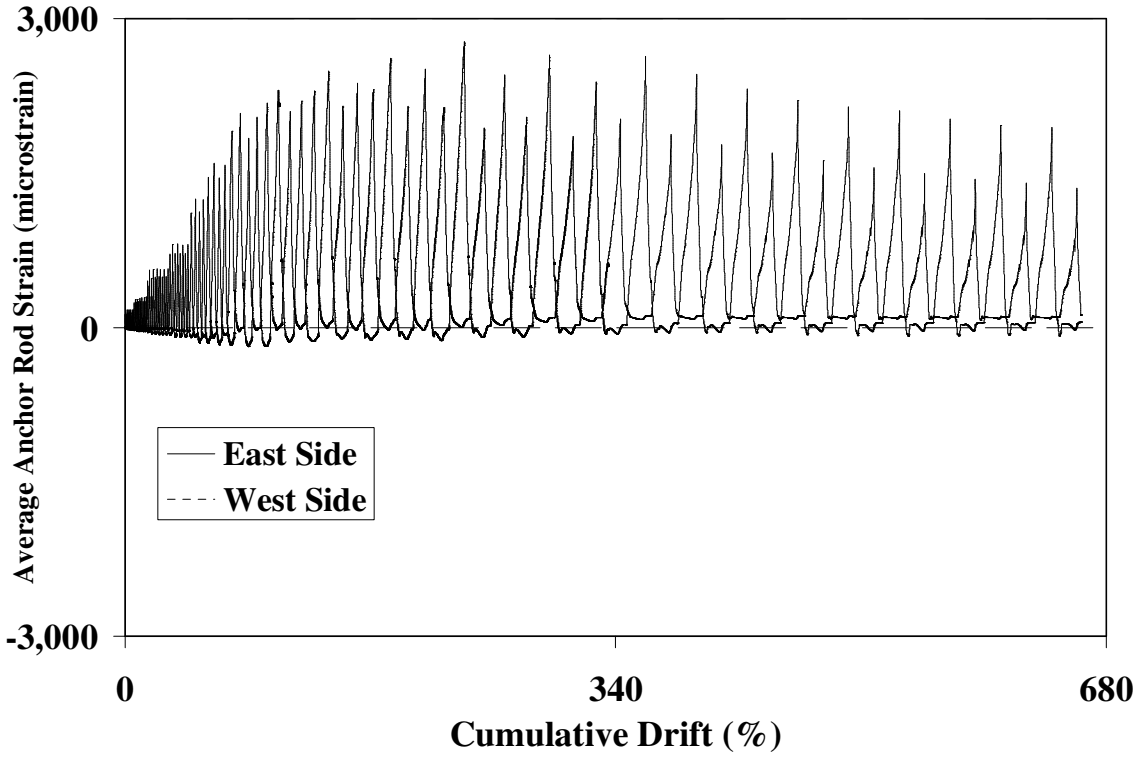

Figure B.23 – Cumulative drift versus inner anchor rod strain data for Test #3

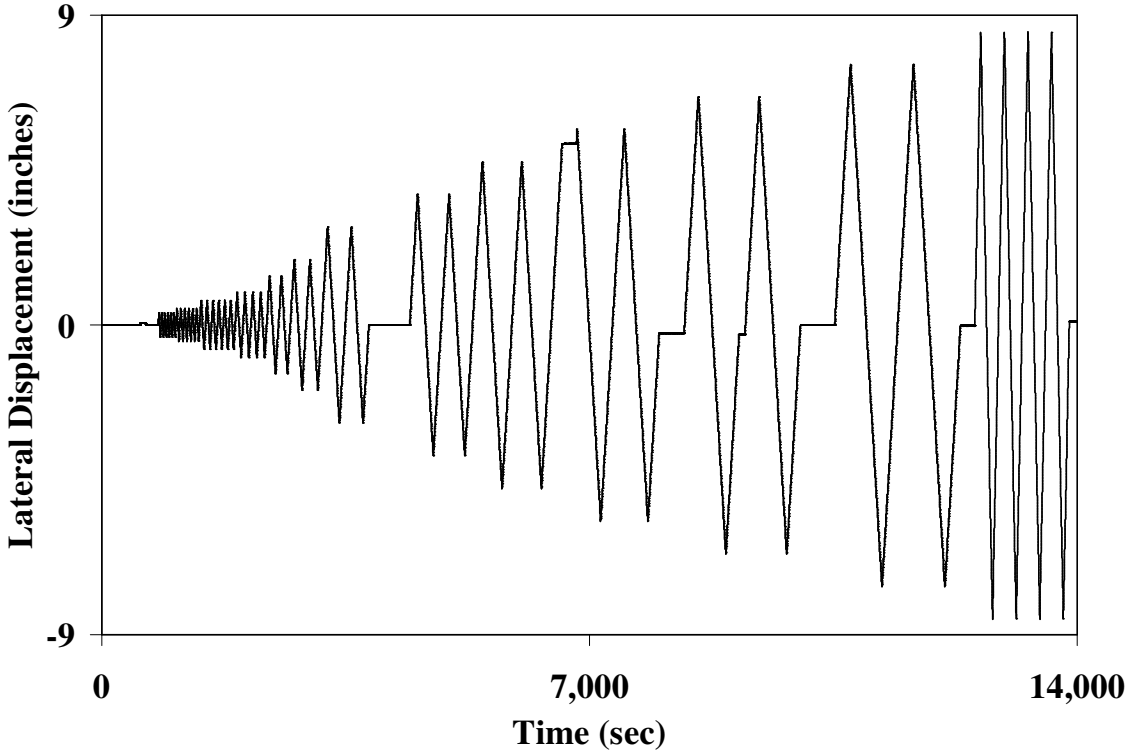

Figure B.24 – Time versus lateral displacement data for Test #4

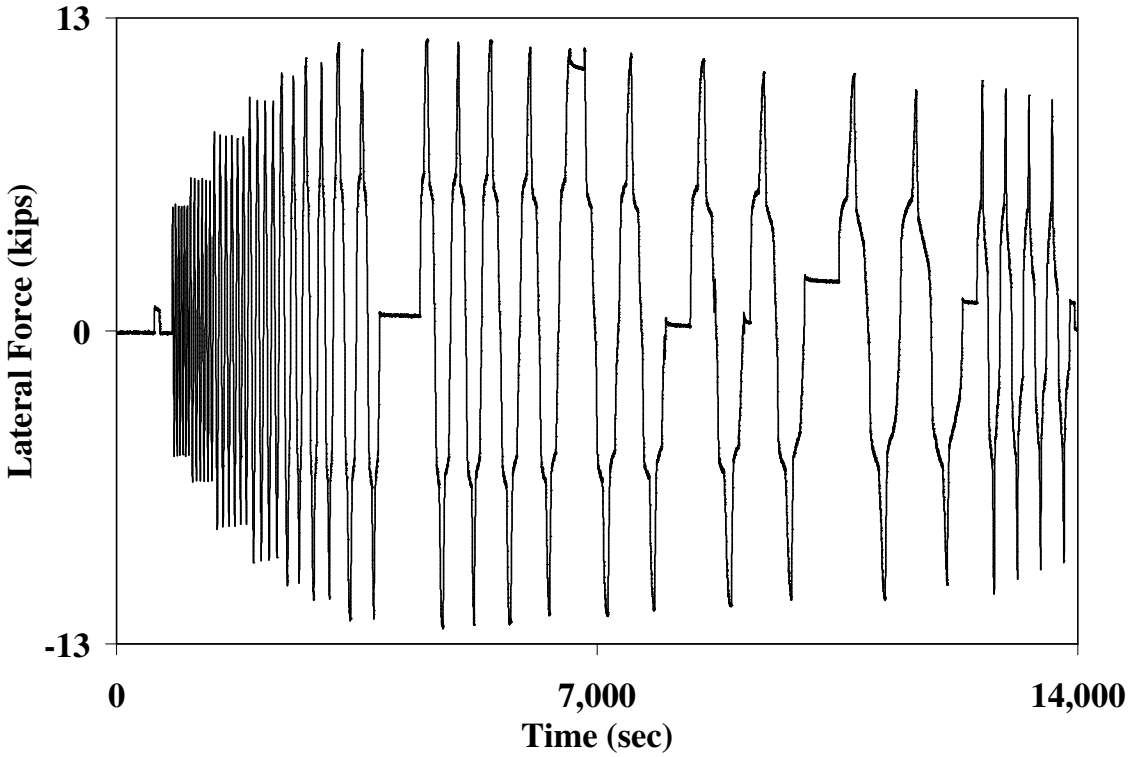

Figure B.25 – Time versus lateral force data for Test #4

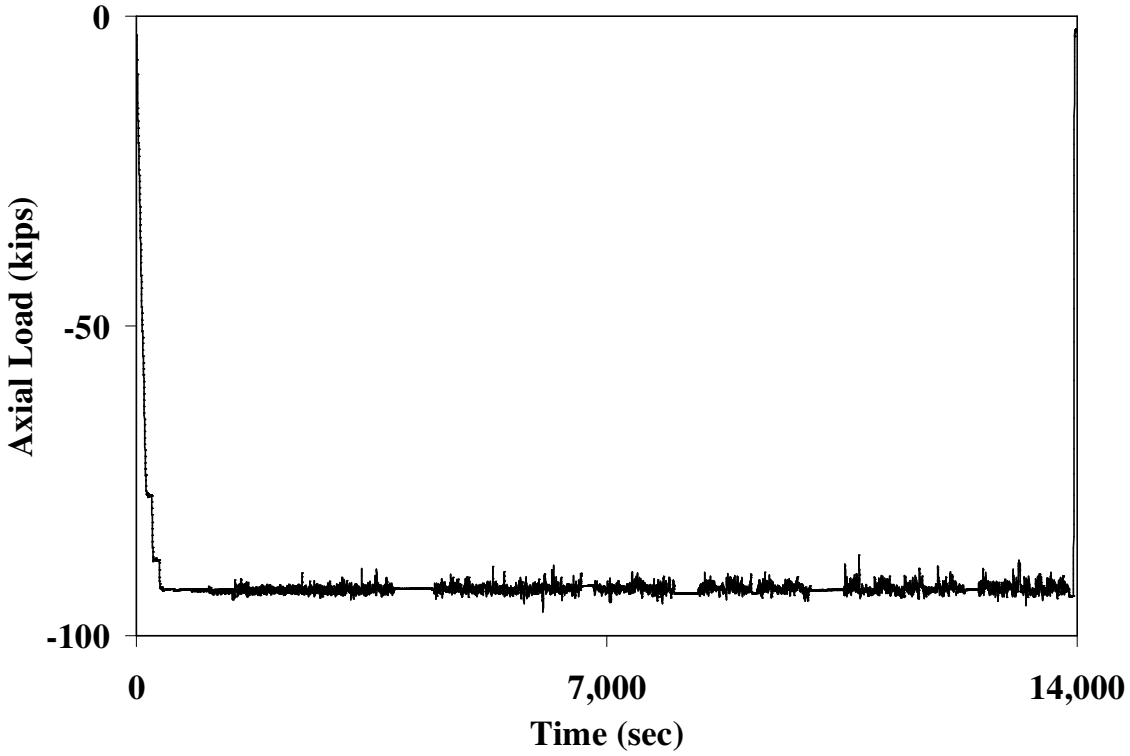

Figure B.26 – Time versus axial load data for Test #4

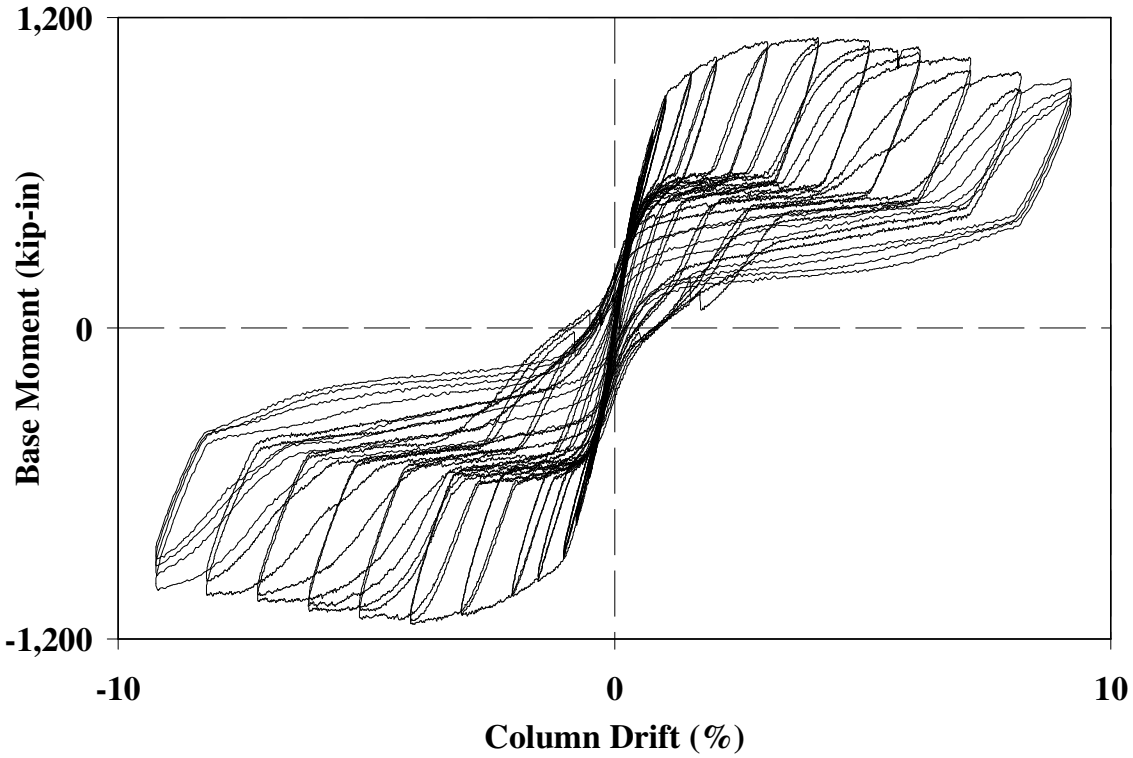

Figure B.27 – Column drift versus base moment data for Test #4

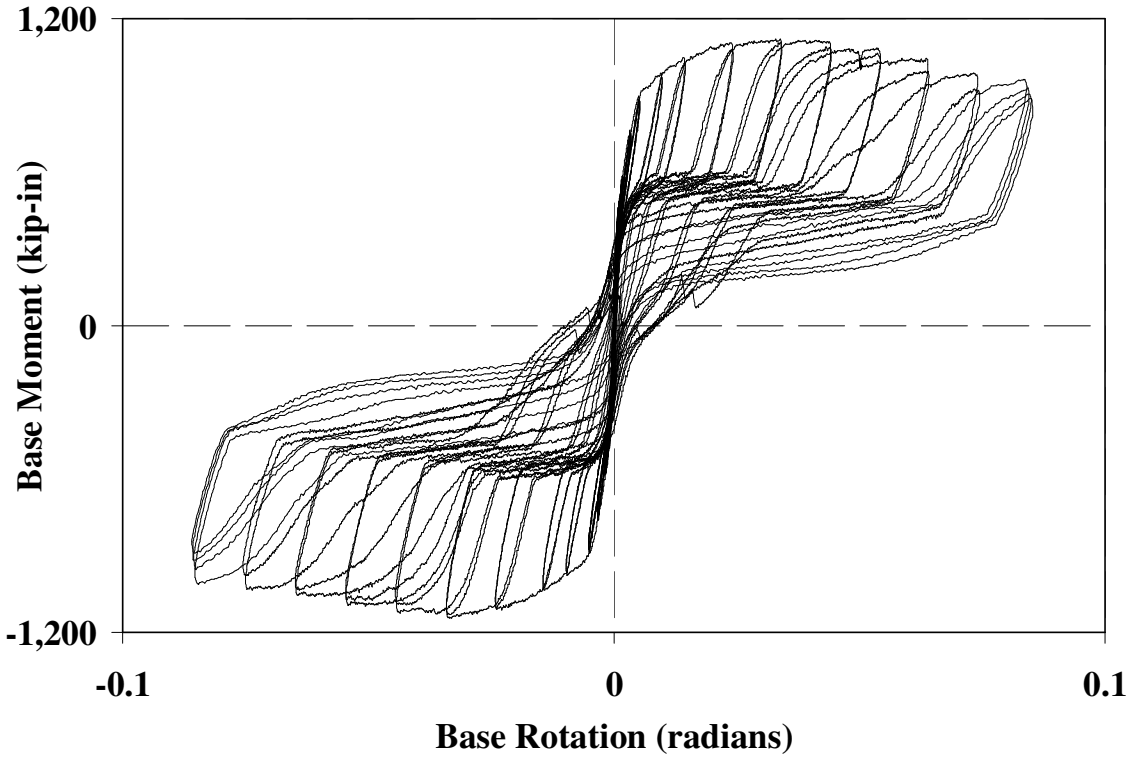

Figure B.28 – Base rotation versus base moment data for Test #4

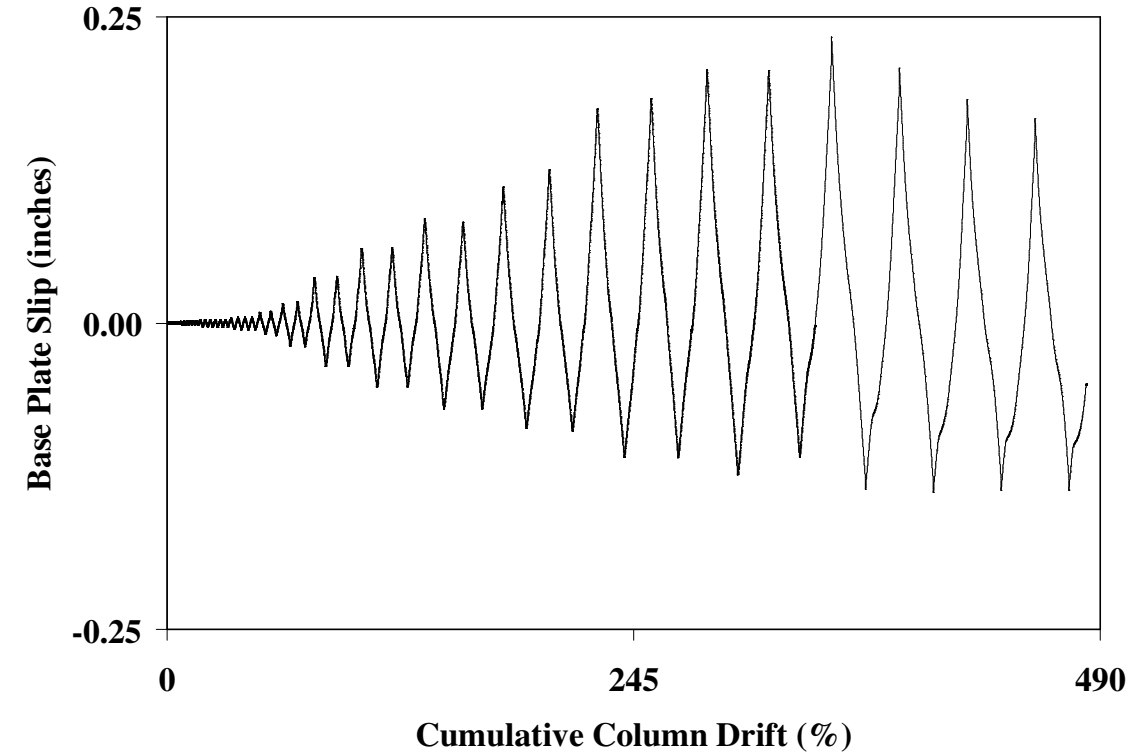

Figure B.29 – Cumulative column drift versus base plate slip data for Test #4

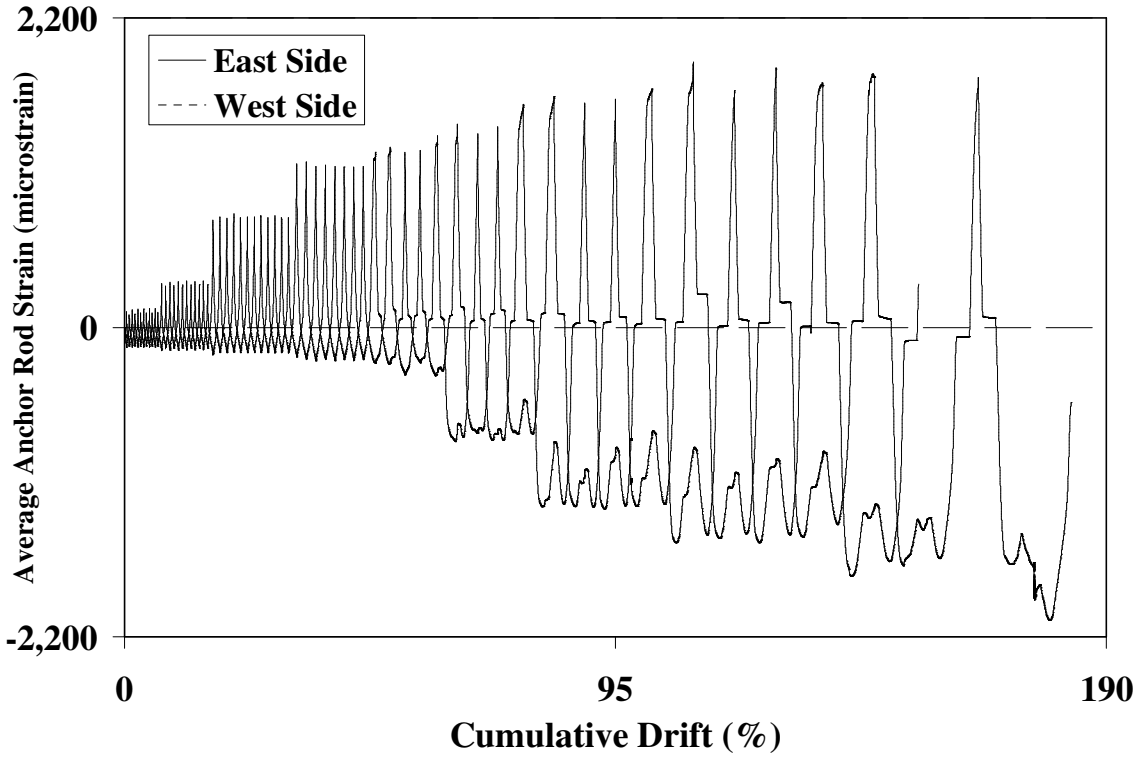

Figure B.30 – Cumulative drift versus anchor rod strain data for Test #4

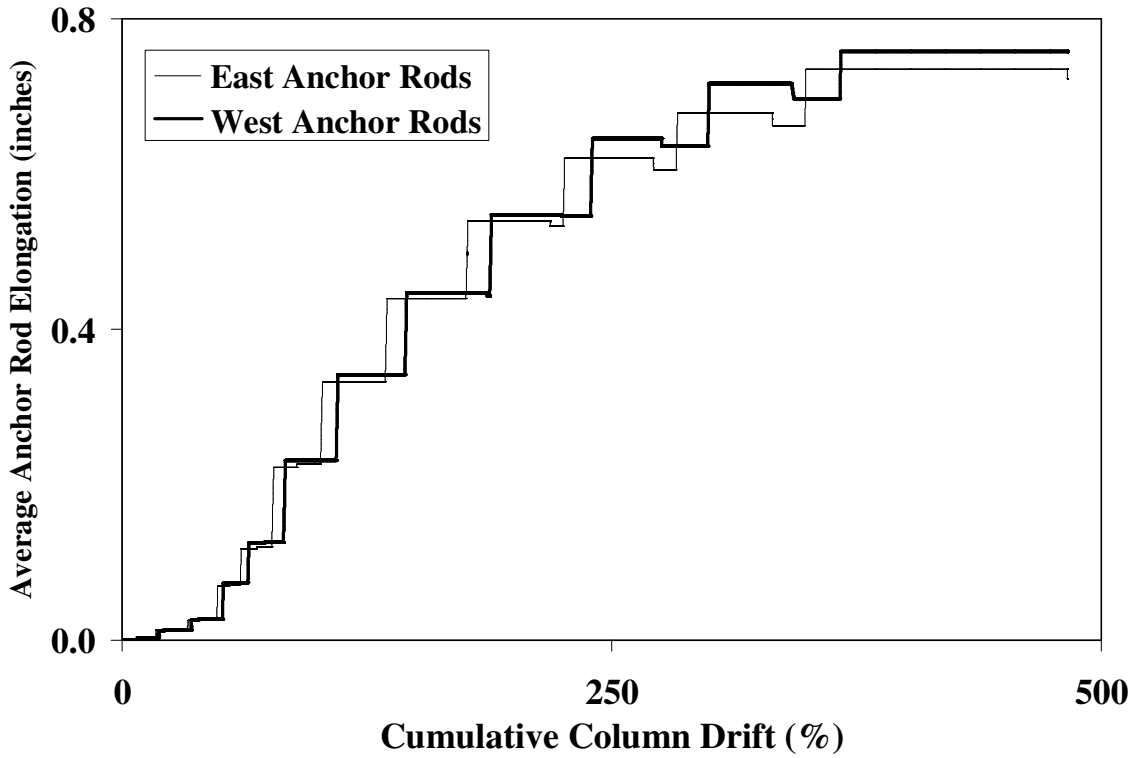

Figure B.31 – Cumulative column drift versus anchor rod elongation data for Test #4

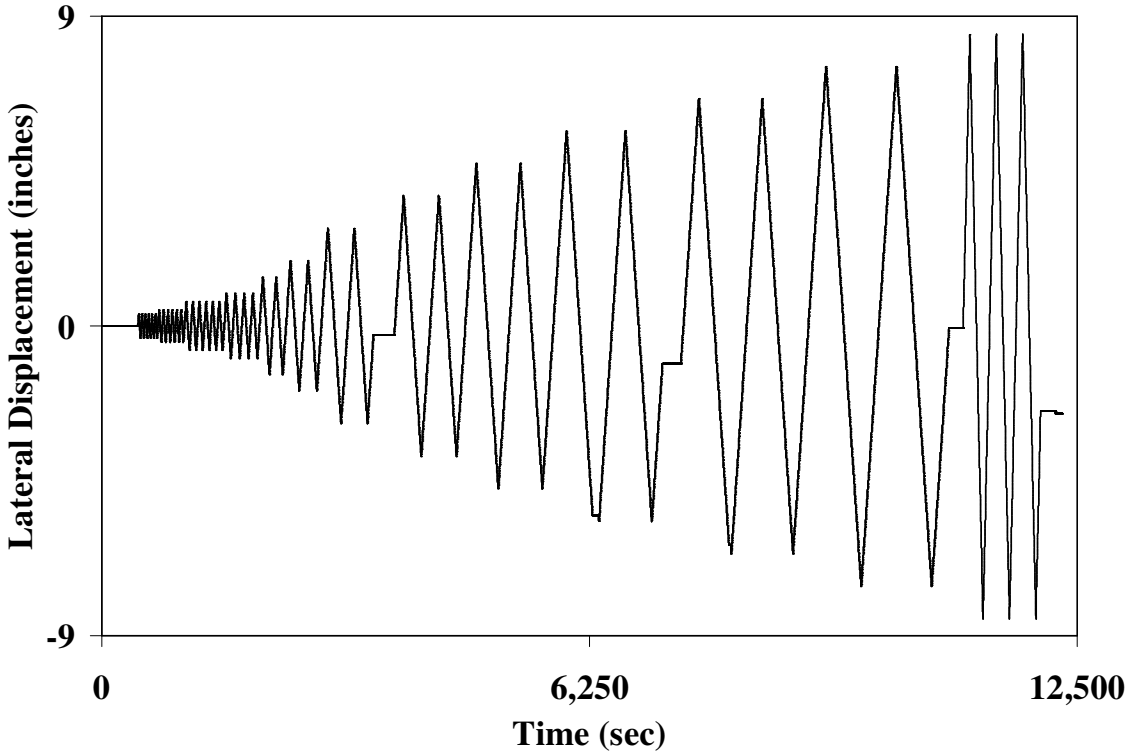

Figure B.32 – Time versus lateral displacement data for Test #5

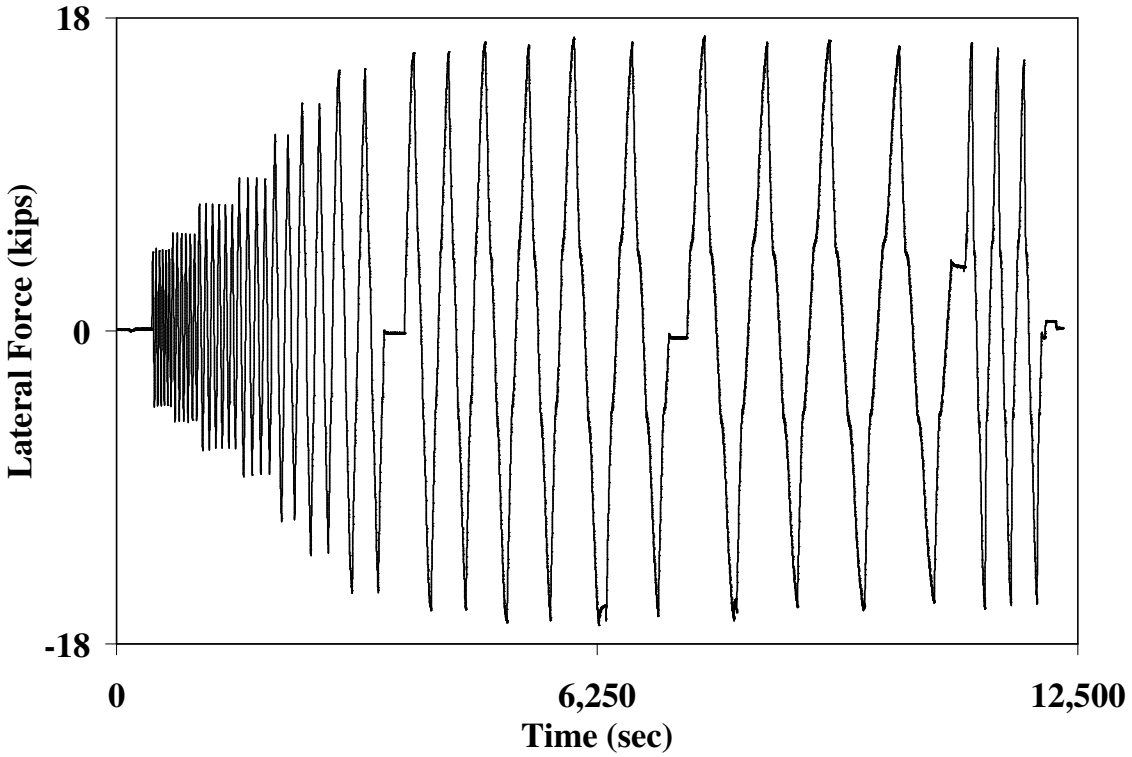

Figure B.33 – Time versus lateral force data for Test #5

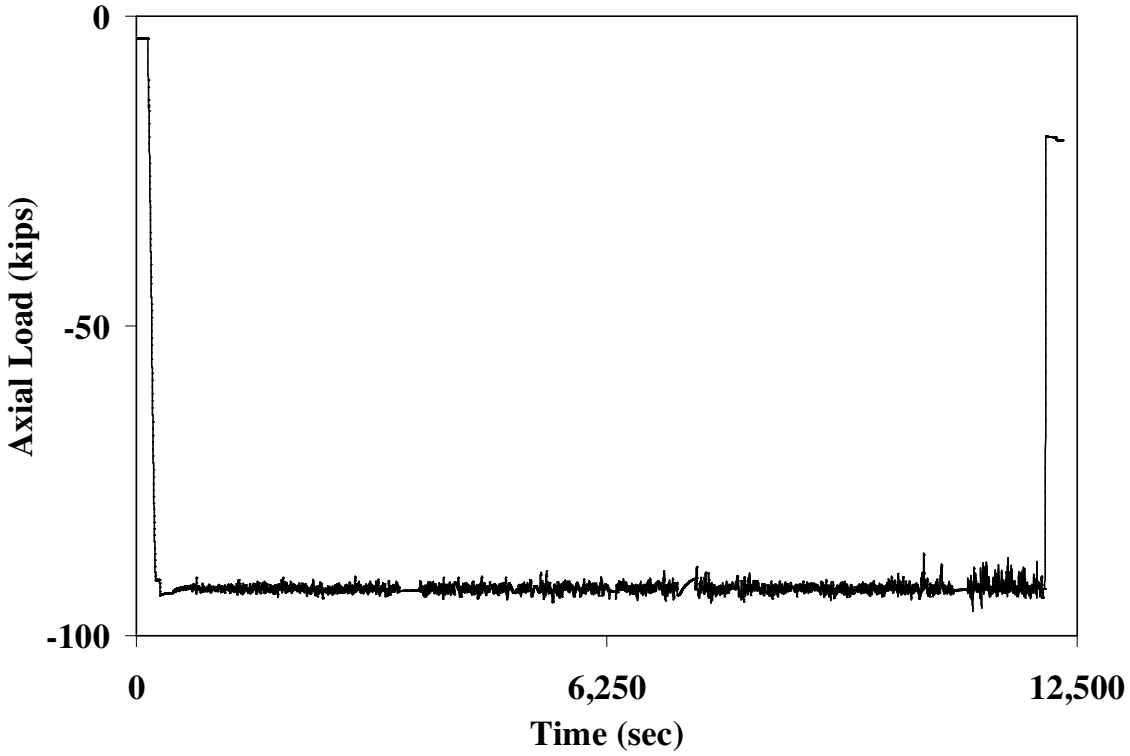

Figure B.34 – Time versus axial load data for Test #5

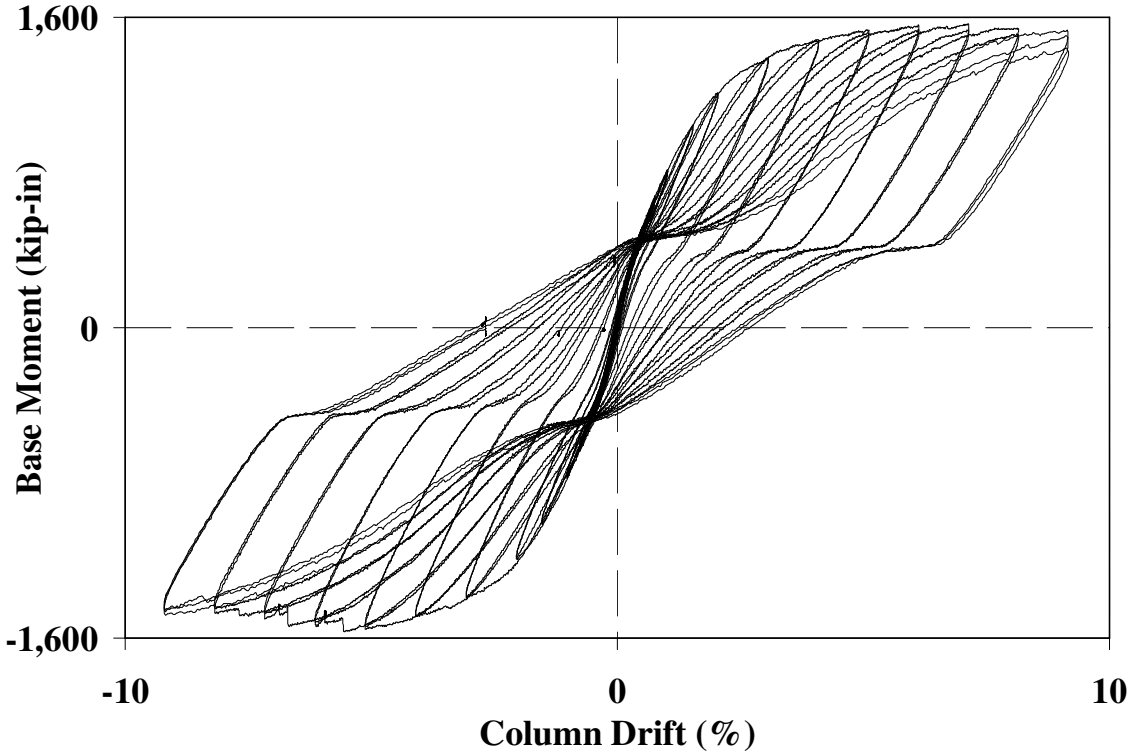

Figure B.35 – Column drift versus base moment data for Test #5

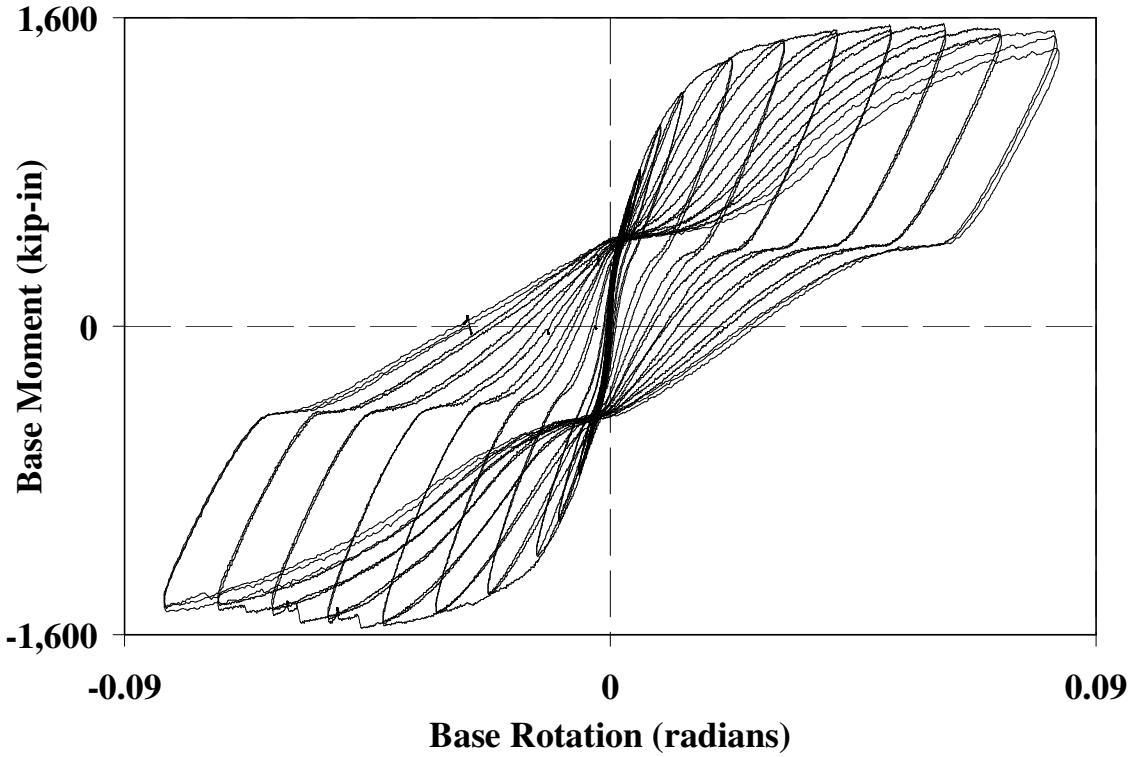

Figure B.36 – Base rotation versus base moment data for Test #5

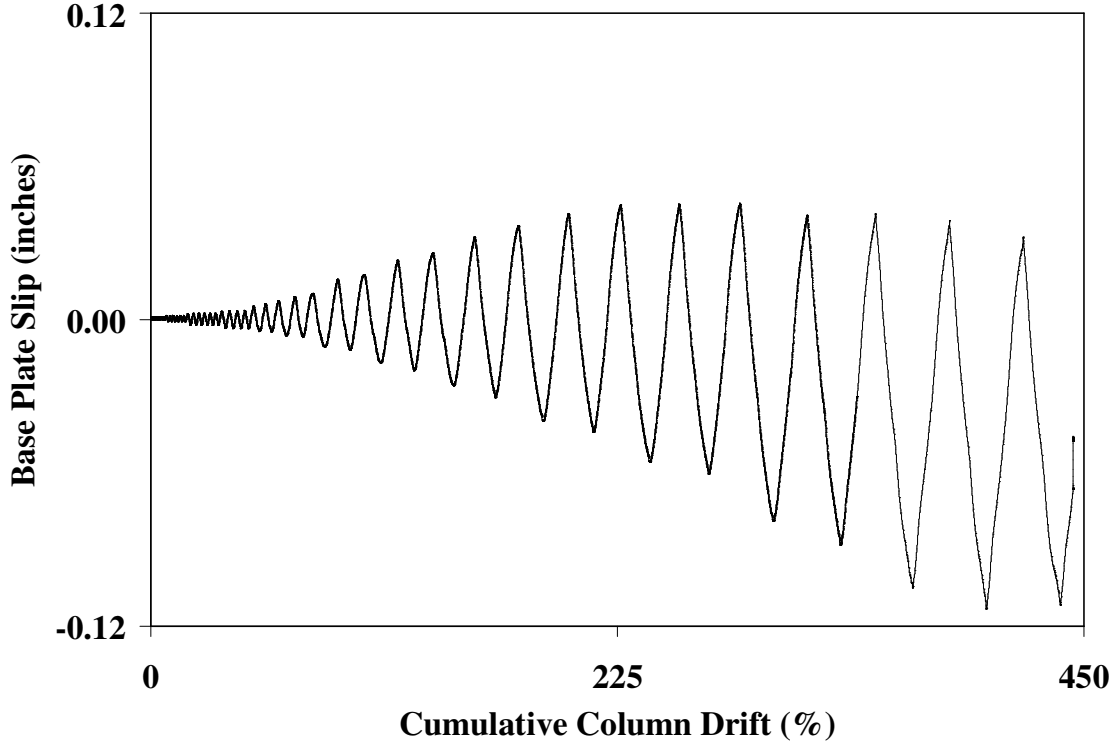

Figure B.37 – Cumulative column drift versus base plate slip data for Test #5

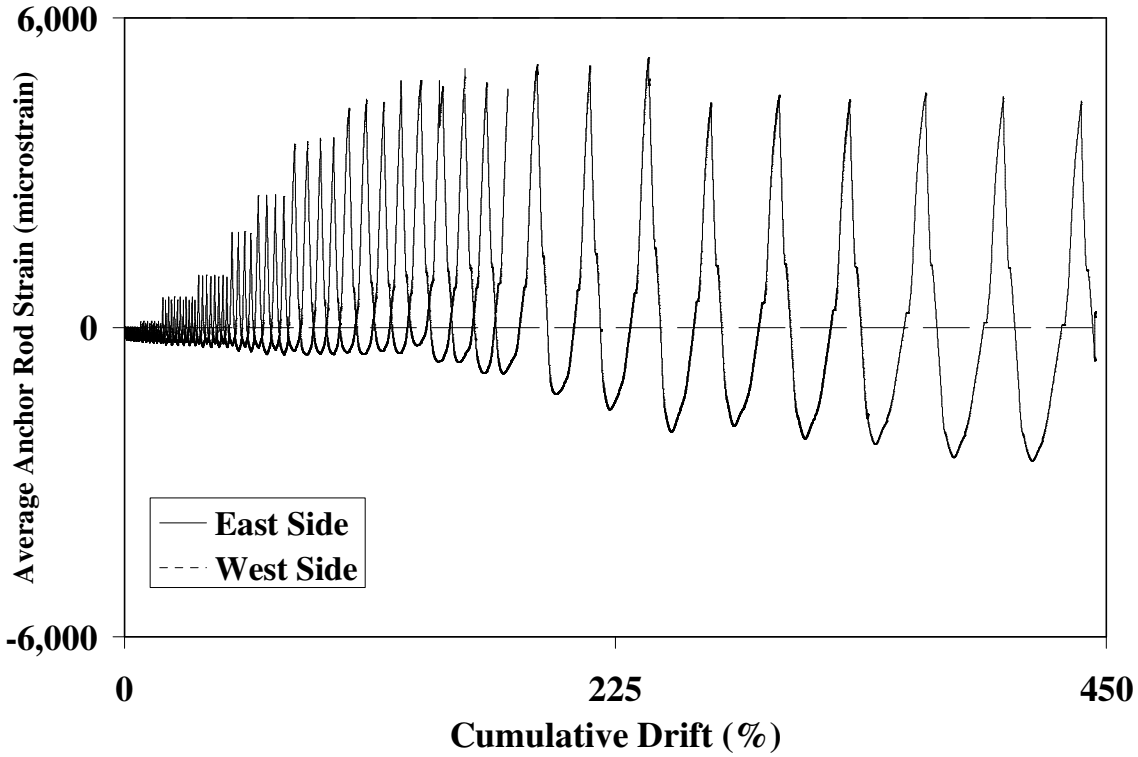

Figure B.38 – Cumulative drift versus anchor rod strain data for Test #5

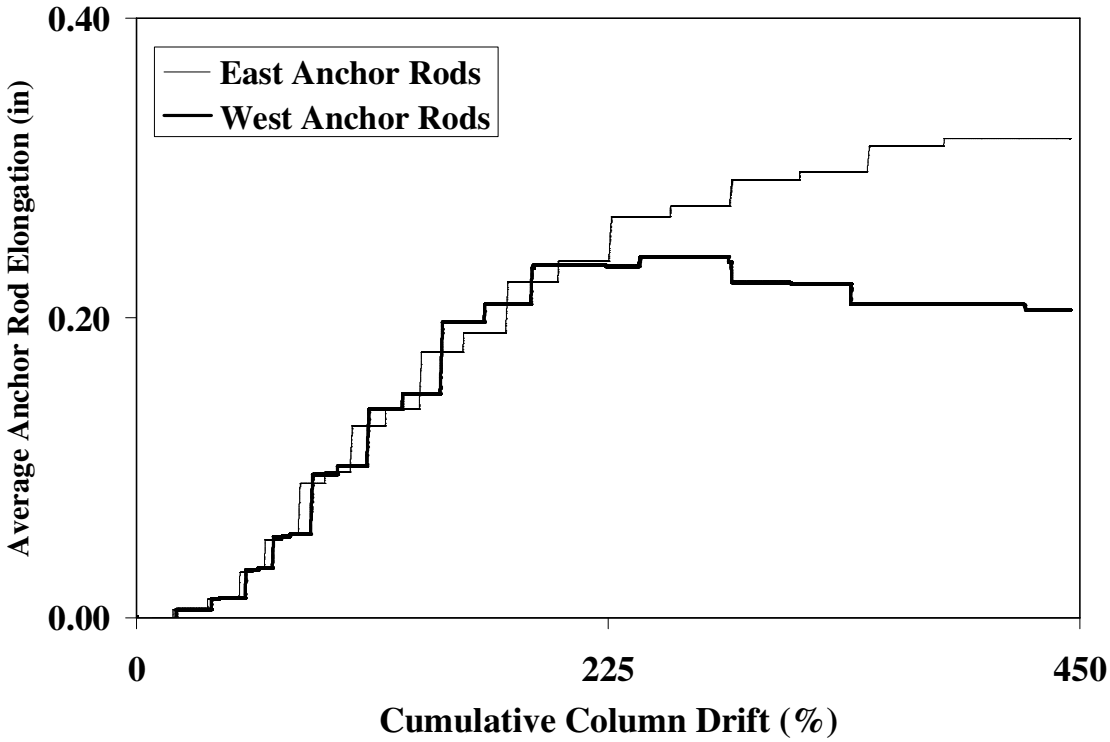

Figure B.39 – Cumulative column drift versus anchor rod elongation data for Test #5

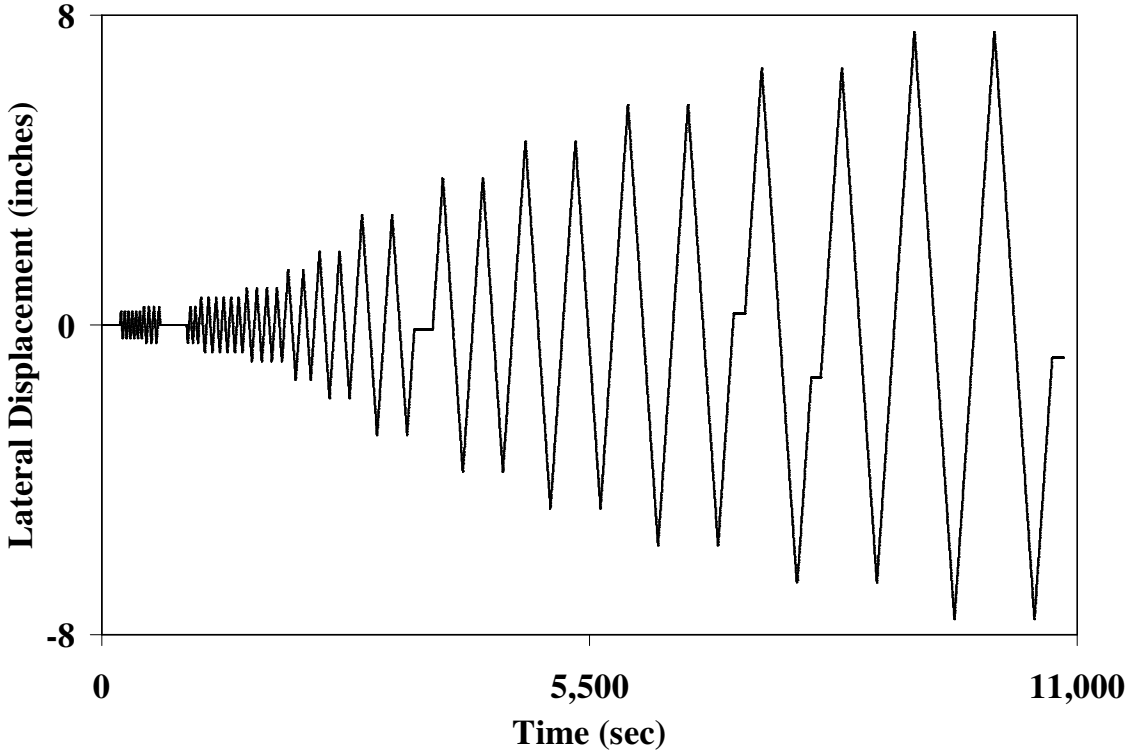

Figure B.40 – Time versus lateral displacement data for Test #6

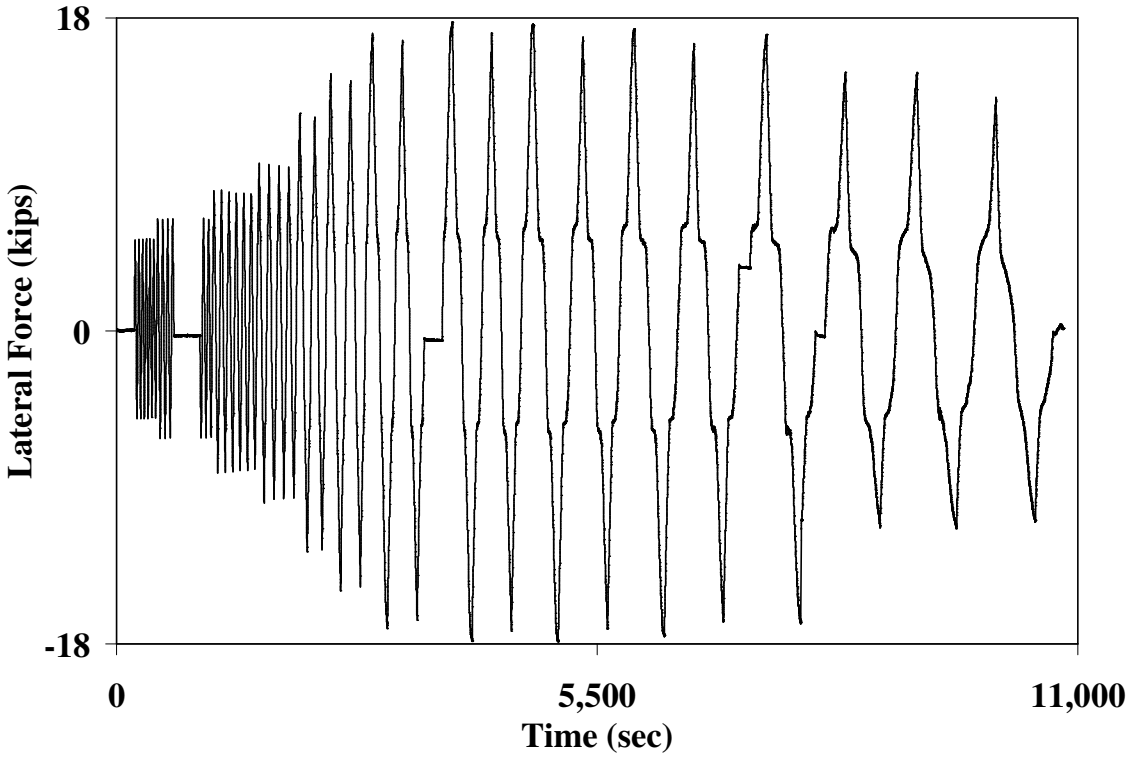

Figure B.41 – Time versus lateral force data for Test #6

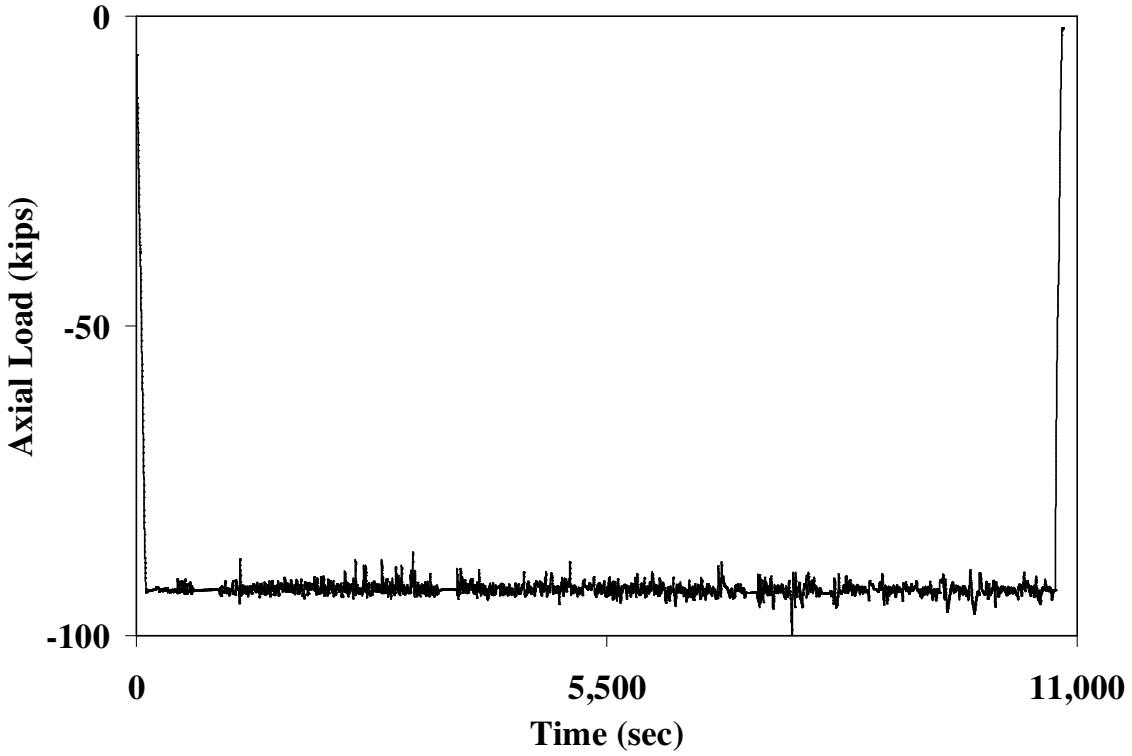

Figure B.42 – Time versus axial load data for Test #6

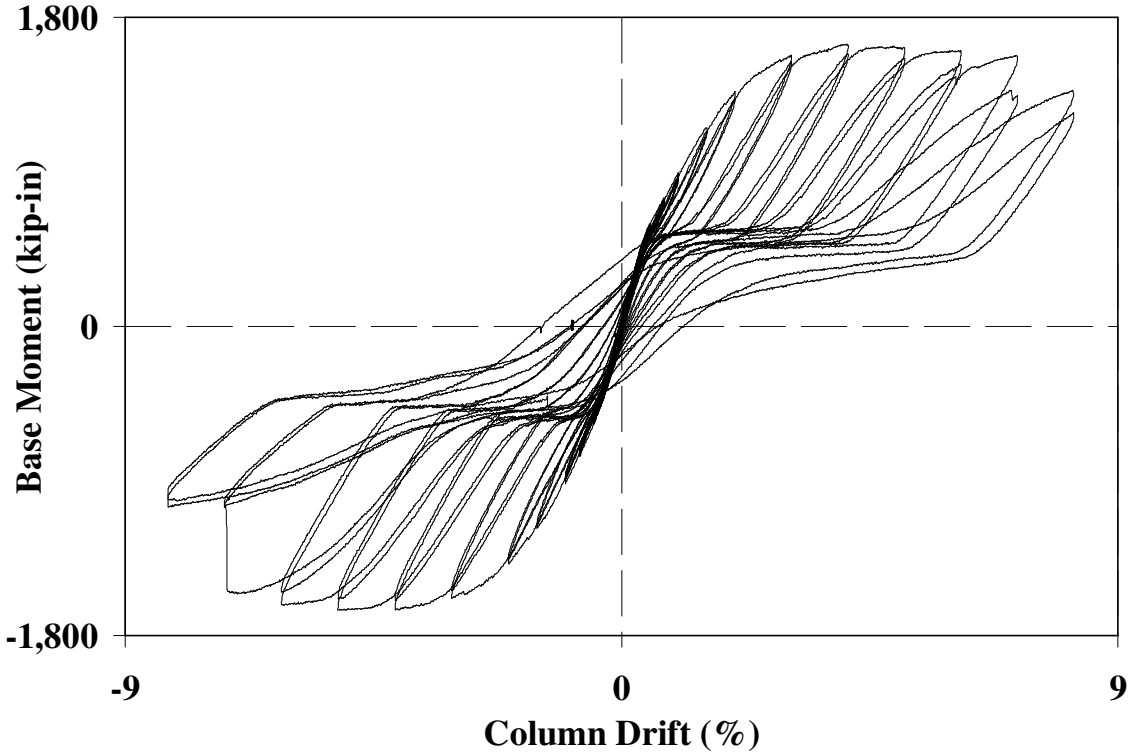

Figure B.43 – Column drift versus base moment data for Test #6

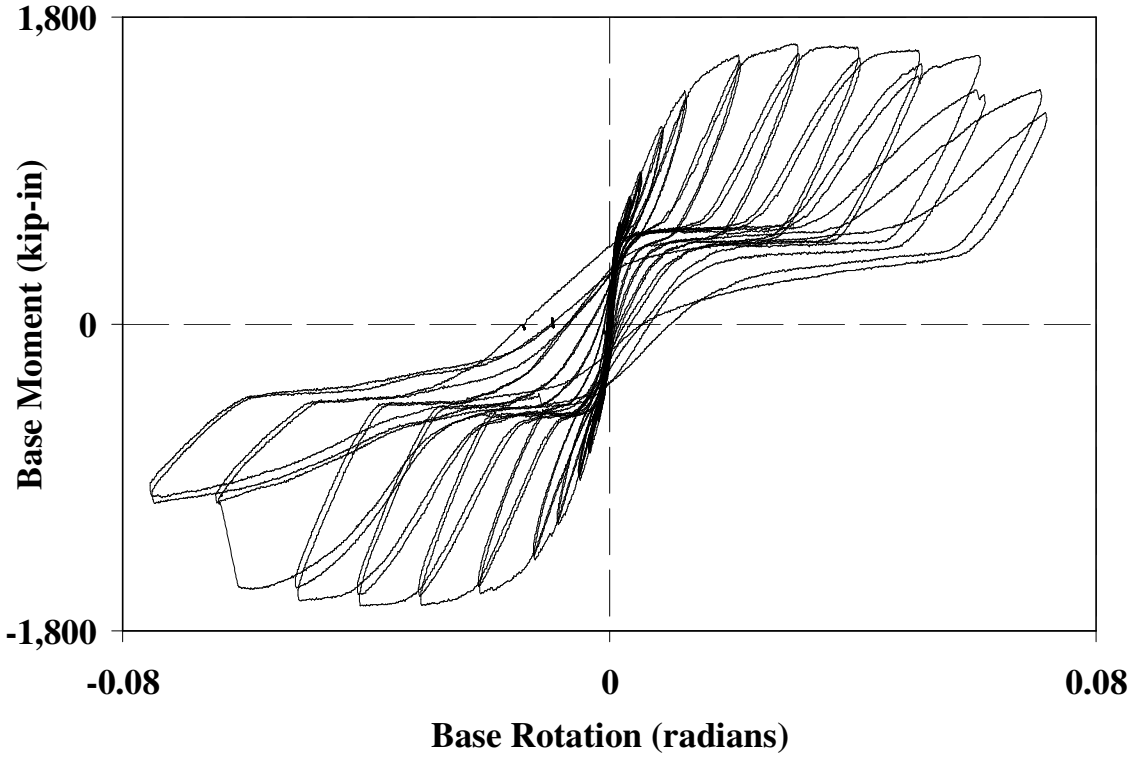

Figure B.44 – Base rotation versus base moment data for Test #6

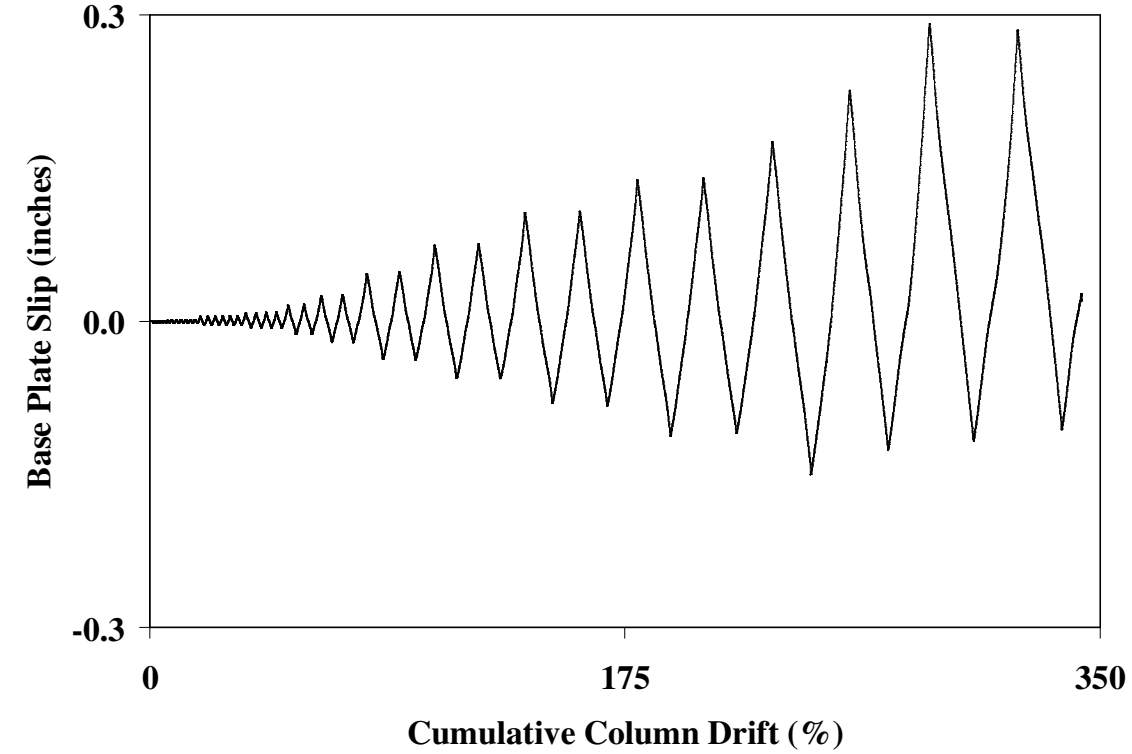

Figure B.45 – Cumulative column drift versus base plate slip data for Test #6

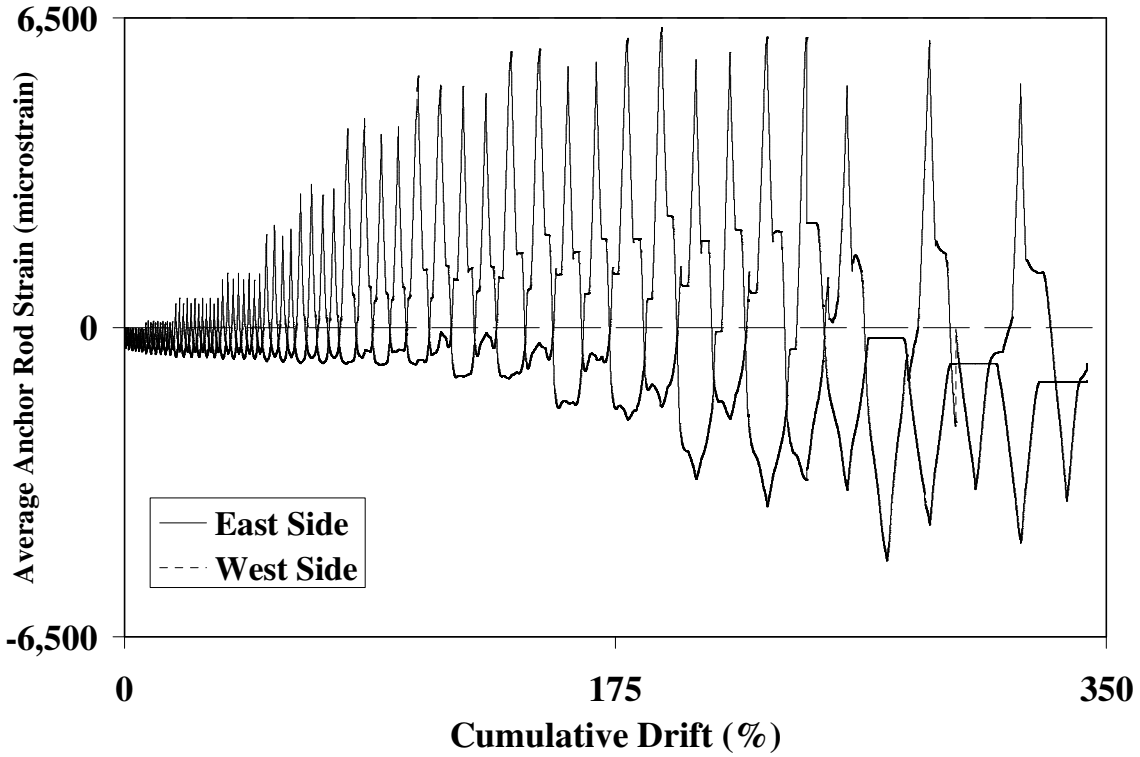

Figure B.46 – Cumulative drift versus anchor rod strain data for Test #6

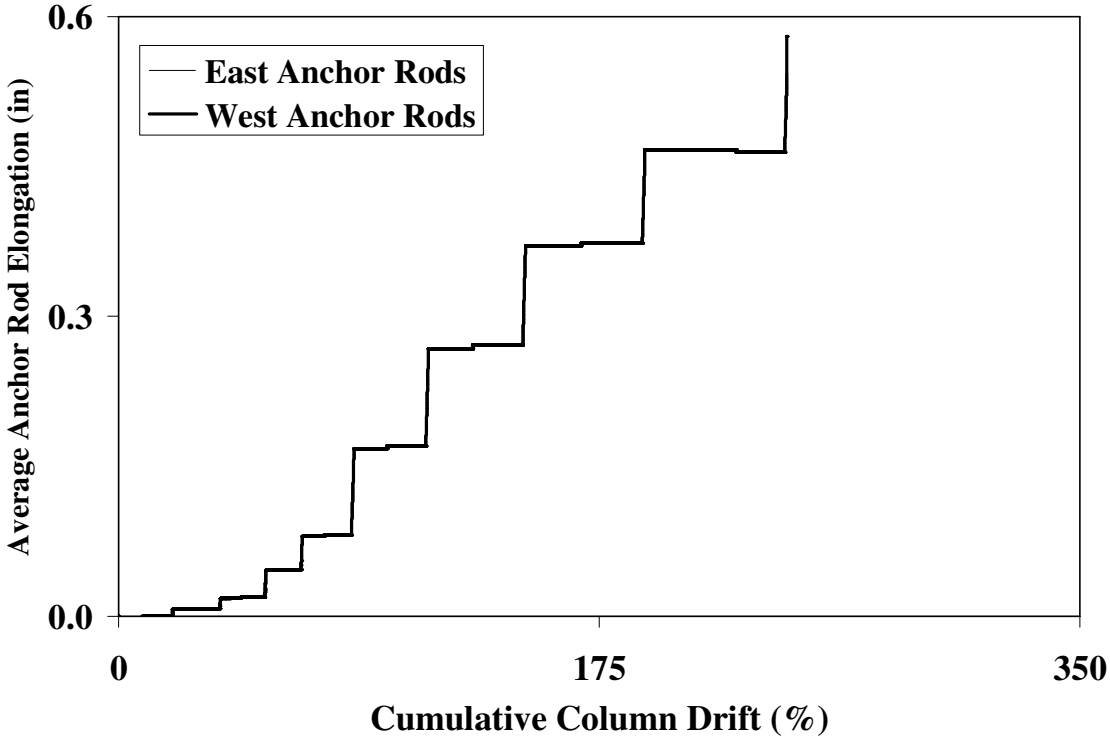

Figure B.47 – Cumulative column drift versus anchor rod elongation data for Test #6

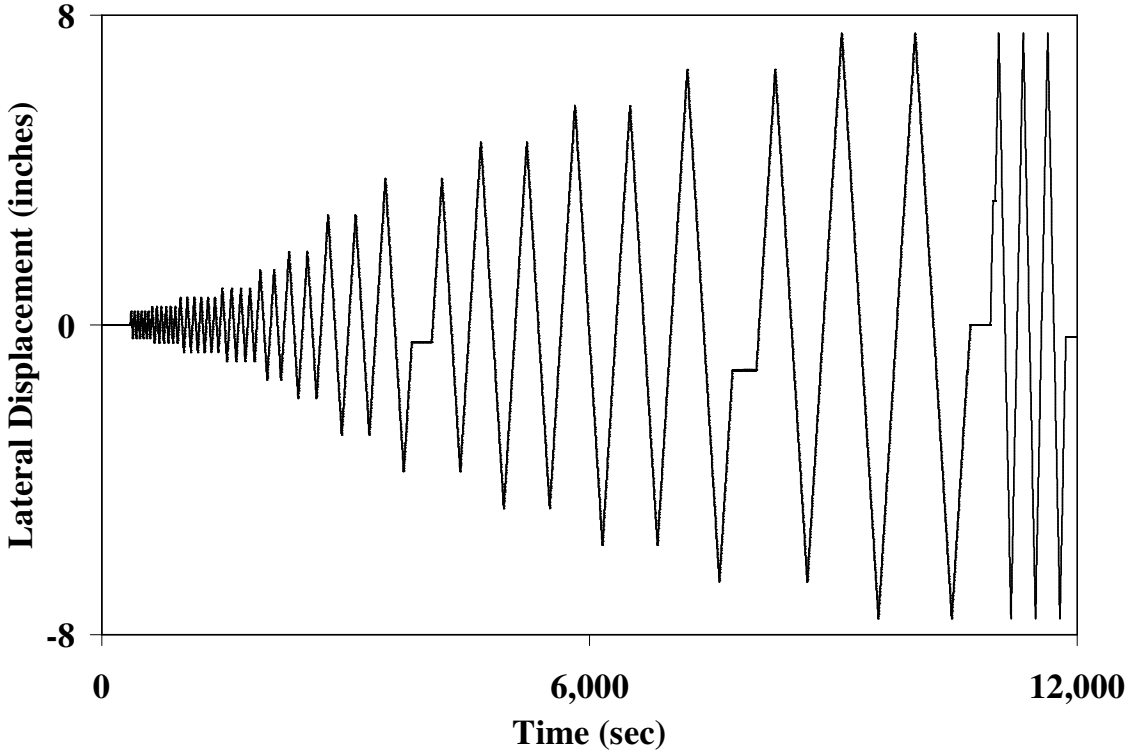

Figure B.48 – Time versus lateral displacement data for Test #7

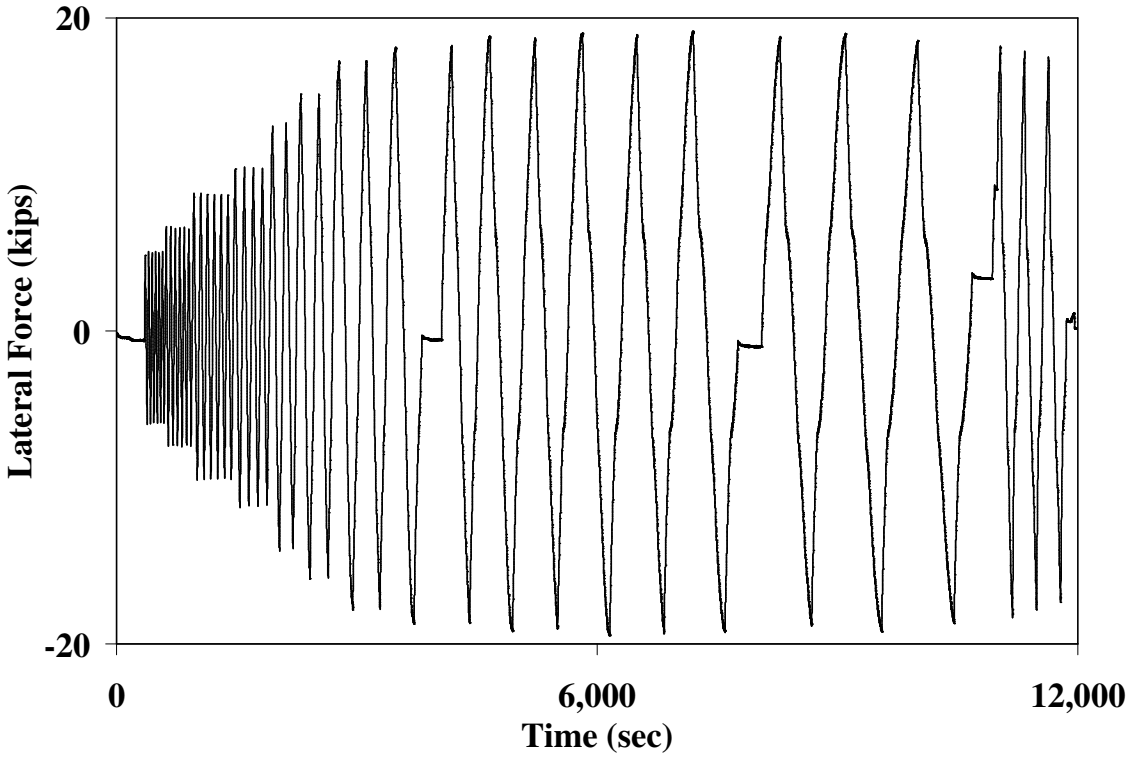

Figure B.49 – Time versus lateral force data for Test #7

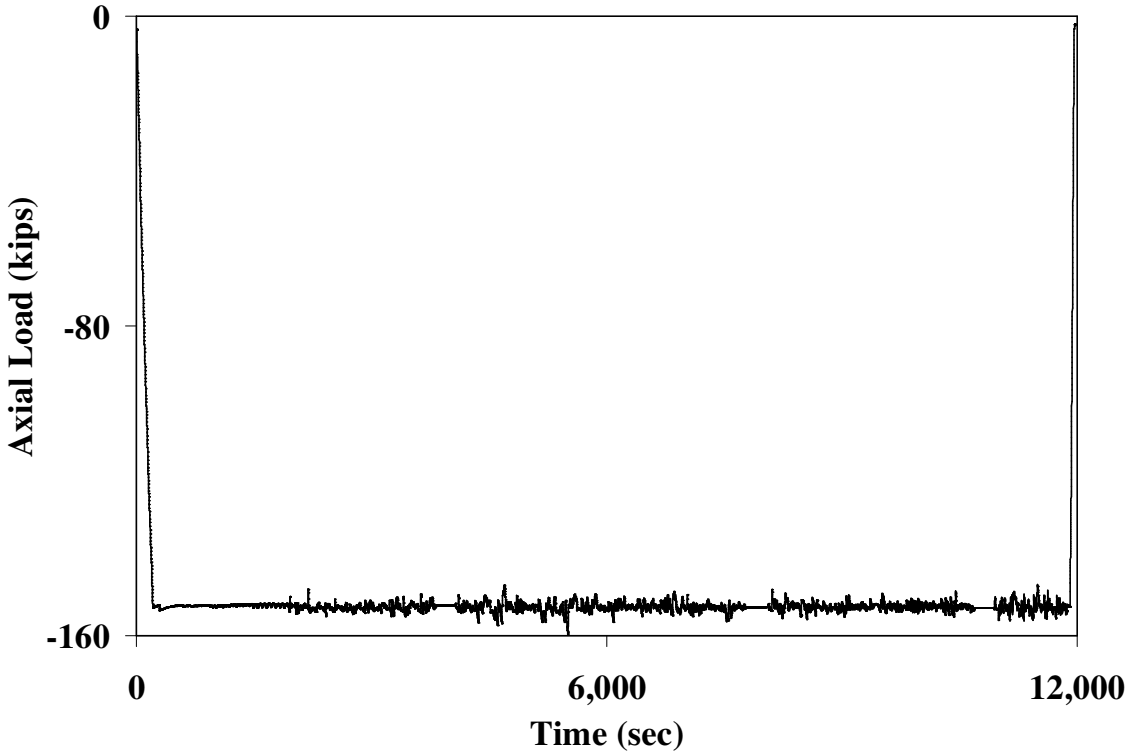

Figure B.50 – Time versus axial load data for Test #7

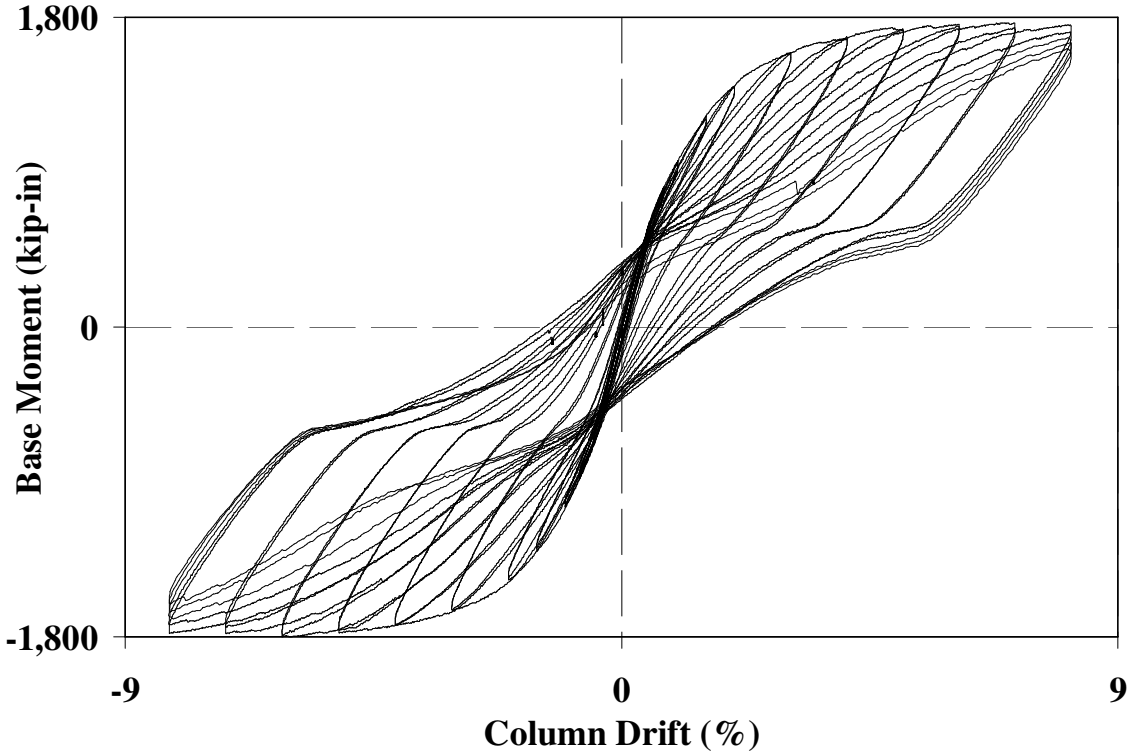

Figure B.51 – Column drift versus base moment data for Test #7

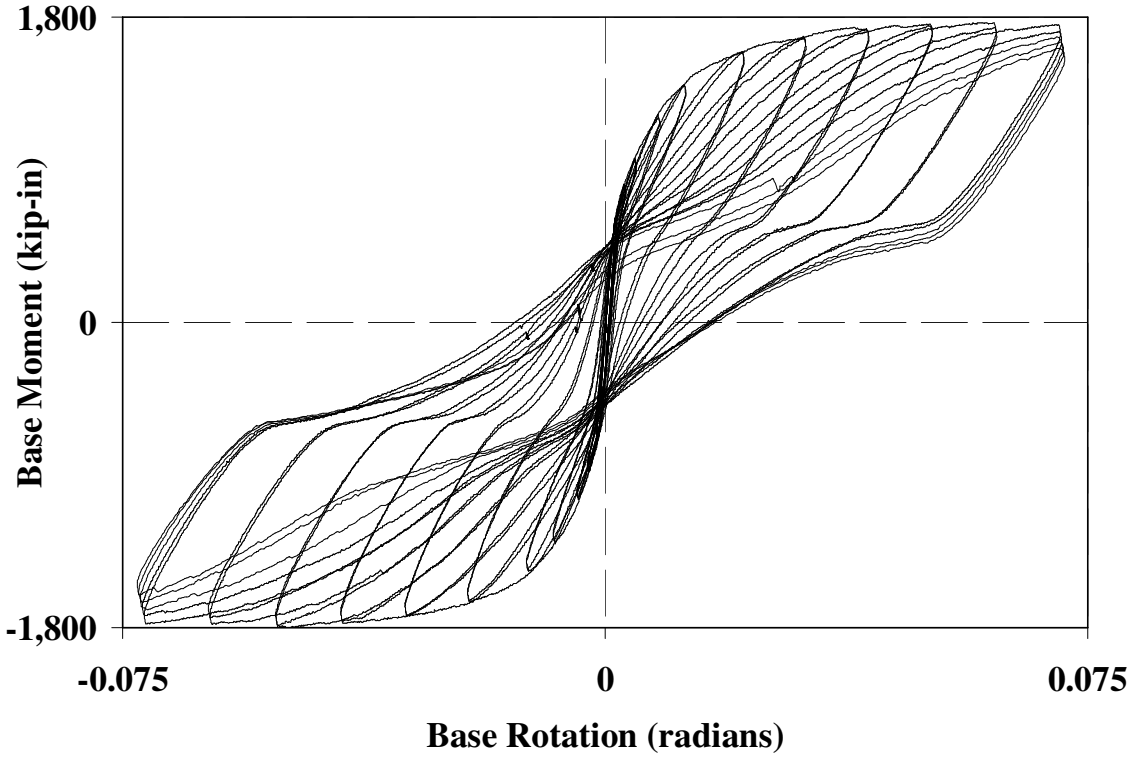

Figure B.52 – Base rotation versus base moment data for Test #7

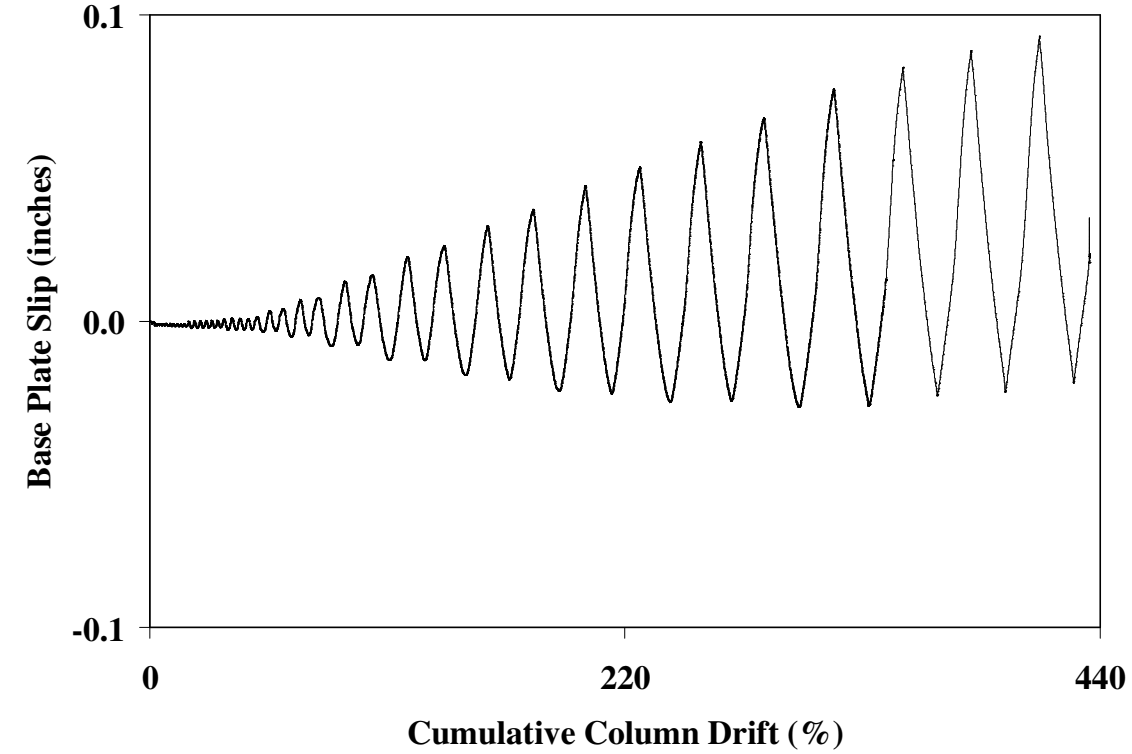

Figure B.53 – Cumulative column drift versus base plate slip data for Test #7

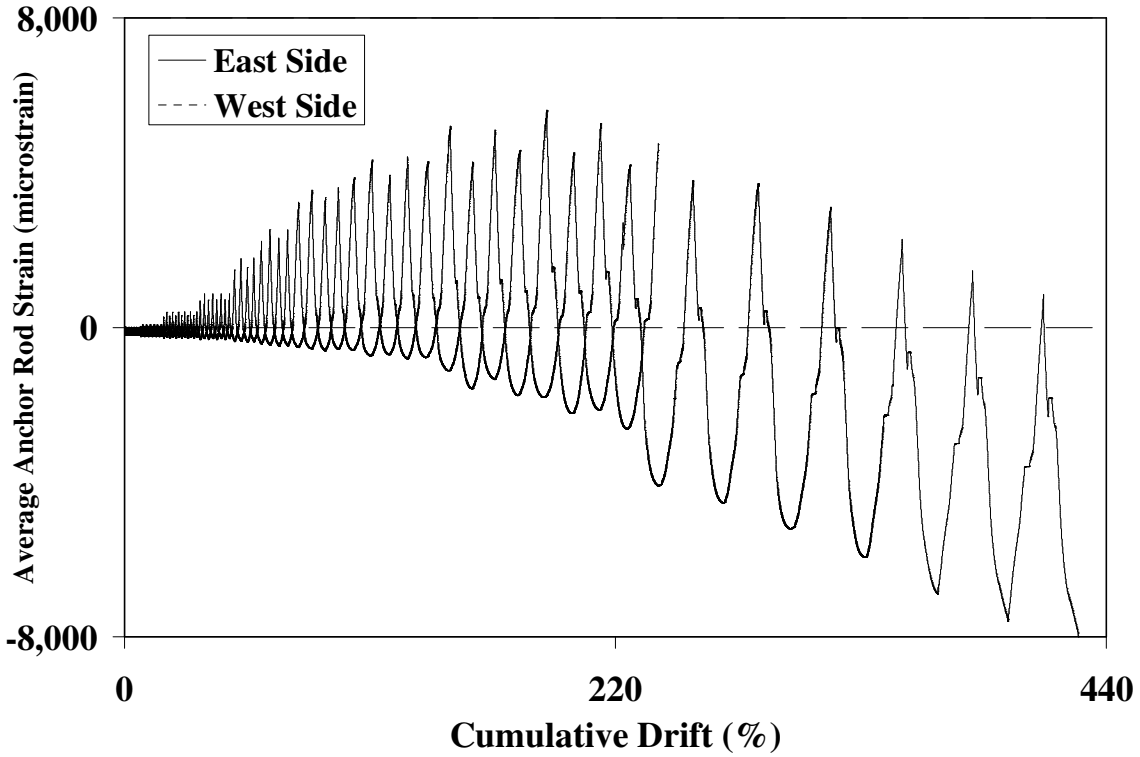

Figure B.54 – Cumulative drift versus anchor rod strain data for Test #7

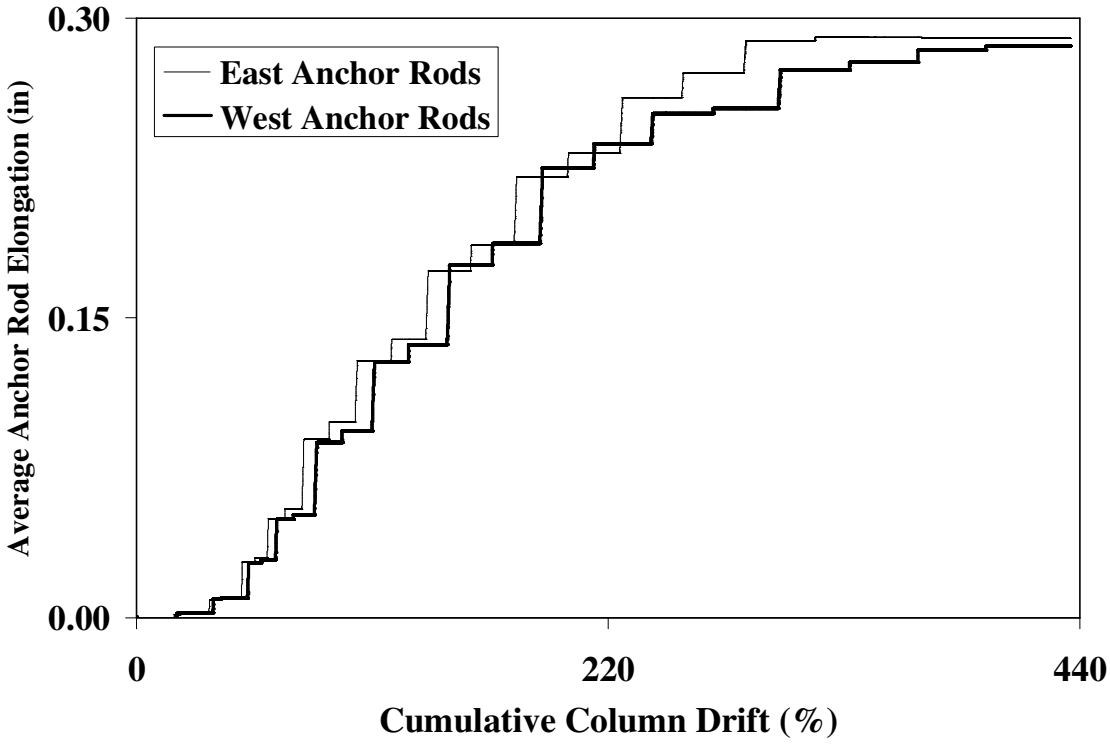

Figure B.55 – Cumulative column drift versus anchor rod elongation data for Test #7

Appendix C

Anchor Rod Forces

Anchor rod strain data collected from the large scale tests (refer Chapter 3 and Appendix B) can be converted to force values for a better assessment of the base connection response. Since the anchor rods undergo yielding under reversed cyclic loading, it is not possible to directly convert the anchor rod strain data to force through elastic analysis. Accordingly, a uniaxial cyclic plasticity model, with kinematic hardening, is calibrated to the anchor rod coupon tension test stress-strain data presented Chapter 3 and Appendix A. Note that the anchor rod coupon tension tests were loaded monotonically and thus do not provide information about cyclic hardening. However, for the purposes of this report's analysis, where the main objective is a qualitative evaluation of design methods, it is assumed that the cyclic hardening is only kinematic and isotropic hardening is negligible.

The material model used to convert the cyclic anchor rod strain data to force values is the Steel01 Material from the Open System for Earthquake Engineering Simulation (OpenSees, 2006). This model is used to construct a uniaxial bilinear steel material object with kinematic hardening and optional isotropic hardening described by a non-linear evolution equation. The parameters of the material model are listed in Table C.1 and Figure C.1 shows an overlay of the calibrated uniaxial stress-strain model on the uniaxial coupon test data for both types of anchor rods.

Figures C.2-C.9 plot the calculated anchor rod forces for every large scale test.

Table C.1 – Steel01 Material Model Parameters

Anchor rod grade	Yield strength "F_y" (ksi)	Initial elastic tangent "E_0" (ksi)	Strain-hardening ratio[1] "b"
36	29,440	48.5	0.0001
105	29,440	100	0.15

[1]Ratio between post-yield tangent and initial elastic tangent

Note: Isotropic hardening parameters (a_1,a_2,a_3,a_4) are set to default, i.e. no isotropic hardening

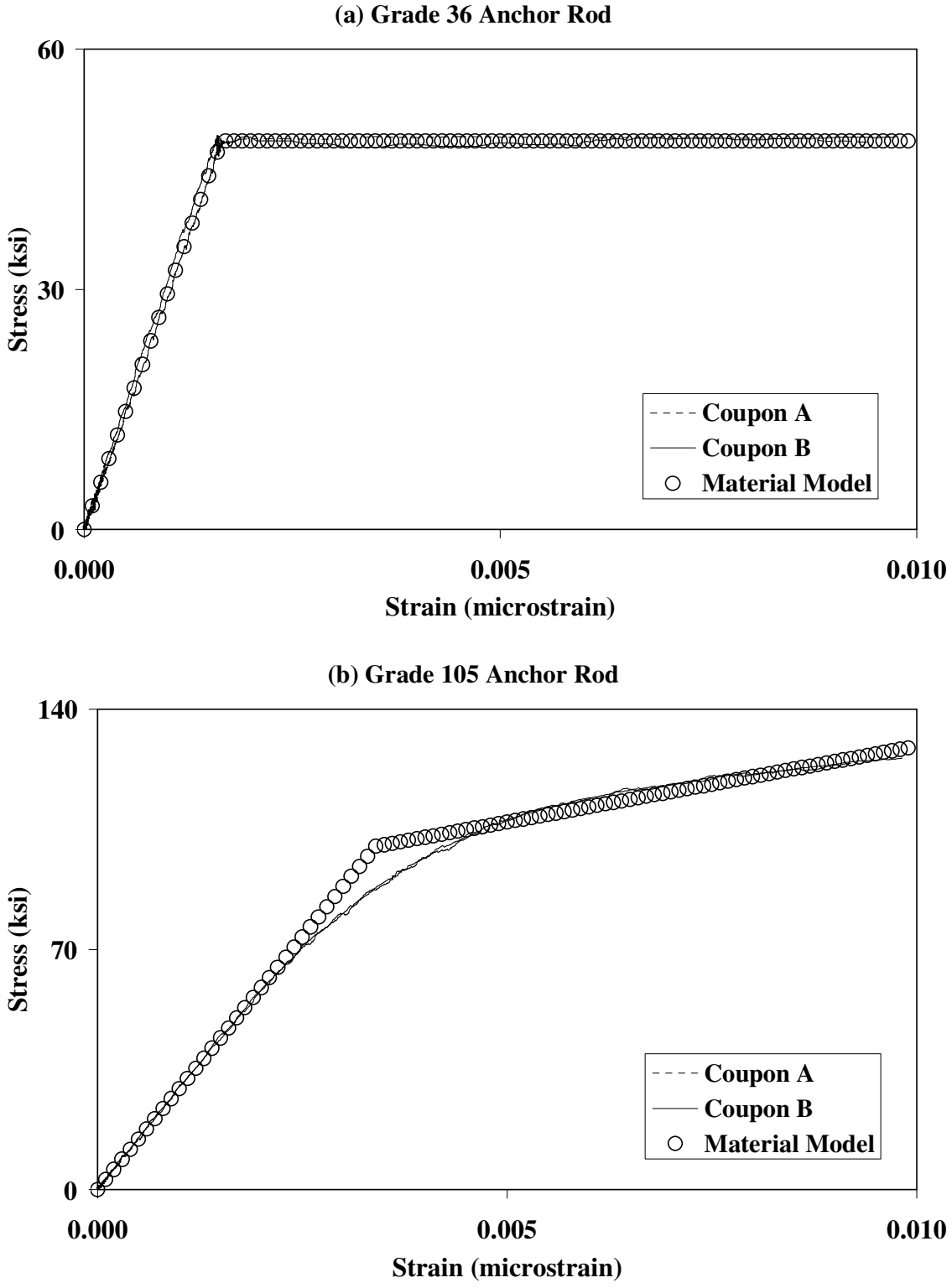

Figure C.1 – Overlays of the calibrated uniaxial stress-strain model on the uniaxial coupon test data for (a) the Grade 36 anchor rods and (b) the Grade 105 anchor rods

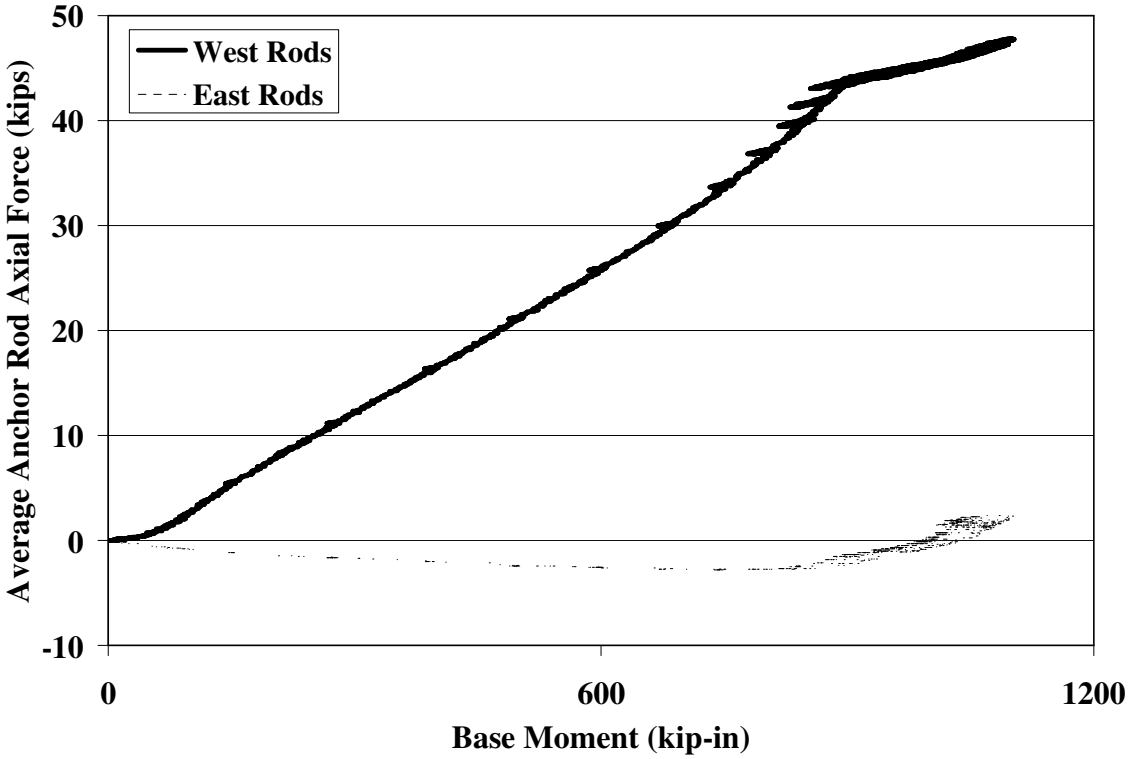

Figure C.2 – Calculated anchor rod forces for Test #1

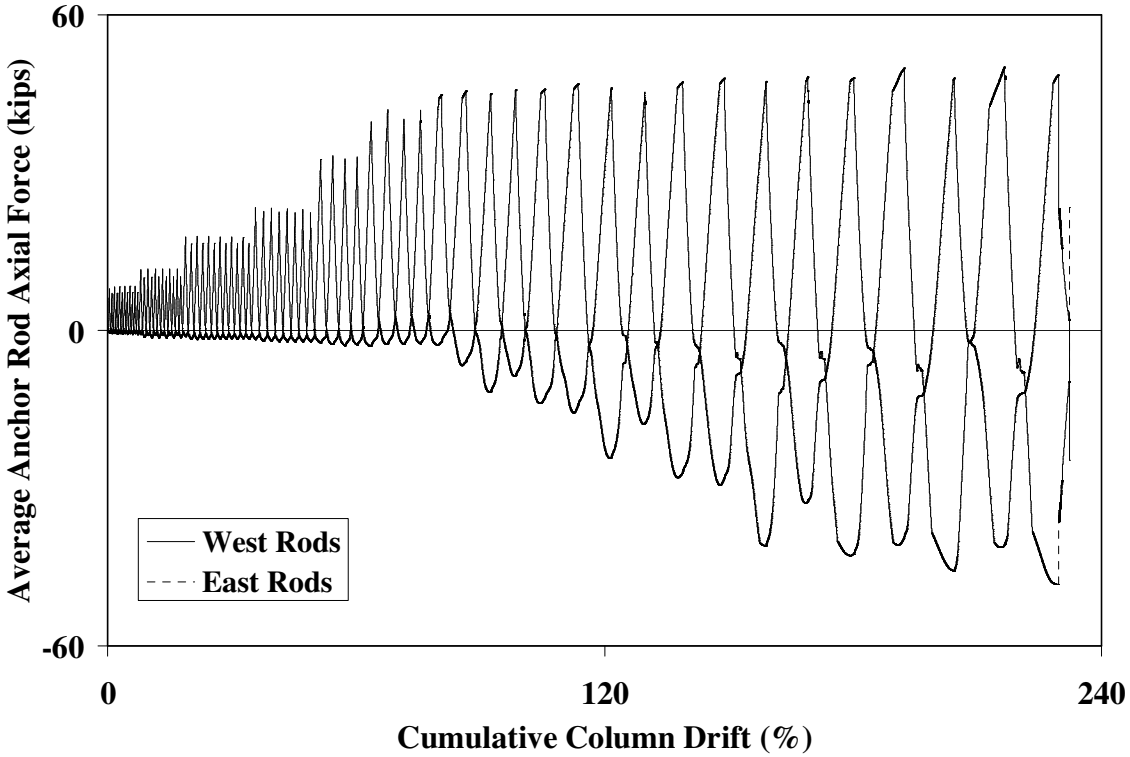

Figure C.3 – Calculated anchor rod forces for Test #2

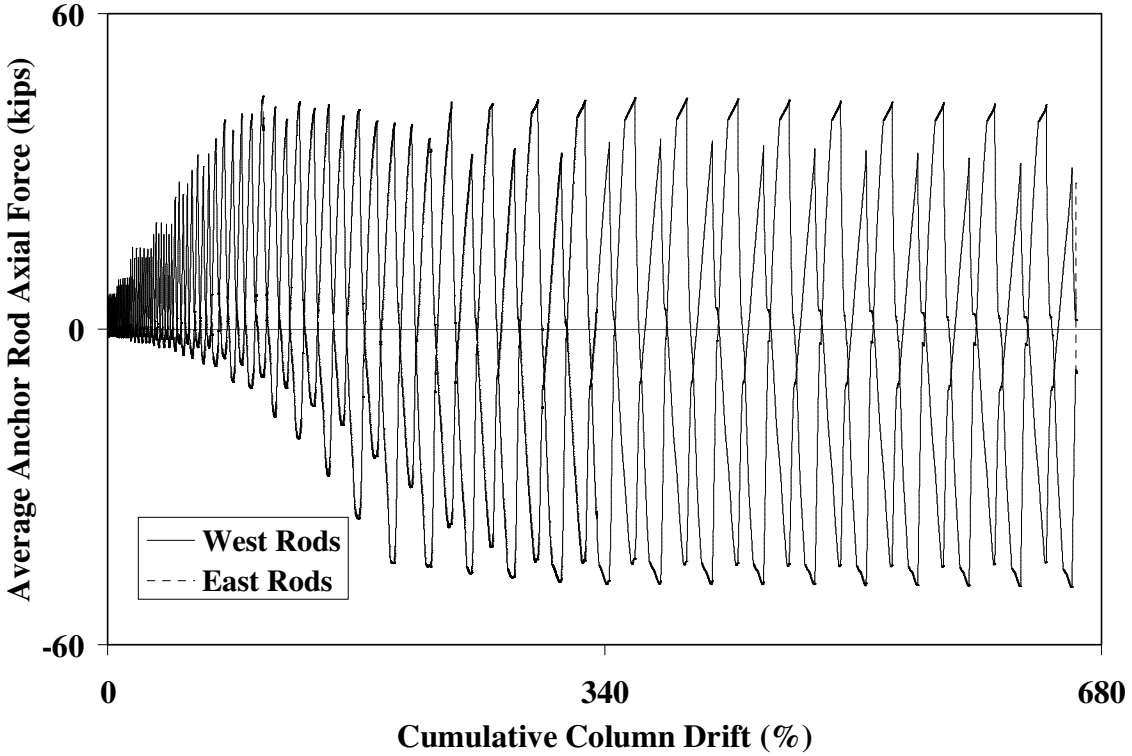

Figure C.4 – Calculated outer anchor rod forces for Test #3

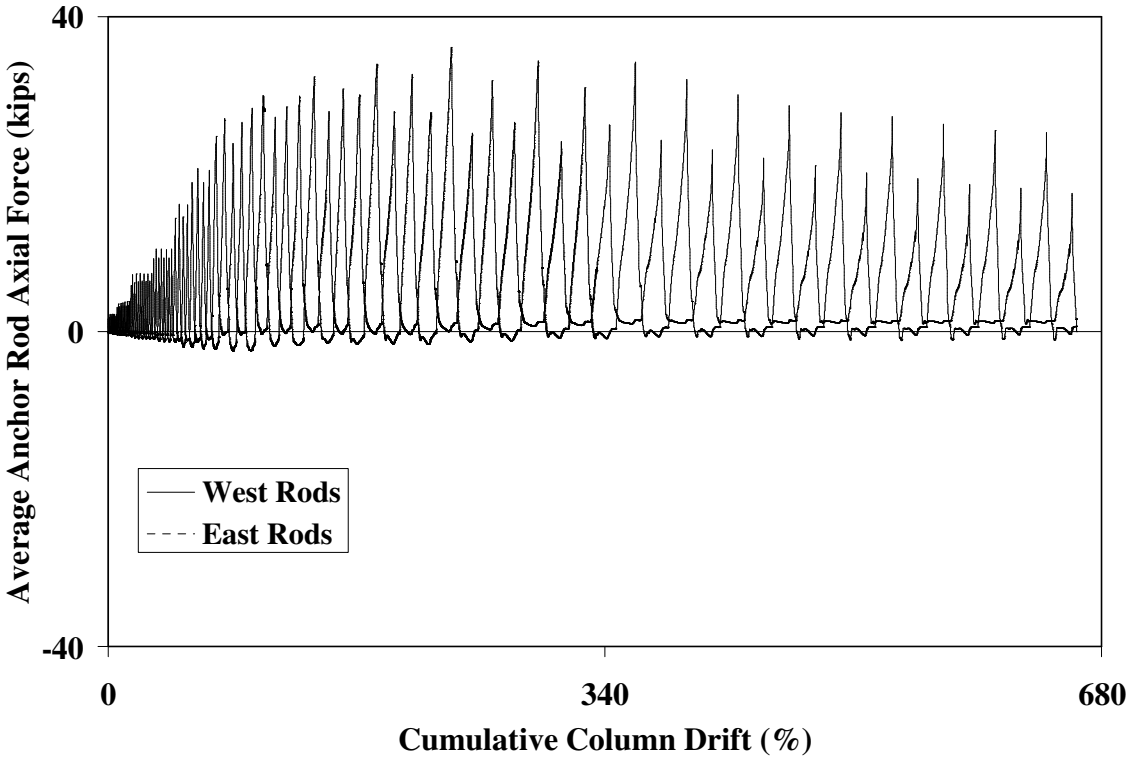

Figure C.5 – Calculated outer anchor rod forces for Test #3

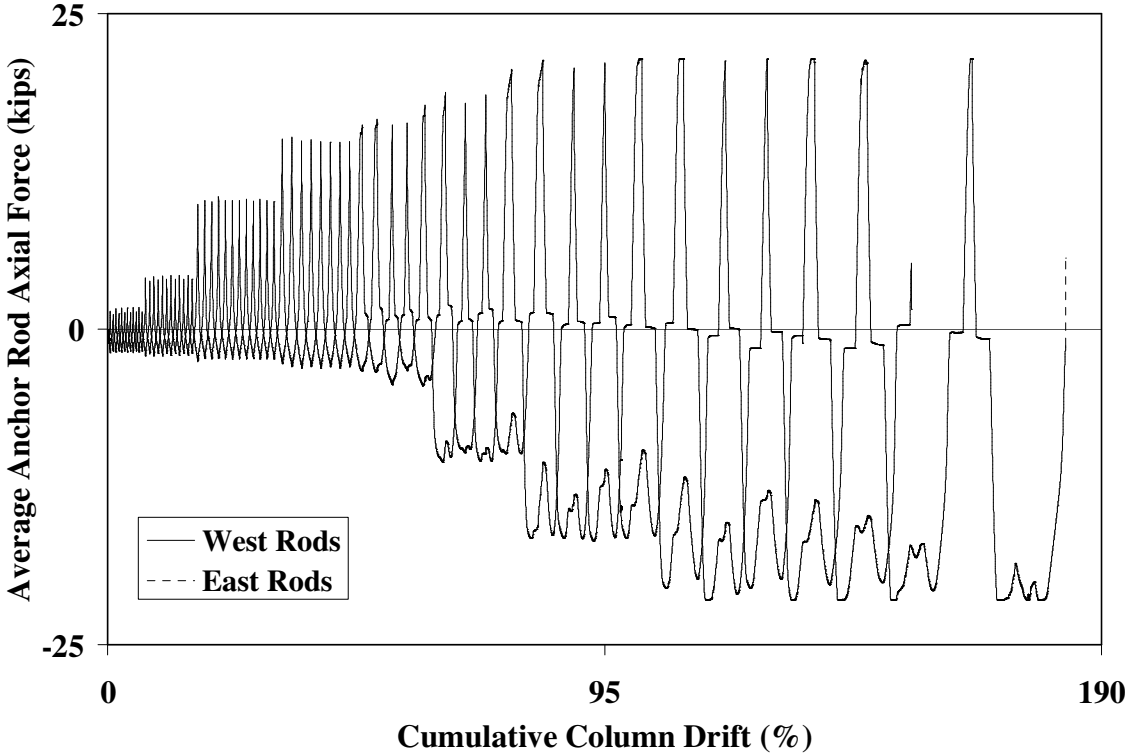

Figure C.6 – Calculated anchor rod forces for Test #4

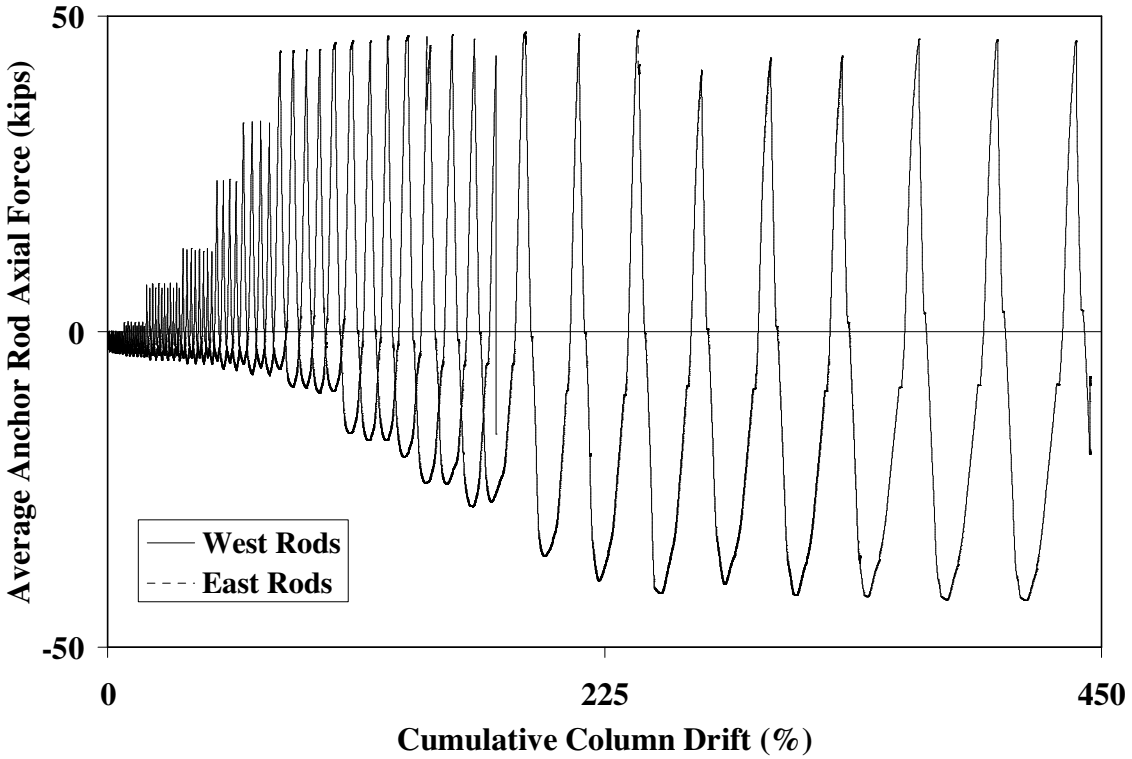

Figure C.7 – Calculated anchor rod forces for Test #5

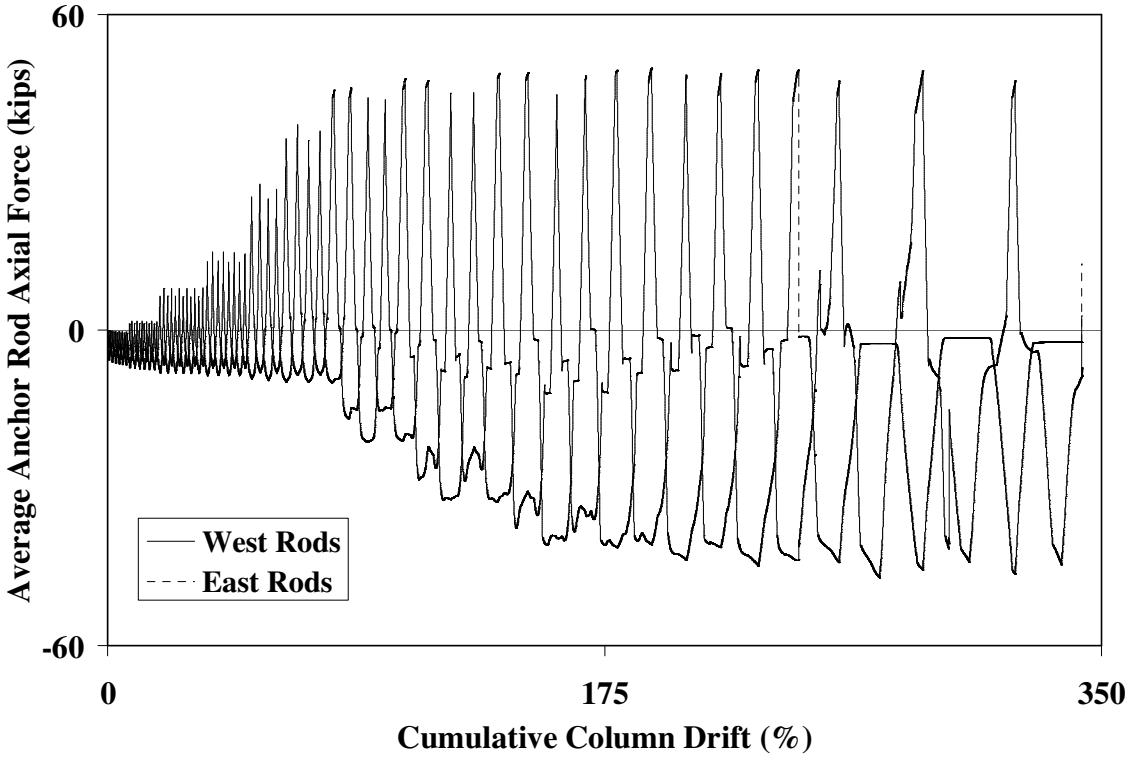

Figure C.8 – Calculated anchor rod forces for Test #6

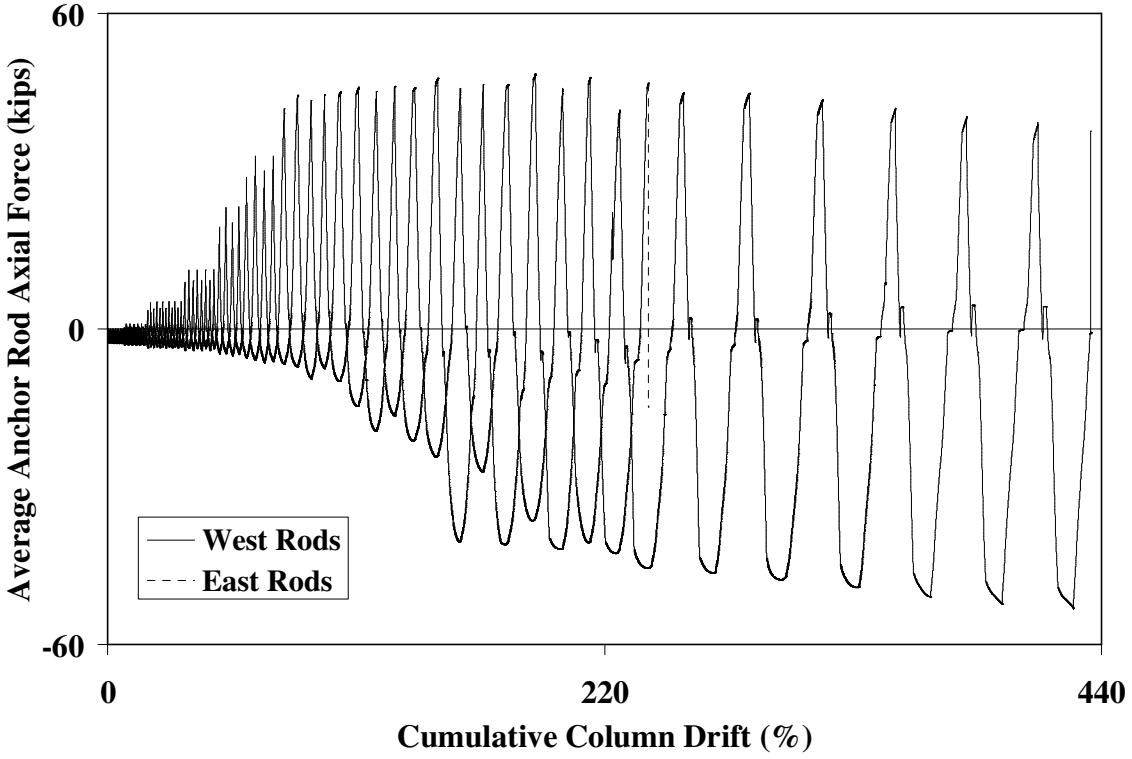

Figure C.9 – Calculated anchor rod forces for Test #7

Appendix D

Base Connection Design Procedures

Three methods for the design of exposed column bases under combined axial compression and strong axis flexural loading are presented. Two of these methods, the Triangular Stress Block (TSB) method and the Rectangular Stress Block (RSB) method, are adapted from design procedures featured in the AISC *Steel Design Guide 1* (Fisher & Kloiber, 2006) and are based on the work of Drake and Elkin (1999), Doyle and Fisher (2005) and others. These methods rely on the basic assumption that, under large load eccentricities, the applied base moment (and applied axial compressive load) is resisted through a combination of anchor rod tension and bearing stresses in the grout/concrete. Owing to the leveling nut detail investigated in this study, a third approach is proposed. Denoted as the Leveling Nut (LNT) method, this model assumes that the applied forces to the base connection are resisted only through a combination of tensile and compressive forces in the anchor rods.

The design methods provided in this Appendix calculate the geometry of the bearing stress distribution, the anchor rod force and the associated component capacities from which the various failure modes may be analyzed. Refer to Chapter 4 for a comprehensive analysis of the base connection strength capacity.

NOTATION USED IN THE APPENDIX

A_1 = bearing area

A_2 = maximum area of the portion of the supporting foundation that is geometrically similar to and concentric with the loaded area

A_b = unthreaded area of anchor bolt

B = base plate width

C = anchor rod compression force

d = column depth

e = load eccentricity = M/P

e_{crit} = critical eccentricity

e_{kern} = kern of base plate

F_y = yield strength

F_u = ultimate strength

f_c' = compressive strength of concrete

f_g' = compressive strength of grout

f, f_1, f_2 = bearing stresses

f_{max} = maximum bearing stress

g = edge distance of anchor rod

L = distance between anchor rods

m = plate bending cantilever length

n = number of anchor rods

M = base moment

N = base plate length

P = axial compressive load

T = anchor rod tensile force

t_p = base plate thickness

Y = bearing length

Z_x = plastic section modulus

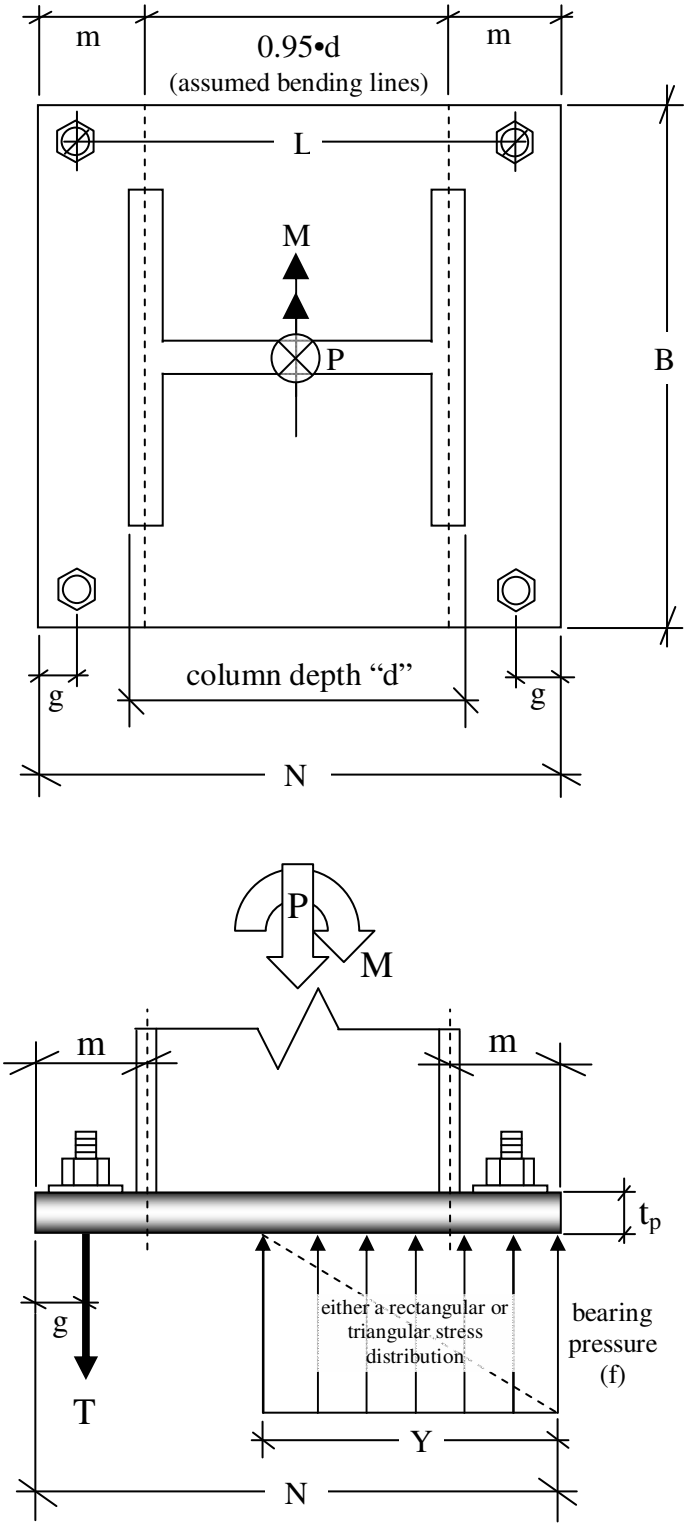

Figure D.1 – Schematic illustration of the base connection design variables

D.1 THE TRIANGULAR STRESS BLOCK (TSB) METHOD

Given an axial compressive load (P), base moment (M), base plate width (B) and length (N), maximum bearing pressure (f_{max}) and anchor rod edge distance (g), four load cases of the TSB method are illustrated in Figure D.2. Case (a) and Case (b) represent conditions whereby the base plate is assumed not to uplift from the grout/concrete foundation, while Case (d) represents an uplift condition. For Case (a) applied forces to the base connection are resisted by a trapezoidal bearing stress distribution on the grout/concrete. For Case (b) applied forces to the base connection are resisted by a rectangular bearing stress distribution on the grout/concrete. These two conditions are separated by a load eccentricity of one-sixth the length of the base plate ($e_{\ker n} = N/6$), also known as the kern of the base plate. The kern is calculated by taking force and moment equilibrium on Figure D.2a and setting the bearing stress f_2 to zero. For Case (d), applied forces to the base connection are resisted through bearing and tension in the anchor rods due to plate uplift. The uplift and no uplift conditions, defined as small and large eccentricity conditions, are separated by a critical eccentricity, i.e. Case (c), where the bearing stress on the extreme compression edge is set to the bearing capacity of the concrete/grout. This critical eccentricity is calculated by taking force and moment equilibrium on Figure D.2c:

$$e_{crit} = \frac{N}{2} - \frac{2 \cdot P}{3 \cdot B \cdot f_{\max}} \qquad \text{(D.1)}^{1}$$

Taking force and moment equilibrium on Case (a), i.e. Figure D.2a, yields –

$$P = \frac{(f_1 + f_2) \cdot B \cdot N}{2} \qquad \text{(D.2)}$$

$$M = \frac{(f_1 - f_2) \cdot B \cdot N^2}{12} \qquad \text{(D.3)}$$

[1] Note that the definition of the critical eccentricity in Equation (4.1) is different than the critical eccentricity defined by *Steel Design Guide 1* (Fisher & Kloiber, 2006). See Chapter 4 for a discussion of this discrepancy.

Solving Equations (D.2) and (D.3) gives –

$$f_1 = \frac{P \cdot N + 6 \cdot M}{B \cdot N^2} \tag{D.4}$$

$$f_2 = \frac{P \cdot N - 6 \cdot M}{B \cdot N^2} \tag{D.5}$$

Taking force and moment equilibrium on Case (b), i.e. Figure D.2b, yields –

$$P = \frac{f \cdot Y \cdot B}{2} \tag{D.6}$$

$$M = \frac{f \cdot Y \cdot B}{2} \cdot \left(\frac{N}{2} - \frac{Y}{3} \right) \tag{D.7}$$

Solving Equations (D.6) and (D.7) gives –

$$Y = 3 \cdot \left(\frac{N}{2} - \frac{M}{P} \right) \tag{D.8}$$

$$f = \frac{4 \cdot P^2}{3 \cdot P \cdot B \cdot N - 6 \cdot M \cdot B} \tag{D.9}$$

Taking force and moment equilibrium on Case (d), i.e. Figure D.2d, yields –

$$P = \frac{f_{\max} \cdot Y \cdot B}{2} - T \tag{D.10}$$

$$M = \frac{f_{\max} \cdot Y \cdot B}{2} \cdot \left(\frac{N}{2} - \frac{Y}{3} \right) + T \cdot \left(\frac{N}{2} - g \right) \qquad \text{(D.11)}$$

Solving Equations (D.6) and (D.7) leads to a quadratic solution –

$$Y = \frac{\frac{f_{\max} \cdot B \cdot (N-g)}{2} - \sqrt{\left(\frac{f_{\max} \cdot B \cdot (N-g)}{2} \right)^2 - 4 \cdot \left(\frac{f_{\max} \cdot B}{6} \right) \cdot \left(P \cdot \left[\frac{N}{2} - g \right] + M \right)}}{\frac{f_{\max} \cdot B}{3}} \qquad \text{(D.12)}^2$$

$$T = 1.5 \cdot \left[\frac{\frac{f_{\max} \cdot B \cdot (N-g)}{2} -}{\sqrt{\left(\frac{f_{\max} \cdot B \cdot (N-g)}{2} \right)^2 - 4 \cdot \left(\frac{f_{\max} \cdot B}{6} \right) \cdot \left(P \cdot \left[\frac{N}{2} - g \right] + M \right)}} \right] - P \qquad \text{(D.13)}$$

[2] While two solutions are possible, only one is physically admissible; refer Section D.7.

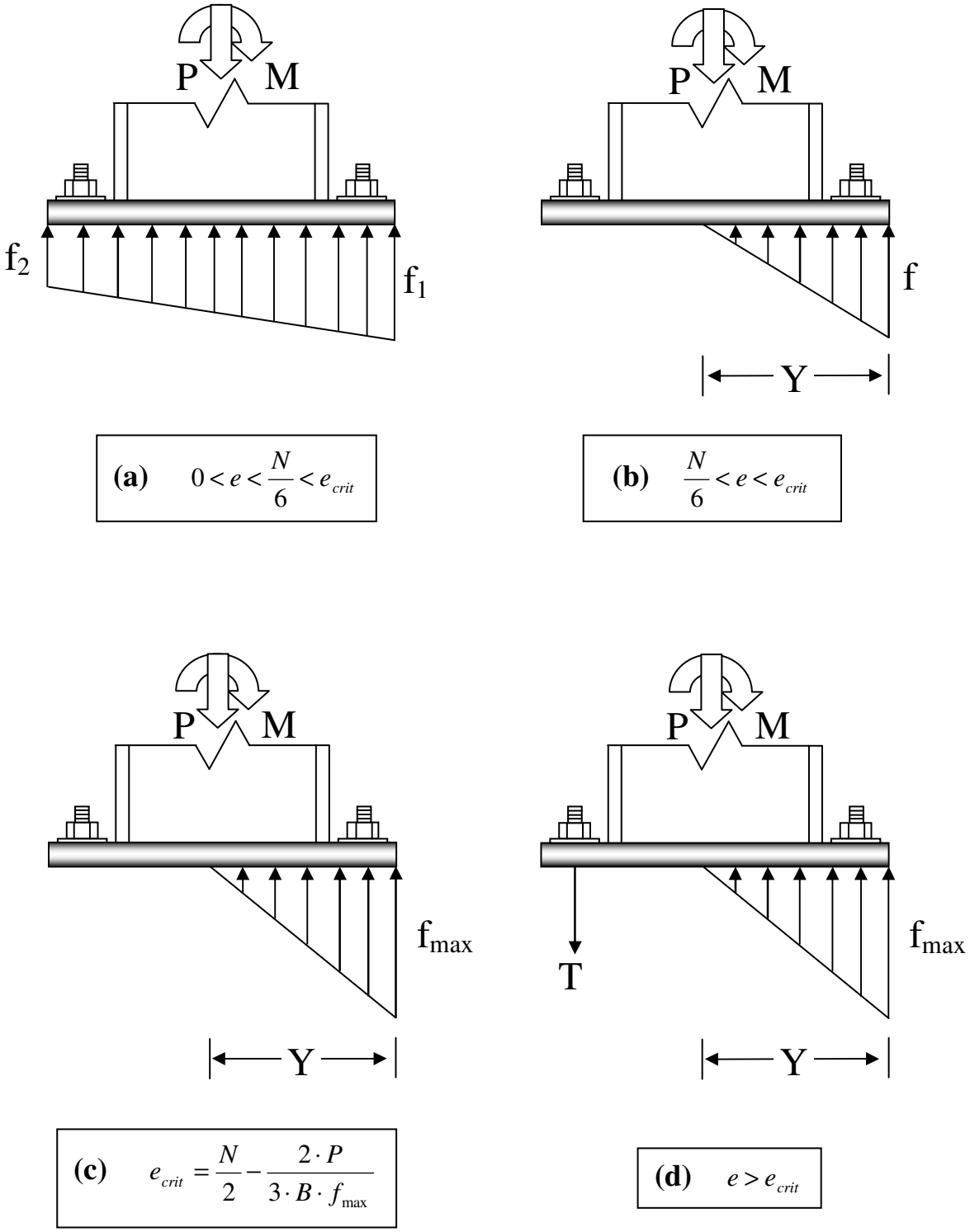

Figure D.2 – Free body diagrams of three cases (as defined by the equations on the right) of the triangular stress block (TSB) method (e = M/P)

D.2 THE RECTANGULAR STRESS BLOCK (RSB) METHOD

Given an axial compressive load (P), base moment (M), base plate width (B) and length (N), maximum bearing pressure (f_{max}) and anchor rod edge distance (g), three load cases of the RSB method are illustrated in Figure D.3. Case (a) and Case (c) represent conditions whereby the base plate is assumed not to uplift and uplift from the grout/concrete foundation, respectively. For Case (a), the no uplift condition, applied forces to the base connection are resisted solely through bearing on the grout/concrete. For Case (c), the uplift condition, applied forces to the base connection are resisted through bearing and tension in the anchor rods. These two conditions, also defined as small and large moment/eccentricity conditions, are separated by a critical eccentricity condition, i.e. Case (b), whereby the bearing stress reaches a maximum (as defined by the grout/concrete bearing strength). This critical eccentricity, is calculated from taking force and moment equilibrium on Figure D.3b –

$$e_{crit} = \frac{N}{2} - \frac{P}{2 \cdot B \cdot f_{\max}} \tag{D.14}$$

Taking force and moment equilibrium on Case (a), i.e. Figure D.3a, yields -

$$P = f \cdot Y \cdot B \tag{D.15}$$

$$M = f \cdot Y \cdot B \cdot \left(\frac{N}{2} - \frac{Y}{2} \right) \tag{D.16}$$

Solving Equations (D.15) and (D.16) gives –

$$f = \frac{P^2}{P \cdot B \cdot N - 2 \cdot M \cdot B} \tag{D.17}$$

$$Y = N - \frac{2 \cdot M}{P} \tag{D.18}$$

Taking force and moment equilibrium on Case (c), i.e. Figure D.2c, yields -

$$P = f_{\max} \cdot Y \cdot B - T \tag{D.19}$$

$$M = f_{\max} \cdot Y \cdot B \cdot \left(\frac{N}{2} - \frac{Y}{2} \right) + T \cdot \left(\frac{N}{2} - g \right) \tag{D.20}$$

Solving Equations (D.21) and (D.22) gives –

$$Y = (N - g) - \sqrt{(N - g)^2 - \frac{2 \cdot \left[M + P \cdot \left(\frac{N}{2} - g \right) \right]}{f_{\max} \cdot B}} \tag{D.23}$$[3]

$$T = f_{\max} \cdot B \cdot \left((N - g) - \sqrt{(N - g)^2 - \frac{2 \cdot \left[M + P \cdot \left(\frac{N}{2} - g \right) \right]}{f_{\max} \cdot B}} \right) - P \tag{D.24}$$

[3] While two solutions are possible, only one is physically admissible; refer Section D.7.

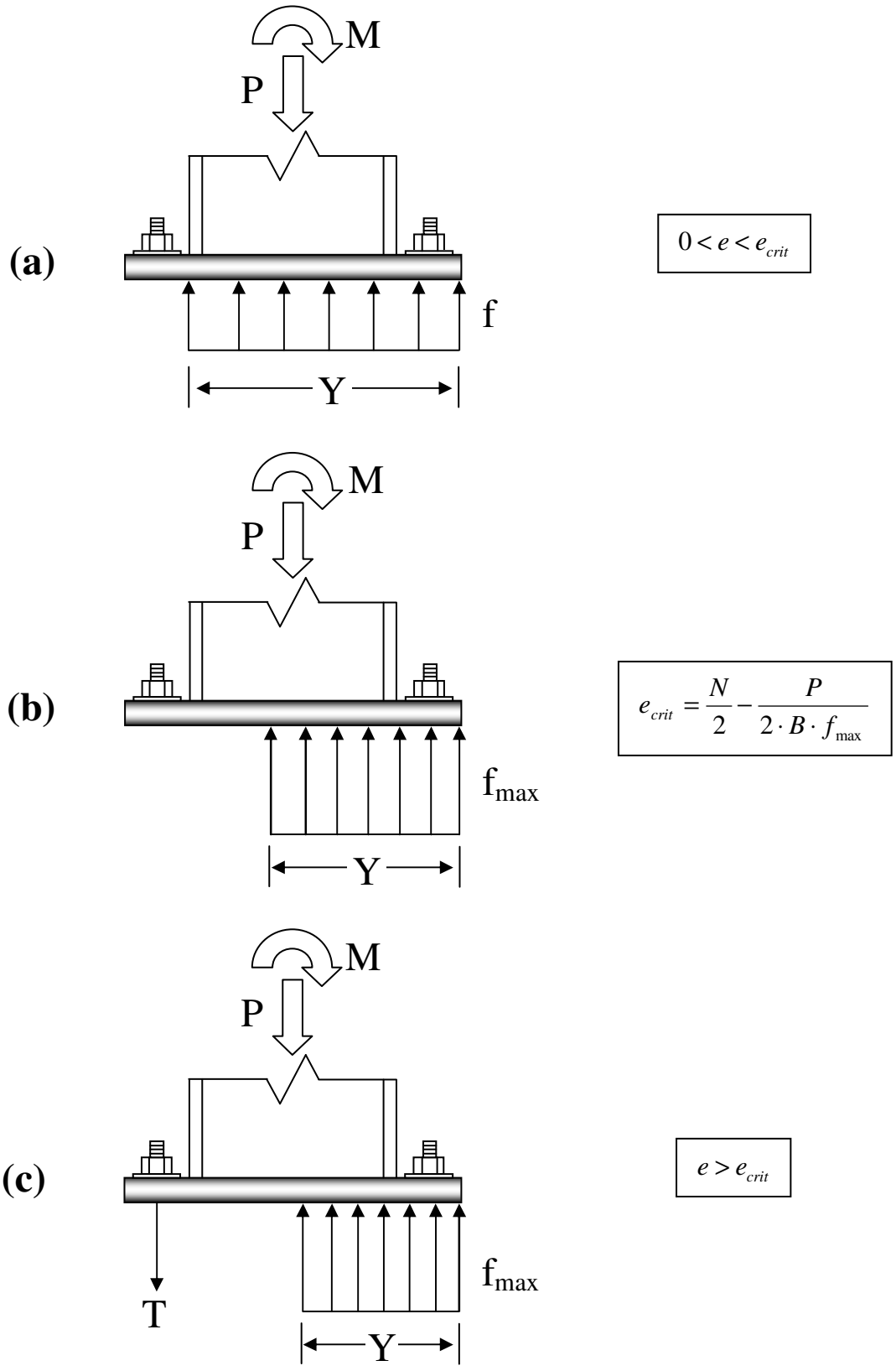

Figure D.3 – Free body diagrams of three cases (as defined by the equations on the right) of the rectangular stress block (RSB) method (e = M/P)

D.3 THE LEVELING NUT (LNT) METHOD

Given an axial compressive load (P), base moment (M) and distance between anchor rods (L), the free body diagram of the LNT method is illustrated in Figure D.4. The base plate is modeled as a simply supported beam and tension and compression loads below the plate are resisted solely by the anchor rods.

Taking force and moment equilibrium on Figure D.4, yields -

$$P = C - T \tag{D.19}$$

$$M = \frac{L}{2}(T + C) \tag{D.20}$$

Solving Equations (D.19) and (D.20) gives –

$$T = \frac{M}{L} - \frac{P}{2} \tag{D.21}$$

$$C = \frac{M}{L} + \frac{P}{2} \tag{D.22}$$

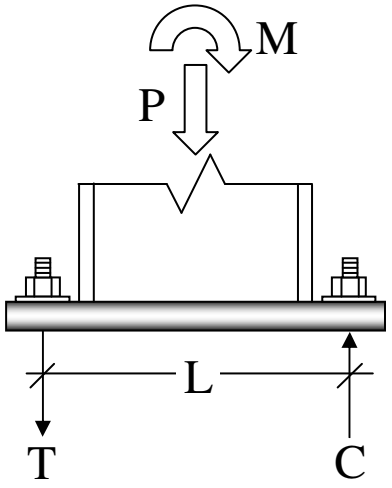

Figure D.4 – Free body diagrams of the Leveling Nut (LNT) method

D.4 BASE PLATE BENDING RESISTANCE

The nominal bending resistance of a per unit width of the base plate, is given as –

$$R_{plate} = \frac{Z_x \cdot F_y}{B} = \frac{F_y \cdot t_p^2}{4} \tag{D.23}$$

Based on Figure D.2, the compression side base plate flexural demand per unit width for the TSB method is determined as –

$$M_{pl,comp} = \begin{Bmatrix} \left[f_1 - (f_1 - f_2)\cdot\left(\frac{m}{N}\right)\right]\cdot\left(\frac{m^2}{2}\right) + \left[(f_1 - f_2)\cdot\left(\frac{m}{N}\right)\right]\cdot\left(\frac{m^2}{3}\right) & for\ e < \frac{N}{6} \\ \left[f - f\cdot\left(\frac{m}{Y}\right)\right]\cdot\left(\frac{m^2}{2}\right) + \left(\frac{f\cdot m^3}{3\cdot Y}\right) & for\ e < e_{crit}\ \&\ Y \geq m \\ \left(\frac{f\cdot Y}{2}\right)\cdot\left(m - \frac{Y}{3}\right) & for\ e < e_{crti}\ \&\ Y < m \\ \left[f_{\max} - f_{\max}\cdot\left(\frac{m}{Y}\right)\right]\cdot\left(\frac{m^2}{2}\right) + \left(\frac{f_{\max}\cdot m^3}{3\cdot Y}\right) & for\ e > e_{crit}\ \&\ Y \geq m \\ \left(\frac{f_{\max}\cdot Y}{2}\right)\cdot\left(m - \frac{Y}{3}\right) & for\ e > e_{crti}\ \&\ Y < m \end{Bmatrix} \tag{D.24}$$

Based on Figure D.3, the compression side base plate flexural demand per unit width for the RSB method is determined as –

$$M_{pl,comp} = \begin{Bmatrix} f\cdot\left(\frac{m^2}{2}\right) & for\ e < e_{crit}\ \&\ Y \geq m \\ f\cdot Y\cdot\left(m - \frac{Y}{2}\right) & for\ e < e_{crit}\ \&\ Y \geq m \\ f_{\max}\cdot\left(\frac{m^2}{2}\right) & for\ e > e_{crit}\ \&\ Y \geq m \\ f_{\max}\cdot Y\cdot\left(m - \frac{Y}{2}\right) & for\ e > e_{crit}\ \&\ Y \geq m \end{Bmatrix} \tag{D.25}$$

The tension side base plate flexural demand per unit width for both the TSB and RSB methods is determined as –

$$M_{pl,ten} = \frac{T \cdot (m - g)}{B} \tag{D.27}$$

D.5 ANCHOR ROD TENSILE RESISTANCE

The 2005 AISC Specification specifies the nominal tensile strength of a fastener as –

$$R_{rod} = n \cdot (0.75 \cdot F_u \cdot A_b) \tag{D.28}$$

D.6 MAXIMUM BEARING STRESS

The design bearing strength of concrete is defined in ACI 318-02, Section 10.17, as –

$$P_p = 0.85 \cdot f_c' \cdot A_1 \cdot \left(\sqrt{\frac{A_2}{A_1}} \right) \leq 1.7 \cdot f_c' \cdot A_1 \tag{D.29}$$

Thus, the maximum bearing stress under the base plate, also assuming the bearing strength of the grout, is calculated as –

$$f_{\max} = \min \left\{ 0.85 \cdot f_c' \cdot \left(\sqrt{\frac{A_2}{A_1}} \right) \leq 1.7 \cdot f_c', 0.85 \cdot f_g' \right\} \tag{D.30}$$

D.7 VALIDITY OF THE TSB AND RSB METHODS

Owing to geometric admissibility and the quadratic solution from Equations (D.10) and (D.11) for the TSB method and Equations (D.19) and (D.20) for the RSB method, the validity of these methods is addressed. Limiting the bearing length as the distance between the base plate edge and the further anchor rods (based on geometric admissibility; i.e. $Y \le N - g$) results in only one physically admissible (i.e. negative root) solution for Equation (D.12) and Equation (D.21). In addition, the value within the square root must be greater or equal to zero to give a real solution. From algebra this results in the following condition –

$$e \le \left\{ \begin{array}{ll} \dfrac{3 \cdot f_{\max} \cdot B \cdot (N-g)^2}{8 \cdot P} - \dfrac{N}{2} + g & for\ TSB \\ \dfrac{f_{\max} \cdot B \cdot (N-g)^2}{2 \cdot P} - \dfrac{N}{2} + g & for\ RSB \end{array} \right\} \tag{D.31}$$

For conditions of zero axial load, the load eccentricity is infinite. This issue can be resolved easily by defining zero axial load as a very small value such as 0.0001 kips.

Appendix E

Computer Code of TSB and RSB Methods and Results

Annotated computer code for the Triangular Stress Block (TSB) method and Rectangular Stress Block (RSB) method is presented based on the mathematical formulation. The computer code is written in the MATLAB programming language. Also presented in this Appendix are the solutions provided by the computer code for each large-scale base connection tests as well as the predicted-to-test ratio of the anchor rod forces for every test.

PARAMETER INPUTS FOR THE COMPUTER CODE

P = axial compressive load

B = base plate width

N = base plate length

d = column depth

g = edge distance of anchor rod

f_c' = compressive strength of concrete

f_g' = compressive strength of grout

A_2 = maximum area of the portion of the supporting foundation that is geometrically similar to and concentric with the loaded area

E.1 COMPUTER CODE FOR THE TRIANGULAR STRESS BLOCK (TSB) METHOD

```
P = P + 0.0001; %% Modification to Preclude Infinite Value

m = (N-0.95*d)/2; %% Plate Cantilever Dimension
A2A1 = A2/(N*B); %% Ratio of Footing Area to Plate Area

%% ACI Concrete Bearing Pressure Capacity
f_max = min(0.85*f_g,min(0.85*f_c*sqrt(A2A1),1.7*f_c));

e_crit = N/2-(2*P)/(3*B*f_max); %% Critical Eccentricity
e_kern = N/6; %% Base Plate Kern

%% Maximum Valid Eccentricity
e_max = (3*f_max*B*(N-g)^2)/(8*(P+10e-10))-N/2+g;

for i=1:10e100
M(i) = i; %% Applied Moment

%% Eccentricity
e = M(i)/P;

if e < e_crit %% "Small Moment" Condition

if e < e_kern %% Trapezoidal Stress Distribution

f1 = (P*N+6*M(i))/(B*N*N); %% Larger Bearing Pressure
f2 = (P*N-6*M(i))/(B*N*N); %% Smaller Bearing Pressure

%% Base Plate Flexure Demand
M_pl_comp(i) = (f1-(f1-f2)*(m/N))*0.5*(m^2)+((f1-f2)*m^3)/(3*N);

elseif e > e_kern %% Triangular Stress Distribution

Y = 3*(N/2 - M(i)/P); %% Bearing Length
f = (4*P^2)/(3*P*B*N-6*M(i)*B); %% Bearing Pressure

%% Moment per Unit Width at Compression Fold Line
if Y >= m %% Bearing Length Extends Past Plate Cantilever Length
M_pl_comp(i) = (f-f*(m/Y))*0.5*(m^2)+(f*m^3)/(3*Y);
elseif Y < m %% Bearing Length is Shorter Than Plate Cantilever Length
M_pl_comp(i) = (f*Y/2)*(m-Y/3);

end
end

T(i) = 0;
M_pl_ten(i) = 0;

elseif e > e_crit & e < e_max %% "Large Moment" Condition
```

```
%% Bearing Length
Y = ((f_max*B*(N-g)/2) - ...
    sqrt(((f_max*B*(N-g)/2))^2-4*(f_max*B/6)*(P*(N/2-g)+M(i))))/...
    (f_max*B/3);

%% Tension Force for BOTH Rods
T(i) = 1.5*((f_max*B*(N-g)/2) - ...
    sqrt(((f_max*B*(N-g)/2))^2-4*(f_max*B/6)*(P*(N/2-g)+M(i))))-P;

%% Moment per Unit Width at Tension Fold Line
M_pl_ten(i) = (T(i)*(m-g)/B);

%% Moment per Unit Width at Compression Fold Line
if Y >= m
M_pl_comp(i) = (f_max-f_max*(m/Y))*0.5*(m^2)+(f_max*m^3)/(3*Y);
elseif Y < m
M_pl_comp(i) = (f_max*Y/2)*(m-Y/3);

end

elseif e > e_max %% "Invalid" Condition
M(i) = nan;
T(i) = nan;
M_pl_comp(i) = nan;
M_pl_ten(i) = nan;
break

end
end
```

E.2 COMPUTER CODE FOR THE RECTANGULAR STRESS BLOCK (RSB) METHOD

```
P = P + 0.0001; %% Modification to Preclude Infinite Value

m = (N-0.95*d)/2; %% Plate Cantilever Dimension
A2A1 = A2/(N*B); %% Ratio of Footing Area to Plate Area

%% ACI Concrete Bearing Pressure Capacity
f_max = min(0.85*f_g,min(0.85*f_c*sqrt(A2A1),1.7*f_c));

e_crit = N/2-P/(2*B*f_max); %% Critical Eccentricity

%% Maximum Valid Eccentricity
e_max = (f_max*B*(N-g)^2)/(2*(P+10e-10))-N/2+g;

for i=1:10e100
M(i) = i; %% Applied Moment

%% Eccentricity
e = M(i)/P;

if e < e_crit %% "Small Moment" Condition

Y = N - 2*M(i)/P; %% Bearing Length
f = (P^2)/(P*B*N-2*M(i)*B); %% Bearing Pressure

%% Moment per Unit Width at Compression Fold Line
if Y >= m %% Bearing Length Extends Past Plate Cantilever Length
M_pl_comp(i) = f*0.5*(m^2);
elseif Y < m %% Bearing Length is Shorter Than Plate Cantilever Length
M_pl_comp(i) = (f*Y)*(m-Y/2);
end

T(i) = 0;
M_pl_ten(i) = 0;

elseif e > e_crit & e < e_max %% "Large Moment" Condition

%% Bearing Length
Y = (N-g)-sqrt((N-g)^2-(2/(f_max*B))*(M(i)+P*(N/2-g)));

%% Tension Force for BOTH Rods
T(i) = f_max*B*(N-g-sqrt((N-g)^2-(2/(f_max*B))*(M(i)+P*(N/2-g))))-P;

%% Moment per Unit Width at Tension Fold Line
M_pl_ten(i) = (T(i)*(m-g)/B);

%% Moment per Unit Width at Compression Fold Line
if Y >= m %% Bearing Length Extends Past Plate Cantilever Length
M_pl_comp(i) = f_max*0.5*(m^2);
elseif Y < m %% Bearing Length is Shorter Than Plate Cantilever Length
M_pl_comp(i) = (f_max*Y)*(m-Y/2);
end
```

```
elseif e > e_max %% "Invalid" Condition
M(i) = nan;
T(i) = nan;
M_pl_comp(i) = nan;
M_pl_ten(i) = nan;
break
end
end
```

Table E.1 – Input parameters for each large scale test

Input Parameter	**Large Scale Test Number**						
	1	**2**	**3**	**4**	**5**	**6**	**7**
P (kips)	0	0	0	92.45	92.35	92.55	152.55
f_c' (psi)$_1$	3,965	4,016	4,140	4,247	4,314	4,347	4,394
f_g' (psi)	7,413	7,854	8,923	9,245	9,349	9,401	9,475
A_2 (in^2)	576						
B (in)	14						
N (in)	14						
d (in)	8.5						
g (in)	1.5						

[1]Due to tests observations and limitations of the concrete bearing stress equation, concrete failure is not considered when calculating the base connection load demands; the concrete strength is listed here for reference

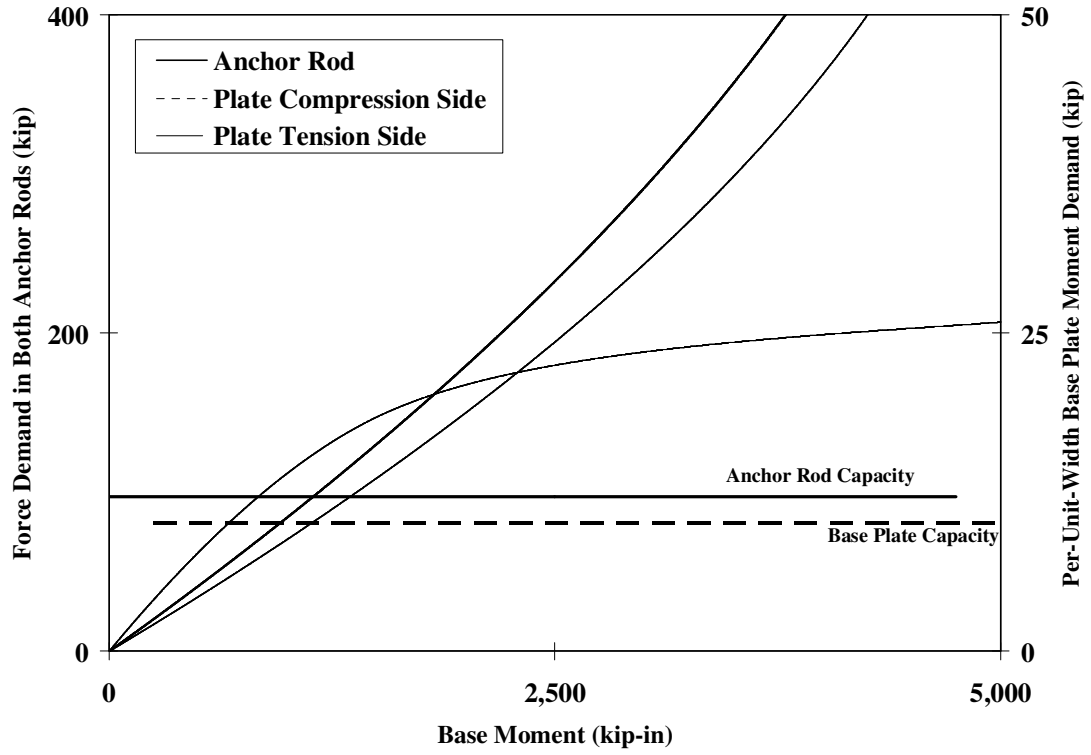

Figure E.1 – Calculated capacity and demand values for Test #1 (TSB Method)

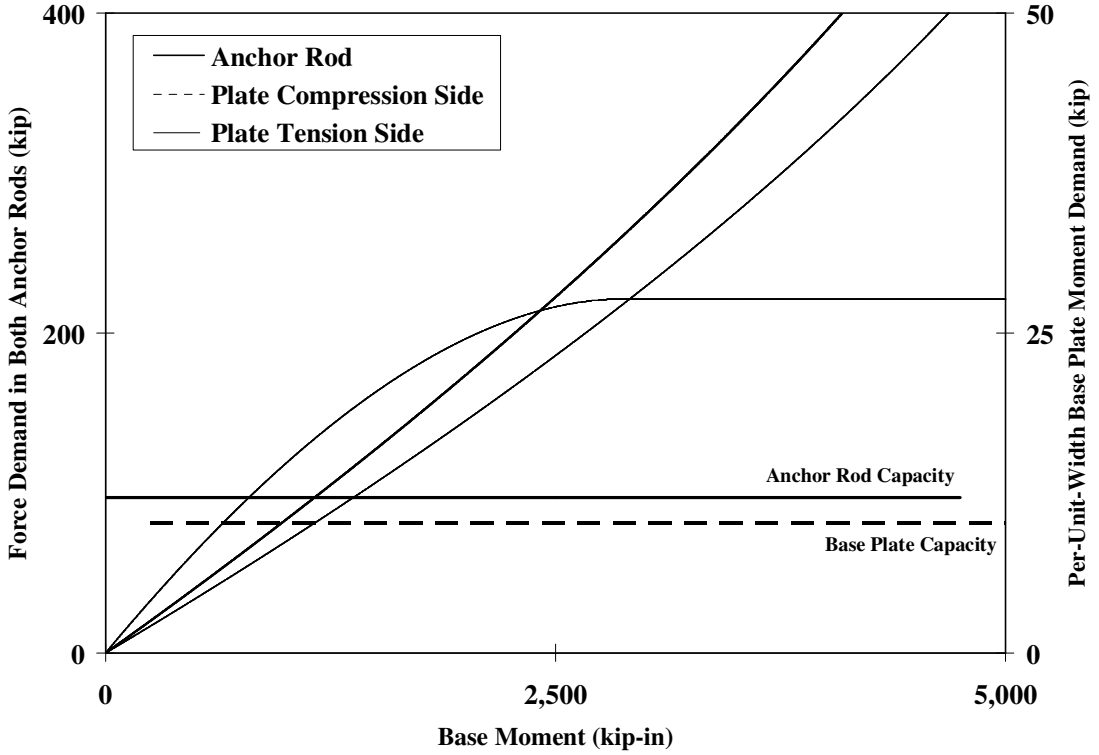

Figure E.2 – Calculated capacity and demand values for Test #1 (RSB Method)

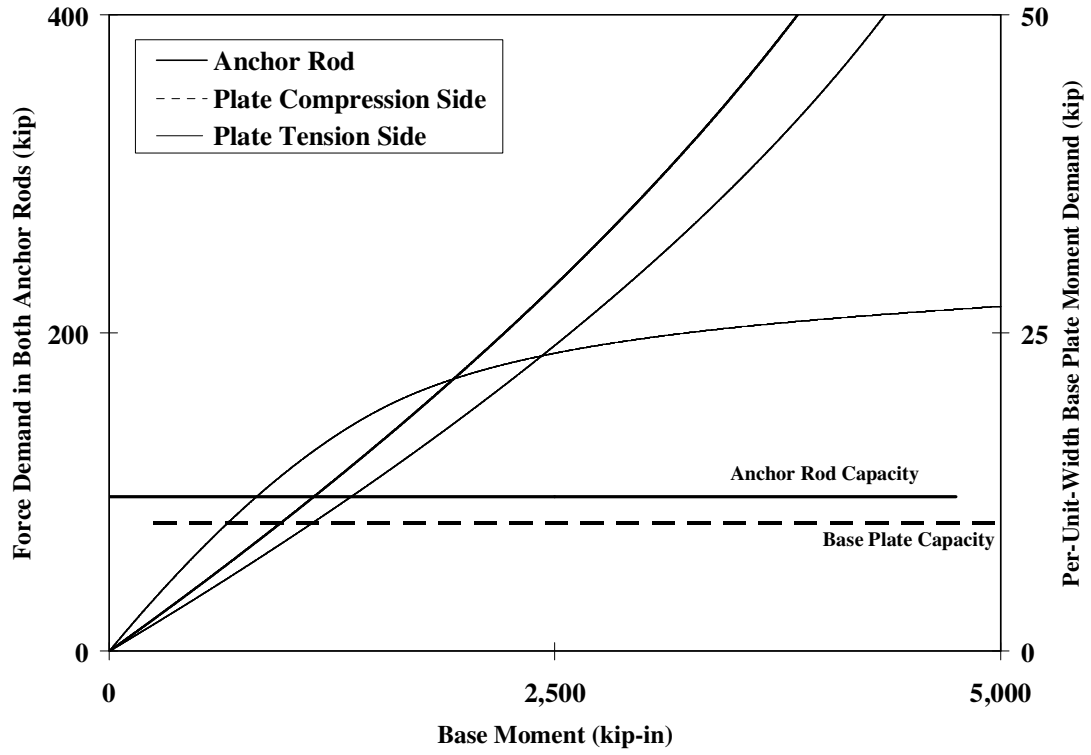

Figure E.3 – Calculated capacity and demand values for Test #2 (TSB Method)

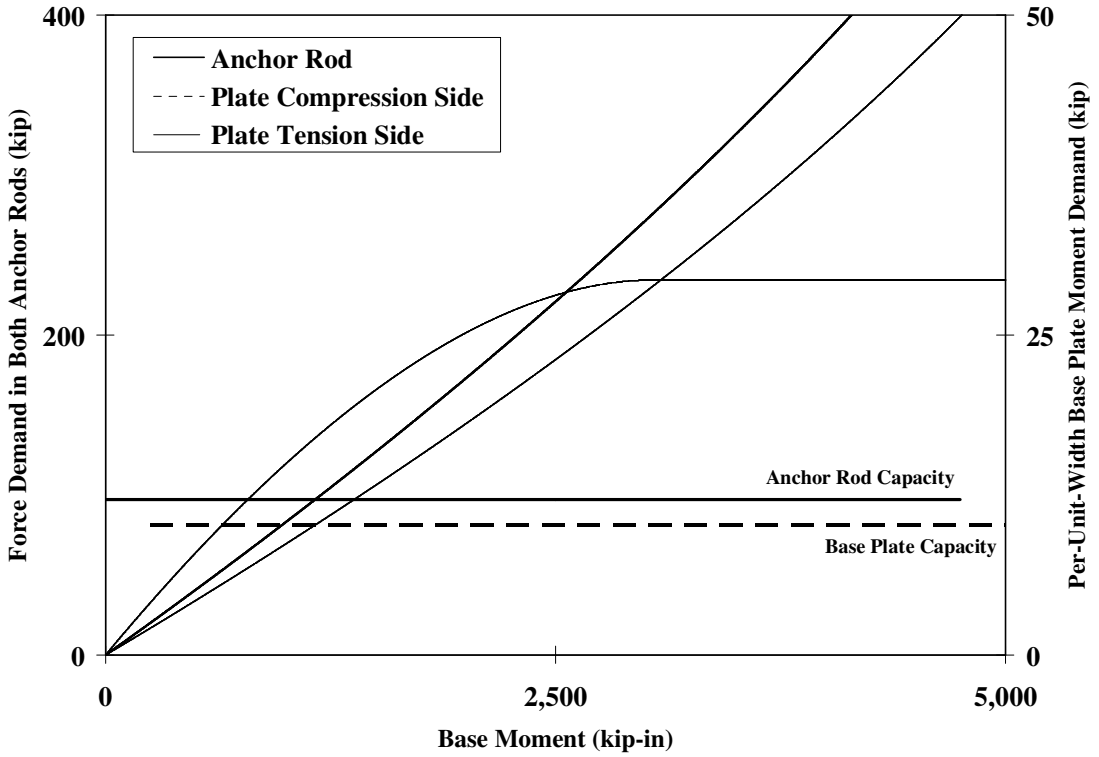

Figure E.4 – Calculated capacity and demand values for Test #2 (RSB Method)

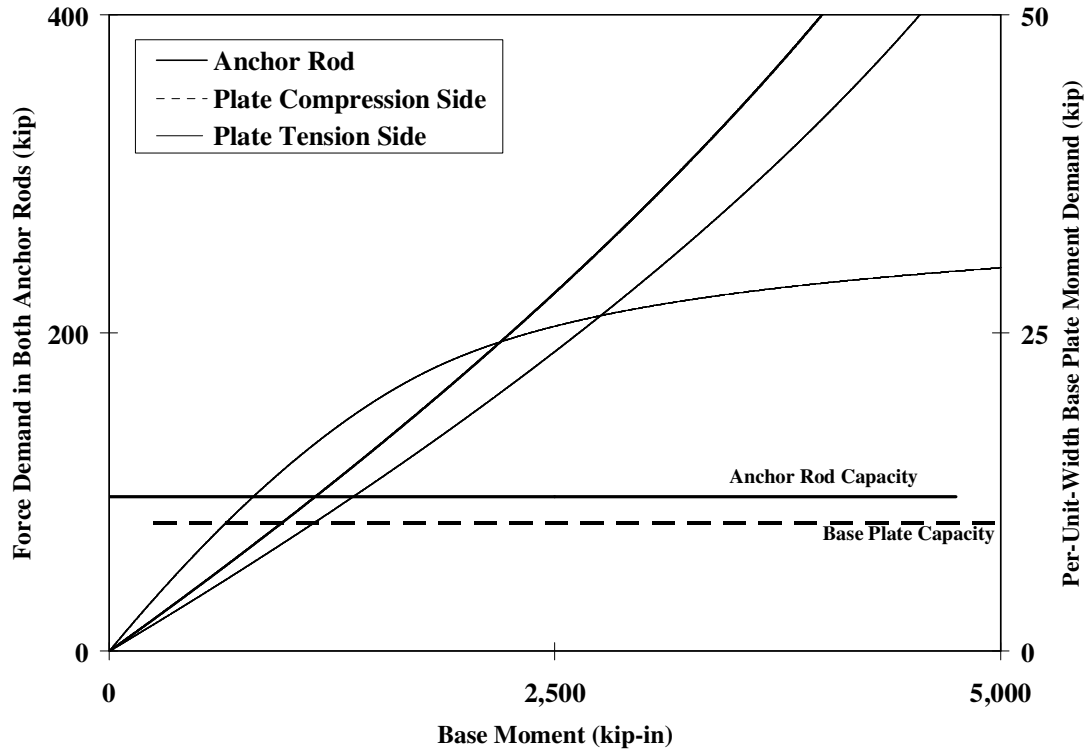

Figure E.5 – Calculated capacity and demand values for Test #3 (TSB Method)

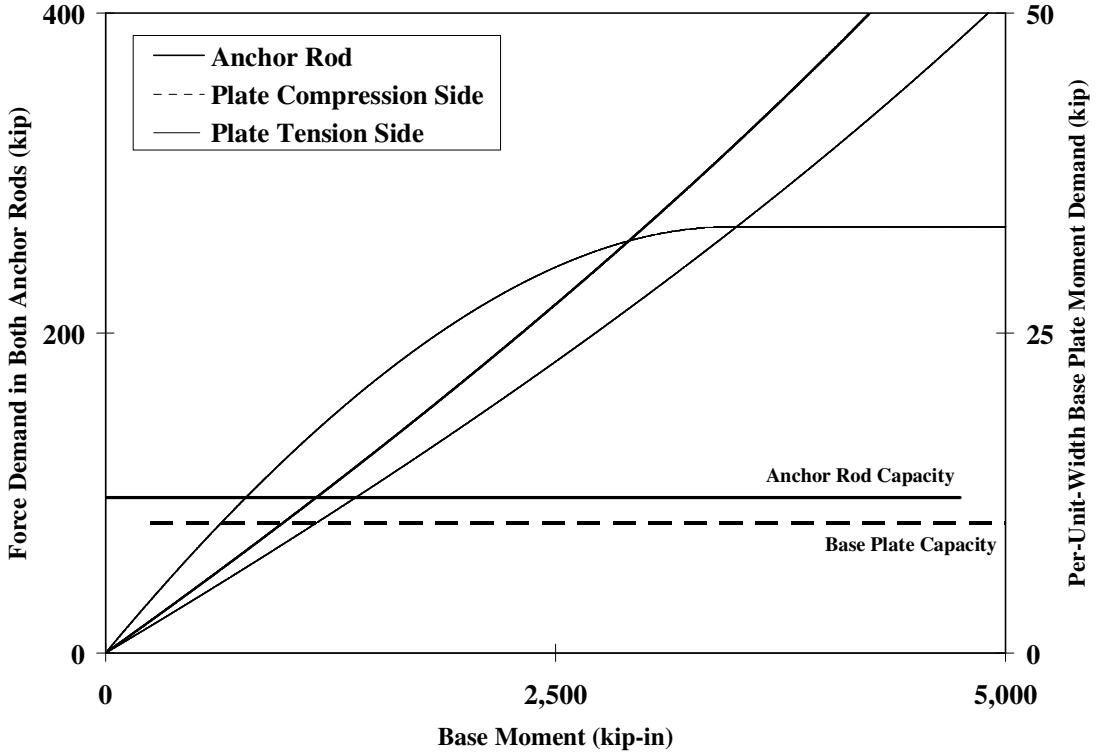

Figure E.6 – Calculated capacity and demand values for Test #3 (RSB Method)

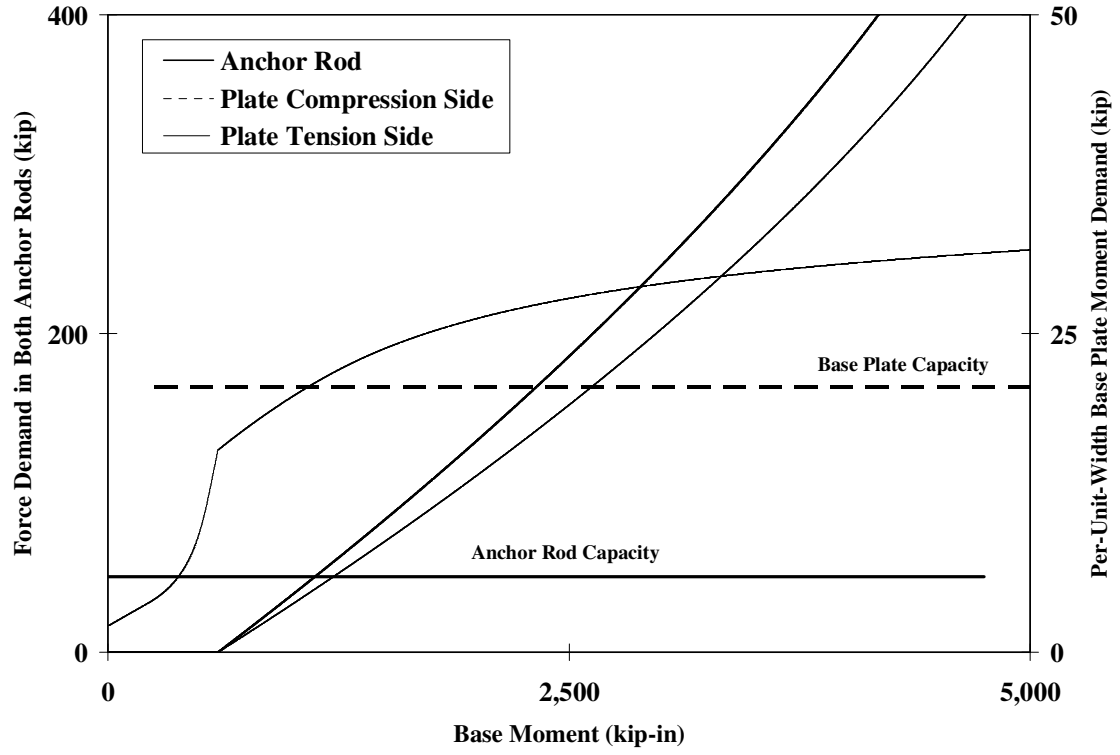

Figure E.7 – Calculated capacity and demand values for Test #4 (TSB Method)

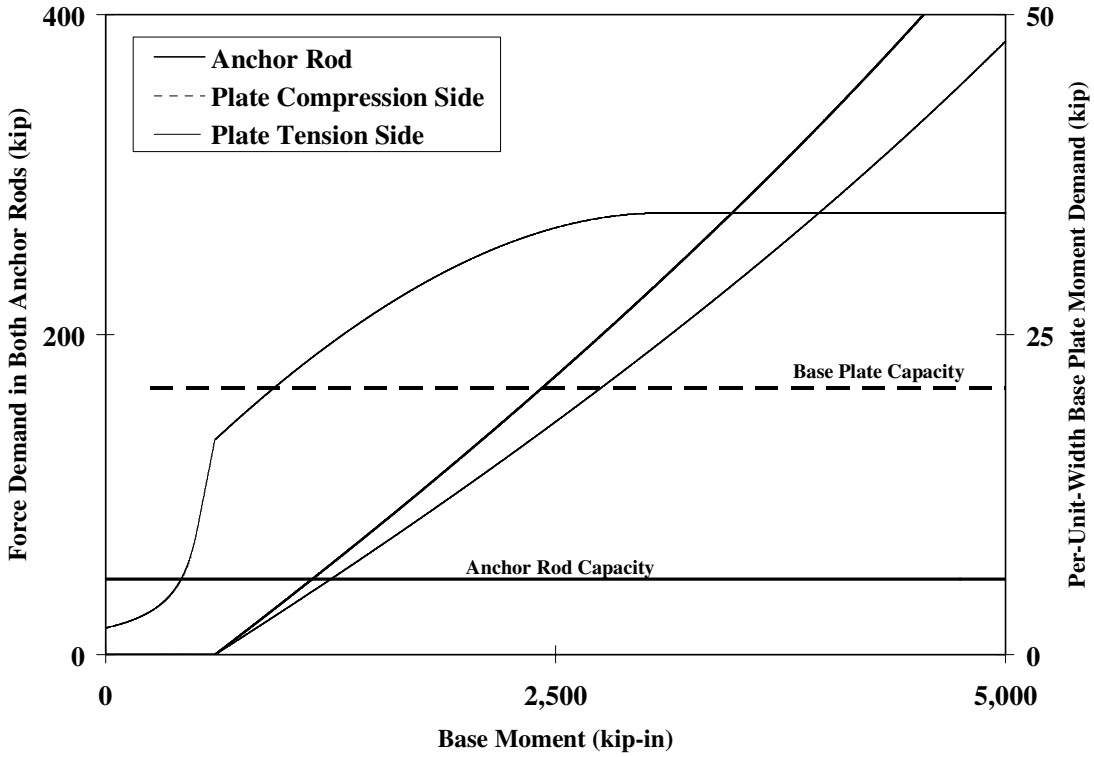

Figure E.8 – Calculated capacity and demand values for Test #4 (RSB Method)

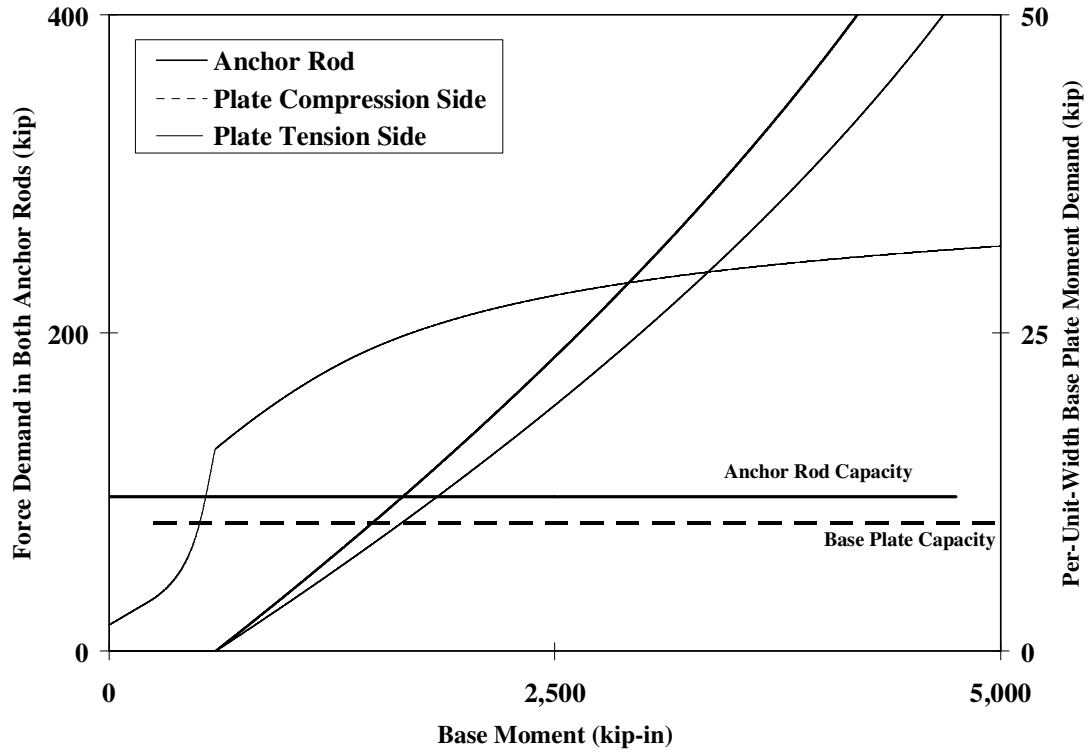

Figure E.9 – Calculated capacity and demand values for Test #5 (TSB Method)

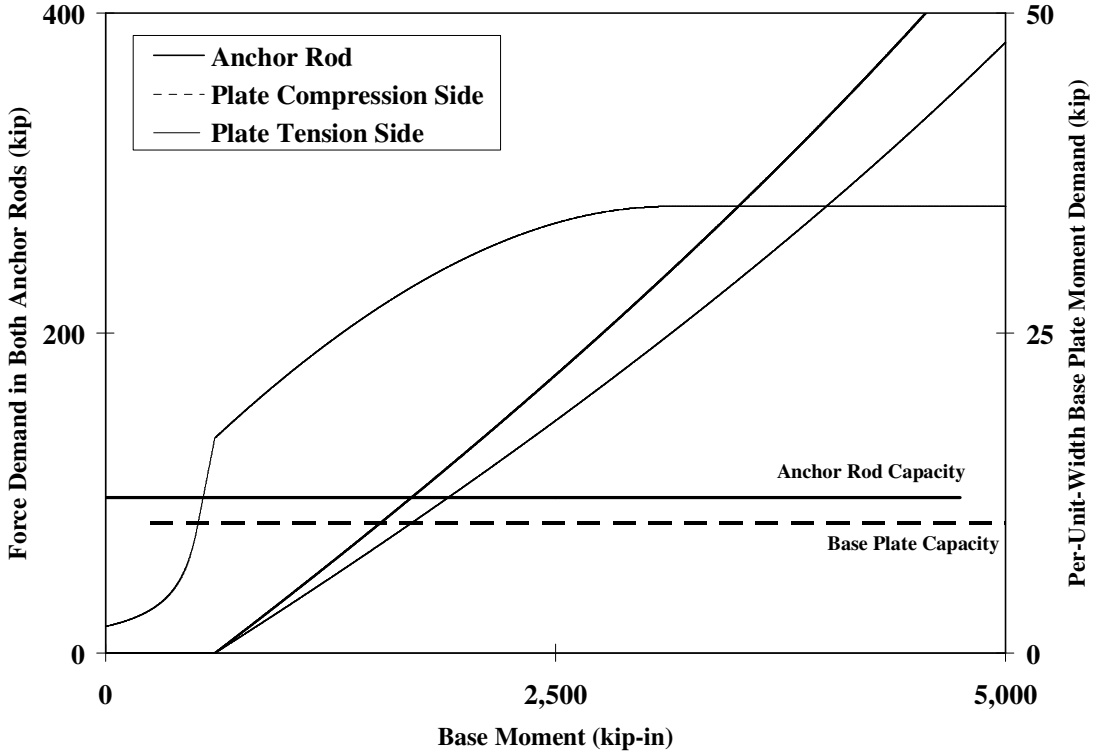

Figure E.10 – Calculated capacity and demand values for Test #5 (RSB Method)

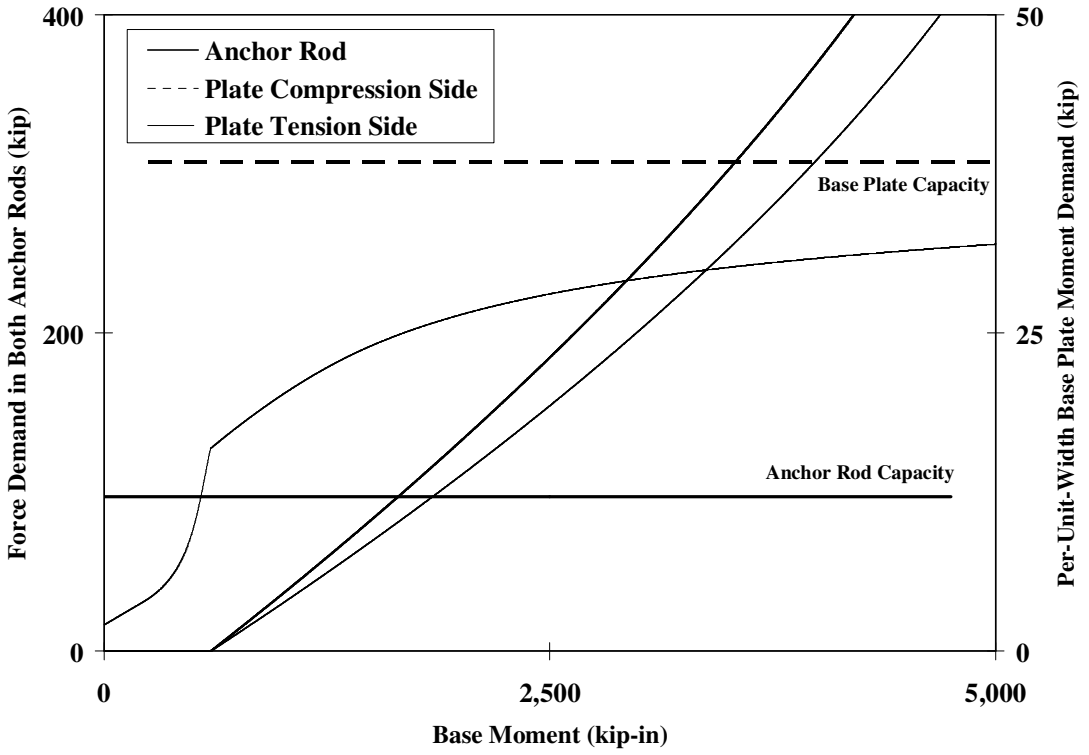

Figure E.11 – Calculated capacity and demand values for Test #6 (TSB Method)

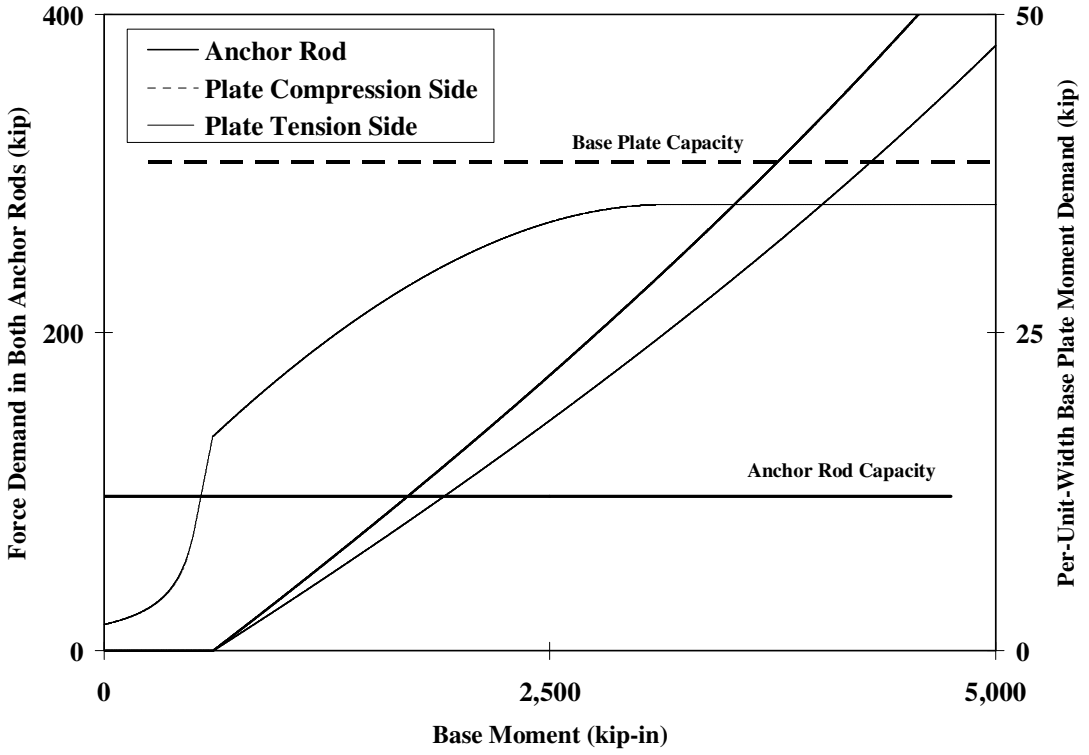

Figure E.12 – Calculated capacity and demand values for Test #6 (TSB Method)

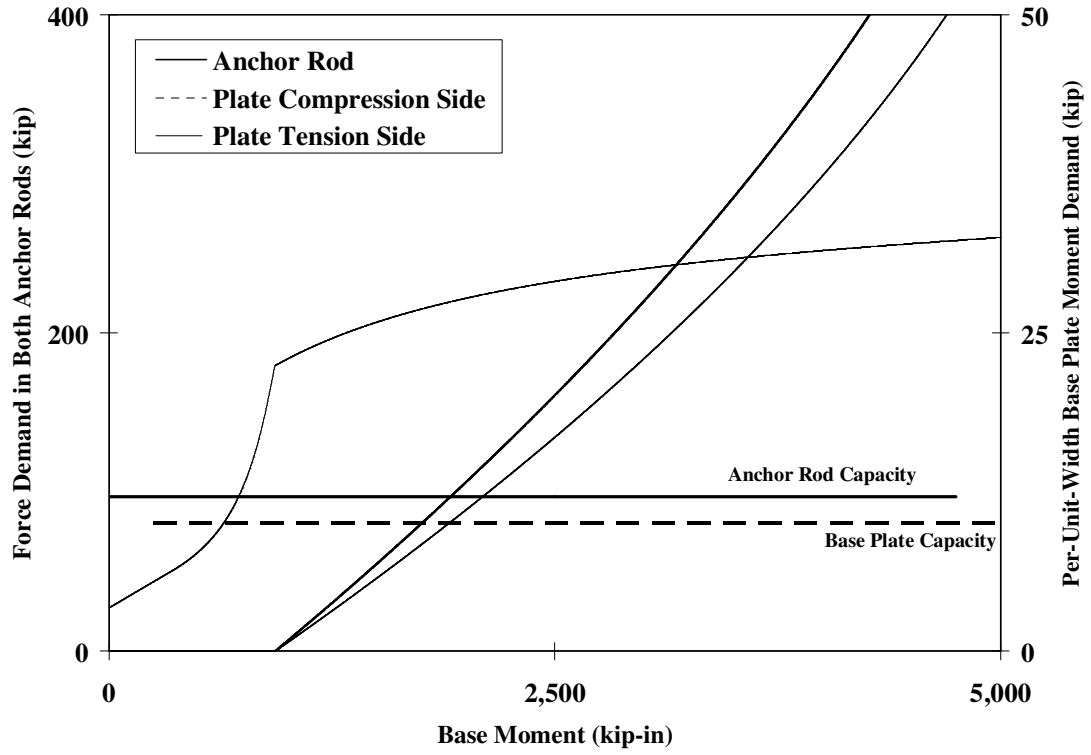

Figure E.13 – Calculated capacity and demand values for Test #7 (TSB Method)

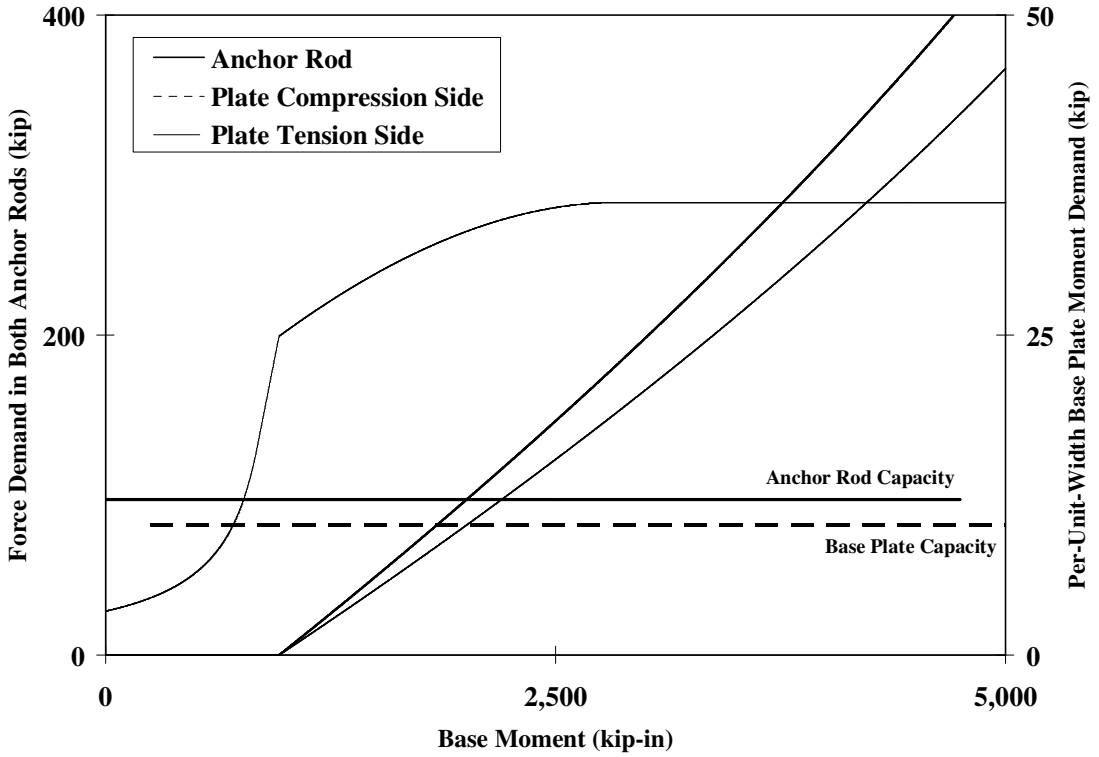

Figure E.14 – Calculated capacity and demand values for Test #7 (RSB Method)

Appendix F

Previous Base Connection Experiments

Based on an extensive literature search, a database of past published experimental programs from around the world on exposed column base connections under flexural loading is presented. Refer to the synthesis report sponsored by the AISC (Grauvilardell *et al.*, 2005) for an extensive description of past experimental programs on column base connections. Table F.1 indicates whether each listed experimental program was referenced in the synthesis report.

Table F.1 - Past experimental programs

Investigator	Year	Loading Type	Investigating Country	Publication Language	Number of Tests	Referenced in Synthesis Report	Main Test Parameters	Main Failure Modes
Eberbach	1959	Axial plus moment (from eccentricity)	Canada	English	5	No	• Base plate thickness	• Column failure by yielding of the tension reinforcement • Base plate yielding
LaFraugh & Magura	1966	Axial plus moment (from eccentricity)	USA	English	23	No	• Size and thickness of base plate • Diameter of anchor bolts • Eccentricity of the applied load	• Column failure • Bolt yielding • Plate yielding
DeWolf & Sarisley	1980	Axial plus moment (from eccentricity)	USA	English	16	Yes	• Axial load eccentricity • Anchor rod diameter • Plate thickness	• Concrete crushing • Anchor rod yielding • Base plate yielding
Stephenson & Tarpy	1981	Moment	USA	English	12	No	• Base plate size • Bending axis • Anchor rod size • Number of anchor rods • Connection type (clip angle or weld)	• Weld failure • Grout cracking • Concrete spalling
Akiyama *et al.*	1984	Axial plus moment (cyclic)	Japan	Japanese	5	Yes	• End detail and depth of anchor rod • Shape of column and base plate	• Concrete crushing • Anchor rod pull-out

Investigator	Year	Loading Type	Investigating Country	Publication Language	Number of Tests	Referenced in Synthesis Report	Main Test Parameters	Main Failure Modes
Picard & Beaulieu	1985	(1) Moment (2) Axial plus moment (from eccentricity)	Canada	English	25	Yes	• Column section • Number of anchor rods	• Grout crushing • Anchor rod fracture
Thambiratnam & Parimasivam	1986	Axial plus moment (from eccentricity)	Singapore	English	12	Yes	• Base plate thickness • Eccentricity of axial load	• Concrete block failure • Base plate yielding • Anchor rod yielding
Picard & Beaulieu	1987	Axial plus moment	Canada	English	14	Yes	• Shape of column • Base plate area and thickness • Number of anchor rods	• Column buckling in the direction of weak axis
Sato	1987	Axial plus moment (cyclic)	Japan	English	6	Yes	• Size of base plate • Column axial load • Yield strength of anchor rod	• Anchor rod fracture • Concrete failure • Anchor rod yielding
Hon & Melchers	1988	Axial plus moment (from eccentricity)	Australia	English	26	Yes	• Base plate thickness • Anchor rod size	• Anchor rod failure • Base plate yielding
Penserini & Colson	1989	Axial plus moment (cyclic)	France	English	N.A.	No	N.A.	N.A.
Astaneh *et al.*	1992	Axial plus moment (cyclic)	USA	English	6	Yes	• Base plate thickness • Column axial load	• Column and plate yielding • Rod and weld fracture • Grout crushing

Investigator	Year	Loading Type	Investigating Country	Publication Language	Number of Tests	Referenced in Synthesis Report	Main Test Parameters	Main Failure Modes
Igarashi *et al.*	1992	Moment (cyclic)	Japan	English	4	Yes	• Type of anchor rod	• Concrete riser and grout cracking and crushing • Anchor rod yielding
Melchers	1992	Moment (cyclic)	Australia	English	10	Yes	• Base plate thickness • Number and size of anchor rod • Anchor rod yield strength	• Base plate yielding • Anchor rod yielding
Cook & Klingner	1992	(1) Moment (2) Shear	USA	English	90	No	• Load eccentricity • Anchor type • Number of anchor rods • Base plate flexibility	• Yielding and fracture of anchors • Yielding of base plate
Carrato	1992	Moment	USA	English	8	No	• Plate thickness • Bolt stiffness (size)	• Base plate yielding • Anchor fracture
Targowski *et al.*	1993	Moment	Belgium	English	12	Yes	• Column section • Base plate thickness	• Base plate yielding • Anchor rod elongation

Investigator	Year	Loading Type	Investigating Country	Publication Language	Number of Tests	Referenced in Synthesis Report	Main Test Parameters	Main Failure Modes
Wald *et al.*	1994	(1) Axial (2) Axial plus moment (3) Moment	Czech Republic	English	14	Yes	• Base plate thickness	N.A.
Yoshimori *et al.*	1997	Moment (cyclic)	Japan	Japanese	5	No	N.A.	N.A.
Kallolil *et al.*	1998	Axial plus moment (from eccentricity)	India	English	3	No	• Anchor bolt size • Base plate thickness • Ratio of the moment to the axial load	• Yielding and fracture of anchor rods • Yielding of base plate
Akiyama *et al.*	1998	Moment (shaking table)	Japan	Japanese	2	Yes	• Base plate thickness	• Anchor rod elongation • Base plate yielding
Jaspart & Vandegans	1998	Axial plus moment	Belgium	English	12	Yes	• Base plate thickness • Number of anchor rods	• Failure of anchor rod and concrete • Yielding of base plate and column
Burda & Itani	1999	Axial plus moment (cyclic)	USA	English	6	Yes	• Base plate area • Base plate thickness	• Fracture of the weld between column and base plate
Fahmy	1999	Moment (cyclic)	USA	English	3	Yes	• Number of anchor rods • Weld material	• Fracture of the weld between column and base plate
Yoshimori & Nakashima	1999	Moment (cyclic)	Japan	Japanese	3	No	• Anchor rod layout and number	N.A.

Investigator	Year	Loading Type	Investigating Country	Publication Language	Number of Tests	Referenced in Synthesis Report	Main Test Parameters	Main Failure Modes
Adany *et al.*	2000	Moment (cyclic)	Hungary Portugal	English	5	Yes	• End-plate thickness • Anchor bolt pre-tensioning	• Base plate yielding • Anchor rod yielding • Column local buckling
Li *et al.*	2000	Axial plus moment (cyclic)	Japan	English	7	Yes	• Column section • Concrete filling • Anchor rod strength	• Anchor rod yielding • Buckling of steel tube
Lee & Goel	2001	Moment (cyclic)	USA	English	4	Yes	• Number of anchor rods • Weld material	• Fracture of the weld between column and base plate
Miyasaka *et al.*	2001	Moment	Japan	Japanese	8	Yes	• Base plate thickness • Location of anchor rods	• Base plate deformation and yielding
Liu	2001	Moment	UK	English	8	No	• Base plate thickness • Number of anchor rods	• Plate yielding • Anchor yielding
Korekoda *et al.*	2001	Axial plus moment (cyclic)	Japan	Japanese	5	No	• Base plate thickness • Anchor layout • Number of anchor rods	N.A.
Zhang *et al.*	2001	Moment (dynamic/static)	USA	English	17	No	• Loading protocol • Base plate flexibility • Cracked/uncracked concrete • Reinforcement details • Anchor type • Load eccentricity	• Anchor fracture • Concrete breakout

Investigator	Year	Loading Type	Investigating Country	Publication Language	Number of Tests	Referenced in Synthesis Report	Main Test Parameters	Main Failure Modes
Somiya *et al.*	2002	Axial and moment	Japan	Japanese	12	Yes	• Different initial axial load and load rate • Plate and tube thickness	• Base plate Yielding • Anchor rod yielding
Takamatsu & Tamai	2005	Axial plus moment (cyclic)	Japan	English	9	No	• Number of anchor rods • Level of axial load • Moment application (monotonic/cyclic) • Use of wedge device	• Yielding of anchor rods
Park *et al.*	2005	Moment (cyclic)	Korea	English	1	No	N.A.	• Anchor yielding
Kim *et al.*	2007	Axial plus moment (cyclic)	USA	English	2	No	• Number of anchor rods • Full scale frame	• Plastic hinging at column top • Inelastic flexural-torsional buckling
Di Sarno *et al.*	2007	Axial plus moment	Italy	English	4	No	• Axial load level • Connection type	• Fracture of anchor bolts • Plastic hinging of column (for socket connection)
Myers *et al.*	2009	Moment (cyclic)	USA	English	5	No	• Weld detail • Loading history	• Weld failure

Investigator	Year	Loading Type	Investigating Country	Publication Language	Number of Tests	Referenced in Synthesis Report	Main Test Parameters	Main Failure Modes
Cui *et al.*	2009	Axial plus moment	Japan	English	8	No	• Column embedment type	• Fracture of anchor bolts
Gomez *et al.*	2009	(1) Moment (monotonic/cyclic) (2) Axial plus moment (cyclic)	USA	English	7	No	• Number of anchor rods • Anchor rod strength • Base plate thickness • Level of axial load • Cyclic/monotonic moment	• Anchor rod Yielding and fracture • Grout crushing • Plate yielding